Modeling, Analysis and Optimization of Integrated Energy Systems for Multigeneration Purposes

By

Pouria Ahmadi

A Thesis Submitted in Partial Fulfillment

of the Requirements for the Degree of Doctor of Philosophy

in

Mechanical Engineering

Faculty of Engineering and Applied Science,

University of Ontario Institute of Technology

Oshawa, Ontario, Canada

Abstract

Energy use is directly linked to well-being and prosperity across the world. Meeting the growing demand for energy in a safe and environmentally responsible manner is an important challenge. There are around seven billion people on Earth and population growth will likely lead to an increase in energy demand, which depends on the adequacy of energy resources. In addition, increasing population and economic development in many countries have serious implications for the environment, since energy generation processes (e.g., generation of electricity, heating, cooling, and shaft work for transportation and other applications) emit pollutants, many of which are harmful to ecosystems. Utilizing advanced technologies to mitigate global warming and increase the efficiency of energy systems are key objectives, with ways to meet them proposed and tested in many countries. Among these technologies, multigeneration processes stand out as a possibility for making important contributions due to their potential for high efficiencies as well as low operating costs and pollution emissions per energy output.

In this PhD thesis, three novel multigeneration energy systems are considered, analyzed and optimized. The aim is to consider both renewable- and non-renewable-based multigeneration systems. A non-renewable-based multigeneration system is composed of a gas turbine as a prime mover, a double pressure heat recovery steam generator, a single effect absorption chiller, a domestic water heater, an ejector cooling system and PEM electrolyzer. This proposed multigeneration system can produce electricity, heating, cooling, hot water and hydrogen simultaneously. The overall exergy efficiency of the system is 60%, which is 30% higher than the power generation system. Observations show that shifting from a conventional power generation system to a multigeneration cycle leads to a decrease in CO_2 emissions of approximately 120 kg/kWh, providing significant motivation to convert to multigeneration cycles. For renewable-based multigeneration systems, biomass-based and integrated ocean thermal energy conversion (OTEC)-based were selected as candidates to meet the requirements of producing electricity, heating, cooling, hot and fresh water and hydrogen.

The biomass-based multigeneration system is composed of a biomass combustor, an ORC cycle for producing electricity, a double-effect absorption chiller for cooling, a heat exchanger for heating, a proton exchange membrane (PEM) electrolyzer for producing hydrogen, a domestic water heater for producing hot water and a reverse osmosis (RO) desalinator for producing fresh water. Pine sawdust is used as the biomass fuel and burned in a biomass

combustor. This multigeneration system increases the exergy efficiency by about 20% and reduces CO_2 emissions by about 3500 kg/MWh compared to a conventional power generation system.The last multigeneration energy system examined is an ocean thermal energy conversion (OTEC)-based system integrated with a PV/T solar collector and a single-effect absorption chiller to provide the cooling load of the system. An OTEC system utilizes low-grade energy and has a low energy efficiency. This integrated system uses warm surface seawater to evaporate a working fluid like ammonia or a Freon refrigerant, which drives an ORC turbine to produce electricity, which in turn is used to drive a PEM electrolyzer to produce hydrogen. A reverse osmosis (RO) desalination unit is used to produce fresh water. The exergy efficiency of this integrated system is 37%, which is higher than single generation systems and, in addition, this integrated system has no emissions as it uses ocean energy instead of fuel.

Multigeneration processes can make important contributions due to their potential for high efficiency as well as low operating costs and pollution emissions per energy output. Issues such as fossil fuel depletion and climate change amplify the advantages and significance of efficient multigeneration energy systems.

Acknowledgements

First and foremost, I would like to express my deep and sincere gratitude to my supervisor, Dr. Ibrahim Dincer, and my co-supervisor, Dr. Marc A. Rosen, for their valuable guidance and never-ending support. Their enthusiasm and passion have been constant sources of inspiration and encouragement.

Moreover, I would like to thank my friends, Halil S. Hamut and Nader Javani for their support throughout my time at the University. I would also like to thank my sister Kamilia and her husband Ahmadreza for their help, support and encouragement throughout my education.

Furthermore, the financial support provided by the Natural Sciences and Engineering Research Council of Canada is gratefully acknowledged.

Last but not least; I would like to thank my parents Morad and Batoul and my brother Pedram for their understanding and encouragement throughout my education.

Table of Contents

ABSTRACT **2**

ACKNOWLEDGEMENTS **4**

TABLE OF CONTENTS **5**

LIST OF TABLES **7**

LIST OF FIGURES **8**

NOMENCLATURE **14**

CHAPTER 1: INTRODUCTION **18**

1.1 Overview 18
1.2 Benefits of multigeneration energy systems 23
1.3 Prime Movers 24
1.3.1 Gas turbine prime mover 25
1.3.2 Fuel cell prime mover 27
1.4 Multigeneration Energy Systems 29

CHAPTER 2: MOTIVATION AND OBJECTIVES **32**

2.1 Motivation 32
2.2 Objectives 33

CHAPTER 3: LITERATURE REVIEW **36**

3.1 Introduction 36
3.1 Cogeneration heat and power (CHP) systems 36
3.2 Trigeneration systems 38
3.3 Multigeneration energy systems 46

CHAPTER 4: DESCRIPTIONS OF SYSTEMS **49**

4.1 System I: Multigeneration system based on gas turbine prime mover 49
4:2 System II: Biomass based multigeneration system 50
4.3 System III: Integrated ocean thermal energy conversion multigeneration system 54

CHAPTER 5: MODEL DEVELOPMENT AND ANALYSES **58**

5.1 Thermodynamic analyses 58
5.1.1 Mass balance equation 58
5.1.2 Energy balance equation 59
5.1.3 Entropy balance equation 59
5.1.4 Exergy analysis 59
5.2 Thermoeconomic analysis 60
5.2.1 Cost balance equation 61
5.2.2 Capital recovery factor 61
5.3 Environmental impact assessment 61
5.4 Optimization 62
5.4.1 Objective functions and system criteria 63
5.4.2 Decision variables 63
5.4.3 Constraints 63
5.4.4 Optimization methods 64
5.5 Analyses of System I 68
5.5.1 Thermodynamic analysis 68
5.5.2 Exergy analysis 79
5.5.3 Economic analysis of system I 86

5.5.4 Environmental impact assessment 92
5.6 ANALYSES OF SYSTEM II 93
5.6.1 Thermodynamic analysis 93
5.6.2 Exergy analysis of system II 101
5.6.3 Economic analysis of system II 103
5.7 ANALYSES OF SYSTEM III 104
5.7.1 Thermodynamic analyses 104
5.7.2 Exergy analysis of system II 110
5.7.3 Economic analysis of system III 112
CHAPTER 6: RESULTS AND DISCUSSION 114
6.1 INTRODUCTION 114
6.2 RESULTS OF SYSTEM I 115
6.2. 1 Modeling results 115
6.2. 2 Exergy and economic analyses results 119
6.2. 3 Environmental impact assessment 133
6.2.4 Multi-objective optimization 139
6.3 RESULTS OF SYSTEM II 156
6.3. 1 Modeling results 156
6.3. 2 Exergy and economic analyses results 158
6.3. 3 Environmental impact assessment 172
6.3.4 Multi-objective optimization 174
6.4 RESULTS OF SYSTEM III 186
6.4. 1 Modeling results 186
6.4. 2 Exergy and economic analyses results 188
6.4.3 Multi-objective optimization of integrated OTEC based multigeneration system 201
6.5 COMPARISON AND GENERALIZATION 214
CHAPTER 7: CONCLUSIONS AND RECOMMENDATIONS 217
7.1 CONCLUSIONS 217
7.2 RECOMMENDATIONS 221
REFERENCES 222

List of Tables

Table 5.1: Values for parameters in Eqs. (5.18, 5.20). 62
Table 5. 2: Expressions for exergy destruction rates for components of the system. 81
Table 5.3: Partial pressures and molar fractions of various constituents of air [47]. 82
Table 5.4: Standard chemical values for selected substances at T_0 = 298.15 K and P_0 = 1 atm [47, 98]... 83
Table 5.5: Composition of pine sawdust biomass. 94
Table 5.6: Expressions for exergy destruction rates for components of the system 102
Table 5.7: Expressions for exergy destruction rates for components of the system 111
Table 6.1: Input parameters used to simulate the system. 116
Table 6.2: Input parameters used to model PEM electrolysis [111]. 117
Table 6.3 : Parameter values resulting from energy and exergy analyses of the system. 118
Table 6.4: Optimization constraints and their rationales 141
Table 6.5: Optimized values for design parameters of the system based on multi-objective optimization 144
Table 6.6: Thermodynamic characteristics of three different points on the Pareto frontier. 144
Table 6.7: Input parameters used to simulate the system. 157
Table 6.8: Parameter values from modeling and energy and exergy analyses of the system 158
Table 6.9: Optimization constraints and their rationales 176
Table 6.10: Optimized values for design parameters of the system based on multi-objective optimization 178
Table 6. 11: Thermodynamic characteristics of three different points on the Pareto frontier. 179
Table 6. 12: Input data for the system simulation of OTEC system. 189
Table 6.13: Input parameters used to model PEM electrolysis. 189
Table 6.14: Parameter values resulting from energy and exergy analyses of the system. 190
Table 6.15: Optimization constraints and their rationales. 202
Table 6.16: Optimized values for design parameters of the system based on multi-objective optimization. 205
Table 6.17: Thermodynamic characteristics of three different points on the Pareto frontier. 205
Table 6.18: Comparison of three different multigeneration systems 215
Table 6.19: Comparison of normalized cost for each multigeneration system. 216

List of Figures

Figure 1.1: A typical trigeneration energy system. 22
Figure 1.2: A multigeneration energy system for producing electricity, cooling, heating, hot water and hydrogen [7]. 23
Figure 1.3: A multigeneration energy system for producing electricity, cooling, heating, hot water, hydrogen and fresh water [7]. 23
Figure 1.4: The schematic diagram of a gas turbine prime mover used in CHP [4]. 27
Figure 1.5: Schematic of combined gas turbine power plant with SOFC [12]. 28
Figure 1.6: Schematic of a multigeneration system for electricity, heating, cooling and hot water production. 30
Figure 1.7: Schematic diagram of a multigeneration energy system for desalination purpose [13]. 31
Figure 4.1: Schematic diagram of a multigeneration energy system based on a micro gas turbine, a dual pressure heat recovery steam generator, an absorption chiller, an ejector refrigeration cycle. 51
Figure 4. 2: Schematic of biomass based a multigeneration energy system for the provision of heating, cooling, electricity, hydrogen, fresh water and hot water. 54
Figure 4.3: Schematic of an integrated renewable based multigeneration energy system for the provision of cooling, electricity, hydrogen, fresh water. 57
Figure 5.1: A control volume for mass balance equation. 58
Figure 5. 2: Multi-objective optimization with two objective functions OF1 and OF2 that are to be minimized, showing the (a) dominant designs and (b) the Pareto frontier. 67
Figure 5.3: Temperature profile of HRSG. 71
Figure 5.4: Pressure profile in ejector, modified from [95]. 74
Figure 5.5: Ejector modeling flowchart. 76
Figure 5.6: 84Variation of standard chemical exergy ($ex_{ch,0}$), chemical exergy due to dissolution (ex_{dis}) and total chemical exergy as a function of LiBr mass basis concentration at T0 = 25 0C. 84
Figure 5.7: *T-S* diagram of the ocean thermal energy conversion (OTEC). 106
Figure 6.1: Comparison of present model with experimental data for PEM electrolyzer. 117
Figure 6.2: Variation of electrolyzer overpotentials at various current densities. 118
Figure 6.3: Exergy destruction rates for the multigeneration system and its components. 119
Figure 6.4: Dimensionless exergy destruction ratio for the multigeneration system and its components. 120
Figure 6.5: Energy and exergy efficienies for the subsystems of the multigeneration system. 121

Figure 6.6: Variations with compressor pressure ratio of the trigeneration exergy efficiency for several gas turbine isentropic efficiencies 122
Figure 6.7: Variations with compressor pressure ratio of energy and exergy efficiencies..... 123
Figure 6.8: Variations with compressor pressure ratio of exergy efficiency and exergy. 124
destruction rate for the trigeneration system. 124
Figure 6. 9: Variations with compressor pressure ratio of combustion chamber and gas turbine mass flow rate. 124
Figure 6.10: Variations with compressor pressure ratio of heating and cooling load of the multigeneration. 125
Figure 6.11: Variations with compressor pressure ratio of heating and cooling load of the multigeneration. 125
Figure 6.12: Variations with gas turbine inlet temperature of total exergy destruction rate and exergy efficiency. 126
Figure 6.13: Variations of gas turbine inlet temperature of exergy efficiency. 127
Figure 6.14: Variations with gas turbine inlet temperature of total exergy destruction rate and exergy efficiency. 127
Figure 6.15: Variations with gas turbine inlet temperature of heating and cooling load of the system. . 128
Figure 6.16: Variations with gas turbine inlet temperature of steam and ORC power output. 129
Figure 6.17: Variations with gas turbine inlet temperature of hydrogen production and hot water mass flow rate. 129
Figure 6.18: Variations with pressure of high-pressure steam, P_{HP}, on system energy and exergy efficiencies. 130
Figure 6.19: Variations with HRSG high pressure of steam cycle and ORC power output. 131
Figure 6.20: Variations with T_{EVP} of various system exergy efficiencies. 131
Figure 6.21: Variations with high pressure pinch point temperature of exergy efficiency and total exergy destruction rate. 132
Figure 6.22: Variations with high pressure pinch point temperature of total cost rate and total exergy destruction rate. 132
Figure 6.23: Comparison of exergy efficiency and unit CO_2 emissions of selected types of plants. ….133
Figure 6.24: Unit CO emissions of selected types of plants. 134
Figure 6.25: Variations of unit CO_2 emissions with compressor pressure ratio for selected cases. 134
Figure 6.26: Variations of unit CO emissions with compressor pressure ratio for selected cases. 135
Figure 6.27: Variations with compressor pressure ratio of sustainability index and cost rate of environmental impact. 136

Figure 6.28: Variations with compressor pressure ratio of total exergy destruction rate and sustainability index. 137
Figure 6.29: Variations with compressor pressure ratio of total cost rate and cost of environmental impact. 137
Figure 6.30: Variations of gas turbine inlet temperature (*GTIT*) on normalized CO_2 emissions. 138
Figure 6.31: Variations of gas turbine inlet temperature (GTIT) on normalized CO emissions. 138
Figure 6.32: Variations with gas turbine inlet temperature of sustainability index and cost rate of environmental impact. 139
Figure 6.33: Pareto Frontier: Best trade off values for the objective functions. 142
Figure 6.34: Results of all evaluations during 300 generations using genetic algorithm. A clear approximation of the Pareto front is visible on the lower part of the figure. 142
Figure 6.35: Scattered distribution of decision variables with population in Pareto frontier: compressor isentropic efficiency (a), gas turbine isentropic efficiency (b), gas turbine inlet temperature (c) and compressor pressure ratio (d). 145
Figure 6.36: Scattered distribution of decision variables with population in Pareto frontier: HRSG low pressure (a), HRSG high pressure (b), low pressure pinch point temperature (c) and high pressure pinch point temperature (d). 146
Figure 6.37: Scattered distribution of decision variables with population in Pareto frontier: HRSG steam turbine isentropic efficiency (a), pump isentropic efficiency (b), absorption chiller evaporator temperature (c) and condenser pressure (d). 147
Figure 6.38: Scattered distribution of decision variables with population in Pareto frontier: ORC turbine inlet pressure (a), ORC turbine extraction pressure (b) and ORC evaporator pressure (c). 148
Figure 6.39: Effects of design parameters on both objective functions: compressor isentropic efficiency (a), gas turbine isentropic efficiency (b), gas turbine inlet temperature (c) and compressor pressure ratio (d). 150
Figure 6.40: Effects of design parameters on both objective functions HRSG low pressure (a), HRSG high pressure (b), low pressure pinch point temperature (c) and high pressure pinch point temperature (d). . 152
Figure 6.41: Effects of design parameters on both objective functions, steam turbine isentropic efficiency (a), pump isentropic efficiency (b), absorption chiller evaporator efficiency (c) and condenser pressure (d). 154
Figure 6.42: Scattered distribution of decision variables with population in Pareto frontier: ORC turbine inlet pressure (a), ORC turbine extraction pressure (b) and ORC evaporator pressure (c). 155
Figure 6.43: Exergy destruction rates for the multi-generation system and its components. 159
Figure 6.44: Effect of varying pinch point temperature on exergy efficiency for several cycles. 160

Figure 6.45: Effects of varying pinch point temperature on heating and cooling loads of the system. ... 161
Figure 6. 46: Effects of varying pinch point temperature on hot water and hydrogen production rates. 161
Figure 6.47: Effects of varying pinch point temperature on exergy efficiency and total exergy destruction rate. ... 162
Figure 6.48: Effects of varying pinch point temperature on net power output and fresh water mass flow rate. ... 163
Figure 6.49: Effects of varying pinch point temperature total cost rate and fresh water mass flow rate. 163
Figure 6.50: Effects of varying ORC turbine inlet pressure on exergy efficiency. ... 164
Figure 6.51: Effects of varying ORC turbine inlet pressure on heating and cooling loads of the system. ... 165
Figure 6.52: Effects of varying ORC turbine inlet pressure on the power to heating and cooling ratios. 166
Figure 6.53: Effects of varying ORC turbine inlet pressure on hydrogen production and total exergy destruction rate. ... 166
Figure 6.54: Effects of varying ORC turbine inlet pressure on exergy destruction rate for ORC cycle and absorption chiller. ... 167
Figure 6.55: Effects of varying ORC turbine inlet pressure on total cost rate and total exergy destruction rate. ... 167
Figure 6.56: Effects of varying ORC turbine inlet pressure on total cost rate net power output. ... 168
Figure 6.57: Effects of varying ORC pump inlet temperature on exergy efficiency and total exergy destruction rate. ... 169
Figure 6.58: Effects of varying ORC pump inlet temperature on heating and cooling loads of the system. 169
Figure 6.59: Effects of varying ORC pump inlet temperature on exergy efficiency. ... 170
Figure 6.60: Effects of varying ORC pump inlet temperature on net power output. ... 170
Figure 6.61: Effects of varying ORC pump inlet temperature on power to heating and cooling ratios. . 171
Figure 6.62: Effects of varying ORC pump inlet temperature on total cost rate and exergy efficiency. . 171
Figure 6.63: Comparison of exergy efficiencies and environmental impacts for three types of plants. .. 172
Figure 6. 64: Effect of varying ORC turbine inlet pressure on CO_2 emissions. ... 173
Figure 6.65: Effects of varying ORC pump inlet temperature on CO_2 emissions. ... 174
Figure 6.66: Effects of varying pinch point temperature on CO_2 emissions. ... 174
Figure 6.67: Pareto Frontier: Best trade off values for the objective functions ... 177
Figure 6.68:Results of all evaluations during 300 generations using genetic algorithm. A clear approximation of the Pareto front is visible on the lower part of the figure. ... 178

Figure 6.69: Scattered distribution of decision variables with population in Pareto frontier: biomass flow rate (a), ORC pump inlet temperature (b), ORC turbine inlet pressure (c) and ORC turbine inlet temperature (d)..... 180
Figure 6.70: Scattered distribution of decision variables with population in Pareto frontier: inch point temperature (a), ORC turbine isentropic efficiency (b), ORC pump isentropic efficiency (c) and absorption chiller evaporator temperature (d). 181
Figure 6.71: Effects of biomass flow rate on both objective functions. 182
Figure 6.72: Effects of turbine inlet pressure on both objective functions. 183
Figure 6.73: Effects of turbine inlet pressure on both objective functions. 184
Figure 6.74: Effects of evaporator pinch point temperature on both objective functions. 185
Figure 6.75: Effects of turbine isentropic efficiency on both objective functions. 186
Figure 6.76: Effects of pump isentropic efficiency on both objective functions. 187
Figure 6.77: Effects of absorption chiller on both objective functions. 187
Figure 6.78: Exergy destruction rates for the Integrated OTEC based multigeneration system and its components. 191
Figure 6.79: Dimensionless exergy destruction ratio for the multigeneration system and its components. 191
Figure 6.80: Effect of varying inlet air mass flow rate and PV/T length on exergy efficiency of the PV/T collector. 192
Figure 6.81: Effects of varying PV/T length and width on electricity generated by the PV/T collector. 193
Figure 6. 82: Effects of varying PV/T length and width on electricity generated by the PV/T collector. 193
Figure 6.83: Effects of varying seawater warm surface mass flow rate on the system exergy efficiency and exergy destruction rate of the system. 194
Figure 6.84: Effects of varying seawater warm surface mass flow rate on the net power output and total cost rate of the system. 195
Figure 6.85: Effects of varying solar radiation intensity on the exergy efficiency of the system. 196
Figure 6.86: Effects of varying condenser temperature on the net power output the system. 196
Figure 6.87: Effects of varying solar intensity on the total exergy destruction of the system. 197
Figure 6.88: Effects of varying solar intensity on the total exergy destruction of the system. 198
Figure 6.89:Effects of varying pinch point temperature on the exergy efficiency and total exergy destruction rate of the system. 198
Figure 6.90: Effects of varying pinch point temperature on the hydrogen production and total cost rate of the system. 199

Figure 6.91: Effects of varying PV/T length and inlet air mass flow rate on the exergy efficiency of the system. 200
Figure 6.92: Effects of varying PV/T length and inlet air mass flow rate on cooling load of the system. 200
Figure 6.93: Effects of varying PV/T length and inlet air mass flow rate on total cost rate of the system. 201
Figure 6.94: Pareto Frontier: Best trade off values for the objective functions. 203
Figure 6.95: Results of all evaluations during 300 generations using genetic algorithm. A clear approximation of the Pareto front is visible on the lower part of the figure. 204
Figure 6.96: Scattered distribution of decision variables with population in Pareto frontier: PV/T length (a), warm surface mass flow rate (b), pinch point temperature (c) and turbine isentropic efficiency (d). 207
Figure 6.97: Scatterd distribution of decision variables with population in Pareto frontier: Pump isentropic efficiency (a), chiller evaporator temperature (b), condenser temperature (c) PV/T mass flow rate (d). 208
Figure 6.98: Scattered distribution of decision variables with population in Paretoe frontier: PV/T width. 209
Figure 6.99: Effects of PV/T length on both objective functions. 209
Figure 6.100: Effects of warm surface mass flow rate on both objective functions. 210
Figure 6.101: Effects of OTEC evaporator pinch point temperature on both objective functions. 211
Figure 6.102: Effects of turbine isentropic efficiency on both objective functions. 211
Figure 6.103: Effects of pump isentropic efficiency on both objective functions. 212
Figure 6.104: Effects of chiller evaporator temperature on both objective functions. 213
Figure 6.105: Effects of condenser temperature on both objective functions. 213
Figure 6.106: Effects of PV/T inlet air mass flow rate on both objective functions. 214
Figure 6.107: Effects of PV/T width on both objective functions. 215

Nomenclature

A	Surface area (m^2)
C_p	Specific heat at constant pressure (kJ/kg K)
C	Cost ($)
c_f	Fuel specific cost ($/MJ)
D_{eq}	Equivalent diameter (m)
D_s	Mass diffusivity (m^2/s)
F	Faraday constant, (C/mol)
ex	Specific exergy (kJ/kg)
$\overline{ex}$	Specific exergy (kJ/kmol)
$\dot{E}x$	Exergy flow rate (kW)
$\dot{E}x_D$	Exergy destruction rate (kW)
G	Gibb's free energy, (kJ)
h	Specific enthalpy (kJ/kg)
$\bar{h}$	Specific molar enthalpy, (kJ/kmol)
$\dot{I}$	Solar radiation intensity (W/m^2)
J	Current density, (A/m^2)
J_o	Exchange current density, (A/m^2)
J_i^{ref}	Pre-exponential factor, (A/m^2)
L	Length, (m)
LHV	Lower heating value (kJ/kg)
$\overline{LHV}$	Lower heating value (kJ/kmol)
M	molar mass, (kg/kmol)
$\dot{m}$	Mass flow rate (kg/s)
$\dot{N}$	Molar flow rate, (mol/s)
P	Pressure (kPa, bar)
$\dot{Q}$	Heat rate (kW)
R	Gas constant (kJ/kg K)
$\bar{R}$	Universal gas constant (kJ/kmolK)
R_{PEM}	Proton exchange membrane resistance (Ω)

s	Specific entropy (kJ/kg K)
T	Temperature (K, ^{0}C)
U_L	Overall heat transfer coefficient (W/m^{2}K)
V	Velocity (m/s)
V_0	Reversible potential (V)
V_{act}	Activation overpotential (V)
$V_{act,a}$	Anode activation overpotential (V)
$V_{act,c}$	Cathode activation overpotential (V)
$\dot{W}$	Work rate (kW)
$\dot{Z}$	Purchase cost rate ($/s)

Greek Letters

β	Chemical exergy/energy ratio
Δ	Change in variable
ε	Normalized CO_2 emissions, (kg/MWh)
γ	Specific heat ratio
δ	Clearance
η	Isentropic efficiency
θ	Dimensionless temperature
λ	Fuel to air ratio
λ_a	Water content at anode-membrane interface (Ω^{-1})
λ_c	Water content at cathode-membrane interface (Ω^{-1})
$\lambda(x)$	Water content at location x in the membrane (Ω^{-1})
μ	Dynamic viscosity (kg/m.s)
σ_{PEM}	Proton conductivity in PEM (s/m)
$\sigma(x)$	Local ionic PEM conductivity (s/m)
ζ	H/C atomic ratio
ρ	Density (kg/m^3)
Φ	Maintenance factor
Ψ	Exergy efficiency
ω	Entrainment ratio

Subscripts

a	Air
Abs	Absorber
AC	Air compressor
act	Actual
CC	Combustion chamber
CHP	Combined heat and power
Cond	Condenser
Cooling	Cooling load
COP	Coefficient of performance
CRF	Capital recovery factor
D	Destruction
D_P	Depletion number
Dif	Diffuser
DWH	Domestic water heater
e	Exit condition
env	Environment
eq	Equivalent
EVP	Evaporator
Exv	Expansion valve
ex	Exergy
f	Fuel
FPC	Flat plat collector
FWP	Feed water pump
g	Combustion gases
Gen	Generator
GTIT	Gas turbine inlet temperature
HEX	Heat exchanger
hr	Hour
GT	Gas turbine
Heating	Heating load

HP	High pressure
HRSG	Heat recovery steam generator
i	Inlet condition
is	Isentropic
LP	Lower pressure
mix	Mixture
multi	Multigeneration
net	Net output power
Noz	Nozzle
ohm	Ohmic
ORC	Organic Rankine cycle
OTEC	Ocean thermal energy conversion
out	Outlet condition
PEM	Polymer exchange membrane
Pf	Primary flow
PP	Pinch point
PV/T	Photo voltaic thermal collector
R	Compressor pressure ratio
Re	Reynolds number
RR	Recovery ratio for desalination unit
RO	Reverse osmosis desalination
Sc	Schmidt number
Sf	Secondary flow
ST	Steam turbine
T_{pz}	Flame temperature
tot	Total
WS	Warm surface
WF	Working fluid
CS	Cold surface

Superscripts

.	rate
Ch	Chemical

Chapter 1: Introduction

1.1 Overview

Energy use is directly linked to well-being and prosperity across the world. Meeting the growing demand for energy in a safe and environmentally responsible manner is an important challenge. A key driver of energy demand is the human desire to sustain and improve ourselves, our families and our communities. There are around seven billion people on Earth and population growth will likely lead to an increase in energy demand, which depends on the adequacy of energy resources. In addition, increasing population and economic development in many countries have serious implications for the environment, because energy generation processes (e.g., generation of electricity, heating, cooling, and shaft work for transportation and other applications) emit pollutants, many of which are harmful to ecosystems. Burning fossil fuels results in the release of large amounts of greenhouse gases, particularly carbon dioxide.

Energy drives processes and is essential to life. Energy exists in several forms, e.g. light, heat, and electricity. Concerns exist regarding limitations on easily accessible supplies of energy resources and the contribution of energy processes to global warming as well as other environmental concerns such as air pollution, acid precipitation, ozone depletion, forest destruction, and radioactive emissions [1]. There are various alternative energy options to fossil fuels, including solar, geothermal, hydropower, wind and nuclear energy. The use of many of the available natural energy resources is limited due to their reliability, quality and energy density. Nuclear energy has the potential to contribute a significant share of large scale energy supply without contributing to climate change. Advanced technologies, aimed at mitigating global warming, are being proposed and tested in many countries. Among these technologies, multigeneration processes, including trigeneration, can make important contributions due to their potential for high efficiencies as well as low operating costs and pollution emissions per energy output. Issues like fossil fuel depletion and climate change amplify the advantages and significance of efficient multigeneration energy systems.

Global warming, which is one the facets of global climate change, refers to an increase in the average temperature of the atmosphere and oceans, which appears to have occurred in recent decades and is projected to continue. The drivers of climate change are generally agreed to be

changes in the atmospheric concentrations of greenhouse gases (GHGs) and aerosols. According to the Intergovernmental Panel on Climate Change (IPCC), most of the increase in global average temperatures since the mid-20th century is linked to the observed increase in anthropogenic GHG concentrations. A greenhouse gas is a gas in an atmosphere that absorbs and emits radiation within the thermal infrared range [2]. This process is the fundamental cause of the greenhouse effect.

The primary greenhouse gases in the Earth's atmosphere are water vapor, carbon dioxide, methane, nitrous oxide, and ozone. The greenhouse effect is a process by which thermal radiation from a planetary surface is absorbed by atmospheric greenhouse gases, and is re-radiated in all directions. Since part of this re-radiation is back towards the surface and the lower atmosphere, it results in an elevation of the average surface temperature above what it would be in the absence of the gases [2]. Global warming is agreed by many to be a direct effect of GHG emissions, which have increased notably over the last century.

Human activity since the Industrial Revolution has increased the amount of greenhouse gases in the atmosphere, leading to increased radioactive forcing from CO_2, methane, tropospheric ozone, chlorofluorocarbons (CFCs) and nitrous oxide. The effect of greenhouse gases on global warming is assessed using an index called global warming potential (GWP), which is a measure of how much a given mass of GHG contributes to global warming relative to a reference gas (usually CO_2) for which the GWP is set to 1. For a 100-year time horizon, GWPs of CO_2, CH_4 and N_2O are reported to be 1, 25 and 298, respectively [3]. Using this index, one can calculate the equivalent CO_2 emissions by multiplying the emission of a GHG by its GWP. The main causes of global warming are listed as follows [3]:

- Carbon dioxide emissions from fossil fuel burning power plants.
- Carbon dioxide emissions from burning gasoline for transportation.
- Methane emissions from animals, agriculture such as rice paddies, and from Arctic sea beds.
- Deforestation, especially tropical forests for wood, pulp, and farmland.
- Use of chemical fertilizers on croplands.

CO_2 is widely believed to be a significant cause of global warming. Research shows that concentrations of CO_2 and methane have increased by 36% and 148% respectively since 1750 [3]. Fossil fuel combustion is responsible for about three-quarters of the increase in CO_2 from

human activity over the past 20 years. The rest of this increase is caused mostly by changes in land use, particularly deforestation. The main source of CO_2 emissions is fossil fuel-based electricity generation units, which account for about 32% of the total CO_2 emissions. The next largest source of CO_2 emissions are caused by heating and cooling, which account for about 33% of total CO_2 emissions, followed by emissions from cars and trucks, which account for 23% of total global CO_2 emissions, and other major transportation, which accounts for 12% [3]. Hence, about 65% of the total CO_2 emissions are attributable to electricity generation and heating and cooling, both of which are directly associated with energy needs of human beings.

Cogeneration, or combined heat and power (CHP), represents a relatively simple, integrated multigeneration energy system involving the use of waste or other heat from electricity generation to produce heating. The overall energy efficiency of a cogeneration system, defined as the part of the fuel converted to both electricity and useful thermal energy, is typically 40–50% [4]. Recently, researchers have extended CHP to trigeneration, a system for the simultaneous production of heating, cooling and electricity from a common energy source. Trigeneration often utilizes the waste heat of a power plant to improve overall thermal performance [5], and is suitable for some energy markets.

The benefits of integrating energy systems became prominent with the application of cogeneration for heat and electricity production. In this simple energy system, waste or other heat is used to produce either cooling or heating. In general, cogeneration is the production of heat and electricity in one process using a single energy source, which often yields considerable reductions in input energy compared to separate processes. Cogeneration is often associated with the combustion of fossil fuels, but can also be carried out using certain renewable energy sources, nuclear energy, and waste thermal energy (obtained directly or by burning waste materials). The recent trend has been to use cleaner fuels for cogeneration, such as natural gas. The strong long-term prospects for cogeneration in global energy markets are related to its ability to provide significant operational, environmental and financial benefits. The product thermal energy from cogeneration can be used for domestic hot water heating, space heating, pool heating, laundry heating processes and absorption cooling. The more the product heat from cogeneration can be used in existing systems, the more financially attractive the system is. Cogeneration helps overcome a drawback of many conventional electrical and thermal systems: significant heat losses, which detract greatly from efficiency [5]. Heat losses are reduced and

efficiency is increased when cogeneration is used to supply heat to various applications and facilities.

The overall energy efficiency of a cogeneration system is the percent of the fuel converted into both electricity and useful thermal energy. Typical cogeneration systems have overall efficiencies of 45–60%. Recently, researchers have extended CHP to have more output purposes. In this regard, trigeneration energy systems have become more suitable for energy markets. Trigeneration is the simultaneous production of heating, cooling and electricity from a common energy source. Trigeneration utilizes the waste or other heat of a power plant to improve overall thermal performance, often utilizing the free energy available from waste energy. In a trigeneration system, waste heat from the plant's prime mover (e.g, gas turbine or diesel engine or Rankine cycle [6]), sometimes with temperature enhancement, drives heating and cooling devices. The heat can be used for space heating, domestic hot water production or steam production for process heating. The heat can also be used for cooling, by driving an absorption chiller. Several studies on trigeneration have been conducted in the last few years, likely due to its benefits and plans for applications. Trigeneration can be applied widely, e.g., in chemical and food industries, airports, shopping centres, hotels, hospitals, and houses. Fig. 1.1 illustrates a trigeneration energy system, consisting of the following four major parts:

- A power generation unit, i.e. a prime mover, such as a gas turbine.
- A cooling unit, such as a single-effect absorption chiller.
- A heating unit, such as a boiler or heat recovery steam generator.

The following processes occur in a trigeneration plant:

- Mechanical power is produced via a generator unit, such as a gas turbine.
- The mechanical power is used to drive an electrical generator.
- Waste heat exits the mechanical generator unit directly or via heated materials like exhaust gases.

As shown in Fig. 1.1, with a single prime mover we can produce heating, cooling and electricity simultaneously. Recently, researchers have extended trigeneration to produce more products like hot water, hydrogen and potable water using a single prime mover by implementing a system called multigeneration.

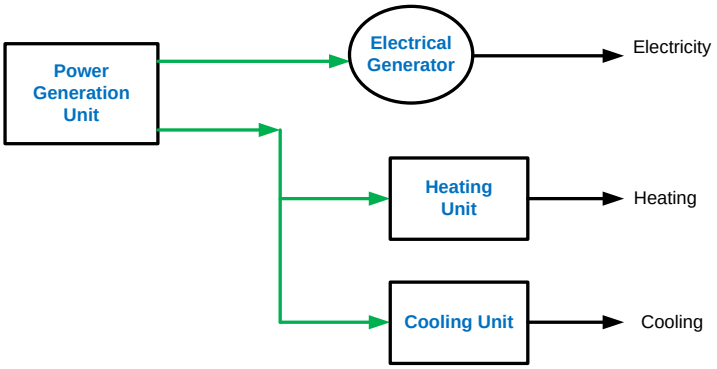

Figure 1.1: A typical trigeneration energy system.

The efficiency for multigeneration energy systems is often higher than those for either trigeneration or CHP because of the additional products (hydrogen, potable and hot water, etc.). Fig. 1.2 and Fig 1.3 illustrate two multigeneration energy systems. The system in Fig. 1.2 produces electricity, cooling, heating, hot water and hydrogen. To produce hydrogen, an electrolyzer is used, which is driven by part of the electricity generated by a solar concentrating collector. Hot water enters the electrolyzer and is reacted electrochemically to split its molecules into hydrogen and oxygen. The heating system is composed of two parts, one for hot water production and another for space heating. Heat rejected from the storage system enters the absorption cooling system to produce cooling and air conditioning. If the system is extended to produce potable water, a desalination system must be used—such a multigeneration energy system is shown in Fig. 1.3. In this case, a portion of the heat produced by the solar concentrator is used to run a desalination system, while part of the electricity generated by the power unit drives the pumps. Other parts of the system are the same as in Fig. 1.2. These two figures are representative of typical multigeneration energy systems that use only solar energy as an input. Other configurations that combine renewable and conventional energy sources are also possible, and are discussed subsequently.

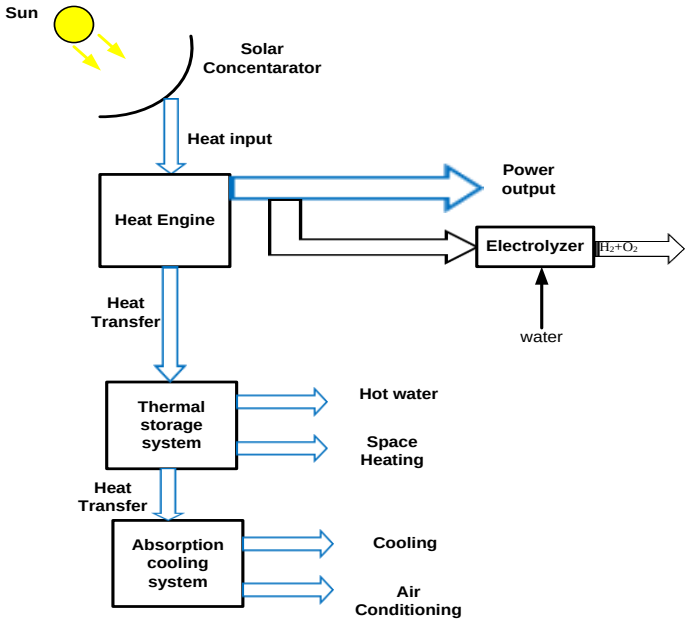

Figure 1.2: A multigeneration energy system for producing electricity, cooling, heating, hot water and hydrogen [7].

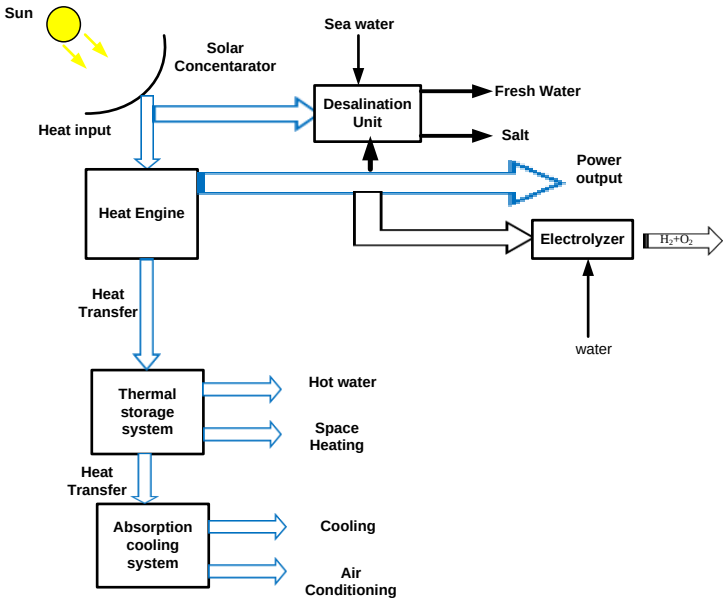

Figure 1.3: A multigeneration energy system for producing electricity, cooling, heating, hot water, hydrogen and fresh water [7].

1.2 Benefits of multigeneration energy systems

There are many benefits of multigeneration energy systems, including higher plant efficiency, reduced thermal losses and wastes, reduced operating costs, reduced greenhouse gas emissions, better use of resources, shorter transmission lines, fewer distribution units, multiple generation

options, increased reliability, and less grid failure [7]. These benefits are discussed below. Multigeneration improves the overall efficiency of the plant and reduces operating costs. The overall efficiency of conventional power plants that use fossil fuel with a single prime mover is usually less than 40%. That is, more than 60% of the heating value of the fuel entering a conventional power plant is lost. On the other hand, the overall efficiency of a conventional power plant that produces electricity and heat separately is around 60% [8].

However, with the utilization of the waste heat from the prime mover, the efficiency of multigeneration plants could reach up to 80% [9]. In a multigeneration plant, the waste heat from the electricity generation unit is used to operate the cooling and heating systems without the need for extra fuel, unlike a conventional power plant that requires extra energy resources. Thus, a multigeneration plant uses less energy to produce the same output as a conventional plant, and has correspondingly lower operating costs.

Multigeneration also reduces GHG emissions. Since a multigeneration energy system uses less fuel to produce the same output compared to a conventional power plant, a multigeneration plant emits less GHGs. Although the GHG emissions from multigeneration plants are less than conventional plants, there are some limitations of using multigeneration plants in a distributed manner because of their on-site gas emissions. Another important benefit of using multigeneration energy systems is that they reduce costs and energy losses due to the fact that they need fewer electricity transmission lines and distribution units. The conventional production of electricity is usually from a centralized plant that is generally located far from the end user. The losses from transmission and distribution of electricity from a centralized system to the user can be about 9% [8].

These benefits have encouraged researchers and designers to develop multigeneration energy systems. The improvement in efficiency is often the most significant factor in implementing a multigeneration energy system. Further assessments before selecting multigeneration plants, such as evaluations of initial capital and operating costs, are needed to ensure efficient and economic multigeneration plant construction and performance [8].

1.3 Prime Movers

In a multigeneration energy system, it is important to select a proper prime mover to meet the required demand. Hence, selection of this component is one of the major concerns for engineers

and designers. Examples of prime mover types are internal combustion engines (ICE), external combustion engines (e.g. Stirling engines), steam turbines, gas turbines, micro turbines, biomass combustors and fuel cells. When selecting a prime mover, there are key criteria to be thoroughly considered. These include:

- The demand of the electricity load should be determined by consideration of the power efficiency and possibility of having more than one prime mover.
- The total amount of heat needed for heating and/or cooling demands should be determined. Based on these demands, the power to cooling and heating ratios of the desired plant is calculated.
- The operating range of the prime movers can be extended. For example, a reheating system for a multi-stage prime mover can be used for this purpose.
- The location of the plant could have a restriction on the acceptable noise level, on-site emissions, and the multigeneration plant size. Therefore, it is important to consider the prime mover's noise level, emissions, and power density.
- If the prime mover is going to be used for emergency application, the startup time must be considered.
- The type of fuel has an impact on both operation and maintenance costs. The fuel type may affect the internal coating life time of the prime mover and, therefore, more frequent maintenance may be needed [10].

After selection of a prime mover based on the above criteria, thermal, economic and environmental analysis all need to occur, along with an optimization study to enhance the understanding of the system.

1.3.1 Gas turbine prime mover

Gas turbines are one of the most suitable prime movers for multigeneration energy systems. A gas turbine, also called a combustion turbine, is a type of internal combustion engine which has an upstream rotating compressor coupled with a downstream turbine, and a combustion chamber in between. Energy is added to the gas stream in the combustion chamber, where fuel is mixed with hot air and then ignited. In the high pressure environment of the combustor, combustion of the fuel increases the temperature. The products of the combustion are forced into the turbine section to produce shaft work. There, the high velocity and volume of the gas flow is

directed through a nozzle over the turbine blades, spinning the turbine that powers the compressor and, for some turbines, drives their mechanical output. The energy given up to the turbine comes from the reduction in the temperature and pressure of the exhaust gas. In a practical gas turbine, gasses are first accelerated in either a centrifugal or radial compressor. These gasses are then slowed down using a diverging nozzle known as a diffuser; these processes increase the pressure and temperature of the flow. In an ideal system this process is isentropic. However, in practice energy is lost in the form of heat, due to friction and turbulence. Gasses then pass from the diffuser to a combustion chamber or similar device, where heat is added. In an ideal system this occurs at constant pressure [11]. As there is no change in pressure, the specific volume of the gasses increases. In practical situations this process is usually accompanied by a slight loss in pressure due to friction. Finally, this larger volume of gasses is expanded and accelerated by nozzle guide vanes before energy is extracted by a turbine.

Micro gas turbines are a kind of gas turbine that has become widespread in distributed power generation units, combined heat and power applications and trigeneration systems. They are one of the most promising technologies for powering hybrid electric vehicles. They range from hand held units producing less than a kilowatt, to commercial sized systems that produce tens or hundreds of kilowatts. The basic principles of micro turbines are based on micro combustion [11]. Gas turbines have the following advantages:

- Very high power-to-weight ratio compared to reciprocating engines.
- Smaller than most reciprocating engines of the same power rating.
- Moves unidirectionally, with far less vibration than a reciprocating engine.
- Fewer moving parts than reciprocating engines.
- Low operating pressures.
- High operation speeds.
- Low lubricating oil cost and consumption.
- Can run on a wide variety of fuels.

Although gas turbines have various advantages, they have some disadvantages:

- Cost is very high.
- Less efficient than reciprocating engines at idle speed.
- Longer startup than reciprocating engines.
- Less responsive to changes in power demand compared to reciprocating engines.

Fig. 1.4 shows a micro gas turbine used in a CHP system. This system has two major parts. The main part is a gas turbine Brayton cycle and the bottoming cycle is a single pressure heat recovery steam generator (HRSG). Hot flue gases from the gas turbine enter the HRSG to produce saturated water at P = 20 bar and $\dot{m} = 33$ kg/s. The net power output of this gas turbine is 50 MW. As Fig. 1.4 shows, the thermal efficiency of the CHP system is higher than in a simple gas turbine cycle because the waste energy of hot flue gases is being utilized in a heat exchanger (HRSG) to produce the heating load, which in this case is saturated water.

Selection of the HRSG is based on the size of the gas turbines; large capacity gas turbines have the ability to produce steam in double or triple pressure levels of HRSG. These gas turbines are usually used for power generation purposes. Therefore, gas turbines can be considered a good candidate for multigeneration energy systems according to the advantages discussed above.

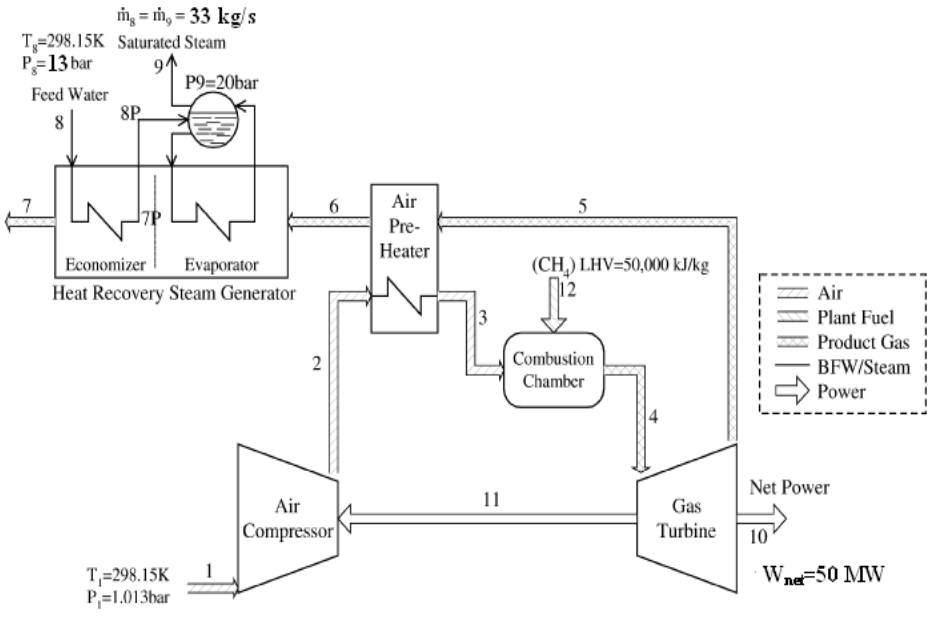

Figure 1.4: The schematic diagram of a gas turbine prime mover used in CHP

1.3.2 Fuel cell prime mover

A fuel cell is a device that generates electricity by a chemical reaction. Every fuel cell has two electrodes, one positive and one negative called, respectively, the anode and cathode. The reactions that produce electricity take place at the electrodes. Each fuel cell also has an electrolyte, which carries electrically charged particles from one electrode to the other, and a catalyst, which speeds the reactions at the electrodes. Hydrogen is the basic fuel; however fuel

cells also require oxygen. One of the greatest advantages of fuel cells is that they can generate electricity with very little pollution, since much of the hydrogen and oxygen used in generating electricity ultimately combines to form a harmless byproduct: water. There are various types of fuel cells:

- Alkaline
- Molten carbonate
- Phosphoric acid
- Proton exchange membrane
- Solid oxide

Fig. 1.5 shows the schematic of a power generation system with both a gas turbine and a fuel cell to produce electricity. Selection of each fuel cell should be based on temperature range and desired output power. For example, a SOFC operates at sufficiently high temperatures to allow direct internal reforming. The anode exhaust gasses contain enough high-pressure steam to provide the water necessary for the reforming reaction. The heat that is needed for this endothermic reaction is supplied by the surroundings via convection and radiation. One of the advantages of the SOFC is that either hydrogen or carbon monoxide can be used as fuel.

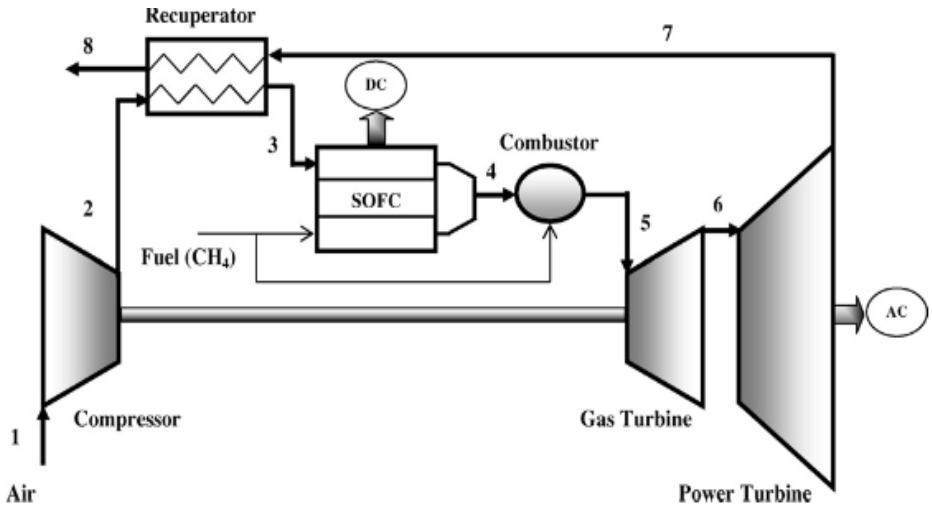

Figure 1.5: Schematic of combined gas turbine power plant with SOFC [12].

1.4 Multigeneration Energy Systems

A multigeneration energy system refers to a system with more than three different purposes from the same source of input energy (the prime mover). These purposes can include electricity, cooling, heating, hot water, hydrogen and fresh water. These systems should be considered for residential application, power plants and other places where numerous useful outputs are required. It must be noted that the location and requirements of its application are major factors the design of a multigeneration energy system. As a clear example, in a place where the need for fresh water is vital, any multigeneration system meant to address the need must prioritize this purpose. In the literature, there are not yet any studies on focused on analyzing and optimizing multigeneration energy systems. These systems are now being considered as a solution to global warming problems, which among the major challenges in this century. It is worth mentioning that different methods are available to achieve each purpose of multigeneration energy systems; this is why the application of each subsystem is very important in meeting the system's requirements. Fig. 1.6 shows a practical multigeneration energy system to produce electricity, cooling, power and domestic hot water that works based on a gas turbine Brayton cycle.

In order to produce saturated steam in this multigeneration system, a dual pressure heat recovery steam generator (HRSG) is used. High pressure saturated steam enters a steam turbine to produce electricity while lower pressure steam works as an absorption chiller heat input into the generator. In order to produce the cooling demand, a single effect absorption chiller with Li-Br water as working fluid is employed. Saturated liquid leaves the generator, which is then used to heat up water using a domestic water heater. According to the concept of a Rankine cycle, the condenser rejects an amount of heat. This heat could be considered either for the space heating application or for a thermochemical water splitting cycle to produce hydrogen. As illustrated in this figure, where the fuel is just injected into the combustion chamber, it can be concluded that this system has less environmental impact compared to GT cycles, CHP systems and trigeneration energy systems. The reason is due to this fact that waste heat from GT and CHP systems is used to produce cooling and heating applications. Energy efficiency of this cycle could be higher than 70%. This multigeneration system could be used to produce hydrogen, another valuable purpose. In this case, a part of the produced electricity could be used to run an electrolyzer to produce hydrogen, which could then be used for either hybrid electric vehicles or to produce electricity using a fuel cell. As shown in Fig. 1.7, flue gases leave the HRSG at a

temperature around 150 ^{0}C. To increase the efficiency of this multigeneration system, the energy of these flue gases could be utilized in a heat exchanger and produce more electricity and cooling by using an ejector refrigeration system. With this configuration, the efficiency of the system could be higher than 85%.

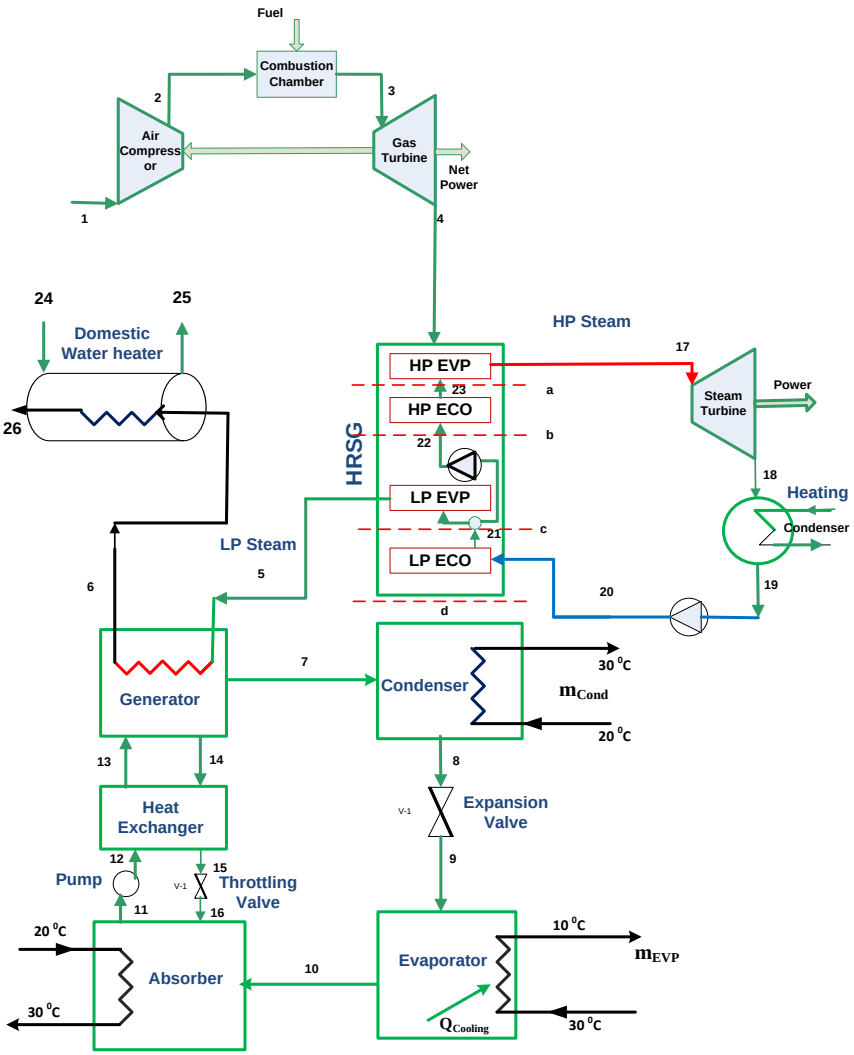

Figure 1.6: Schematic of a multigeneration system for electricity, heating, cooling and hot water production.

Fig. 1.7 shows another multigeneration energy system for production of electricity, heating, cooling and fresh water. A photovoltaic solar panel is selected to use solar energy in order to run triple effect absorption to provide cooling. A triple effect absorption cooling system is also considered for the cooling demand of the system, and a desalination unit is applied to

produce fresh water. These two figures clearly show the vast potential of multigeneration energy systems. There are many more options in the design multigeneration energy systems, which will be discussed in detail in the following chapters.

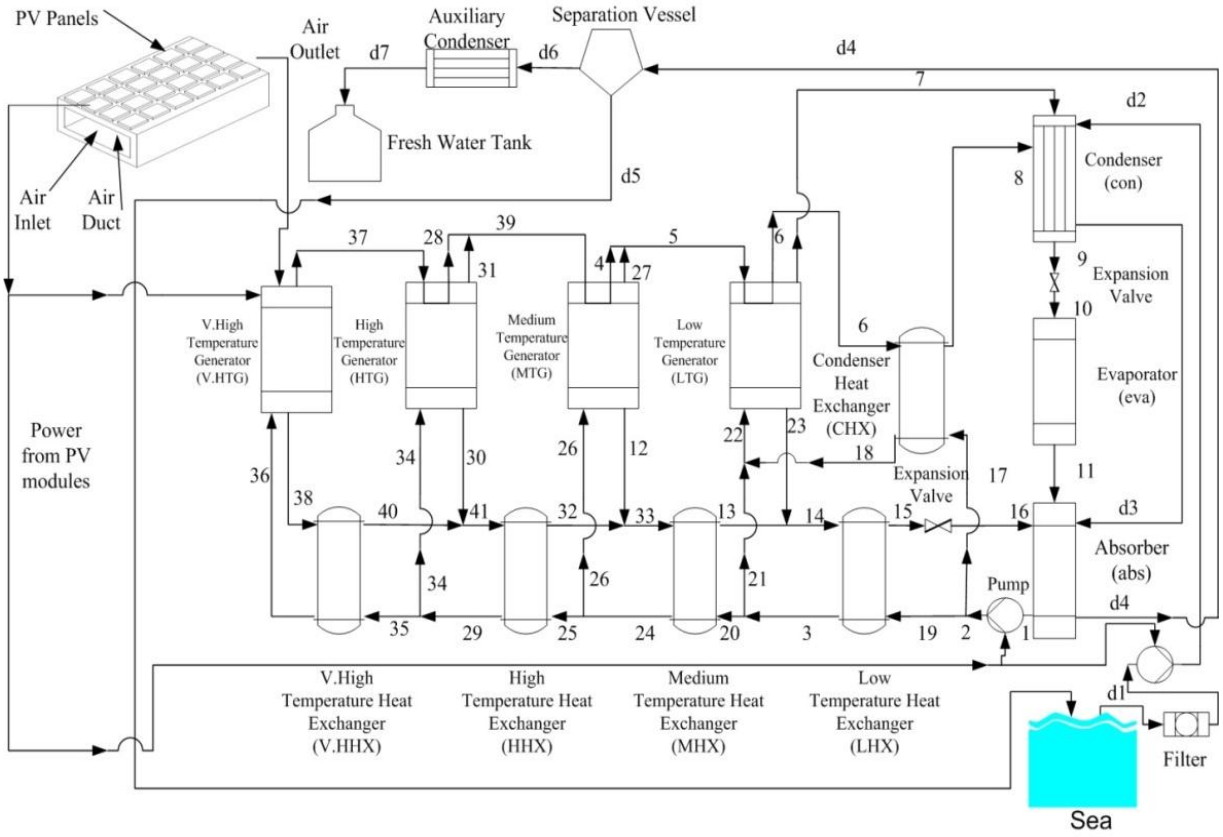

Figure 1.7: Schematic diagram of a multigeneration energy system for desalination purpose [13].

Chapter 2: Motivation and Objectives

2.1 Motivation

Energy plays a critical role in driving almost all practical processes and is essential to sustain life. Energy exists in several forms, e.g., light, heat, electricity. Concerns exist regarding limitations on easily accessible supplies of energy resources and the contribution of energy processes to global warming as well as various other environmental concerns as air pollution, acid precipitation, ozone depletion, forest destruction, and radioactive emissions. There are various alternative energy options to fossil fuels, including solar, geothermal, hydropower, wind and nuclear energy. The use of available natural energy resources is limited due to their reliability, quality and density. Nuclear energy has the potential to contribute a significant share of large scale energy supply without contributing to climate change. Many advanced systems to mitigate global warming have been proposed and tested. Among such systems, multigeneration processes, including trigeneration, can make important contributions due to their potential for high efficiencies as well as low operating costs and pollution emissions per unit energy output. Issues such as fossil fuel depletion and climate change amplify the advantages and significance of efficient multigeneration energy systems. A multigeneration energy system produces several useful outputs form one or more kinds of energy inputs. The main purposes of using multigeneration are to increase efficiency and sustainability and reduce environmental impact and cost. Such systems often provide significant potential for global warming mitigation. Possible products of a multigeneration system include electricity, heating, cooling, hot water, fresh water and hydrogen.

The literature review section shows that there are not enough studies performed that are related to multigeneration energy system. Studies show that integration of energy system always leads to an increase in the thermal efficiency of the system. For example, trigeneration could increase the system thermal energy efficiency up to 70% [6]. Therefore, the lack of study especially for renewable based multigeneration energy systems to produce several commodities simultaneously has made this system quit interesting.

On the other side, there are a few studies in the literature about exergy, exergoeconomic and exergoenvironmental optimization of multigeneration energy systems. Therefore, in this PhD

thesis, a comprehensive analysis is conducted to model, analyze and optimize some novel multigeneration energy systems based on both conventional and renewable energy sources. To enhance the understanding of the system performance, exergy analysis as a potential tool is conducted. Exergy analysis can investigate the areas of irreversibilities and recommend ways to improve the overall efficiency of the system. The comprehensive thermodynamic modeling of each system is conducted by the combination of some software in order to fully model the system. Matlab software is used as the main software to simulate all parts of the multigeneration energy system. Since Matlab software does not have the properties of refrigerant, water and flue gases, Engineering Equation Solver (EES) software and Refprop software are also used to determine the properties of the refrigerant and coolant at each stage of the system. This software is linked to Matlab software to finalize the modeling and analysis section. The advantages of using Matlab software is the ability of conducting an evolutionary algorithm based multi objective optimization to find the best optimal design parameters of the system. To conduct an optimization, various objective functions including exergy efficiency, total cost of the plant and greenhouse gas emission are considered with respect to certain proper constraints. It must be noted that genetic algorithm is used as the optimization method, which is developed in Matlab software based on fast and elitist non-dominated sorting genetic algorithm (NSGA-II) [14].

To have a comprehensive system performance analysis, a parametric study is carried out to see the variation of the system performance. The importance of parametric study is to predict a performance assessment of the studied system in order to find the proper design parameters for the optimization study. Although parametric study is important, it cannot give the best optimal design parameters of the system. Those parameters from parametric study that have significant effect on exergy efficiency, total cost rate and environmental impacts are selected as decision variable. Also, a sensitivity analysis which is an important part of each optimization problem is performed. In this case the effect of each decision variables on the variation of the objective functions is discussed in details.

2.2 Objectives

The originality of this PhD thesis is to comprehensively model, analyze and optimization of three novel multigeneration energy systems which have not been previously considered in the literature. in addition, exergy, exergoeconomic and environmental impact assessment are

conducted to enhance the performance analysis of the system. Another important originality and innovativeness of this thesis is the use of multi objective evolutionary based optimization to optimize three different sets of objective functions, exergy efficiency of systems (to be maximized), total cost of the system including cost of environmental impacts (to be minimized) and greenhouse gas emission (to be minimized) with respect to some proper constraints. Moreover, the Pareto frontier solution for these multigeneration systems is obtained via an evolutionary algorithm based multi-objective optimization.

In the direction of this PhD thesis, the model is developed and the thesis is prepared. This PhD research thesis consists of some main objectives as follows:

a) To develop a mathematical model for our three novel multigeneration energy systems:
    - Comprehensive thermodynamic modeling of a multigeneration system based on gas turbine prime move, double pressure heat recovery steam generator, a single effect absorption chiller, an ejector refrigeration system, a domestic water heater and a PEM electrolyzer for hydrogen production.
    - Thermodynamic modeling of a biomass based multigeneration system with double effect absorption chiller, an organic Rankine cycle, a PEM electrolyzer for hydrogen production, a domestic water heater and a reverse osmosis desalination unit to produce fresh water.
    - Thermodynamic modeling of a novel multigeneration system based on an ocean thermal energy conversion (OTEC) technology assisted with PV/T solar collector and absorption chiller to provide cooling load and a reverse osmosis desalination unit to produce fresh water.
b) To perform a model validation for each part of multigeneration system to ensure the correctness of developed simulation code.
    - Single effect absorption chiller model validation with some references form literature.
    - Double pressure heat recovery steam generator model validation.
    - Double effect absorption chiller model validation.
    - PEM PEM electrolyzer validation with experimental data from literature,

c) To perform the exergy analysis of each multigeneration system.
    - Calculation of exergy flow rate of each stream of the systems.
    - Determination of exergy destruction rate and exergy efficiency of each component.
    - Calculation of various dimensionless exergy numbers such as the exergy destruction ratio, waste exergy ratio and exergy destruction factor.

d) To conduct exergoeconomic analyses for each multigeneration system.
    - Calculation of equipment purchase cost for each system.
    - Calculation of total cost rate of each system.

e) To perform the environmental impact assessment of the system
    - Calculation of CO_2 emissions of the system.
    - Determination of sustainability index and finding the relation between exergy, economic and environmental impacts.

f) To perform a complete parametric study and the performance assessment of the system.
    - A comprehensive parametric study of each system separately to understand the effects of design parameters on the system performance including exergy efficiency and environmental impacts.
    - Effect of environment condition on the performance assessment of each studied system.

g) To perform an optimization of multigeneration energy systems using an evolutionary based algorithm developed in Matlab software to find the best design parameters.
    - Proposing various objective functions; exergy efficiency (to be maximized), total cost rate of the plant including damage cost of environmental impacts (to be minimized), and greenhouse gas emission (to be minimized).
    - Applying the optimization methods based on some reasonable constraints.
    - Finding the best decision variables using multi objective optimization code developed in Matlab software.
    - Conducting a comprehensive sensitivity analysis to observe the variation of each objective function by change in each decision variables.

Chapter 3: Literature Review

3.1 Introduction

In the literature, there have been various studies associated with CHP and trigeneration energy systems, though a comprehensive study of a multigeneration energy system has not yet appeared. Because of the environmental concerns and technological developments in the last decade, both the need for and the capability of producing multipurpose energy solutions have been amplified considerably. The related papers, their aims, method of analysis and brief conclusions are presented in this section. In this chapter, an attempt is made to cover the most recent studies regarding cogeneration of heat and power (CHP), trigeneration and multigeneration energy systems. Since there are several papers about CHP and trigeneration systems, the literature has been categorized based on thermodynamic modeling, exergy and exergoeconomic analysis and optimization study. This chapter begins with the details of the literature review and then provides a summary of recent publications.

3.1 Cogeneration heat and power (CHP) systems

A multigeneration energy system produces several useful outputs from one or more kinds of energy inputs. The main purposes of using multigeneration are to increase efficiency and sustainability and to reduce environmental impact and cost. Such systems often provide significant potential for global warming mitigation. Possible products of a multigeneration system include electricity, heating, cooling, hot water, fresh water and hydrogen. Cogeneration, or combined heat and power (CHP), represents a relatively simple process that produces two commodities in an integrated fashion, including the use of waste heat from electricity generation to produce heating. The overall energy efficiency of a cogeneration system, defined as the part of the fuel energy content converted to both electricity and useful thermal energy, is typically 40-50% and, in some cases, much higher [8].

A micro-scale building cooling, heating and power (BCHP) system with an adsorption chiller was experimentally studied by Huangfu et al. [15]. The authors observed the performance of an adsorption chiller under different heating conditions. They concluded that there was an almost linear relation between the adsorption chiller and the change in hot water inlet

temperature for the two investigated models. Mago et al. [16] analyzed and optimized the use of CHP-ORC systems for small commercial buildings. In another study, Mago et al. [17] reported on the evaluation of the potential emission reductions from the use of CHP systems in different commercial buildings. Mago and Hueffed [18] evaluated a turbine-driven combined cooling, heating and power (CCHP) system for large office buildings under various operating strategies, and explored the use of carbon credits to show how the possible reduction in carbon dioxide emissions via a CCHP system could translate into economic benefits.

Bianchi et al. [19] studied the performance analysis of an integrated CHP system with thermal and electric energy storage for residential application. Athanasovici et al. [4] proposed a unified comparison method for the thermodynamic efficiency of CHP plants, and used this method to compare various separate and combined energy production processes. Havelsky [10] analyzed the problem of efficiency evaluation of systems for combined heat, cold and electricity production, and developed equations for energy efficiency and primary energy savings. The energy analysis of trigeneration plants with heat pumps was examined by Miguez et al. [20, 21]. They concluded that the heat pump is important for plant efficiency enhancement.

Khaliq et al. [9] carried out an exergy analysis of a combined electrical power and refrigeration cycle, as well as a parametric study of the effects of exhaust gas inlet temperature, pinch point and gas composition on energy and exergy efficiencies, electricity to cold ratio, and exergy destruction rate for a cogeneration system and its components. Cihan et al. [22] carried out energy and exergy analyses for a combined cycle located in Turkey and suggested modifications to decrease the exergy destruction in CCPPs. Their results showed that combustion chambers, gas turbines and HRSGs are the main sources of irreversibilities, representing over 85% of the overall exergy losses.

Barelli et al. [23] conducted an exergetic analysis of a residential CHP system based on a PEM fuel cell. They also conducted a complete parametric study to see the effect of fuel cell design parameters such as temperature, pressure and relative humidity on the system performance. Bingol et al. [24] reported the exergy based performance analysis of high efficiency polygeneration systems for sustainable building applications. El-Emam and Dincer [25] conducted the energy and exergy analyses of a CHP system with a molten carbonate fuel cell (MCFC) and a gas turbine system. They performed a parametric study by changing some design parameters of the system in order to assess the system performance. The results showed

that the maximum output work of the MCFC is estimated to be 314.3 kW for an operating temperature of 650 ^{0}C. The overall energy and exergy efficiencies achieved for this system were 42.89% and 37.75%, respectively.

Akkaya et al. [26] conducted the exergy analysis for a hybrid CHP system using a SOFC and a gas turbine. They also performed a complete parametric study of the system. The results showed that a design based on an exergy performance coefficient criterion has considerable advantage in terms of entropy generation rate. Al-Sulaiman et al. [27] demonstrated an efficiency gain of more than 22% using a trigeneration plant compared with a power cycle (SOFC and organic Rankine cycle). They also determined the maximum efficiencies of 74% for the trigeneration plant, 71% for heating cogeneration, 57% for cooling cogeneration and 46% for net electricity generation, and concluded that exergy analysis is a significant tool for both CHP and trigeneration cycles.

In recent decades, exergoeconomics and thermoeconomics have been increasingly utilized by researchers, combining thermodynamics with economics. Many such studies have been reported, especially for power generation and cogeneration (CHP). Rosen and Dincer [28] performed an exergoeconomic analysis of a coal fired electricity generating station, and found the ratio of thermodynamic loss rate to the capital cost to be a significant parameter in evaluating plant performance that may allow thermodynamics and economics to be successfully traded-off in plant designs. Ahmadi et al. [29] carried out energy, exergy and exergoeconomic analyses of a steam power plant in Iran, and considered the effect of the load variations and ambient temperature on component exergy destruction rate. The results showed that energy losses are mainly associated with the condenser, where the energy loss rate to the environment was 307 MW, while the boiler energy loss rate was only 68 MW. However, the irreversibility rate of the boiler was significantly higher than the irreversibility rates of the other components. Exergy and exergoeconomic analyses of CHP plants [30-32] have demonstrated the usefulness of these methods for thermal systems.

3.2 Trigeneration systems

Trigeneration is the simultaneous production of heating, cooling and electricity from a common energy source. Trigeneration utilizes waste or other heat from a power plant to improve overall thermal performance, often utilizing the free energy available via waste energy. In a trigeneration

system, waste heat from the plant's prime mover (e.g., gas turbine, diesel engine, or Rankine cycle [6]), sometimes with temperature enhancement, drives heating and cooling devices. The heat can be used for space heating, domestic hot water production, or to produce steam for process heating. The heat can also be used for cooling, by driving an absorption chiller. Pospisil et al. [33] performed an energy analysis of a trigeneration system and compared cogeneration and trigeneration plants for a typical building. The results showed that cogeneration can increase the efficiency by about 31% while trigeneration systems increase efficiency by about 39% compared to a single generation system. Al-Sulaiman et al. [34] reported the performance comparison of three trigeneration systems using organic Rankine cycles. The systems they considered consist of SOFC-trigeneration, biomass-trigeneration, and solar-trigeneration. Martins et al. [35] studied the thermodynamic performance assessment of a trigeneration cycle considering the influence of operational variables. Calva et al. [36] studied the thermal integration of trigeneration systems. They focused on trigeneration schemes where a gas turbine is used as a prime mover for power production and cooling is generated by a typical compression refrigeration system. Huang et al. [37] reported a biomass fuelled trigeneration system in selected buildings. This trigeneration system consisted of an internal combustion (IC) engine integrated with biomass gasification. In their system the gas generated by the biomass gasifier was used to provide electricity for a typical building using an IC engine. The waste heat is then recovered from the engine cooling system and exhaust gases are utilized to supply hot water for space heating; excess heat was also used to drive an absorption cooling system.

Rocha et al. [38] studied the performance tests of two small trigeneration pilot plants. The first system was based on a 30 kW natural gas powered micro turbine, and the second used a 26 kW natural gas powered IC engine coupled with an electrical generator as a prime mover. They also used an ammonia water absorption refrigeration chiller for producing chilled water. Huicochea et al. [39] carried out a thermodynamic analysis of a trigeneration system consisting of a micro gas turbine and a double effect absorption chiller. The system consisted of a microturbine to produce electrical power, a double effect absorption water LiBr chiller for air conditioning and a heat exchanger to produce hot water.

Chicco and Mancarella [40] proposed some energy indicators to assess the fuel efficiency of a trigeneration plant. Chicco and Mancarella [41] applied these energy indicators to introduce a planning criterion called equivalent gas price. Aghahosseini et al. [42] reported the

thermodynamic analysis of an integrated gasification and Cu-Cl cycle for trigeneration of hydrogen, steam and electricity .They used Aspen HYSYS to simulate the system. The results showed that using oxygen instead of air for the gasification process, in which oxygen is provided by the integrated Cu-Cl cycle, led to a 20% increase in the hydrogen content of produced syngas. Minciuc et al. [43] presented a method for analyzing trigeneration systems and established limits for the best performance of gas turbine trigeneration with absorption chilling from a thermodynamic point of view.

Moya et al. [44] studied the performance assessment of a trigeneration system consisting of a micro gas turbine and an air cooled, indirect fired, ammonia water absorption chiller. They also conducted a parametric study by changing some major design parameters, including variation of output power of the micro gas turbine, ambient temperature for the absorption unit, chilled water outlet temperature and thermal oil inlet temperature. Velumani et al. [45] proposed a new integrated trigeneration system consisting of a micro gas turbine, a solid oxide fuel cell and a single effect absorption chiller. The results showed that the energy efficiency of this cycle is about 70%.

Buck and Fredmann [46] studied the performance of a trigeneration plant based on a micro turbine assisted by a small solar tower. They conducted an economic analysis on the use of single and double effect absorption chillers. The authors recommended using the double effect chiller since it showed better thermal performance and lower operating cost compared to the single effect absorption chiller.

Exergy is a useful tool for determining the location, type and true magnitude of exergy losses, which appear in the form of either exergy destructions or waste exergy emissions [47]. Therefore, exergy can assist in developing strategies and guidelines for more effective use of energy resources and technologies. Recently, exergy analysis has become a very popular tool for analyzing thermal systems. Some studies have applied exergy analyses to CHP and trigeneration energy systems based on IC engines.

Santo et al. [48] conducted the energy and exergy analyses of a IC engine based trigeneration system under two different operating strategies for buildings. They presented a computational hourly profile method that combined fittings from the literature and actual data from manufacturer into a single algorithm curve in order to obtain the mathematical representations of physical phenomena and thermodynamic properties. The developed simulation

method was used to predict the performance of a given cogeneration concept under two different operational strategies.

Ebrahimi et al. [49] carried out energy and exergy analyses of a micro steam CCHP cycle for a residential building. They analyzed a trigeneration energy system consisting of a steam turbine and an ejector refrigeration system to provide the cooling load for residential buildings. They also optimized the system using a genetic algorithm to determine its maximum overall efficiency. The exergy analysis results revealed that the greatest exergy destruction rate takes place in the steam generator for both summer and winter seasons.

Khaliq [50] conducted the exergy analysis for a trigeneration system. The system studied consisted of a gas turbine cycle, a single pressure heat recovery steam generator to provide heating and a single effect LiBr absorption chiller to provide sufficient cooling. He also conducted a comprehensive parametric study to investigate the effects of compressor pressure ratio, gas turbine inlet temperature, combustion chamber pressure drop, and evaporator temperature on the exergy destruction rate in each component, first law efficiency, electrical to thermal energy ratio, and second law efficiency of the system. The exergy analysis results indicated that that maximum exergy destruction rate occurred in the combustion and steam generation process, which represented over 80% of the total exergy destruction rate in the overall system.

Kong et al. [51] conducted the energy and economic analyses of a trigeneration plant using a Stirling engine as a prime mover with a conventional plant with a separate production of cooling, heating and power. They concluded that the trigeneration plant with the Stirling engine can save more than 33% of the primary energy compared to the conventional plant. Ziher and Poredos [52] addressed the economics of using a trigeneration plant in a hospital. They calculated the cooling, heating, and power price per kWh on a monthly basis for one year. In order to obtain the cooling capacity, the authors suggested that the use of steam absorption and compression chillers with a cold storage system in the plant. Ahmadi et al. [6] carried out an exergoenvironmental analysis of a trigeneration system based on a micro gas turbine and an organic Rankine cycle (ORC), and performed a parametric study involving the main design parameters of the trigeneration system.

Temir and Bilge [53] studied a thermoeconomic analysis of a trigeneration system that produces electrical power with a natural gas fed reciprocating engine and that yields absorption

cooling by making use of the system's exhaust gases. Ehyaei and Mozafari [54] performed energy, economic and environmental impact assessment of a micro gas turbine employed for on-site combined heat and power production, and examined the optimization of the micro turbine application to meet the electrical, heating and cooling loads of a building. Mago and Hueffed [18] evaluated a turbine driven combined cooling, heating and power (CCHP) system for large office buildings under various operating strategies, and explored the use of carbon credits to show how the possible reduction in carbon dioxide emissions via a CCHP system could translate into economic benefits.

Ozgener et al. [55] developed an exergoeconomic model for a vertical ground source heat pump (GSHP) residential heating system. They calculated the ratio of thermodynamic loss rate to capital cost values to be in the range of 0.18 to 0.43, and provided a linear correlation between the value of this parameter and ambient temperatures. They also drew attention to the compressor as the component where the most exergy destruction occurred.

Ozgener and Hepbasli [56] conducted an exergoeconomic analysis for a solar assisted ground source heat pump heating system with a 50 meter vertical and 32 millimeter nominal diameter U bend ground heat exchanger. They determined that the total exergy loss values were between 0.010 kW and 0.480 kW and found the largest energy and exergy losses in the greenhouse compressor. Moreover, they have calculated the ratio of thermodynamic loss rate to capital cost values to be in the range of 0.035 to 1.125.

Many reports in the literature consider environmental aspects of thermal systems. Dincer [57] and Dincer and Rosen [47] considered the environmental and sustainability aspects of hydrogen and fuel cell systems. The exergetic and environmental aspects of drying systems have also been examined [17]. Ahmadi and Dincer [4] conducted an exergoenvironmental optimization of a CHP system using a genetic algorithm, and a sensitivity analysis of how optimized design parameters vary with the fuel cost. A thermodynamic analysis of post-combustion CO_2 capture in a natural gas fired power plant has been reported by Amrolahi et al. [58]. Petrakopoulou et al. [59] studied exergoeconomic and exergoenvironmental analyses of a combined cycle power plant with chemical looping technology. This research provided an evaluation of chemical looping combustion technology from an economic and environmental perspective by comparing it with a reference plant, a combined cycle power plant that includes no CO_2 capture.

For various reasons, it is important to optimize processes so that a chosen quantity, known as the objective function, is maximized or minimized. For example, the output, profit, productivity, product quality, etc., may be maximized, or the cost per item, investment, energy input, etc., may be minimized. The success and growth of industries today is strongly based on their ability to optimize designs and systems. With the advent in the recent years of new materials, such as composites and ceramics, and new manufacturing processes, several traditional industries (e.g., steel) have faced significant challenges and, in some cases, diminished in size, while many new fields have emerged. It is important to exploit new techniques for product improvement and cost reduction in traditional and new industries. Even in an expanding area, such as consumer electronics, the prosperity of a company is closely connected to its ability to apply optimization to new and existing process and system designs. Consequently, engineering design, which has always been important, has become increasingly coupled with optimization [47].

Optimization is a significant tool in engineering for determining the best, or optimal, value for the decision variable of a system. Energy engineering is a field where optimization plays a particularly important role. Engineers involved in thermal energy engineering, for instance, are required to answer the questions such as

- What processes or equipment should be selected for a system, and how should the parts be arranged for the best outcome?
- What are the best characteristics for the components (e.g., size, capacity, cost)?
- What are the best process parameters (e.g., temperature, pressure, flow rate and composition) of each stream interacting with the system?

In order to answer such questions, engineers are required to formulate an appropriate optimization problem. Proper formulation is usually the most important and sometimes the most difficult step in optimization. To formulate an optimization problem, there are numerous elements that need to be defined, including system boundaries, optimization criteria, decision variables and objective functions.

Sahoo [60] carried out an exergoeconomic analysis and optimization of a cogeneration system which produces 50 MW of electricity and 15 kg/s of saturated steam at 2.5 bar. He optimized the unit using exergoeconomic principles and evolutionary programming, and showed that the cost of electricity production is 9.9% lower for the optimum case in terms of

exergoeconomics compared to a base case. Sayyaadi and Sabzaligol [61] performed an exergoeconomic optimization of a 1000 MW light water nuclear power generation system using a genetic algorithm and considering ten decision variables, and showed that the fuel cost of the optimized system is greater than that for a base case. Shortcomings in the optimized system are compensated by larger monetary savings in other economic sectors. Haseli et al. [62] found the optimum temperatures in a shell and tube condenser with respect to exergy. The optimization problem in that study considered condensation of the entire vapor flow and was solved with sequential quadratic programming (SQP).

Saayaadi and Nejatolahi [63] analyzed cooling tower assisted vapor compression refrigeration machines with respect to total exergy destruction rate and total product cost objective functions. They used energy and exergy analyses for the thermodynamic model and incorporated Total Revenue Requirement (TRR) for the economic model. They have optimized the system with respect to single objective thermodynamic, single objective economic and multi-objective criteria. For the multi-objective optimization, they selected final solutions from the Pareto frontier curve. Finally, they compared the results obtained from the three optimizations and calculated that the percentage deviation from ideal results for thermodynamic and economic criteria is 40.09% for thermodynamically optimized system, 82.46 % for economically optimized system and 22.51% for the multi-objective optimized system and therefore determined that the multi-objective optimization satisfies the generalized engineering criteria more than the other two single-objective optimized designs.

Ahmadi et al. [64] conducted a comprehensive exergy, exergoeconomic and environmental impact analyses and a multi-objective optimization for combined cycle power plants (CCPPs) with respect to the exergy efficiency, total cost rate and CO_2 emissions of the overall plant. They determined that the largest exergy destructions occurred in the CCPP combustion chamber and that increasing the gas turbine inlet air temperatures decreases the CCPP cost of exergy destruction. They derived the expression for the Pareto optimal point curves for the determined exergy efficiency range and concluded that the increase in total cost per unit exergy efficiency is considerably high after exergy efficiencies over 57% and therefore a point below this should be chosen on the Pareto optimal curve.

Sayyaadi and Babaelahi [65] analyzed a liquefied natural gas re-liquefaction plant with respect to multi-objective approach which simultaneously considers exergy and exergoeconomic

objectives. They used MATLAB multi-objective optimization algorithm of NSGA-II, which is based on the Genetic Algorithm, and obtained Pareto optimal frontier to find the Pareto optimal solutions. They compared the final optimal system with the base case and found that the exergetic efficiency in the multi-objective optimum design is 11.11% higher than that of the exergoeconomic optimized system, while the total product cost of the multi-objective optimal design is 16.7 higher than that of the exergoeconomic optimal system

Ghaebi et al. [66] conducted the exergoeconomic optimization of a trigeneration system for heating, cooling and power production purpose based on total revenue requirement (TRR) method and using evolutionary algorithm. The system studied consists of an air compressor, a combustion chamber, a gas turbine, a dual pressure heat recovery steam generator and an absorption chiller in order to produce cooling, heating and power. The economic model used in their research was the TRR and the cost of the total system product was defined as our objective function and optimized using a genetic algorithm technique.

Kavvadias and Maroulis [67] investigated the multi-objective optimization of a trigeneration plant. This optimization was carried out on technical, economical, energetic and environmental performance indicators in a multi-objective optimization framework. The results showed that trigeneration plants can be more economically attractive, energy efficient and environmental friendly than conventional cogeneration plants.

Al-Sulaiman et al. [68] studied the thermoeconomic optimization of three trigeneration systems using organic Rankine cycles. The three systems considered were SOFC-trigeneration, biomass-trigeneration, and solar-trigeneration systems. The results showed that solar based trigeneration system has the highest net available exergy as compared to the other two systems. Therefore, it has the highest potential to have the highest exergy if the solar collector performance is improved.

Wang et al. [69] conducted multi-objective optimization of an organic Rankine cycle (ORC) for low grade waste heat recovery using evolutionary algorithm. The multi-objective optimization of the ORC with R134a as the working fluid was conducted in order to achieve the system optimization design from both thermodynamic and economic aspects using non-dominated sorting genetic algorithm (NSGA-II). The decision variables considered for multi-objective optimization were turbine inlet pressure, turbine inlet temperature, pinch temperature

difference, approach temperature difference and condenser temperature difference are selected as the decision variables.

Shirazi et al. [70] conducted a comprehensive thermodynamic modeling and multi-objective optimization of an internal reforming solid oxide fuel cell gas turbine hybrid system. They validated the model using available data in the literature. They used genetic algorithm to optimize the system. In the multi-objective optimization procedure, the exergy efficiency and the total cost rate of the system (including the capital and maintenance costs, operational cost and social cost of air pollution for CO, NO_x, and CO_2) were considered as objective functions. They also performed sensitivity analyses of the variation of each objective function with major design parameters of the system.

3.3 Multigeneration energy systems

A multigeneration energy system refers to a system with more than three different useful outputs with a same source of input energy (e, g prime mover). These outputs could be electricity, cooling, heating, hot water, hydrogen and fresh water. It is of great importance that these systems could be considered for residential application, power plants and other places where numerous useful outputs are required. It must be noticed that location and the requirements of application is a major factors in designing a multigeneration energy system.

Hosseini et al. [71] conducted a comprehensive thermodynamic model for an integrated energy system. The system studied consists of a gas turbine, a SOFC fuel cell, a single pressure HRSG and a multi effect desalination to produce electricity, heating, cooling and fresh water. They also performed a comprehensive parametric study to see the effect of some major design parameters on the system performance. The results showed that the integrated system could increase the system efficiency by about 25% compared to a single generation system.

Ahmadi et al. [6] studied a new integrated trigeneration energy system consisting of a gas turbine, a double pressure heat recovery steam generator and a single effect absorption chiller and an organic Rankine cycle. They also performed a parametric study to see the variation of exergy efficiency, cooling and heating load and cost of environmental impact. The results of this study demonstrated that system performance is notably affected by the compressor pressure ratio, the gas turbine inlet temperature and the gas turbine isentropic efficiency.

Ratlamwala et al. [72] studied a performance assessment of an integrated PV/T and triple effect cooling system for hydrogen and cooling production. The also conducted a comprehensive parametric study on the effect of average solar radiation for different months, operating time of the electrolyzer, inlet air temperature and PV area module on the power production and hydrogen production rate. In another study, Ratlamwala et al. [73] analyzed the performance of a novel integrated geothermal system for multigeneration, based on a geothermal double flash power generating unit, an ammonia water quadruple effect absorption unit and an electrolyzer system for cooling, heating, power, hot water and hydrogen production. Increasing the geothermal source temperature, pressure and mass flow rate was observed to increase the output power and hydrogen production rate.

Ozturk and Dincer [74] conducted a thermodynamic analysis of a solar based multigeneration system with hydrogen production. The solar based multigeneration considered for this analysis consists of four main sub systems: Rankine cycle, organic Rankine cycle, absorption cooling and heating, and hydrogen production and utilization. The exergy efficiency and exergy destruction rate for the subsystems and the overall system show that the parabolic dish collectors have the highest exergy destruction rate among constituent parts of the solar-based multigeneration system

Dincer and Zamfirescu [7] performed energy and exergy analyses of renewable-energy-based multigeneration, considering several options for producing such products as electricity, heat, hot water, cooling, hydrogen, and fresh water. Ahmadi et al. [75] studied the exergo-environmental analysis of an integrated organic Rankine cycle for polygeneration to produce electricity, heating, cooling and hot water. The system analyzed consists of a gas turbine cycle, an organic Rankine cycle (ORC), a single effect absorption chiller and a domestic water heater. The exergy efficiency of the trigeneration system is found to be higher than that of typical combined heat and power systems or gas turbine cycles. The results also indicate that carbon dioxide emissions for the trigeneration system are less than for the aforementioned systems. The exergy results show that combustion chamber has the largest exergy destruction of the cycle components, due to the irreversible nature of its chemical reactions and the high temperature difference between the working fluid and flame temperature.

Ahmadi et al. [76] studied a thermodynamic modeling and assessment of an integrated biomass-based multigeneration energy system. They analyzed a new multigeneration system

based on a biomass combustor, an organic Rankine cycle (ORC), an absorption chiller and a proton exchange membrane electrolyzer to produce hydrogen, and a domestic water heater for hot water production, is proposed and thermodynamically assessed. Also, they conducted exergy analysis to determine the irreversibilities in each component and the system performance. In addition, an environmental impact assessment of the multi-generation system was performed, and the potential reduction in CO_2 emissions when the system shifts from power generation to multi-generation are investigated.

Ahmadi et al. [8] carried out an exergy-based optimization of a multigeneration energy system. They considered a multigeneration energy system with a gas turbine as the prime mover to produce electricity, heating, cooling and domestic hot water, and applied a multi-objective evolutionary based optimization to find the best design parameters of the system considering exergy efficiency and total cost of the system as two objective functions.

The research reported to date suggests that multigeneration is often advantageous for mitigating global warming and increasing efficiency. However, complete energy, exergy, and environmental impact assessments of a multigeneration based on micro gas turbine and ejector refrigeration system, biomass based multigeneration system and ocean thermal energy conversion based multigeneration system have not been reported in the literature. Also, a fast and elitist non-dominated sorting genetic algorithm (NSGA-II) based multi-objective optimization for such complex systems has not been used yet in such research.

Chapter 4: Descriptions of Systems

In this PhD thesis three different multigeneration energy systems are modeled, analyzed and optimized. It is aimed to select three novel multigeneration energy systems to produce electricity, heating, cooling, hot water, fresh water and hydrogen. It is tried to use different sources of energies as a heat source from conventional to renewable energy sources. This chapter is categorized in there subsections to describe each system.

4.1 System I: Multigeneration system based on gas turbine prime mover

As it was completely discussed in literature, gas turbine is one of the good candidates to be considered as a prime mover because of the reasons discussed earlier. Therefore, one of the multigeneration energy systems here is based on this prime mover. This system is composed of five different subsystems. As it is shown in Fig. 4.1, electricity is produced by a gas turbine and a steam turbine while cooling is produce based on two different cycles, a single effect absorption chiller and an ejector refrigeration cycle. To produce hydrogen, a PEM electrolyzer working by electricity produced from ejector is used. Finlay a domestic water heater is used to make use of the energy from absorption generator. A complete explanation of each subsystem is given bellow.

Fig. 4.1 illustrates an integrated multigeneration system containing a compressor, a combustion chamber (CC), a gas turbine, a double pressure heat recovery steam generator (HRSG) to produce superheated steam, a single effect absorption chiller, a heat recovery vapor generator (HRVG) to produce ORC vapor that is driven by heat from flue gases from the HRSG, an organic Rankine cycle (ORC) ejector refrigeration system, a PEM electrolyzer for hydrogen production and a domestic water heater for hot water production. Air at ambient conditions enters the air compressor at point 1 and exits after compression (point 2). The hot air enters the combustion chamber (CC) into which fuel is injected, and hot combustion gases exit (point 3) and pass through a gas turbine to produce shaft power. The hot gas expands in the gas turbine to point 4. Hot flue gases enter the double pressure HRSG to provide high and low pressure steam at points 5 and 14. High pressure steam enters the steam turbine to generate shaft power while the low pressure steam enters the generator of the absorption system to provide the cooling load

of the system. The low pressure line leaving the generator has adequate energy for use in a domestic water heater that provides hot water at 50ºC. Furthermore, flue gases leaving the HRSG at point *C* enter a heat recovery vapor generator to provide electricity and cooling. Since the flue gases have a low temperature, around 160ºC, an ORC cycle is used, consisting of an ORC turbine to generate electricity and a steam ejector to provide the system cooling load. These flue gases enter the HRVG at point *d* to produce saturated vapor at point 29, which leaves the HRVG at point 28. Saturated vapor at point 29 enters the ORC turbine and work is produced.

The extraction turbine and ejector play important roles in this combined cycle. The high pressure and temperature vapor is expanded through the turbine to generate power, and the extracted vapor from the turbine enters the supersonic nozzle of the ejector as the primary vapor. The stream exiting the ejector (point 33) mixes with turbine exhaust (point 31) and is cooled in the preheater and enters the condenser where it becomes a liquid by rejecting heat to the surroundings. Some of the working fluid leaving the condenser enters the evaporator after passing through the throttle valve (point 39), and the remainder flows back to the pump (point 37). The ORC pump increases the pressure (point 40), and high pressure working fluid is heated in the preheater (point 41) before entering the HRVG. The low pressure and temperature working fluid after the valve (point 39) enters the evaporator, providing a cooling effect for space cooling. Some of the electricity is considered for residential applications while some directly drives a PEM electrolyzer to produce hydrogen. In this analysis, waste heat is used as a heat source to stimulate the multigeneration system and R123 is selected as the working fluid because it is a non-toxic, non-flammable and non-corrosive refrigerant with suitable thermophysical characteristics.

4:2 System II: Biomass based multigeneration system

Renewable energy is a source of energy which comes from natural resources such as sunlight, wind, rain, tides, waves, geothermal heat and biomass. These are naturally replenished when used. Biomass, as a renewable energy source, is biological material from living, or recently living, organisms [77].

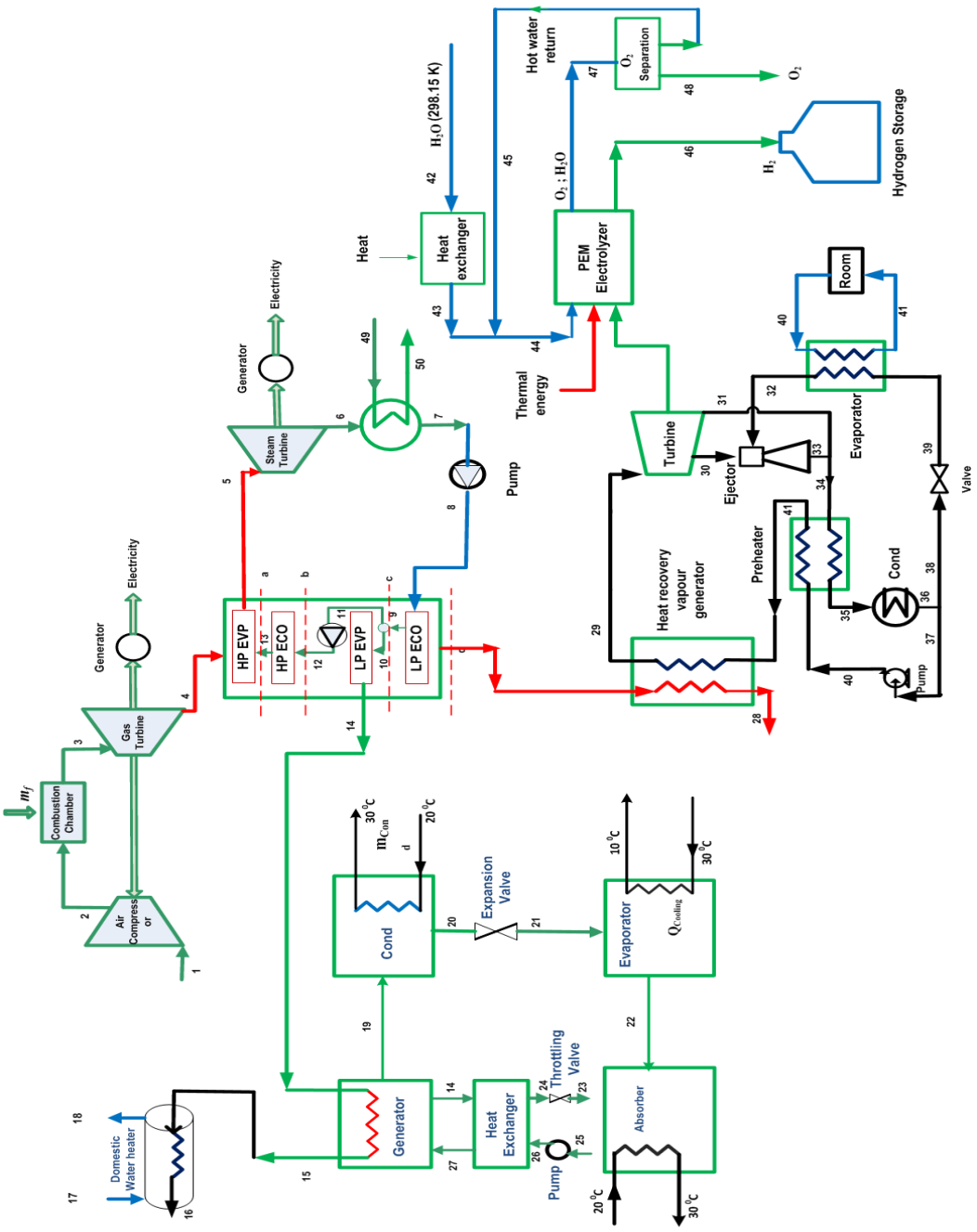

Figure 4.1: Schematic diagram of a multigeneration energy system based on a micro gas turbine, a dual pressure heat recovery steam generator, an absorption chiller, an ejector refrigeration cycle.

Comprehensively, biomass comprises all the living matter present on Earth and, as an energy source, biomass can either be used directly, or converted into other energy products such as biofuels [77]. Currently, biomass resources are mainly used in the production of heating, cooling and electricity. Direct combustion of biomass with coal is the most common method of conversion and provides the greatest potential for large scale utilization of biomass energy in the

near term [78]. Other thermochemical conversion technologies such as gasification and pyrolysis are technically feasible and potentially efficient, compared to combustion, for power generation. However, these technologies either lack of maturity and reliability or are not economically viable for large scale utilization [79]. Biomass based cogeneration systems are studied over many years by numerous researchers for various industries (e.g., sugar, rice, palm oil, paper and wood) as a means of waste disposal and energy recovery [80].

Fig. 4.2 illustrates an integrated multigeneration system containing a biomass combustor, an ORC cycle to produce electricity, a double-effect absorption chiller for cooling, a heat exchanger for heating, a proton exchange membrane (PEM) electrolyzer to produce hydrogen, a domestic water heater to produce hot water and a reverse osmosis (RO) desalination to produce fresh water. Pine sawdust is used as the biomass fuel and burned in a biomass combustor. The heat from the biomass combustor is input to the ORC cycle. The waste heat from the ORC is utilized to produce steam in the heating process via the heat exchanger, and to produce cooling using a double-effect absorption chiller. To have an efficient ORC, its working fluid should have a high critical temperature so that the waste heat can be used more efficiently [75]. A typical organic fluid used in ORCs is n-octane, which has a relatively high critical temperature (569 K) [76]. This organic fluid is selected here as the working fluid of the ORC. The ORC cycle produces electricity, part of which is used for residential applications depending on electricity needs of the building, and the remainder of which drives a PEM electrolyzer for hydrogen production and RO desalination to produce fresh water. The hydrogen and fresh water are stored in a hydrogen tank and fresh water tank respectively. Since the flue gases leaving the ORC evaporator still have energy, they are utilized to produce hot water in a domestic water heater.

As shown in Fig. 4.2 biomass enters the combustor at point 30 and air enters at point 29. Hot flue gases leave the biomass combustor at point 31 and then enter a cyclone to remove the ash. Hot flue gases without ash enter an ORC evaporator to produce steam at point 27 to rotate the ORC turbine blades and produce shaft work. The high-pressure and temperature vapor at point 27 is expanded through the turbine to generate power, and the extracted vapor from the turbine enters the heat exchanger for the heating process. Saturated vapor leaves the heating process unit at point 24. This saturated steam enters the generator of the double-effect absorption system to provide the cooling load of the system. Saturated liquid leaves the absorption generator and enters the ORC pump at point 25. ORC pump increase the pressure of ORC working fluid

and high pressure ORC fluid enters the ORC evaporator at point 26 to close the ORC power generation unit. Since flue gases leaving the ORC evaporator still have energy, a domestic water heater is used to utilize the energy of the hot gases at point 33. Water enters the domestic water heater at point 35 and hot water leave the domestic water heater at point 36. Reverse osmosis (RO) desalination is used to produce fresh water as shown right bottom side of Fig. 4.2.

Sea water at point 37 enters a filter to remove dissolved species and then passes through the absorber of the double-effect absorption chiller to increase the temperature to improve the efficiency of the OR desalination unit. A high pressure RO pump is used to increase the pressure of the water. High pressure sea water leaves the RO pump and enters the RO unit at point 40. Fresh water is produced at point 41 and stored in a fresh water tank for the later use while high pressure brine water enters a hydraulic turbine to reduce the pressure and generate electricity.

Finally, low pressure brine water leaves the RO unit and sends back to the sea. The cooling load of the system is provided by a double-effect absorption chiller. Weak Li-Br solution at point a is pumped through an high pressure solution leaves the pump at point 2 then passes through a high temperature heat exchanger to increase the temperature. High temperature weak solution then enters the high temperature heat exchanger at point 3 and the high temperature weak solution enters the high temperature generator. In high temperature generator water is removed from the solution and the strong solution sends back to the absorber after passing through the high and low temperature heat exchangers. On the other side, vapor leaves the high temperature generator at point 17 and enters the low temperature generator. The refrigerant steam produced by the low pressure generator is condensed by the cooling water and then enters the expansion valve at point 8 to reduce the pressure and enters the evaporator at point 9. This low pressure vapor enters the evaporator and saturated vapor leaves the evaporator at point 10 and enters the absorber. The absorption heat is removed by the sea water entering the absorber at point 38 to improve the efficiency of the RO desalination unit.

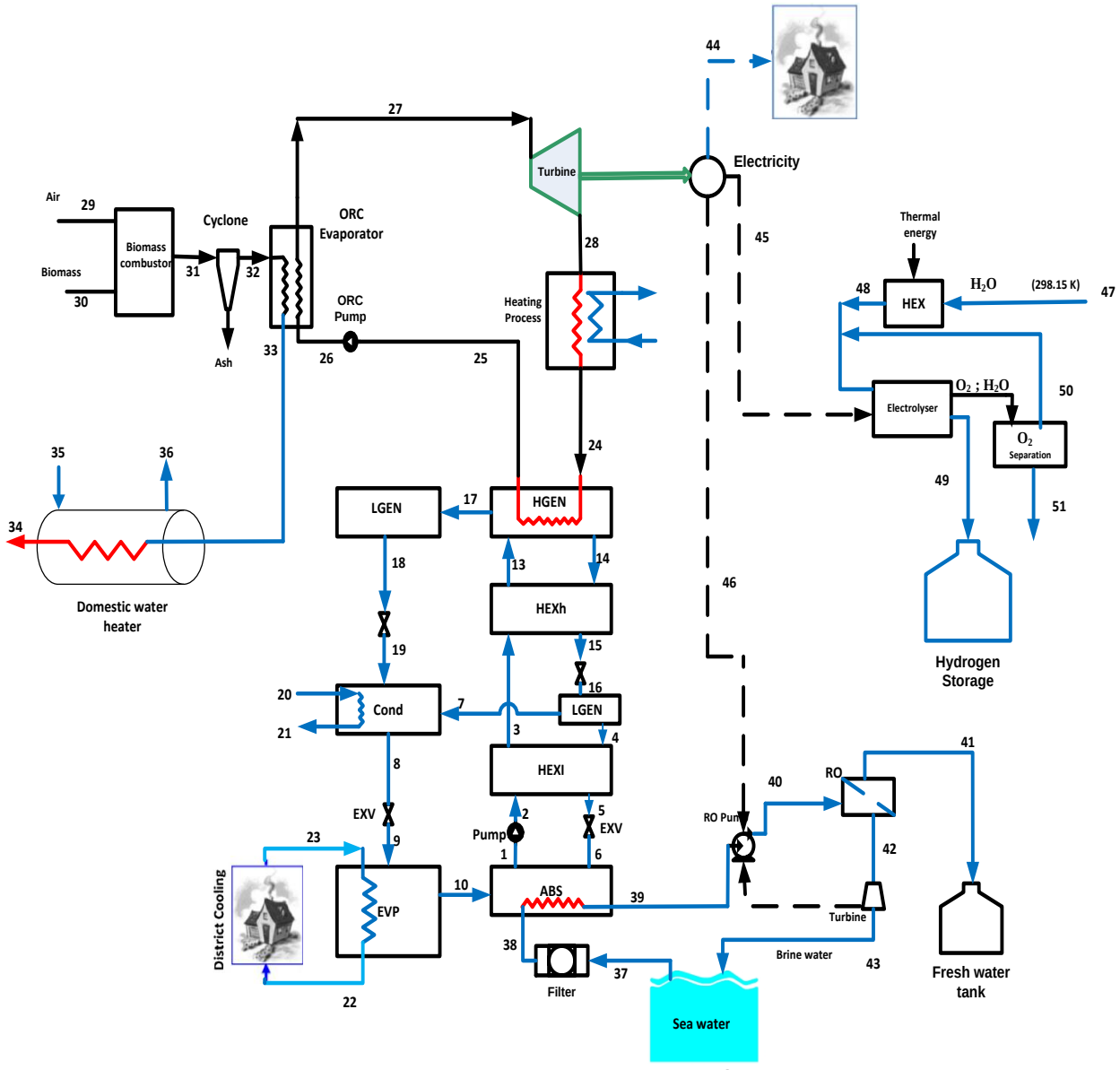

Figure 4. 2: Schematic of biomass based a multigeneration energy system for the provision of heating, cooling, electricity, hydrogen, fresh water and hot water.

4.3 System III: Integrated ocean thermal energy conversion multigeneration system

A large amount of solar energy is stored as heat in the surface waters of the world's oceans, providing a source of renewable energy. Ocean thermal energy conversion (OTEC) is a process for harnessing this renewable energy in which a heat engine operates between the relatively warm ocean surface, which is exposed to the sun, and the colder (about 5ºC) water deeper in the ocean, in order to produce electricity. OTEC usually incorporates a low-temperature Rankine

cycle engine which boils a working fluid such as ammonia to generate a vapor which turns the turbine to generate electricity, and then is condensed back into a liquid in a continuous process. 80 % of the energy that is received from the sun by the earth is stored in the world's oceans [81, 82], and many regions of the world have access to this OTEC resource. OTEC can produce fuels by using its product electricity to produce hydrogen, which can be used in hydrogen fueled cars as well as in the development of synthetic fuels. For a small city, millions of tons of CO_2 are generated annually through fossil fuel use while with OTEC the value is zero, during the operation of devices. OTEC has a potential to replace some fossil fuel use, perhaps via OTEC ships travelling the seas of the world.

An OTEC system utilizes low-grade energy and has a low energy efficiency (approximately 3–5 %). Therefore, achieving a high electricity generating capacity with OTEC requires the use of large quantities of seawater, and a correspondingly, large amounts of pumping power. These factors have negative impact on the cost-effectiveness of this technology and therefore OTEC is not commercially viable today. In order to improve the effectiveness and economics of OTEC cycles, it is proposed to integrate them with industrial operations so that, apart from generating electricity, they could be used for fresh water production, air conditioning and refrigeration, cold water agriculture, aquaculture and mariculture, and hydrogen production [81]. Potential markets for OTEC have been identified, most of which are in the Pacific Ocean, and about 50 countries are examining its implementation as a sustainable source of energy and fresh water, including India, Korea, Palau, Philippines, the U.S. and Papua New Guinea [83]. In 2001, as a result of cooperation between Japan and India, a 1-MW OTEC plant was built in India [83], and others are planned to be constructed in the near future [84].

Considerable research has been directed to the development of OTEC recently. Uehara [85-87] conducted numerous theoretical and experimental studies on the major components of an OTEC plant, and showed that ammonia is a suitable working fluid for an OTEC plant employing a closed organic Rankine cycle (ORC). The energy efficiency of the Rankine cycle in an OTEC plant is usually limited to around 5% due to the small temperature differences between surface water and deep water of the ocean. Thus, in order to improve the efficiency of OTEC, other thermodynamic cycles such as the Kalina cycle and the Uehara cycle that use an ammonia–water mixture as the working fluid are being considered [88]; they are reported to have better energy efficiencies than a Rankine cycle at the same temperature difference [88]. Increasing in the

temperature difference between the hot heat source and the cold heat sink can improve the efficiency of OTEC plants, as can the integration of OTEC with other energy technologies. Saitoh and Yamada [88] proposed a conceptual design of a multiple Rankine-cycle system using both solar thermal energy and ocean thermal energy in order to improve the cycle efficiency.

Fig. 4.3 shows a schematic diagram of an integrated OTEC system equipped with a flat plate and PV/T solar collector, a reverse osmosis (RO) desalination unit, a single effect absorption chiller and PEM electrolyzer. This integrated system uses the warm surface seawater to evaporate a working fluid such as ammonia or a Freon refrigerant, which drives an ORC turbine to produce electricity, which in turn is used to drive a PEM electrolyzer to produce hydrogen. After passing through the turbine, the vapor is condensed in a heat exchanger that is cooled by cold deep seawater. The working fluid is then pumped back through the warm seawater heat exchanger, and the cycle is repeated continuously. Warm surface water is pumped from the ocean surface at point 1. A warm surface pump increase the pressure where the high pressure warm water enters a flat plate collector at point 2 to increase its temperature. Water enters an evaporator at point 3 and after a heat exchange with the ORC fluid, leaves the evaporator at point 4 where it is flushed back to the ocean surface.

A PV/T solar panel is considered to provide the cooling load of the system. Air enters the PV/T panel at point 41 and, after absorbing the sun's heat using its panels, its temperature increases. Next, the hot air leaves the PV/T at point 40 and enters the absorption chiller generator in order to run the chiller. The electricity generated by PV/T is directed to derive a RO desalination plant to produce fresh water. In this multigeneration system, a provision of the electricity generated by OTEC plant is used to produce hydrogen using a PEM electrolyzer at point 22. The produced hydrogen is stored in a hydrogen storage tank for later usage.

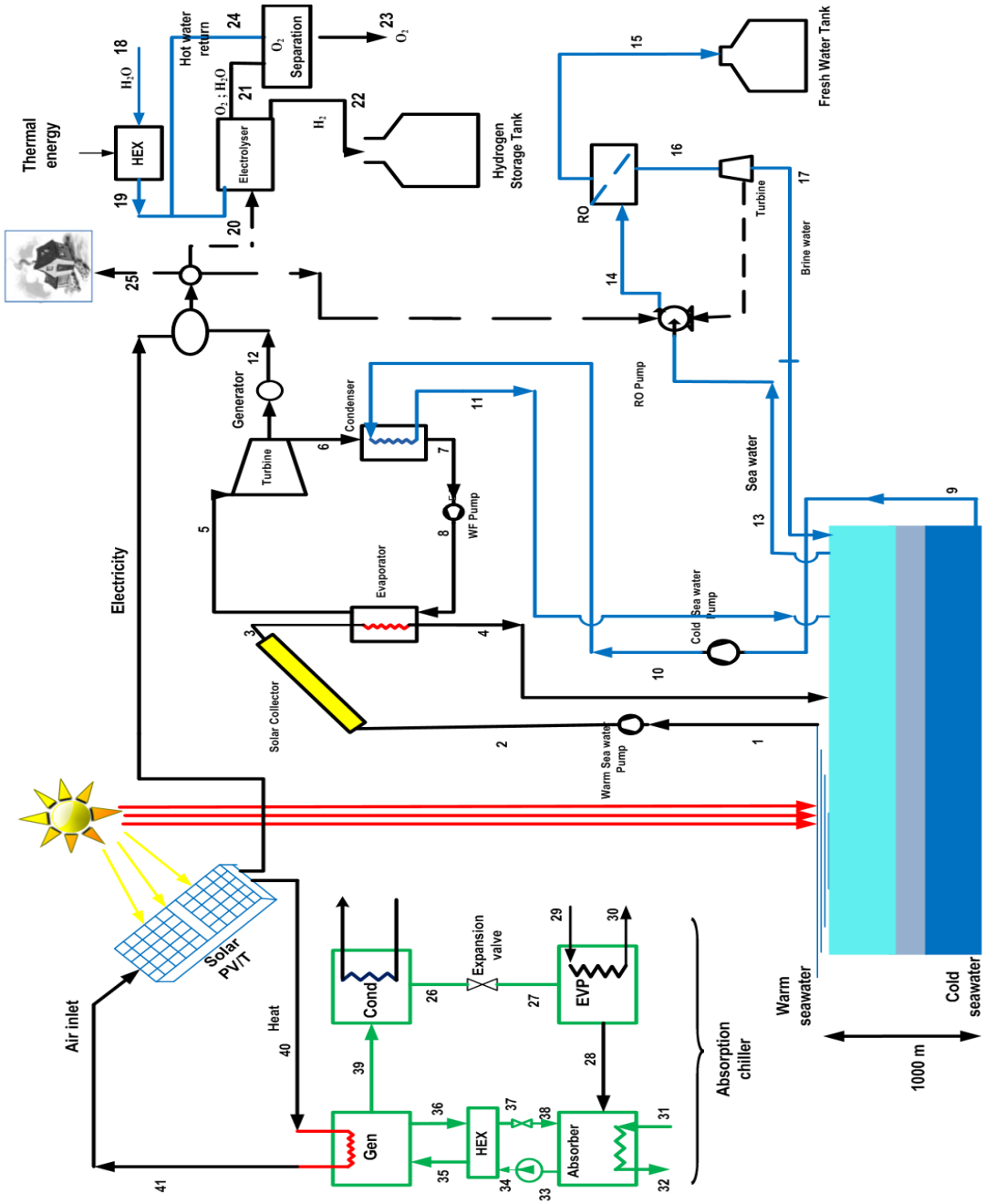

Figure 4.3: Schematic of an integrated renewable based multigeneration energy system for the provision of cooling, electricity, hydrogen, fresh water.

Chapter 5: Model Development and Analyses

In this chapter we will have some introductory explanations. It starts with general thermodynamic principles to exergy and economic analyses.

5.1 Thermodynamic analyses

Thermodynamic analyses are composed of mass balance equation, entropy balance equation and energy and exergy balance equations as follows:

5.1.1 Mass balance equation

The conservation of mass principle is a fundamental principle in analyzing any thermodynamic systems. This principle is defined for a control volume, as shown in Fig. 5.1 as follows:

$$\sum_k \dot{m}_i - \sum_k \dot{m}_e = \frac{dm_{cv}}{dt} \qquad (5.1)$$

where m and $\dot{m}$ are the mass and mass flow rate, respectively, and the subscripts i and e refer to the inlet of the control volume and exit of the control volume, respectively. The subscript cv indicates the control volume.

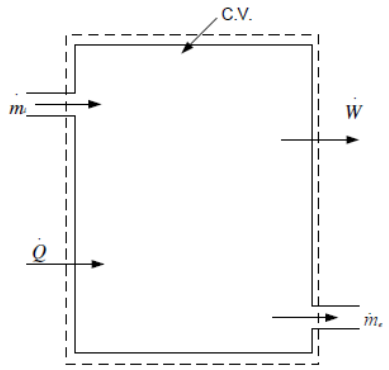

Figure 5.1: A control volume for mass balance equation.

5.1.2 Energy balance equation

The energy balance of a control volume deals with all the input and output energy components of a selected control volume. The first law of thermodynamics which is known as the conservation of energy principle, is defined as

$$\dot{Q} - \dot{W} + \sum_i \dot{m}_i(h_i + \frac{{V_i}^2}{2} + gZ_i) - \sum_e \dot{m}_{ie}(h_e + \frac{{V_e}^2}{2} + gZ_e) = \frac{dE_{cv}}{dt} \quad (5.2)$$

where E,$\dot{Q}$,$\dot{W}$ and t are the energy, heat transfer rate, work rate and time, respectively. The other symbols, h, V, g and Z, stand for specific enthalpy, velocity, standard acceleration of gravity, and elevation respectively.

5.1.3 Entropy balance equation

Entropy generation is associated with the losses in the system. The entropy generated within a process is called entropy generation and it is denoted by S_{gen}. The entropy generation rate for a control volume is defined as [89]:

$$\dot{S}_{gen} = \sum_e \dot{m}_e s_e - \sum_i \dot{m}_e s_i - \sum_k \frac{\dot{Q}}{T_k} + \frac{dS_{cv}}{dt} \quad (5.3)$$

where $\dot{S}_{gen}$ is entropy generation rate and s is specific entropy.

5.1.4 Exergy analysis

Exergy analysis can help develop strategies and guidelines for more efficient and effective use of energy, and is utilized to study various thermal processes, especially power generation, CHP, trigeneration and multigeneration. The exergy of a substance is often divided into four components. Two common ones are physical and chemical exergy. The two others, kinetic and potential exergy, are assumed to be negligible here, as elevation changes are small and speeds are relatively low [29, 47, 76]. Physical exergy is defined as the maximum useful work obtainable as a system interacts with an equilibrium state. Chemical exergy is associated with the departure of the chemical composition of a system from its chemical equilibrium and is considered important in processes involving combustion and other chemical changes [90]. Through the second law of thermodynamics, the following exergy rate balance is written as

$$\dot{E}x_Q + \sum_i \dot{m}_i\, ex_i = \sum_e \dot{m}_e\, ex_e + \dot{E}x_W + \dot{E}x_D \quad (5.4)$$

where subscripts *i* and *e* denote the control volume inlet and outlet flow, respectively, $\dot{E}x_D$ is the exergy destruction rate and other terms are given as follows:

$$\dot{E}x_Q = (1 - \frac{T_0}{T_i})\dot{Q}_i \quad (5.5)$$

$$\dot{E}x_w = \dot{W} \quad (5.6)$$

$$ex = ex_{ph} + ex_{ch} \quad (5.7)$$

Here, $\dot{E}x_Q$ is the exergy rate of heat transfer crossing the boundary of the control volume at absolute temperature *T*, the subscript 0 refers to the reference environment conditions and $\dot{E}x_W$ is the exergy rate associated with shaft work. Also, ex_{ph} is defined as follows:

$$ex_{ph} = (h - h_0) - T_0(s - s_0) \quad (5.8)$$

The chemical exergy for gas mixtures is defined as follows [90]:

$$ex_{mix}^{ch} = [\sum_{i=1}^{n} x_i ex_i^{ch} + RT_0 \sum_{i=1}^{n} x_i \ln x_i] \quad (5.9)$$

The above equation cannot be used to evaluate fuel exergy. Here, fuel exergy is approximated with the following simplification [29, 90]:

$$\xi = \frac{ex_f}{LHV_f} \quad (5.10)$$

The ratio of chemical exergy to LHV_f is usually close to unity for common gaseous fuels, e.g., $\xi_{CH_4} = 1.06, \xi_{H_2} = 0.985$

For a general gaseous fuel with composition C_xH_y, the following experimental correlation can be used for ξ [90]:

$$\xi = 1.033 + 0.0169\ \frac{y}{x} - \frac{0.0698}{x} \quad (5.11)$$

5.2 Thermoeconomic analysis

Thermoeconomics is the branch of engineering that appropriately combines, at the level of system components, thermodynamic evaluations based on an exergy analysis and economic principles, in order to provide information that is useful to the design and operation of a cost-effective system, but not obtainable by conventional energy and exergy analyses and economic analysis [12]. Some suggest that, when exergy costing is not applied, the general term thermoeconomics is more appropriate as it characterizes any combination of thermodynamic and economic analysis.

5.2.1 Cost balance equation

For each flow in a system, a parameter called flow cost rate $\dot{C}$ (\$/h) is defined, and a cost balance is written for each component as

$$\dot{C}_{q,k} + \sum_i \dot{C}_{i,k} + \dot{Z}_k = \sum_e \dot{C}_{e,k} + \dot{C}_{w,k} \quad (5.12)$$

Cost balances are generally written so that all terms are positive. Using Eq. (5.12), one can write [90]:

$$\sum(c_e \dot{E}x_e)_k + c_{w,k}\dot{W}_k = c_{q,k}\dot{E}x_{q,k} + \sum(c_i \dot{E}x_i)_k + \dot{Z}_k \quad (5.13)$$

$$\dot{C}_j = c_j \dot{E}x_j \quad (5.14)$$

$$\dot{Z} = \frac{Z_k CRF \Phi}{N \times 3600} \quad (5.15)$$

where Z_k is the purchase cost of the k^{th} component, and *CRF* is the capital recovery factor.

5.2.2 Capital recovery factor

Capital recovery factor (CRF) depends on the interest rate and equipment life time, and is determined as

$$CRF = \frac{i \times (1+i)^n}{(1+i)^n - 1} \quad (5.16)$$

Here, *i* denotes the interest rate and *n* the total operating period of the system in years. Also, *N* is the annual number of operation hours for the unit, and φ is the maintenance factor, which is often 1.06 [4, 66, 90].

5.3 Environmental impact assessment

An important measure for reducing environmental impact, including emissions of carbon dioxide, a primary greenhouse gas, is increasing efficiency and thereby decreasing fuel use. Although numerous exergy and exergoeconomic analyses have been reported for CHP and trigeneration, many do not incorporate environmental impact. Addressing this deficiency is one objective of this article, in which emissions of CO, CO_2 and NO_x are considered. The amount of CO and NO_x produced in the combustion chamber due to the combustion reaction depends on various combustion characteristics including the adiabatic flame temperature [91]. The adiabatic flame temperature in the primary zone of the combustion chamber can be expressed as follows:

$$T_{pz} = A\sigma^{\alpha} \exp(\beta(\sigma+\lambda)^2)\pi^{x^*}\theta^{y^*}\xi^{z^*} \quad (5.17)$$

Here, π denotes the dimensionless pressure (P/P_{ref}), θ the dimensionless temperature (T/T_{ref}) and ξ the H/C atomic ratio. Also, $\sigma = \phi$ for $\phi \leq 1$, where ϕ is the mass or molar ratio and $\sigma = \phi - 0.7$ for $\phi \geq 1$. Further, *x*, *y* and *z* are quadratic functions of σ based on the following equations:

$$x^* = a_1 + b_1\sigma + c_1\sigma^2 \tag{5.18}$$

$$y^* = a_2 + b_2\sigma + c_2\sigma^2 \tag{5.19}$$

$$z^* = a_3 + b_3\sigma + c_3\sigma^2 \tag{5.20}$$

Here, the values of the parameters are listed in Table 5.1. The amount of CO and NO_x produced in a combustion chamber depends on various combustion characteristics including the adiabatic flame temperature [92]. Here, the emissions for these species (in grams per kilogram of fuel) are determined as follows [92]:

$$m_{NO_x} = \frac{0.15\times10^{16}\tau^{0.5}\exp(\frac{-71100}{T_{PZ}})}{P_3^{0.05}(\frac{\Delta P_{in}}{P_{in}})^{0.5}} \tag{5.21}$$

$$m_{CO} = \frac{0.179\times10^{9}\exp(\frac{7800}{T_{PZ}})}{P_3^{2}\tau(\frac{\Delta P_{in}}{P_{in}})^{0.5}} \tag{5.22}$$

Table 5.1: Values for parameters in Equations. (5.18-5.20).

Constants	$0.3 \leq \varphi \leq 1.0$			$1.0 \leq \varphi \leq 1.6$	
	$0.92 \leq \theta \leq 2$	$2 \leq \theta \leq 3.2$		$0.92 \leq \theta \leq 2$	$2 \leq \theta \leq 3.2$
A	2361.764	2315.75		916.826	1246.177
α	0.115	-0.049		0.288	0.381
β	-0.948	-1.114		0.145	0.347
λ	-1.097	-1.180		-3.277	-2.036
a_1	0.014	0.010		0.031	0.036
b_1	-0.055	-0.045		-0.078	-0.085
c_1	0.052	0.048		0.049	0.051
a_2	0.395	0.568		0.025	0.009
b_2	-0.441	-0.550		0.260	0.502
c_2	0.141	0.131		-0.131	-0.247
a_3	0.005	0.010		0.004	0.017
b_3	-0.128	-0.129		-0.178	-0.189
c_3	0.082	0.084		0.098	0.103

5.4 Optimization

The first step in any optimization problem is to define the system boundaries. All subsystems that affect system performance should be included. When the system is overly complex, it is

often desirable to break it down into smaller subsystems. In this case, optimization should be done on each subsystem independently, i.e., sub-optimization of the subsystems is performed.

5.4.1 Objective functions and system criteria

The next step in an optimization problem is to define the system criteria, which is sometimes called the objective function. The objective function is based on the desire or purpose of the decision maker, and it can be either maximized or minimized.

Optimization criteria can vary widely. For instance, it can be based on efficiency (energy, exergy or other efficiencies), economic (total capital investment, total annual levelized costs, cost of exergy destruction, and cost of environmental impact), technological (production rate, production time and total weight) and/or environmental (rate of emitted pollutants). Note that we can consider more than one objective function to find the optimal solution for an optimization problem. This method is called multi-objective optimization [47].

5.4.2 Decision variables

Another essential element in formulating an optimization problem is the selection of the independent decision variables that adequately characterized the possible design options. To select these decision variables, it is important to (a) include all important variables that could affect the performance and cost effectiveness of the system, (b) not include variables with minor importance, and (c) distinguish among independent variables whose values are amenable to change. In each optimization problem, only decision variables are changing. Variables whose values are calculated from the independent variables using mathematical models are dependent variables.

5.4.3 Constraints

The constraints in a given design problem arise due to limitations on the ranges of the physical variables, basic conservation principles which must be satisfied and other limitations. The restrictions on the variables may arise due to the space, equipment, and materials that are being employed. These may restrict, for example, the dimensions of the system, the highest temperature that the components can safely attain, the allowable pressure, the material flow rate, the force generated, and so on. Also, minimum values of the temperature may be specified for

thermoforming of a plastic and for ignition to occur in an engine. Thus, both minimum and maximum values of the design variables may be involved in constraints.

Many constraints in thermal systems arise because of conservation laws, particularly those related to mass, momentum, and energy. For instance, under steady-state conditions, mass inflow to the system must equal mass outflow. This condition gives rise to an equation that must be satisfied by the relevant design variables, thus restricting the values that may be employed in the search for an optimum. Similarly, energy balance considerations are important in thermal systems and may limit the range of temperatures, heat fluxes, dimensions, etc., that may be used. Several such constraints are often satisfied during modeling and simulation because the governing equations are based on conservation principles. In this way, the objective function being optimized already considers these constraints. In such cases, only the additional limitations that define the boundaries of the design domain remain to be considered.

5.4.4 Optimization methods

There are several methods for optimization described as follows:

5.4.4.1. Classical optimization

Classical optimization techniques are useful in finding the optimum solution or unconstrained maximum or minimum of continuous and differentiable functions. Some specifications for classical optimization can be selected based on this understanding, as described below:

- These are analytical methods that make use of differential calculus in locating the optimum solution.
- Classical methods have limited scope in practical applications as some involve objective functions which are not continuous and/or differentiable.
- These methods assume that the function is differentiable twice with respect to the design variables and that the derivatives are continuous.
- Three main types of problems can be handled by classical optimization techniques:
    - ✓ Single variable functions.
    - ✓ Multivariable functions with no constraints.
    - ✓ Multivariable functions with both equality and inequality constraints. In problems with equality constraints the Lagrange multiplier method can be used. If the

problem has inequality constraints, the Kuhn-Tucker conditions can be used to identify the optimum solution.

5.4.4.2 Numerical method optimization

This optimization technique can be categorized according to specific method, as follows:

- **Linear programming:** Studies the case in which the objective function *f* is linear and the set *A*, where *A* is the design variable space, is specified using only linear equalities and inequalities.
- **Integer programming:** Studies linear programs in which some or all variables are constrained to take on integer values.
- **Quadratic programming:** Allows the objective function to have quadratic terms, while the set *A* must be specified with linear equalities and inequalities.
- **Nonlinear programming**: Studies the general case in which the objective function or the constraints or both contain nonlinear parts.
- **Stochastic programming:** Studies the case in which some of the constraints depend on random variables.
- **Dynamic programming:** Studies the case in which the optimization strategy is based on splitting the problem into smaller sub-problems.
- **Combinatorial optimization:** Concerns problems where the set of feasible solutions is discrete or can be reduced to a discrete one.
- **Evolutionary algorithm:** Involves numerical methods based on random search.

5.4.4.3 Evolutionary algorithm

An evolutionary algorithm utilizes techniques inspired by biological evaluation reproduction, mutation, recombination, and selection. Candidate solutions to the optimization problem play the role of individuals in a population, and the fitness function determines the environment within which the solutions "live." Evolutionary algorithm methods include *genetic algorithms* (GAs), *artificial neural networks* (ANNs), and *fuzzy logic* [93]. These approaches are discussed further below. Each of the approaches is available in toolboxes developed by Math Works and can thus be used easily with MATLAB software.

Genetic algorithm

A genetic algorithm is a search method used for obtaining an optimal solution which is based on evolutionary techniques that are similar to processes in evolutionary biology, including inheritance, learning, selection and mutation. The process starts with a population of candidate solutions called individuals, and progresses through generations, with the fitness of each individual being evaluated. Fitness is defined based on the objective function. Then multiple individuals are selected from the current generation based on fitness and modified to form a new population. This new population is used in the next iteration and the algorithm progresses toward the desired optimal point [94, 95].

Artificial neural network

Artificial neural networks are interconnected groups of processing elements, called artificial neurons, similar to those in the central nervous system of the body. The approach is thus analogous to some elements of neuroscience. The characteristics of the processing elements and their interconnections determine the processing of information and the modeling of simple and complex processes. Functions are performed in parallel and the networks have both non-adaptive and adaptive elements, which change with the inputs and outputs and the problem. The ANN approach leads to nonlinear, distributed, parallel, local processing and adaptive representations of systems [93].

Fuzzy logic

Fuzzy logic allows us to deal with inherently imprecise concepts, such as cold, warm, very, and slight, and is useful in a wide variety of thermal systems where approximate, rather than precise, reasoning is needed. Fuzzy logic can be used for the control of systems and in problems where a sharp cut off between two conditions does not exist.

Multi-objective optimization

Optimal conditions are generally strongly dependent on the chosen objective function. However, several aspects of performance are often important in most practical applications. In thermal and energy systems design, efficiency (energy and/or exergy), production rate, output, quality, and heat transfer rate are common quantities that are to be maximized, while cost, input, environmental impact and pressure are quantities to be minimized. Any of these can be chosen as the objective function for a problem, but it is usually more meaningful and useful to consider

more than one objective function. In a single-objective optimization problem, the task is to find the value for the objective function which optimizes a sole objective function. When more than one objective function is considered in the optimization, we refer to the procedure as multi-objective optimization. One of the common approaches for dealing with multiple objective functions is to combine them into a single objective function that is to be minimized or maximized. For example, in the design of heat exchangers and cooling systems for electronic equipment, it is desirable to maximize the heat transfer rate. However, this often comes at the cost of increased fluid flow rates and corresponding frictional pressure losses.

Another approach which has attracted much attention in recent years is multi-objective optimization. With this approach, two or more objective functions that are of interest in a given problem are considered and a strategy is developed to balance or trade off each objective function relative to the others [14].

To illustrate, we consider two objective functions OF_1 and OF_2. We assume that these are to be minimized (although maximization can be similarly handled since it is equivalent to minimization of the negative of the function). Fig. 5.2.a shows values for the two objective functions at five design points. As shown in this figure, design 2 is clearly preferable to design 4 because both objective functions are smaller for design 2 compared to design 4. Similarly, design 3 is preferable to design 5. However, designs 1, 2 and 3 are not preferable, or dominated, by any other designs. The set of non-dominated designs is introduced as the Pareto frontier, representing the best collection of design points. This is shown in Fig. 5.2.b. Note that any point on the Pareto frontier can be considered as an optimal design condition. The selection of a specific design from the set of points constituting the Pareto frontier is at the discretion of the decision maker, which may be an engineer or designer.

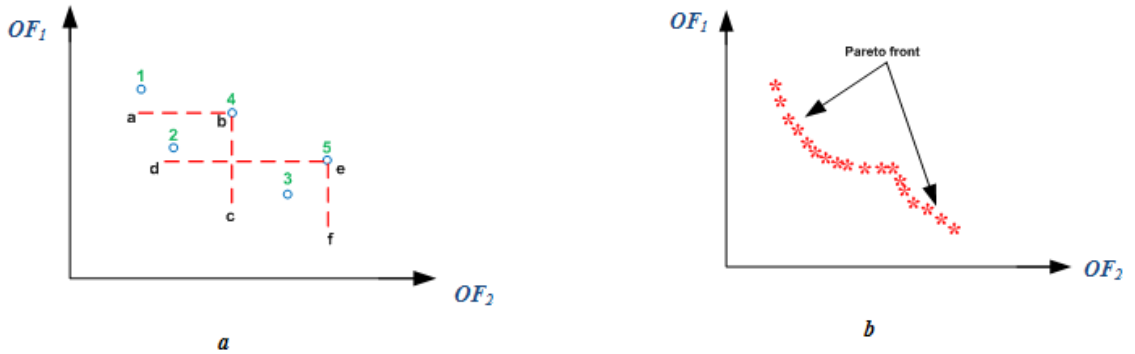

Figure 5. 2: Multi-objective optimization with two objective functions OF1 and OF2 that are to be minimized, showing the (a) dominant designs and (b) the Pareto frontier.

5.5 Analyses of System I

For the analysis of system one thermodynamic analysis, exergy and exergoeconomic analyses are conducted as follows:

5.5.1 Thermodynamic analysis

For thermodynamic modeling, the multigeneration system considered in Fig. 4.1 is divided into six main parts: gas turbine (Brayton) cycle, Rankine cycle with double pressure HRSG, a single effect absorption chiller, organic Rankine cycle (ORC), domestic water heater and PEM electrolyzer. The fuel injected to the combustion chamber is natural gas. We determine the temperature profile in the plant, input and output enthalpy and exergy flow rates, exergy destructions rates, and energy and exergy efficiencies. The energy balances and governing equations for various multigeneration components (see Fig. 4.1) are written as follows:

5.5.1.1 Brayton cycle

Brayton cycle is composed of 4 major components as

- **Air compressor**

Air at ambient pressure and temperature T_1 enters the compressor. The compressor outlet temperature is a function of compressor isentropic efficiency (η_{AC}), compressor pressure ratio (r_{AC}) and specific heat ratio, as follows:

$$T_2 = T_1 \times (1 + \frac{1}{\eta_{AC}} (r_{AC}^{\frac{\gamma_a - 1}{\gamma_a}} - 1)) \quad (5.23)$$

The compressor work rate is a function of air mass flow rate ($\dot{m}_a$), air specific heat and temperature difference, and can be expressed as follows:

$$\dot{W}_{AC} = \dot{m}_a C_{pa} (T_2 - T_1) \quad (5.24)$$

where γ_a is the air specific heat ratio, and C_{pa} is treated as a function of temperature as follows [75]:

$$C_{pa}(T) = 1.048 - \left(\frac{3.83T}{10^4}\right) + \left(\frac{9.45T^2}{10^7}\right) - \left(\frac{5.49T^3}{10^{10}}\right) + \left(\frac{7.92T^4}{10^{14}}\right) \quad (5.25)$$

- **Combustion chamber (CC)**

The outlet properties of the combustion chamber are a function of air mass flow rate, fuel lower heating value (*LHV*) and combustion efficiency, and are related as follows:

$$\dot{m}_a h_2 + \dot{m}_f LHV = \dot{m}_g h_3 + (1 - \eta_{cc})\, \dot{m}_f LHV \quad (5.26)$$

The combustion chamber outlet pressure is defined by considering a pressure drop across the combustion chamber as follows:

$$\frac{P_3}{P_2} = 1 - \Delta P_{CC} \quad (5.27)$$

where ΔP_{cc} is the pressure loss across the combustion chamber and η_{cc} is the combustion efficiency.

The combustion reaction occurring and its species coefficients can be expressed as follows:

$$\lambda \mathrm{C_{x1}H_{y1}} + \left(x_{\mathrm{O_2}}\mathrm{O_2} + x_{\mathrm{N_2}}\mathrm{N_2} + x_{\mathrm{H_2O}}\,\mathrm{H_2O} + x_{\mathrm{CO_2}}\mathrm{CO_2} + x_{\mathrm{Ar}}\mathrm{Ar}\right) \rightarrow y_{\mathrm{CO_2}}\mathrm{CO_2} + y_{\mathrm{N_2}}\mathrm{N_2} +$$

$$y_{\mathrm{O_2}}\mathrm{O_2} + y_{\mathrm{H_2O}}\mathrm{H_2O} + y_{\mathrm{NO}}\mathrm{NO} + y_{\mathrm{CO}}\mathrm{CO} + y_{\mathrm{Ar}}\mathrm{Ar}), \quad (5.28)$$

where

$y_{\mathrm{CO_2}=}(\lambda x_1 + x_{\mathrm{CO_2}} - y_{\mathrm{CO}})$,

$y_{\mathrm{N_2}} = (x_{\mathrm{N_2}} - y_{\mathrm{NO}})$,

$y_{\mathrm{H_2O}} = (x_{\mathrm{H_2O}} + \frac{\lambda \times y_1}{2})$,

$y_{\mathrm{O_2}} = (x_{\mathrm{O2}} - \lambda \times x_1 - \frac{\lambda \times y_1}{4} - \frac{y_{\mathrm{CO}}}{2} - \frac{y_{\mathrm{NO}}}{2})$,

$y_{Ar} = x_{Ar}$, and

$\lambda = \frac{n_f}{n_{air}}$.

- **Gas turbine**

The gas turbine outlet temperature can be written as a function of gas turbine isentropic efficiency (η_{GT}), the gas turbine inlet temperature (T_3) and gas turbine pressure ratio (P_3/P_4) as follows:

$$T_4 = T_3(1 - \eta_{GT}(1 - \left(\frac{P_3}{P_4}\right)^{\frac{1-\gamma_g}{\gamma_g}}) \quad (5.29)$$

The gas turbine output power is also found as

$$\dot{W}_{GT} = \dot{m}_g C_{pg}(T_3 - T_4) \quad (5.30)$$

Here, $\dot{m}_g$ is the gas turbine mass flow rate, which is calculated as

$$\dot{m}_g = \dot{m}_f + \dot{m}_a \tag{5.31}$$

The net output power can be expressed as

$$\dot{W}_{net} = \dot{W}_{GT} - \dot{W}_{AC} \tag{5.32}$$

where C_{pg} is taken to be a function of temperature as follows:

$$C_{pg}(T) = 0.991 + \left(\frac{6.997T}{10^5}\right) + \left(\frac{2.712T^2}{10^7}\right) - \left(\frac{1.2244T^3}{10^{10}}\right) \tag{5.33}$$

5.5.1.2 Bottoming cycle

Energy balances and governing equations for the components of the bottoming cycle (steam turbine cycle and HRSG) are provided here.

- **Dual pressure HRSG**

A dual-pressure HRSG with two economizers (LP and HP) and two evaporators (LP and HP) is used in the multigeneration cycle to provide both low- and high-pressure steam. The LP steam is used to drive the absorption chiller and the HP steam to generate electricity. The temperature profile in the HRSG is shown in Fig. 5.3, where the pinch-point is defined as the difference between the temperature of the gas at the entrance of the evaporator (economizer side) and the saturation temperature. The dual-pressure HRSG has two pinch points (PP_{HP} and PP_{LP}). The temperature differences between the water leaving the economizers (T_{20} and T_{22}) and the saturation temperature (T_5 and T_{17}) are the approach points (AP_{HP} and AP_{LP}), which depend on the economizer's tube layout. Note that the pinch point and approach temperatures are considered constant here. Energy balances for each element of the HRSG are expressed as follows:

$$\dot{m}_{w,HP}(h_5 - h_{13}) = \dot{m}_g C_{Pg}(T_4 - T_a) \tag{5.34}$$

$$\dot{m}_{w,HP}(h_{13} - h_{12}) = \dot{m}_g C_{Pg}(T_a - T_b) \tag{5.35}$$

$$\dot{m}_{w,LP}(h_{11} - h_{10}) = \dot{m}_g C_{Pg}(T_b - T_c) \tag{5.36}$$

$$\dot{m}_w(h_9 - h_8) = \dot{m}_g C_{Pg}(T_c - T_d) \tag{5.37}$$

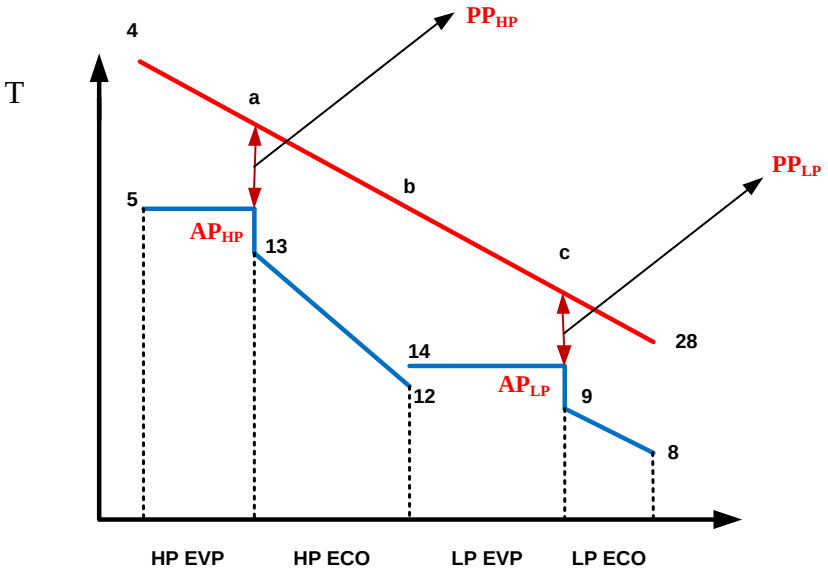

Point number	Specification
4	Hot gases entering HRSG
a	Hot gases exiting high pressure evaporator (HP EVP)
b	Hot gases exiting high pressure economizer (HP ECO)
c	Hot gases exiting low pressure evaporator
28	Hot gases exiting HRSG
8	Cold water entering HRSG
9	Hot water exiting low pressure economizer (LP ECO)
14	Saturated water exiting low pressure evaporator
12	Hot water entering high pressure economizer (HP ECO)
13	Hot water exiting high pressure economizer (HP ECO)
5	Saturated water exiting high pressure evaporator

Figure 5.3: Temperature profile of HRSG.

- **Steam turbine**

An energy balance for the steam turbine shown in Fig. 4.1 and the isentropic efficiency equation are written as follows:

$$\dot{m}_w h_5 = \dot{W}_{ST} - \dot{m}_w h_6 \qquad (5.38)$$

$$\eta_{ST} = \frac{\dot{W}_{ST,act}}{\dot{W}_{ST,is}} \quad (5.39)$$

- **Condenser**

An energy balance for the condenser follows:

$$\dot{m}_6 h_6 = \dot{Q}_{Cond} - \dot{m}_7 h_7 \quad (5.40)$$

- **Pump:**

An energy balance for pump and an isentropic efficiency can be expressed as follows:

$$\dot{m}_w h_7 + \dot{W}_{Pump} = \dot{m}_w h_8 \quad (5.41)$$

$$\eta_{Pump} = \frac{\dot{W}_{is}}{\dot{W}_{act}} \quad (5.42)$$

5.5.1.3 Absorption Chiller

The principle of mass conservation and the first and second laws of thermodynamics are applied to each component of the single-effect absorption chiller. In our analysis, each component is considered as a control volume with inlet and outlet streams, and heat and work interactions are considered. Mass balances are applied for the total mass and each material of the working fluid solution. The governing and conservation equations for total mass and each material of the solution for a steady state and steady flow case follow [96]:

$$\sum \dot{m}_i = \sum \dot{m}_o \quad (5.43)$$

$$\sum (\dot{m}x)_i = \sum (\dot{m}x)_0 \quad (5.44)$$

Here, $\dot{m}$ is the working fluid mass flow rate and x is mass concentration of Li-Br in the solution. For each component of the absorption system, a general energy balance is written as

$$\dot{Q} - \dot{W} = \sum \dot{m}_o h_o - \sum \dot{m}_i h_i \quad (5.45)$$

The cooling load of the absorption chiller is defined as

$$\dot{Q}_{cooling} = \dot{m} \times (h_{22} - h21) \quad (5.46)$$

Further information about the thermodynamic modeling and energy balances for each component is given in [97].

5.5.1.4 Domestic water heater

The hot gases from the heat recovery heat exchanger enter the water heater to warm domestic hot water to 60 ^{o}C. Water enters this heater at a pressure and temperature of 3 bar and 20 ^{o}C, respectively. The energy balance for this component is given as follows:

$$\dot{m}_{w,LP}(h_{15} - h_{16}) = \dot{m}_{w}(h_{18} - h_{17}) \quad (5.47)$$

5.5.1.5 Organic Rankine Cycle

The hot flue gases leaving the HRSG still have energy that can be utilized in a heat recovery vapor generator in an organic Rankine cycle to produce both cooling and electricity. Energy balances and governing equation for various components of ORC cycle (see Fig. 4.1) are provided below.

5.5.1.5.1 Ejector

An ejector, which is a type of pump, uses the Venturi effect of a converging-diverging nozzle to convert the mechanical energy (pressure) of a motive fluid to kinetic energy (velocity), creating a low pressure zone that draws in and entrains a suction fluid. After passing through the throat of the injector, the mixed fluid expands and the velocity is reduced, recompressing the mixed fluids by converting velocity back to pressure. The motive fluid may be a liquid, steam or any other gas.

The process occurring in the ejector (Fig. 5.4) is assumed to be steady state, one dimensional and adiabatic, and no work is done during the process. The velocities at the inlet and outlet of the ejector can be considered negligible [98]. For simplicity the effect of losses in the nozzle, mixing section and diffuser are accounted for by the efficiency for each section of the ejector. In this study, the primary motive flow enters the ejector at point 30, and the suction flow exits the evaporator at point 32. The process in the ejector includes the expansion of the high pressure prime motive flow through the nozzle, mixing with the low pressure secondary flow in the mixing section at constant pressure, and diffusing to the outlet of the ejector (point 33) while the kinetic energy of the mixture is converted to the pressure head. An important parameter for the secondary flow is the entrainment ratio, defined as

$$\omega = \frac{\dot{m}_{32}}{\dot{m}_{30}} \quad (5.48)$$

In the nozzle section in Fig. 5.4, the inlet velocity of primary flow $V_{\mathrm{pf,n1}}$ is negligible, so the exit enthalpy and velocity of primary flow can be expressed as

$$V_{pf,n_2} = \sqrt{2\eta_{Noz}(h_{pf,n_1} - h_{pf,n_2,s})} \quad (5.49)$$

where h_{pf,n_1} is the enthalpy at point 30 and $h_{pf,n_2,s}$ is the exit enthalpy of the primary flow under isentropic expansion and η_{Noz} is the nozzle efficiency.

The momentum conservation equation for the mixing chamber area is

$$\dot{m}_{30}V_{pf,n_2} + \dot{m}_{32}V_{sf,n_2} = (\dot{m}_{30} + \dot{m}_{32})V_{mf,m,s} \quad (5.50)$$

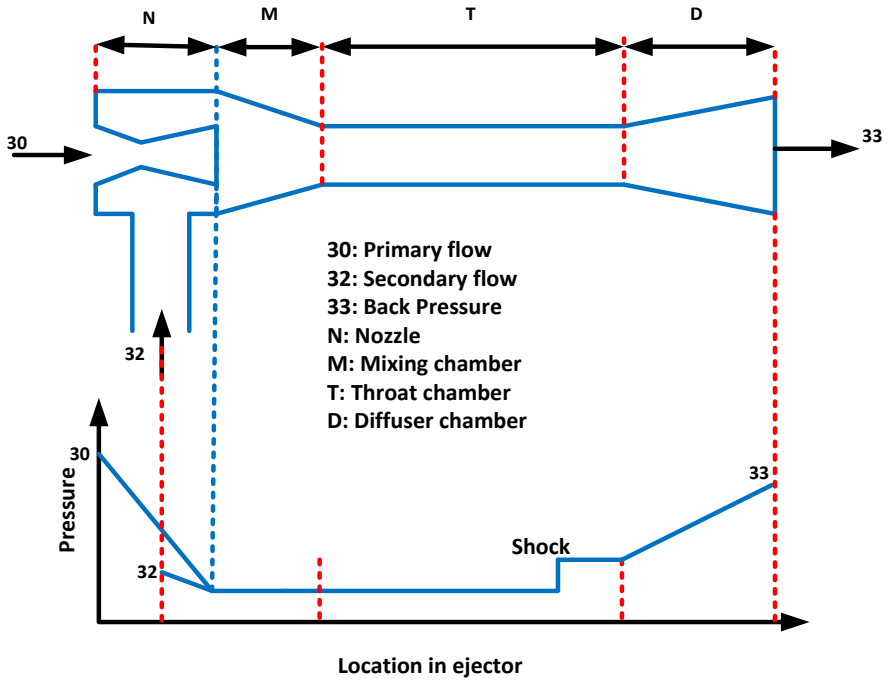

Figure 5.4: Pressure profile in the ejector for system I (modified from [98]).

Neglecting the secondary flow velocity V_{sf,n_2} compared to the primary flow velocity V_{pf,n_2}, the exit velocity of mixed flow $V_{mf,m,s}$ can be expressible as

$$V_{mf,m,s} = \frac{V_{pf,n_2}}{1+\omega} \quad (5.51)$$

The mixing chamber efficiency can be expressed as

$$\eta_{Mix} = \frac{V_{mf,m}^2}{V_{mf,m,s}^2} \quad (5.52)$$

Therfore, the actual velocity of the mixed flow is expressed as

$$V_{mf,m} = \frac{V_{pf,n2}\sqrt{\eta_{Mix}}}{1+\omega} \quad (5.53)$$

The energy equation for the mixing chamber gives

$$\dot{m}_{30}\left(h_{pf,n_2}+\frac{V_{pf,n_2}^2}{2}\right)+\dot{m}_{32}\left(h_{sf,n_2}+\frac{V_{sf,n_2}^2}{2}\right)=\dot{m}_{33}(h_{mf,m}+\frac{V_{mf,m}^2}{2}) \quad (5.54)$$

By simplifying this equation and using equation. (5.48) and (5.53), the enthalpy of mixed flow is obtained:

$$h_{mf,m}=\frac{h_{pf,n_1}+\omega h_{sf,n_2}}{1+\omega}-\frac{V_{mf,m}^2}{2} \quad (5.55)$$

In the diffuser section, the mixed flow converts its kinetic energy to a pressure increase. Assuming the exit velocity of the mixed flow to be negligible and considering the diffuser efficiency, the actual exit enthalpy of the mixed flow is calculated as

$$h_{33}=h_{mf,m}+(h_{mf,d,s}-h_{mf,m})/\eta_{Dif} \quad (5.56)$$

where $h_{mf,d,s}$ is the ideal exit enthalpy of the mixed flow with isentropic compression, and η_{Dif} is the diffuser efficiency.

Using these equations, the entrainment ratio is expressed as [98]:

$$\omega=\sqrt{\eta_{Noz}\eta_{Mix}\eta_{Dif}\frac{h_4-h_a}{h_5-h_b}}-1 \quad (5.57)$$

where $\eta_{Noz}, \eta_{Mix}, \eta_{Dif}$ are the nozzle, mixing chamber and diffuser efficiencies. The flow chart of the ejector modeling is shown in Fig. 5.5.

5.5.1.5.2 Heat recovery vapor generator (HRVG)

As shown in Fig. 4.1, R123 vapor is generated in the HRVG using the hot flue gases leaving the HRSG. An energy rate balance for this component is written as

$$\dot{m}_4 C_p(T_d-T_{28})=\dot{m}_{ORC}(h_{29}-h_{41}) \quad (5.58)$$

5.5.1.5.3 ORC turbine

Saturated vapor at point 29 enters an ORC turbine and part of this vapor leaves the ORC turbine to drive the ejector. Writing the energy rate balance for a control volume around the ORC turbine gives

$$\dot{W}_{ORC,T}=\dot{m}_{29}h_{29}-\dot{m}_{30}h_{30}-\dot{m}_{31}h_{31} \quad (5.59)$$

5.5.1.5.4 Preheater

The hot vapor leaving the ejector at point 34 enters a preheater to increase the temperature of the working fluid at point 40. An energy rate balance for this component can be written as

$$\dot{m}_{34}(h_{34} - h_{35}) = \dot{m}_{40}(h_{40} - h_{41}) \quad (5.60)$$

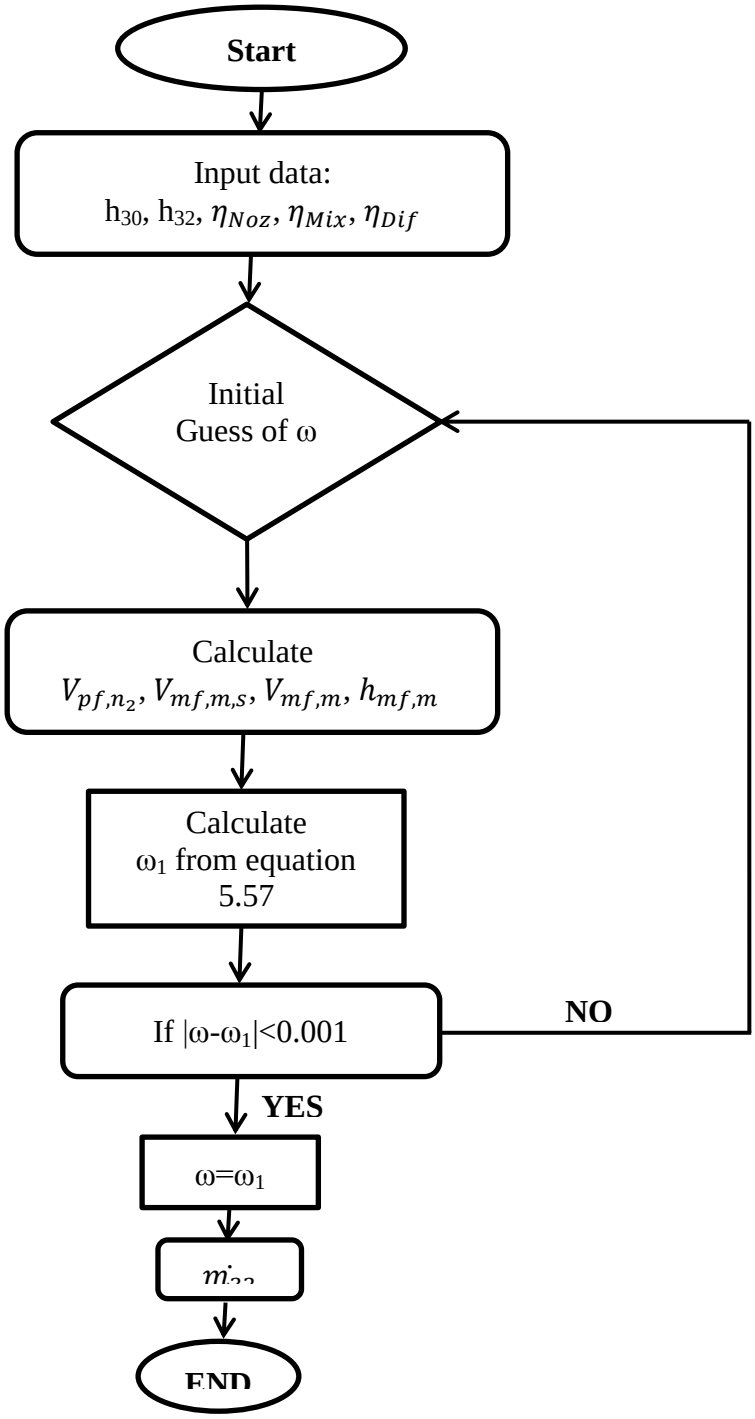

Figure 5.5: Ejector modeling flowchart.

5.5.1.5.5 Condenser

The saturated vapor leaving the preheater at point 35 enters the condenser. The saturated liquid leaves the condenser and is divided into two branches: one to an ORC pump to return to the ORC cycle and another to an expansion valve to provide the cooling capacity of the system. An energy rate balance for the condenser can be written as

$$\dot{Q}_{Cond} = \dot{m}_{35}(h_{35} - h_{36}) \quad (5.61)$$

5.5.1.5.6 ORC pump

The ORC pump work can be expressed using an energy rate balance for a control volume around the ORC pump as follows:

$$\dot{W}_{ORC,Pump} = \dot{m}_{ORC}(h_{40} - h_{37}) \quad (5.62)$$

5.5.1.5.7 Expansion valve

An energy balance for the expansion valve gives

$$h_{38} = h_{39} \quad (5.63)$$

5.5.1.5.8 Evaporator

As shown in Fig. 4.1, an evaporator is used for district cooling. An energy rate balance for this component is written as

$$\dot{Q}_{Cooling} = \dot{m}_{32}(h_{32} - h_{39}) \quad (5.64)$$

5.5.1.6 PEM Electrolyzer

Hydrogen as an energy carrier can facilitate sustainable energy systems. The development of sustainable carbon-neutral energy sources has become one of the most significant issues in the world today. Hydrogen can be produced from various energy sources using methods like biomass conversion, steam methane reforming and water splitting. Hydrogen can be produced in a relatively environmentally benign manner (depending on the source of the input energy) via splitting water by photocatalysis, thermochemical cycles and electrolysis. Currently, both thermochemical and photocatalysis hydrogen production are not economically competitive. Water electrolysis is a mature technology for large scale hydrogen production. Hydrogen production by proton exchange membrane (PEM) electrolysis has numerous advantages, such as low environmental impact and easy maintenance.

The PEM electrolyzer for H_2 production is illustrated on the right side of Fig. 4.1. During electrolysis, electricity and heat are both supplied to the electrolyzer to drive the electrochemical reactions. As shown in Fig. 4.1, liquid water is fed to the PEM electrolyzer at ambient temperature, and enters a heat exchanger that heats it to the PEM electrolyzer temperature before it enters the electrolyzer. Leaving the cathode, the H_2 produced dissipates heat to the environment and cools to the reference environment temperature. The oxygen gas produced at the anode is separated from the water and oxygen mixture and then cooled to the reference environment temperature. The remaining water is returned to the water supply stream for the next hydrogen production cycle. The overall PEM electrolysis reaction is simply water splitting, i.e., electricity and heat are used to separate water into hydrogen and oxygen. Hydrogen is stored in a tank for later usage. Thermochemical modeling is carried out for the PEM electrolyzer, along with energy and exergy analyses. The total energy needed by the electrolyzer can obtained as

$$\Delta H = \Delta G + T\Delta S \tag{5.65}$$

where ΔG is Gibb's free energy and $T\Delta S$ represents the thermal energy requirement. The values of G, S, and H for hydrogen, oxygen and water can be obtained from thermodynamic tables. The total energy need is the theoretical energy required for H_2O electrolysis without any losses. The catalyst used in PEM electrolysis provides an alternative path for the reaction with lower activation energy. The mass flow rate of hydrogen is determined by [99]:

$$\dot{N}_{H_2,out} = \frac{J}{2F} = \dot{N}_{H_2O,reacted} \tag{5.66}$$

Here, J is the current density and F is the Faraday constant. The PEM electrolyzer voltage can be expressed as

$$V = V_0 + V_{act,a} + V_{act,c} + V_{ohm} \tag{5.67}$$

where V_0 is the reversible potential, which is related to the difference in free energy between reactants and products and can be obtained with the Nernst equation as follows:

$$V_0 = 1.229 - 8.5 \times 10^{-4}(T_{PEM} - 298) \tag{5.68}$$

Here, $V_{act,a}$, $V_{act,c}$ and V_{ohm} are the activation overpotential of the anode, the activation overpotential of the cathode, and the ohmic overpotential of the electrolyte, respectively. Ohmic overpotential in the proton exchange membrane (PEM) is caused by the resistance of the membrane to the hydrogen ions transported through it. The ionic resistance of the membrane

depends on the degree of humidification and thickness of the membrane as well as the membrane temperature. The local ionic conductivity $\sigma(\mathrm{x})$ of the proton exchange membrane is expressed as [100]:

$$\sigma_{PEM}[\lambda(x)] = [0.5139\lambda(x) - 0.326]\exp\left[1268\ \left(\frac{1}{303} - \frac{1}{T}\right)\right] \quad (5.69)$$

where x is the distance into the membrane measured from the cathode-membrane interface and $\lambda(\mathrm{x})$ is the water content at a location x in the membrane. The value of $\lambda(\mathrm{x})$ can be calculated in terms of the water content at the membrane-electrode edges:

$$\lambda(x) = \frac{\lambda_a - \lambda_c}{D}\ x + \ \lambda_c \quad (5.70)$$

Here, D is the membrane thickness, and λ_a and λ_c are the water contents at the anode-membrane and the cathode-membrane interfaces, respectively. The overall ohmic resistance can thus be expressed as [100]:

$$R_{PEM} = \int_0^D \frac{dx}{\sigma_{PEM}[\lambda(x)]} \quad (5.71)$$

Based on the Ohm's law, the following equation can be written for the ohmic overpotential:

$$V_{ohm,PEM} = JR_{PEM} \quad (5.72)$$

The activation overpotential, V_{act}, caused by a deviation of net current from its equilibrium and an electron transfer reaction, must be differentiated from the concentration of the oxidized and reduced species. Then,

$$V_{act,i} = \frac{RT}{F}\ \sinh^{-1}\left(\frac{J}{2J_{0,i}}\right)\ ,\ i = a, c \quad (5.73)$$

Here, J_o is the exchange current density, which is an important parameter in calculating the activation overpotential. It characterizes the electrode's capabilities in the electrochemical reaction. A high exchange current density implies a high reactivity of the electrode, which results in a lower overpotential. The exchange current density for electrolysis can be expressed as [99]

$$J_{0,i} = J_i^{ref} exp\left(-\frac{V_{act,i}}{RT}\right)\ ,\ i = a, c \quad (5.74)$$

where J_i^{ref} is the pre-exponential factor and $V_{act,i}$ is the activation energy for the anode and cathode. Further details about PEM electrolysis modeling can be found elsewhere [99, 100].

5.5.2 Exergy analysis

In this section, exergy balance equation for system I is presented using the formula provided in section 5.4.

5.5.2.1 Exergy balance equations of a gas turbine based multigeneration system

Here, the exergy of each flow is calculated at all states and the changes in exergy are determined for each major component. The exergy destructions for all components in this multigeneration system are shown in Table 5.2. Since in this multigeneration energy system, a combustion reaction occurs in combustion chamber, it is important to calculate the chemical exergy where combustion takes place and where the solution is not real such as LiBr solution. Chemical exergy is equal to the maximum amount of work that can be obtained when a substance is brought from the reference-environment state to the dead state by a process including heat transfer and exchange of substances only with the reference environment. The maximum work is attained when the process is reversible. Alternatively, chemical exergy can also be viewed as the exergy of a substance that is at the reference-environment state.

Chemical exergy is also equivalent to the minimum amount of work necessary to produce a substance at the reference-environment state from the constituents in the reference environment. Chemical exergy has two main parts, reactive exergy resulting from the chemical reactions necessary to produce species which do not exist as stable components in the reference environment, and concentration exergy resulting from the difference between the chemical concentration of a species in a system and its chemical concentration in the reference environment [47]. The concentration part is related to the exergy of purifying or diluting a substance, such as separating oxygen from air.

As shown in Fig. 4.1, combustion reaction occurs in combustion chamber where the energy of fuel is converted to increase the temperature at gas turbine inlet temperature. Since chemical component of the gasses leaving the combustion chamber differ from the one in the reference environment, we should use chemical exergy of mixture to calculate the chemical exergy at at point 3 in Fig. 4.1.Therefore, we should first define the partial pressures and molar fractions of various constituents of air. The partial pressure P_i and molar fraction of each of these substances in air at a given relative humidity is given in Table 5.3.

Table 5.2: Expressions for exergy destruction rates for components of the system.

Component	**Exergy destruction rate expression**
Air compressor	$\dot{E}x_{D,AC} = \dot{E}x_1 - \dot{E}x_2 - \dot{W}_{AC}$
Combustion chamber (CC)	$\dot{E}x_{D,CC} = \dot{E}x_2 + \dot{E}x_f - \dot{E}x_3$
Gas turbine (GT)	$\dot{E}x_{D,GT} = \dot{E}x_3 - \dot{E}x_4 - \dot{W}_{GT}$
HRSG	$\dot{E}x_{D,HRSG} = \dot{E}x_4 + \dot{E}x_8 - \dot{E}x_5 - \dot{E}x_c$
Steam turbine (ST)	$\dot{E}x_{D,ST} = \dot{E}x_5 - \dot{E}x_6 - \dot{W}_{ST}$
Steam condenser	$\dot{E}x_{D,Cond} = \dot{E}x_6 + \dot{E}x_{49} - \dot{E}x_7 - \dot{E}x_{50}$
Pump	$\dot{E}x_{D,P} = \dot{E}x_7 - \dot{E}x_8 + \dot{W}_P$
Heat recovery vapor generator	$\dot{E}x_{D,HRVG} = \dot{E}x_c + \dot{E}x_{41} - \dot{E}x_{28} - \dot{E}x_{29}$
ORC turbine	$\dot{E}x_{D,ORC\,T} = \dot{E}x_{29} - \dot{W}_{ORC} - \dot{E}x_{30} - \dot{E}x_{31}$
Ejector	$\dot{E}x_{D,Ejector} = \dot{E}x_{30} + \dot{E}x_{32} - \dot{E}x_{33}$
Preheater	$\dot{E}x_{D,PRH} = \dot{E}x_{34} + \dot{E}x_{40} - \dot{E}x_{35} - \dot{E}x_{41}$
ORC pump	$\dot{E}x_{D,ORC\,Pump} = \dot{E}x_{37} + \dot{W}_{ORC} - \dot{E}x_{40}$
ORC condenser	$\dot{E}x_{D,Cond} = \dot{E}x_{35} - \dot{E}x_{36} - \dot{E}x_{Q,Cond}$
ORC evaporator	$\dot{E}x_{D,EVP} = \dot{E}x_{39} + \dot{E}x_{40} - \dot{E}x_{32} - \dot{E}x_{41}$
ORC expansion valve	$\dot{E}x_{D,EXV} = \dot{E}x_{38} - \dot{E}x_{39}$
Domestic water heater	$\dot{E}x_{D,DWH} = \dot{E}x_{15} + \dot{E}x_{17} - \dot{E}x_{16} - \dot{E}x_{18}$
PEM electrolyzer	$\dot{E}x_{D,PEM} = \dot{E}x_{44} + \dot{W}_{PEM} - \dot{E}x_{46} - \dot{E}x_{47} + \dot{E}x_Q$
Absorption condenser	$\dot{E}x_{D,Cond} = \dot{E}x_{19} - \dot{E}x_{20} - \dot{E}x_Q$
Absorption expansion valve	$\dot{E}x_{D,EXV} = \dot{E}x_{20} - \dot{E}x_{21}$
Absorption evaporator	$\dot{E}x_{D,EVP} = \dot{E}x_{21} - \dot{E}x_{22} + \dot{E}x_Q$
Absorber	$\dot{E}x_{D,Abs} = \dot{E}x_{22} + \dot{E}x_{23} - \dot{E}x_{25} - \dot{E}x_Q$
Absorption pump	$\dot{E}x_{D,P} = \dot{E}x_{25} + \dot{W}_P - \dot{E}x_{26}$
Absorption heat exchanger	$\dot{E}x_{D,HEX} = \dot{E}x_{26} + \dot{E}x_{14'} - \dot{E}x_{24} - \dot{E}x_{27}$
Absorption generator	$\dot{E}x_{D,Gen} = \dot{E}x_{14} + \dot{E}x_{27} - \dot{E}x_{15} - \dot{E}x_{14'} - \dot{E}x_{19}$

Table 5.3: Partial pressures and molar fractions of various constituents of air [47].

Component	P_i (kPa)	Molar fraction (%)
N_2	75.78	75.67
O_2	20.39	20.34
CO_2	0.00335	0.03
H_2O	2.2	3.03
He	0.00048	0.00052
Ne	0.00177	0.0018
Ar	0.906	0.92
Kr	0.000097	0.000076

Using combustion reaction for a control volume around the combustion chamber (equation (5.28)), the mole fraction of the flue gases leaving the combustion chamber can be easily calculated. Therefore, using the following equation, chemical exergy of the flue gases is determined as

$$\overline{ex}_{ch} = \sum x_k \overline{ex}^k_{ch} + RT_0 \sum x_k \ln(x_k) \quad (5.75)$$

where x_k is the molar fraction of each constituent which was calculated in equation (5.28) and $\overline{ex}^k_{ch}$ is standard molar chemical exergy. The standard chemical exergy for selected substances are listed in Table 5.5.

For the absorption cooling system, because water and Li-Br solution is not an ideal, the following expression is used for the chemical exergy calculation as follows:

$$\overline{ex}_{ch} = (1/\bar{M}_{sol})\left[\sum_{i=1}^{n} y_i \, \overline{ex}^k_{ch} + \bar{R}\, T_0 \, \sum_{i=1}^{n} y_i \ln(a_i)\right] \quad (5.76)$$

Extending this equation for LiBr water solution we obtain:

$$\overline{ex}_{ch} = (1/\bar{M}_{sol})\left[\begin{array}{c} y_{\mathrm{H_2O}}\, \overline{ex}^0_{\mathrm{H_2O}} + y_{\mathrm{LiBr}}\, \overline{ex}^0_{\mathrm{LiBr}} + \\ \bar{R}\, T_0\, (y_{\mathrm{H_2O}} \ln(\mathrm{a_{H_2O}}) + y_{\mathrm{LiBr}} \ln(\mathrm{a_{LiBr}}) \end{array}\right] \quad (5.77)$$

Here, $\mathrm{a_{H_2O}}$ is water activity defined as vapor pressure of water in the mixture divided by vapor pressure of pure water and $\mathrm{a_{LiBr}}$ is LiBr activity defined as vapor pressure of LiBr in the mixture divided by vapor pressure of LiBr. This equation consists of two parts, standard chemical exergy of pure species and exergy due to dissolution process defined as follows:

$$\overline{ex}^0_{ch} = \frac{1}{\bar{M}_{sol}} (y_{\mathrm{H_2O}}\, \overline{ex}^0_{\mathrm{H_2O}} + y_{\mathrm{LiBr}}\, \overline{ex}^0_{\mathrm{LiBr}}) \quad (5.78)$$

$$\overline{ex}^{dis}_{ch} = \frac{RT_0}{\bar{M}_{sol}} \left[y_{\mathrm{H_2O}} \ln(\mathrm{a_{H_2O}}) + y_{\mathrm{LiBr}} \ln(\mathrm{a_{LiBr}})\right] \quad (5.79)$$

where y_i is the molar fraction defined as

$$y_{\mathrm{H_2O}} = \frac{(1-x_{1w})\bar{M}_{LiBr}}{(1-x_{1w})\bar{M}_{LiBr}+x_{1w}\bar{M}_{\mathrm{H_2O}}} \quad (5.80)$$

$$y_{\mathrm{LiBr}} = 1 - y_{\mathrm{H_2O}} \quad (5.81)$$

Here, x_{1w} is defined as

$$x_{1w} = \frac{x_{LiBr}}{100} \quad (5.82)$$

where x_{LiBr} is the LiBr water solution concentration in percent and $\bar{M}_{LiBr}$ and $\bar{M}_{\mathrm{H_2O}}$ are 86.85 kg/kmol and 18.02 kg/kmol respectively.

Table 5.4: Standard chemical values for selected substances at T_0 = 298.15 K and P_0 = 1 atm [47, 101].

Element	$\overline{ex}^0_{ch}$ (kJ/mol)	Element	$\overline{ex}^0_{ch}$ (kJ/mol)
Ag (s)	70.2	Kr (g)	34.36
Al (s)	888.4	Li (s)	393.0
Ar (s)	11.69	Mg (s)	633.8
As (s)	494.6	Mn (s_α)	482.3
Au (s)	15.4	Mo (s)	730.3
B (s)	628.8	N_2 (g)	0.72
Ba (s)	747.4	Na (s)	336.6
Bi (s)	274.5	Ne (g)	27.19
Br_2 (l)	101.2	Ni (s)	232.7
C (s, graphite)	410.26	O_2 (g)	3.97
Ca (s)	712.4	P (s, red)	863.6
Cd (s_α)	293.2	Pb (s)	232.8
Cl_2 (g)	123.6	Rb (s)	388.6
Co (s_α)	265.0	S (s, rhombic)	609.6
Cr (s)	544.3	Sb (s)	435.8
Cs (s)	404.4	Se (s, black)	346.5
Cu (s)	134.2	Si (s)	854.6
D_2 (g)	263.8	Sn (s, white)	544.8
F_2 (g)	466.3	Sn (s)	730.2
Fe (s_α)	376.4	Ti (s)	906.9
H_2 (g)	236.1	U (s)	1190.7
He (g)	30.37	V (s)	721.1
Hg (l)	115.9	W (s)	827.5
I_2 (s)	174.7	Xe (g)	40.33
K (s)	366.6	Zn (s)	339.2

To calculate the chemical exergy for other components not listed in Table 5.4, we may refer to some reactions for which the standard chemical exergy of some components are already given in. In this case, we can calculate the chemical exergy for the new components. Since the

standard chemical exergy of Li-Br is not listed in Table 5.5, the following reaction is used in order to calculate the chemical exergy of Li-Br [101]:

$$\overline{ex}^0_{ch} = \Delta\bar{g}^0_f + \sum_{i=1}^{n} \overline{ex}^0_{ch,i} \quad (5.83)$$

$$\mathrm{Li} + \frac{1}{2}\mathrm{Br}_2 \rightarrow \mathrm{LiBr} \quad (5.84)$$

$$\overline{ex}^0_{ch,\mathrm{LiBr}} = \Delta\bar{g}^0_{f,\mathrm{LiBr}} + \overline{ex}^0_{ch,\mathrm{Li}} + \frac{1}{2}\overline{ex}^0_{ch,\mathrm{Br}_2} \quad (5.85)$$

Here, $\Delta\bar{g}^0_{f,\mathrm{LiBr}} = -324\ \frac{\mathrm{kJ}}{\mathrm{mol}}$ [97]

Fig. 5.6 shows the variation of chemical exergy as a function of LiBr mass basis concentration based on equations (5.78) and equation (5.79). As shown in this figure and increase in LiBr concentration results in an increase in total chemical exergy of LiBr water solution.

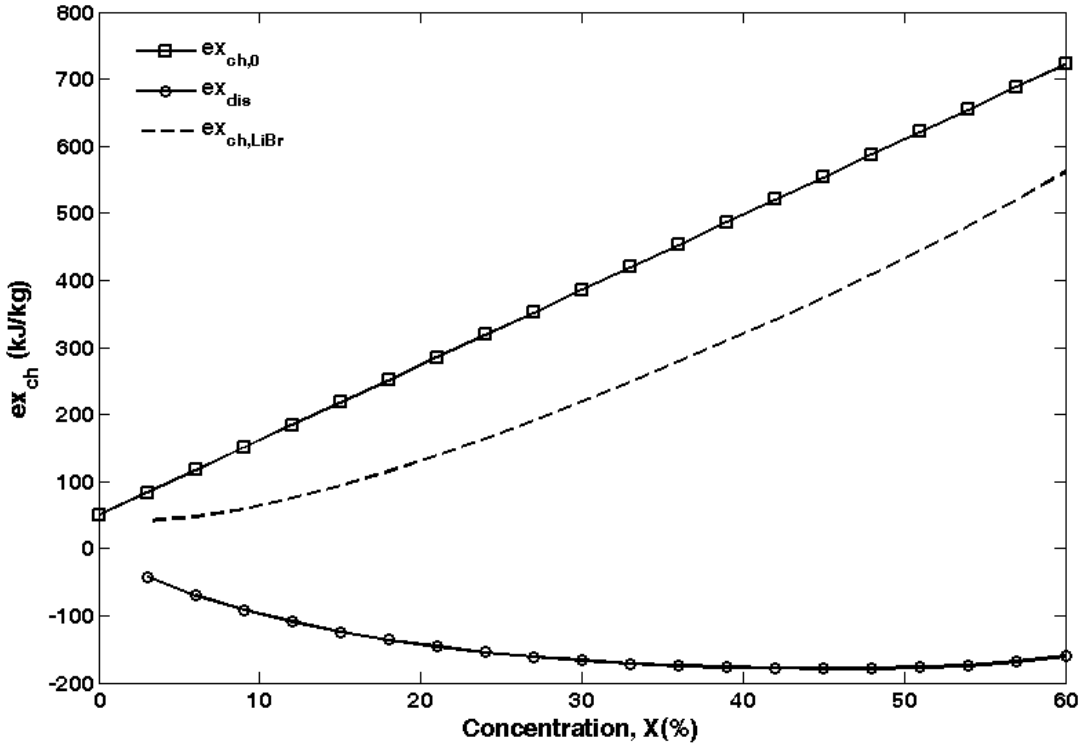

Figure 5.6: Variation of standard chemical exergy ($ex_{ch,0}$), chemical exergy due to dissolution (ex_{dis}) and total chemical exergy as a function of LiBr mass basis concentration at T0 = 25 0C.

Therefore, based on the LiBr concentration the total chemical exergy at each point of the single effect absorption chiller in Fig. 4.1 can be easily calculated using a code developed in Matlab software.

5.5.2.2 Energy efficiency

The energy, or first law, efficiency is defined as the ratio of useful energy produced by the system (cold, heat, electricity) to the input energy of the fuel supplied to the system. In this study, we consider three energy efficiencies for the system: the gas turbine cycle, the CHP portion of the system and the overall multigeneration system, i.e.,

$$\eta_{Power} = \frac{\dot{W}_{net,GT}}{\dot{m}_f LHV_f} \tag{5.86}$$

$$\eta_{CHP} = \frac{\dot{W}_{net,GT} + \dot{Q}_{heating}}{\dot{m}_f LHV_f} \tag{5.87}$$

$$\eta_{multi} = \frac{\dot{W}_{net,GT} + \dot{W}_{net,ST} + \dot{W}_{net,ORC} + \dot{Q}_{heating} + \dot{Q}_{cooling,chiller} + \dot{Q}_{cooling,ORC} + \dot{m}_{H_2} LHV_{H_2} + \dot{m}_{18} h_{18}}{\dot{m}_f LHV_f} \tag{5.88}$$

where LHV_f denotes the lower heating value of the fuel (natural gas) and is assigned a value LHV_f = 50,000 kJ/kg, $\dot{m}_f$ is the mass flow rate of the fuel entering the combustion chamber, and $\dot{W}_{net,GT}$, $\dot{W}_{net,ST}$ and $\dot{W}_{net,ORC}$ denote the net power outputs of the gas turbine cycle, the steam cycle and the ORC cycle. Also, $\dot{Q}_{heating}$ $\dot{Q}_{cooling,chiller}$ and $\dot{Q}_{cooling,ORC}$ denote the heating load of the multigeneration system, the absorption cooling load and ORC cooling load, while the last two terms in the numerator denote the energy values of the hydrogen and hot water products. It can be seen from these expressions the energy efficiency of the multigeneration system must exceed that for the gas turbine (GT) cycle. Note that the multigeneration energy efficiency is often problematic, as the cooling terms in the numerator can cause the energy efficiency to exceed 100 %; this explains in part why exergy efficiencies are more advantageous.

5.5.2.3 Exergy efficiency

The exergy efficiency, defined as the product exergy output divided by the exergy input, for the gas turbine, CHP and overall multigeneration systems, can be expressed as follows:

$$\Psi_{power} = \frac{\dot{W}_{net,GT}}{\dot{E}x_f} \tag{5.89}$$

$$\Psi_{CHP} = \frac{\dot{W}_{net,GT} + \dot{E}x_{heating}}{\dot{E}x_f} \tag{5.90}$$

$$\Psi_{multi} = \frac{\dot{W}_{net,GT}+\dot{W}_{net,ST}+\dot{W}_{net,ORC}+\dot{E}x_{heating}+\dot{E}x_{cooling,chiller}+\dot{E}x_{cooling,ORC}+\dot{E}x_{H_2}+\dot{E}x_{18}}{\dot{E}x_f} \quad (5.91)$$

Here,

$$\dot{E}x_{heating} = \dot{Q}_{cond}\left(1 - \frac{T_0}{T_{cond}}\right) \quad (5.91)$$

$$\dot{E}x_{Cooling} = \dot{Q}_{cooling}\left(\frac{T_0 - T_{EVP}}{T_{EVP}}\right) \quad (5.92)$$

$$\dot{E}x_{H_2} = \dot{m}_{H_2} ex_{H_2} \quad (5.93)$$

5.5.3 Economic analysis of system I

In order to perform the economic analysis and optimization of the three novel multigeneration systems, we should first define a purchase cost of each equipment used in the system as a function of some major design parameters. In this section, the cost function of each component and some economic parameters are defined and explained.

5.5.3.1 Investment cost of a gas turbine based multigeneration system

Investment cost of equipment is most detailed and accurate when obtained from vendors of specific models. A useful handy comprehensive methods to express the investment cost is a detailed plot of mathematical function of the variation of cost with main parameters. Alternatively, these complex data and mathematical cost functions can be presented in an approximate and compact form as listed below:

5.5.3.1.1 Brayton cycle

The investment cost of each component in the gas turbine cycle is given as follows:

- **For air compressor**

Purchase cost of air compressor is a function of air mass flow rate, compressor pressure ratio and compressor isentropic efficiency the cost function can be expressible as follows [102]:

$$Z_{AC}(\$) = C_{11}\dot{m}_{air}\frac{1}{C_{12} - \eta_{AC}}\left(\frac{P_2}{P_1}\right)\ln\left(\frac{P_2}{P_1}\right) \quad (5.94)$$

$$C_{11} = 44.71\,\frac{\$}{\frac{kg}{s}}\,, C_{12} = 0.95 \quad (5.95)$$

- **For combustion chamber (CC)**

Combustion chamber in gas turbine cycle is the main part as the fuel burnt to produce high temperature flue gases. Purchase cost of combustion chamber is a function of air mass flow rate entering the chamber, and gas turbine inlet temperature (GTIT), the expression of the purchases cost of combustion chamber is expressed as

$$Z_{CC}(\$) = C_{21}\dot{m}_{air}\{1 + \exp[C_{22}(T_3 - C_{23})]\}\frac{1}{0.995-\frac{P_3}{P_2}} \quad (5.96)$$

$$C_{21} = 28.98\,\frac{\$}{\frac{kg}{s}}\,, C_{22} = 0.015\,\frac{1}{K}, C_{23} = 1540 \quad (5.97)$$

- **For gas turbine (GT)**

Purchase cost of gas turbine is a function of inlet gas mass flow rate, gas turbine pressure ratio and gas turbine isentropic efficiency. The cost function can be defined as follows [102]:

$$Z_{GT}(\$) = C_{31}\dot{m}_{gas}\frac{1}{C_{32}-\eta_{GT}}\ln(\frac{P_3}{P_4})\{1 + \exp[C_{33}(T_3 - 1570)]\} \quad (5.98)$$

$$C_{31} = 301.45\,\frac{\$}{\frac{kg}{s}}\,, C_{32} = 0.95, C_{23} = 0.025\,\frac{1}{K} \quad (5.99)$$

5.5.3.1.2 Steam cycle

Exhaust gases leaving the gas turbine at point 4 still have energy to produce vapor at point 5. The steam cycle in this multigeneration system consists of a doula pressure heat recovery steam generator (HRSG), a steam turbine, a condenser and a pump. The purchase cost of each component can be calculated as follows:

- **For heat recovery steam generator (HRSG)**

Purchase cost of a double pressure HRSG is a function of several design parameters such as high and low pressure, high and low pressure mass flow rate and flue gas mass flow rate passing over each pressure level. The cost function of a double pressure HRSG can be expressed as follows [102]:

$$Z_{HRSG}(\$) = C_{41}\sum_i\left[f_{p,i}\,f_{T,steam,i}\,f_{T,gas,i}\left(\frac{\dot{Q}}{\Delta T_{ln,i}}\right)^{0.8}\right] + C_{42}\sum_j(f_{p,j}\dot{m}_{steam,j}) + C_{43}\dot{m}_{gas}^{1.2}$$

(5.100)

$$f_{p,i} = 0.0971\ \frac{P_i}{30\ bar} + 0.9029 \tag{5.101}$$

$$f_{T,steam,i} = 1 + \exp(\frac{T_{out,steam,i} - 830}{500\ K}) \tag{5.102}$$

$$f_{T,gas,i} = 1 + \exp(\frac{T_{out,gas,i} - 990}{500\ K}) \tag{5.103}$$

$$C_{41} = 4131.8 \frac{\$}{\left(\frac{kW}{K}\right)^{0.8}}, C_{42} = 13380 \frac{\$}{\frac{kg}{s}}, C_{43} = 1489.7\ \frac{\$}{\frac{kg}{s}} \tag{5.104}$$

- **For steam turbine**

The purchase cost of steam turbine is the function of turbine inlet temperature, steam turbine isentropic efficiency and turbine work which can be expressed as follows:

$$Z_{ST}(\$) = C_{51}\left(\dot{W}_{ST}\right)^{0.7}\left[1 + \left(\frac{0.05}{1-\eta_{ST}}\right)^3\right]\left\{1 + \exp(\frac{T_5 - 866\ K}{10.42\ K})\right\} \tag{5.105}$$

$$C_{31} = 3880.5 \frac{\$}{kW^{0.7}} \tag{5.106}$$

- **For condenser**

To calculate the purchase cost of condenser the following expression can be used:

$$Z_{Cond}(\$) = C_{61} \frac{\dot{Q}_{cond}}{k\Delta T_{\ln}} + C_{62}\dot{m}_{CW} \tag{5.107}$$

$$C_{61} = 280.74 \frac{\$}{m^2}, C_{62} = 746 \frac{\$}{\frac{kg}{s}}, k = 2200 \frac{W}{m^2 K} \tag{5.108}$$

Here, $\dot{m}_{CW}$ is the cooling water mass flow rate and $\Delta T_{\ln}$ is the logarithmic temperature difference.

- **For pump**

The purchase cost of pump is defined as follows:

$$Z_{Pump}(\$) = C_{71}\left(\dot{W}_P\right)^{0.71}(1 + \frac{0.2}{1-\eta_P}) \tag{5.109}$$

$$C_{71} = 705.48 \frac{\$}{kW} \tag{5.110}$$

5.5.3.1.3 ORC cycle

The ORC cycle shown in Fig. 4.1, has several component. The purchase cost of each component in the ORC cycle can be expressed as the following sections:

- **For heat recovery vapor generator (HRVG)**

The purchase cost of HRVG can be calculated as follows [103]:

$$Z_{HRVG}(\$) = 1010\ (A_{HRVG})^{0.8} \tag{5.111}$$

where

$$A_{HRVG} = \frac{\dot{m}_{28}\, Cp_g (T_C - T_{28})}{U_{HRVG} \Delta T_{\ln}} \tag{5.112}$$

Here, U_{HRVG} is the overall heat transfer coefficient for HRVG with the value of $0.88k\ \frac{W}{m^2K}$.

- **For ORC turbine**

The cost function of the ORC turbine can be calculated using the following formula [103]:

$$Z_T(\$) = 4750\ \left(\dot{W}_T\right)^{0.75} \tag{5.113}$$

Here, $\dot{W}_T$ is the work generated by the turbine in kW.

- **For ejector**

The purchase cost of ejector is the function of motive mass flow rate, inlet motive temperature and pressure and the outlet pressure. The cost function can be expressible as follows [104]:

$$Z_{Ejector}(\$) = 1000 \times 15.96 \dot{m}_{30} \left(\frac{T_{30}+273.15}{\frac{P_{30}}{1000}}\right)^{0.05} \left(\frac{P_{33}}{1000}\right)^{-0.75} \tag{5.114}$$

where P is pressure in kPa and T is temperature in ^{0}C.

- **For evaporator**

The purchase cost of ORC evaporator can be calculated as follows [103]:

$$Z_{EVP}(\$) = 309.14(A_{EVP})^{0.85} \tag{5.115}$$

where

$$A_{EVP} = \frac{\dot{Q}_{EVP}}{U_{EVP} \Delta T_{\ln}} \tag{5.116}$$

Here, U_{EVP} is the overall heat transfer coefficient for evaporator with the value of $0.2\ \frac{kW}{m^2K}$.

- **For expansion valve**

The purchase cost of expansion valve can be expressible as follows [103]:

$$Z_{EXV}(\$) = 37\ \left(\frac{P_{38}}{P_{39}}\right)^{0.68} \tag{5.117}$$

- **For preheater**

The cost function of a preheater in ORC cycle can be treated as a heat exchanger that can be calculated as [103]:

$$Z_{Preheater}(\$) = 1000(A_{preheater})^{0.65} \quad (5.118)$$

where

$$A_{preheater} = \frac{\dot{Q}_{preheater}}{U_{preheater}\Delta T_{\ln}} \quad (5.119)$$

Here, $U_{preheater}$ is the overall heat transfer coefficient for preheater with the value of $0.85\ \frac{kW}{m^2K}$.

- **For condenser**

The purchase cost of ORC condenser can be calculated as follows [103]:

$$Z_{Cond}(\$) = 516.62(A_{Cond})^{0.6} \quad (5.120)$$

where

$$A_{EVP} = \frac{\dot{Q}_{Cond}}{U_{Cond}\Delta T_{\ln}} \quad (5.121)$$

Here, U_{Cond} is the overall heat transfer coefficient for evaporator with the value of $0.15\ \frac{kW}{m^2K}$.

- **For pump**

The following expression is used to calculate the cost of ORC pump:

$$Z_{Pump}(\$) = 200(\dot{W}_P)^{0.65} \quad (5.122)$$

5.5.3.1.4 Absorption chiller

The purchase cost of absorption chiller is a function of all the design parameters of the chiller that can be compacted and approximated as function of the cooling load of the chiller as follows [79]:

$$Z_{chiller}(\$) = 1144.3(\dot{Q}_{EVP})^{0.67} \quad (5.123)$$

Here, $\dot{Q}_{EVP}$ is the cooling load of the absorption chiller in kW that can be calculated using the energy balance for the control volume around the evaporator shown in Fig. 4.1.

5. 5.3.1.5 PEM electrolyzer

The purchase cost of the electrolyzer is a function of the inlet electricity to split water which can be expressed as [105]:

$$Z_{PEM}(\$) = 1000\dot{W}_{PEM} \quad (5.124)$$

5. 5.3.1.6 Domestic water heater (DWH)

The cost function of the domestic water heater considered in this system can be expressed as follows [103]:

$$Z_{DWH}(\$) = 0.3m_{DWH} \quad (5.125)$$

Here, m_{DWH} is the hot water production in m^3 that is calculated using the energy balance equation for a control volume around the DWH.

5.5.3.2 Capital recovery factor (CRF)

A capital recovery factor is the ratio of a constant annuity to the present value of receiving that annuity for a given length of time [90]. Using an interest rate *i*, the capital recovery factor is defined as

$$CRF = \frac{i\times(1+i)^n}{(1+i)^n-1} \quad (5.126)$$

Here, *i* denotes the interest rate and *n* the total operating period of the system in years.

5.5.3.3 Cost rate

Since each device in a system is expected to be working in a specific time frame, the cost rate of each device is a good indicator to calculate the cost rate in \$/s represented by $\dot{Z}$. The cost rate of each device is determined as

$$\dot{Z} = \frac{Z_k CRF \Phi}{N\times 3600} \quad (5.127)$$

where Z_k is the purchase cost of the k^{th} component, and *CRF* is the capital recovery factor explained in equation (5.126). Also, *N* is the annual number of operation hours for the unit, and φ is the maintenance factor, which is often 1.06 [90].

5.5.3.4 Cost of environmental impact

The desire of preserving the environment while converting energy resources into different forms can be assessed quantitatively using an environmental index of performance. The outputs of the energy conversion process are not only the desired products like electricity, heating and cooling, but also pollutant emissions (e.g., NO_x and CO), CO_2 emissions, thermal pollution (e.g., warming of local water bodies), solid wastes, etc. Reduction or minimization of these undesired effects may be an objective from an energetic perspective. A single pollutant can be considered in such an environmental impact assessment objective according to its degree of harmfulness. If more than one pollution source is taken into account, their degrees of harmfulness can be introduced as relative weights of each pollutant measure. The weighting may also be considered from economic point of view when the unit damage cost of each pollutant is available. These criteria can also be combined to form a hybrid criterion which includes information from each.

5.5.4 Environmental impact assessment

5.5.4.1 Normalized CO_2 emissions

To assess CO_2 emissions for the system, three cases are considered and the CO_2 emissions are calculated for each case. In the first case, the power cycle is used to produce electricity. In the second, electricity and heating systems are considered simultaneously and, in the last case, the entire system for multiple products is considered. The amount of CO_2 produced in each case can be expressed as

$$\varepsilon_{power} = \frac{\dot{m}_{CO_2}}{\dot{W}_{net}} \tag{5.128}$$

$$\varepsilon_{CHP} = \frac{\dot{m}_{CO_2}}{\dot{W}_{net}+\dot{Q}_{heating}} \tag{5.129}$$

$$\varepsilon_{multi} = \frac{\dot{m}_{CO_2}}{\dot{W}_{net}+\sum \dot{Q}_{heating}+\sum \dot{Q}_{cooling}+\dot{E}_{HW}+\dot{E}_{\mathrm{H}_2}+\dot{E}_{fresh\ water}} \tag{5.130}$$

5.5.4.2 Sustainability analysis

To improve environmental sustainability, it is necessary not only to use sustainable energy sources, but also to utilize non-renewable sources like natural gas fuel more efficiently, and to

limit environmental damage. In this way, society can reduce its use of limited resources and extend their lifetimes. Here, a sustainability index *SI* is used to relate exergy with environmental impact [47]:

$SI = 1/ D_P$ (5.131)

where D_P is the depletion number, defined as the ratio of exergy destruction to input exergy. This relation demonstrates how reducing a system's environmental impact can be achieved by reducing its exergy destruction. Also, the sustainability index is then determined as a measure of how the exergy efficiency affects sustainable development as follows:

$$SI = \frac{1}{1-\psi} \quad (5.132)$$

5.6 Analyses of system II

The analyses of system II is thermodynamic analysis, exergy and exergoeconomic analysis described as follows:

5.6.1 Thermodynamic analysis

The thermodynamic modeling of the multigeneration system considered in chapter 4 (Fig. 4.2) is divided into four sub-systems: 1) biomass combustor, 2) organic Rankine cycle and domestic water heater, and 3) double-effect absorption chiller and proton exchange membrane (PEM) electrolyzer 4) reverse osmosis desalination unit. We determine the temperature profile in the multigeneration plant, input and output enthalpies, exergy flows, environmental impacts, exergy destructions and exergy efficiencies. The relevant energy balances and governing equations for the main sections of the multi-generation plant shown in Fig. 4.2 are described in the following subsections.

5.6.1.1 Biomass combustion

As shown in Fig. 4.2, biomass enters the combustor at point 30 and air enters at point 29. The composition of the biomass considered in this study (pine sawdust) is described in Table 5.5. The chemical equation of biomass combustion with air assuming complete combustion is:

$$C_xH_yO_z + \omega\ H_2O + \lambda(O_2 + 3.76\ N_2) \rightarrow a\ CO_2 + bH_2O + c\ N_2 \quad (5.133)$$

Table 5.5: Composition of pine sawdust biomass.

Composition	Value (%)
Moisture content in biomass (by weight)	10
Elemental analysis (dry basis by weight)	
Carbon (C)	50.54
Hydrogen (H)	7.08
Oxygen (O)	41.11
Sulfur (S)	0.57

where ω is the moisture content in the biomass fuel. The molar mass flow rate of the biomass can be expressed as

$$\dot{n}_{C_xH_yO_z} = \frac{\dot{m}_{biomass}}{M_{C_xH_yO_z}} \quad (5.134)$$

Here, $M_{C_xH_yO_z}$ is the molar mass of the biomass. The coefficients on the right hand side of Eq. (5.75) are determined with element balances:

$$a = x \quad (5.135)$$

$$b = \frac{y+2\omega}{2} \quad (5.136)$$

$$c = \frac{79}{21}\lambda \quad (5.137)$$

where

$$\lambda = \frac{2a+b-\omega-Z}{2} \quad (5.138)$$

To calculate the flue gas temperature leaving the combustor, we write an energy balance for a control volume around the biomass combustor, as follows:

$$\bar{h}_{C_xH_yO_z,30} + \omega\bar{h}_{H_2O,29} + \lambda\bar{h}_{O_2,29} + 3.76\lambda\bar{h}_{N_2,29} = a\bar{h}_{CO_2,31} + b\bar{h}_{H_2O,31} + c\bar{h}_{N_2,31} \quad (5.139)$$

Here, $\bar{h}_{C_xH_yO_z}$ is defined as [106]:

$$\bar{h}_{C_xH_yO_{z,30}} = x\bar{h}_{CO_2,30} + (\frac{y}{2})\bar{h}_{H_2O(l),29} + \overline{LHV}_{biomass}M_{C_xH_yO_z} \quad (5.140)$$

For pure and dry biomass fuels, nitrogen and sulphur are usually negligible and the below formula is used for a biomass with a chemical formula of CH_aO_b:

$$\overline{LHV}_{dry} = \frac{400000+100600y-\frac{b}{1+0.5a}(117600+100600a)}{12+a+16b} \quad (5.141)$$

The lower heating value for biomass with moisture is expressible as [106]:

$$\overline{LHV}_{mois} = [1-\mu_m-H_u]\overline{LHV}_{dry} - 2500H_u \quad (5.142)$$

where μ_m and H_u respectively denote mineral matter content and moisture content in biomass. Once the temperatures at points 29 and 30 are determined, Eq. (5.139) can be solved for the temperature at point 31.

5.6.1.2 ORC cycle

The ORC cycle here has 4 major components as follows:

- **For evaporator**

To determine the temperature and enthalpy for the ORC evaporator, the following energy balance equation for the evaporator can be used:

$$\dot{m}_{32}h_{32} + \dot{m}_{26}h_{26} = \dot{m}_{330}h_{33} + \dot{m}_1h_1 \quad (5.143)$$

Considering a pinch point temperature in the evaporator, the following expression can be used to calculate the gas temperature leaving the evaporator, which is an important parameter for hot water production:

$$T_{PP} = T_{33} - T_{26} \quad (5.144)$$

where T_{PP} is the pinch point temperature difference in the evaporator.

- **For ORC Turbine**

An energy balance for the ORC turbine and condenser yields the following relation:

$$\dot{m}_{27}h_{27} = \dot{W}_T + \dot{m}_{28}h_{28} \quad (5.145)$$

Also,

$$\eta_{ORC,T} = \frac{\dot{W}_{ORC,act}}{\dot{W}_{ORC,is}} \quad (5.146)$$

where h_{27} and h_{28} are the inlet and outlet enthalpies and $\dot{W}_{ORC,act}$ and $\dot{W}_{ORC,is}$ are actual and isentropic turbine power outputs.

- **For ORC Condenser**

An energy balance equation for condenser can be written as

$$\dot{m}_{28}h_{28} = \dot{m}_{24}h_{24} + \dot{Q}_{Cond} \quad (5.147)$$

- **For ORC Pump**

The ORC pump work can be expressed using an energy balance for a control volume around the ORC pump as follows:

$$\dot{W}_{ORC,pump} = \dot{m}_{25}(h_{26} - h_{25}) \quad (5.148)$$

5.6.1.3 Domestic Water Heater

The hot gases leaving the evaporator enter the water heater and heat domestic hot water to 60 ^{0}C. Water enters this heater at a pressure and a temperature of 2 bar and 20 ^{0}C, respectively. An energy balance for this component follows:

$$\dot{m}_{33}C_{pg}(T_{33} - T_{34}) = \dot{m}_{DWH}(h_{36} - h_{35}) \quad (5.149)$$

5.6.1.4 Double-effect absorption chiller

Absorption chillers can be used for air conditioning and cooling purposes. Compared to the more conventional vapor-compression refrigeration systems, absorption refrigeration systems replace the electricity consumption associated with vapor compression by a thermally driven system. This is accomplished by making use of absorption and desorption processes that employ a suitable working pair (a refrigerant and an absorbent). LiBr-water is a common working fluid for absorption systems in various cooling applications, including use in multi-generation systems. The LiBr-water mixture is heated in the generator as shown in Fig. 4.2. Heat provided by saturated water vapor via the heating process unit (point 24 in Fig. 4.2) allows separation of the refrigerant (H_2O) from the absorbent (LiBr solution).To model the LiBr-water absorption system used in this multigeneration system, the principle of mass conservation and the first and second laws of thermodynamics are applied to each component of the single-effect LiBr-water absorption chiller. In our analysis, each component is considered as a control volume with inlet and outlet streams, and heat and work interactions are considered. Mass balances are applied for the total mass and each material of the working fluid solution.

- **For absorber**

Mass balance equation for absorber can be written as

$$\dot{m}_{10} = \dot{m}_1 + \dot{m}_6 \quad (5.150)$$

Concentration balance equation for absorber is as

$$\dot{m}_1 x_1 = \dot{m}_6 x_6 \quad (5.151)$$

Energy balance equation for absorber is expressed as

$$\dot{m}_{10}h_{10} + \dot{m}_6 h_6 = \dot{m}_1 h_1 + \dot{Q}_{ABS} \quad (5.152)$$

$$\dot{Q}_{ABS} = \dot{m}_{38}(h_{39} - h_{38}) \quad (5.153)$$

- **For Pump**

The absorption pump work can be expressed using an energy balance for a control volume around the absorption pump as follows:

$$\dot{m}_1 = \dot{m}_2 \quad (5.154)$$

$$\dot{W}_{pump} = \dot{m}_2(h_2 - h_1) \quad (5.155)$$

- **For HEXI**

Mass balance equation for the first heat exchanger can be written as

$$\dot{m}_2 = \dot{m}_3 \quad (5.156)$$

$$\dot{m}_4 = \dot{m}_5 \quad (5.157)$$

Concentration balance equation is expressed ass

$$x_2 = x_3 \quad (5.158)$$

$$x_4 = x_5 \quad (5.159)$$

Energy balance equation is written as

$$\dot{m}_2 h_2 + \dot{m}_4 h_4 = \dot{m}_3 h_3 + \dot{m}_5 h_5 \quad (5.160)$$

$$T_{14} = T_{24} - PP \quad (5.161)$$

where PP is the pinch point temperature.

- **For low temperature generator (LGEN)**

To determine the temperature and enthalpy for the low temperature generator (LGEN), the following energy and mass balance equation for the LGEN can be used:

$$\dot{m}_{16} = \dot{m}_4 + \dot{m}_7 \quad (5.162)$$

$$\dot{m}_4 x_4 = \dot{m}_{16} x_{16} \quad (5.163)$$

$$\dot{m}_{17} h_{17} - \dot{m}_{18} h_{18} + \dot{m}_{16} h_{16} = \dot{m}_7 h_7 + \dot{m}_4 h_4 \quad (5.164)$$

- **For HEXI**

The mass balance equation for the second heat exchanger can be written as

$$\dot{m}_3 = \dot{m}_{13} \quad (5.165)$$

$$\dot{m}_{14} = \dot{m}_{15} \quad (5.167)$$

Concentration balance equation is expressed as

$$x_3 = x_{13} \quad (5.168)$$

$$x_{14} = x_{15} \quad (5.169)$$

Energy balance equation is written as

$$\dot{m}_3 h_3 + \dot{m}_{14} h_{14} = \dot{m}_{13} h_{13} + \dot{m}_{15} h_{15} \quad (5.170)$$

- **For High temperature generator (HGEN)**

To determine the temperature and enthalpy for the high temperature generator (HGEN), the following energy and mass balance equation for the LGEN can be used:

$$\dot{m}_{13} = \dot{m}_{14} + \dot{m}_{17} \quad (5.171)$$

$$\dot{m}_{14} x_{14} = \dot{m}_{13} x_{13} \quad (5.172)$$

$$\dot{m}_{24}(h_{24} - h_{25}) + \dot{m}_{13} h_{13} = \dot{m}_{17} h_{17} + \dot{m}_{14} h_{14} \quad (5.173)$$

$$h_{17} = h(P_{14}, x = 1) \quad (5.174)$$

- **For low temperature generator (LGEN)**

The mass and energy balance for the second heat exchanger can be written as

$$\dot{m}_{17} = \dot{m}_{18} \quad (5.175)$$

$$\dot{Q}_{LGEN} = \dot{m}_{17} h_{17} - \dot{m}_{18} 18 \quad (5.176)$$

- **For expansion valves**

The mass balance equation is written as

$$\dot{m}_5 = \dot{m}_6 \quad (5.177)$$

$$\dot{m}_{18} = \dot{m}_{19} \quad (5.178)$$

$$\dot{m}_8 = \dot{m}_9 \quad (5.179)$$

$$h_5 = h_6 \quad (5.180)$$

$$h_{18} = h_{19} \quad (5.181)$$

$$h_8 = h_9 \quad (5.182)$$

- **For condenser**

The energy and mass balance equations for condenser can be written as

$$\dot{m}_8 = \dot{m}_{19} + \dot{m}_7 \quad (5.183)$$

$$\dot{m}_{19}h_{19} + \dot{m}_7 h_7 = \dot{m}_8 h_8 + \dot{Q}_{Cond} \quad (5.184)$$

- **For evaporator**

The energy and mass balance equations for evaporator can be written as

$$\dot{m}_9 = \dot{m}_{10} \quad (5.185)$$

$$\dot{Q}_{EVP} = \dot{m}_{10}h_{10} - \dot{m}_9 h_9 \quad (5.186)$$

$$h_{10} = h(T_{EVP}, x = 1) \quad (5.187)$$

5.6.1.5 Reverse osmosis (RO) desalination unit

A typical seawater reverse osmosis-desalination plant consists of four major processes: seawater intake, pre-treatment and the RO system. Here, the RO system is the main process in which the separation occurs. The RO system includes a high pressure pump, the membrane separation unit and an energy recuperation system. The raw water is pressurized by a high pressure pump and then it is supplied to the membranes where the seawater desalination takes place. In this thesis, a standard RO unit based on a typical seawater RO plant consisting of a single RO stage of b trains is considered according to Salcedo et al. [107]. The rejected brine is pressurized at the outlet of the RO stage and then passes through a hydro-turbine in order to recover part of the energy consumed by the high pressure pump. In order to model the RO desalination unit, mass and energy balance are used as follows:

$$\dot{W}_{net} = b_n\left(\dot{W}_{Pump} - \dot{W}_{Turbine}\right) \quad (5.188)$$

Here, b_n is the number of trains which is 7 in our study and $\dot{W}_{Pump}$ and $\dot{W}_{Turbine}$are required RO pump and hydro-turbine which are expressible as follows:

$$\dot{W}_{Pump} = \frac{\Delta P\, \dot{m}_{39}}{\eta_{Pump}\, \rho_{39}} \quad (5.189)$$

$$W_{Turbine} = \frac{\Delta P\, \dot{m}_{42}\, \eta_{Turbine}}{\rho_{42}} \quad (5.190)$$

where ΔP is the transmembrane pressure and η_{Pump} and $\eta_{Turbine}$ are RO pump and hydroturbine isentropic efficiencies respectively. The target fresh water flow rate, $\dot{m}_{41}$ is determined from electricity deriving the RO and the recovery ratio RR, which is one of the technical characteristics of the membrane, as follows:

$$\dot{m}_{41} = \frac{\dot{m}_{37}}{RR} \tag{5.191}$$

The trans-membrane pressure can be expressed by the following equation:

$$\Delta P = J_w \cdot k_m + \Delta\pi \tag{5.192}$$

where k_m is the membrane permeability resistance with the value of $8.03 \times 10^{-11}\ \frac{\mathrm{m^2 s}}{\mathrm{kgPa}}$ and J_w *is* volumetric permeate flow rate expressed as

$$J_w = \frac{\dot{m}_{41}}{\rho_{41} \cdot n\, A_{mem}} \tag{5.193}$$

where *n* is the total number of membrane which is 600 in this study, ρ_{41}density at point 41 and $A_{mem}$is the area of membrane. In equation (5.192), $\Delta\pi$ is the transmembrane osmotic pressure that can be expressed as follows:

$$\Delta\pi = 805.1 \times 10^5 C_w R \tag{5.194}$$

Here, C_w is the membrane wall concentration that can be calculated as

$$C_w = \frac{e^{\left(\frac{j_w}{K_{mass}}\right)} x_{39}}{e^{\left(\frac{j_w}{K_{mass}}\right)} (1-R) + R} \tag{5.195}$$

where *R* denotes the membrane rejection coefficient with the value of 0.9975 in this study based on Salcedo et al. [107]. K_{mass} is the mass transfer coefficient expressed as follows:

$$K_{mass} = 0.04\, Re^{0.75}\, Sc^{0.33}\, \frac{D_s}{d} \tag{5.196}$$

where D_s is the diffusivity and *d* is the feed channel thickness with values of $1.45 \times 7\ \frac{\mathrm{m^2}}{\mathrm{s}}$ and 0.71 mm respectively.

In equation (5.196) the Reynolds number is determined as

$$Re_{39} = \frac{\dot{m}_{39}}{N_{ch}\, MW \cdot \mu_{39} \cdot N_P} \tag{5.197}$$

where N_{ch} and N_P represent the number of feed channel and the number of pressure vessel respectively and μ_{39} is the dynamic viscosity of the water and *MW* is the membrane width. Also, in equation (5.196), *Sc* is the Schmidt number defined as

$$Sc = \frac{\mu_{39}}{\rho_{39}\, D_s} \tag{5.198}$$

5.6.2 Exergy analysis of system II

- **Exergy balance equations of a biomass based multigeneration system**

Here, the exergy of each flow is calculated at all states and the changes in exergy are determined for each major component. The exergy destructions for all components in this multigeneration system (Fig. 4.2) are listed in Table 5.6.

- **Energy efficiency**

The energy, or first law, efficiency is defined as the ratio of useful energy produced by the system (cold, heat, electricity) to the input energy of the fuel supplied to the system. In this study, we consider three energy efficiencies for the system: the biomass ORC cycle, the CHP portion of the system and the overall multigeneration system, i.e.,

$$\eta_{Power} = \frac{\dot{W}_{net,ORC}}{\dot{m}_f LHV_f} \tag{5.199}$$

$$\eta_{CHP} = \frac{\dot{W}_{net,ORC}+\dot{Q}_{heating}}{\dot{m}_f LHV_f} \tag{5.200}$$

$$\eta_{multi} = \frac{\dot{W}_{net,ORC}+\dot{Q}_{heating}+\dot{Q}_{cooling,chiller}+\dot{m}_{H_2} LHV_{H_2}+\dot{m}_{36}h_{36}+\dot{m}_{41}h_{41}}{\dot{m}_f LHV_f} \tag{5.201}$$

where LHV_f denotes the lower heating value of the biomass. For pure and dry biomass fuels, nitrogen and sulphur are usually negligible and the below formula is used for a biomass with a chemical formula of CH_aO_b:

$$\overline{LHV}_{dry} = \frac{400000+100600y-\frac{b}{1+0.5a}(117600+100600a)}{12+a+16b} \tag{5.202}$$

The lower heating value for biomass with moisture is expressible as [106]:

$$\overline{LHV}_{mois} = [1-\mu_m-H_u]\overline{LHV}_{dry} - 2500H_u \tag{5.203}$$

where μ_m and H_u respectively denote mineral matter content and moisture content in biomass. Also, $\dot{Q}_{heating}$ and $\dot{Q}_{cooling,chiller}$ denote the heating load of the multigeneration system, the double- effect absorption cooling load, while the last three terms in the numerator denote the energy values of the hydrogen, hot water and fresh water products. It can be seen from these expressions the energy efficiency of the multigeneration system must exceed that for power generation cycle.

Table 5.6: Expressions for exergy destruction rates for components of the system

Component	Exergy destruction rate expression
Combustor	$\dot{E}x_{D,Comb} = \dot{E}x_{29} + \dot{E}x_{30} - \dot{E}x_{31}$
ORC evaporator	$\dot{E}x_{D,Evp} = \dot{E}x_{32} + \dot{E}x_{26} - \dot{E}x_{27} - \dot{E}x_{33}$
ORC turbine	$\dot{E}x_{D,T} = \dot{E}x_{27} - \dot{W}_T - \dot{E}x_4$
Heating process	$\dot{E}x_{D,heat} = \dot{E}x_{28} - \dot{E}x_Q - \dot{E}x_{24}$
ORC pump	$\dot{E}x_{D,P} = \dot{E}x_{25} + \dot{W}_P - \dot{E}x_{26}$
Absorption condenser	$\dot{E}x_{D,Cond} = \dot{E}x_{19} + \dot{E}x_{20} - \dot{E}x_8 - \dot{E}x_{21}$
Expansion valves	$\dot{E}x_{D,Exv} = \dot{E}x_{18} - \dot{E}x_{19} + \dot{E}x_8 - \dot{E}x_9 + \dot{E}x_{15} - \dot{E}x_{16} + \dot{E}x_5 - \dot{E}x_6$
Absorption evaporator	$\dot{E}x_{D,Evp} = \dot{E}x_9 + \dot{E}x_{21} - \dot{E}x_{23} - \dot{E}x_{10}$
Absorber	$\dot{E}x_{D,Abs} = \dot{E}x_{10} + \dot{E}x_6 + \dot{E}x_{38} - \dot{E}x_1 - \dot{E}x_{39}$
Absorption pump	$\dot{E}x_{D,P} = \dot{E}x_1 + \dot{W}_P - \dot{E}x_2$
Absorption heat exchanger I	$\dot{E}x_{D,HExI} = \dot{E}x_2 + \dot{E}x_4 - \dot{E}x_3 - \dot{E}x_5$
Absorption heat exchanger h	$\dot{E}x_{D,HExh} = \dot{E}x_3 + \dot{E}x_{14} - \dot{E}x_{13} - \dot{E}x_{15}$
High Temperature Absorption generator	$\dot{E}x_{D,Genh} = \dot{E}x_{24} + \dot{E}x_{13} - \dot{E}x_{14} - \dot{E}x_{17} - \dot{E}x_{25}$
Low Temperature Absorption generator	$\dot{E}x_{D,GenL} = \dot{E}x_{17} - \dot{E}x_{18} - \dot{E}x_Q$
PEM electrolyzer	$\dot{E}x_{D,PEM} = \dot{E}x_{22} + \dot{W}_{PEM} - \dot{E}x_{24} - \dot{E}x_{23}$
Domestic hot water heater	$\dot{E}x_{D,DWH} = \dot{E}x_{33} + \dot{E}x_{35} - \dot{E}x_{36} - \dot{E}x_{34}$
RO pump	$\dot{E}x_{D,RO\ Pump} = \dot{E}x_{39} + \dot{W}_P - \dot{E}x_{40}$
RO desalination unit	$\dot{E}x_{D,RO\ desalination} = \dot{E}x_{40} - \dot{E}x_{41} - \dot{E}x_{42}$
RO hydraulic turbine	$\dot{E}x_{D,h\ turbine} = \dot{E}x_{42} - \dot{W}_T - \dot{E}x_{43}$

- **Exergy efficiency**

The exergy efficiency, defined as the product exergy output divided by the exergy input [47], can be expressed for the ORC power generation unit, the CHP unit and the multi-generation system as follows:

$$\Psi_{ORC} = \frac{\dot{W}_{net,ORC}}{\dot{E}x_{biomass}} \tag{5.204}$$

$$\Psi_{CHP} = \frac{\dot{W}_{net,ORC}+\dot{E}x_{heating}}{\dot{E}x_{biomass}} \tag{5.205}$$

$$\Psi_{multi} = \frac{\dot{W}_{net,ORC}+\dot{E}x_{heating}+\dot{E}x_{cooling}+\dot{E}x_{H_2}+\dot{E}x_{36}+\dot{E}x_{41}}{\dot{E}x_{biomass}} \tag{5.206}$$

where

$$\dot{E}x_{heating} = \dot{Q}_{cond}\left(1 - \frac{T_0}{T_{cond}}\right) \tag{5.207}$$

$$\dot{E}x_{cooling} = \dot{Q}_{cooling}\left(\frac{T_0 - T_{EVP}}{T_{EVP}}\right) \tag{5.208}$$

$$\dot{E}x_{H_2} = \dot{m}_{H_2} ex_{H_2} \tag{5.209}$$

$$\dot{E}x_{35} = \dot{m}_{35}(h_{35} - h_0) - T_0(s_{35} - s_0) \tag{5.210}$$

Also, $\dot{E}x_{biomass}$ is the exergy of biomass, defined as [24]:

$$\dot{E}x_{biomass} = \dot{m}_{biomass}\beta LHV_{mois} \tag{5.211}$$

Here, β is defined as

$$\beta = \frac{1.0414+0.0177\left(\frac{H}{C}\right)-0.3328\left(\frac{O}{C}\right)\left\{1+0.0537\left(\frac{H}{C}\right)\right\}}{1-0.4021\left(\frac{O}{C}\right)} \tag{5.212}$$

and *LHV* is as given in equation (5.203).

5.6.3 Economic analysis of system II

In order to perform the economic analysis and optimization of the three novel multigeneration systems, we should first define a purchase cost of each equipment used in the system as a function of some major design parameters. In this section, the cost function of each component and some economic parameters are defined and explained.

5.6.3.1 Investment cost of a biomass based multigeneration system

Biomass based multigeneration system shown in Fig 4.2 has some similar parts as the first multigeneration system. Here, the cost functions of the ones that differ from the first system are provided.

5.6.3.1.1 Biomass combustor and evaporator

The cost function of biomass combustor and evaporator is a function of flue gas energy leaving the combustor, main pressure and temperature of the ORC cycle. The purchase cost function can be expressed as follows [79]:

$$Z_{com}(\$) = 740(H_B)^{0.8}\exp(\frac{0.01P_{27}-2}{14.29})\exp(\frac{T_{27}-350}{446}) \quad (5.213)$$

where

$$H_B = \dot{m}_g h_{31} \quad (5.214)$$

Here, $\dot{m}_g$ is the flue gas mass flow rate in kg/s.

5.6.3.1.2 Heating process unit

Several cost functions are available for the heating process considered for this biomass based multigeneration system. The cost function of heating process here is defined as [103]:

$$Z_{Heating}(\$) = 5714\dot{m}_{28} \quad (5.215)$$

5.6.3.1.3 Reverse osmosis (RO) desalination unit

In this biomass based multigeneration, a RO desalination unit is considered as already discussed. The cost of RO desalination unit can be expressed as follows [108]:

$$Z_{RO}(\$) = 0.98m^3 \quad (5.216)$$

where *m* is the fresh water mass in kg.

5.7 Analyses of system III

5.7.1 Thermodynamic analyses

An OTEC system utilizes low-grade energy and has low energy efficiency (about 3–5%). Therefore, achieving a high electricity generating capacity with OTEC requires the use of large quantities of seawater and a correspondingly large amount of pumping energy. For thermodynamic modeling purposes, the integrated OTEC system for hydrogen production

considered here (Fig. 4.3) is divided into three parts: flat plate solar collector, ocean thermal energy conversion (OTEC) unit and PEM electrolyzer.

Fig. 4.3 shows a schematic diagram of an integrated OTEC system equipped with a flat plate solar collector, a PV/T panel, a single effect absorption chiller, a reverse osmosis (RO) desalination unit and PEM electrolyzer. This integrated system uses the warm surface seawater to evaporate a working fluid like ammonia or a Freon refrigerant, which drives a turbine to produce electricity, which in turn is used to drive a PEM electrolyzer to produce hydrogen. After passing through the turbine, the vapor is condensed in a heat exchanger that is cooled by cold deep seawater. The working fluid is then pumped back through the warm seawater heat exchanger, and the cycle is repeated continuously.

Energy and exergy analyses are used to determine the temperature profile in the plant, input and output enthalpy and exergy flows, exergy destructions rates and energy and exergy efficiencies. The relevant energy balances and governing equations for the main sections of the plant shown in Fig. 4.3 are described in the following subsections.

5.7.1.1 Flat plate solar collector

As shown in Fig. 4.3, water enters the solar collector at point 2 and is heated by the collector. The useful heat gained by the working fluid can be written as

$$\dot{Q}_u = \dot{m} C_p (T_3 - T_2) \tag{5.217}$$

where T_3, T_2, C_p and $\dot{m}$ are the water outlet temperature, inlet temperature, specific heat at constant pressure and mass flow rate. The Hottel-Whillier equation for the heat gained by the flat plate collector considering heat losses from the collector is calculated as [109]:

$$\dot{Q}_u = A_P F_R [S - U_l (T_{in} - T_0)] \tag{5.218}$$

where T_0 is the ambient temperature and the F_R is heat removal factor which is defined as:

$$F_R = \frac{\dot{m} C_p}{U_l A_P} \left[1 - e^{\left\{ -\frac{F' U_l A_P}{\dot{m} C_p} \right\}} \right] \tag{5.219}$$

Here, F' is collector efficiency factor which is around 0.914 for this case [109] and U_l is the overall collector loss coefficient obtained from [109]. In equation (5.218), radiation flux absorbed by the absorber is calculated as

$$\dot{S} = (\tau\alpha)\dot{I} \tag{5.220}$$

where $(\tau\alpha)$ is optical efficiency and $\dot{I}$ is solar radiation intensity. The energy efficiency of the solar flat plate collector is expressed as

$$\eta = \frac{\dot{Q}_u}{IA_P} \tag{5.221}$$

5.7.1.2 Ocean thermal energy conversion (OTEC)

As shown in Fig. 4.3, the electricity production unit is based on an organic Rankine cycle which is suitable for low-grade heat. Fig. 5.7 shows the corresponding temperature-entropy (*T*-*S*) diagram of the ORC. The net power output of the system is expressible as

$$\dot{W}_{net} = \dot{W}_G - (\dot{W}_{WS} + \dot{W}_{CS} + \dot{W}_{WF}) \tag{5.222}$$

where $\dot{W}_G$is the turbine generator power, $\dot{W}_{WS}$ and $\dot{W}_{CS}$ are the warm and cold seawater pumping power, and $\dot{W}_{WF}$ is working fluid working power.

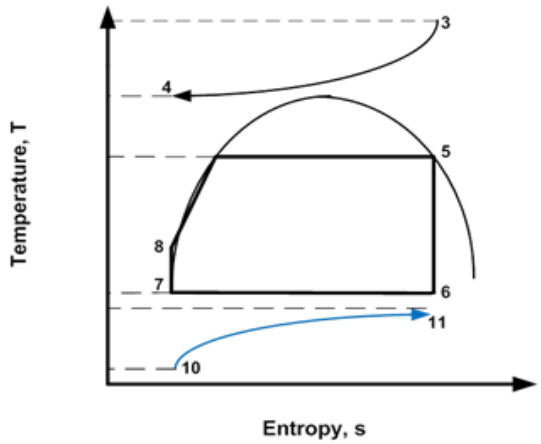

Point number	Specification
3	Warm water entering ORC evaporator
4	War water exiting the ORC evaporator to the ocean
7	Saturated liquid ammonia entering ORC pump
8	Liquid ammonia exiting ORC pump
5	Saturated vapour entering turbine
6	Saturated ammonia entering condenser
10	Cold water entering the condenser
11	Cold water outlet from condenser to the ocean

Figure 5.7: *T*-*s* diagram of the ocean thermal energy conversion (OTEC).

- **Turbine generator power**

The turbine power output is calculated by writing the energy balance for a control volume around a turbine which is the product of working fluid mass flow rate, $\dot{m}_F$ and the adiabatic heat loss between the evaporator and the condenser, as follows:

$$\dot{W}_G = \dot{m}_F \eta_T \eta_G (h_5 - h_6) \tag{5.223}$$

Here, $\eta_T$and $\eta_G$are the turbine isentropic efficiency and generator mechanical efficiency.

- **Warm seawater pumping power**

The warm seawater pumping power can be written as

$$\dot{W}_{WS} = \frac{\dot{m}_{WS}\,\Delta H_{WS}\,g}{\eta_{WSP}} \quad (5.224)$$

where ΔH_{WS} is the total pump head difference of the warm seawater piping [110]:

$$\Delta H_{WS} = (\Delta H_{WS})_P + (\Delta H_{WS})_E \quad (5.225)$$

Here, $(\Delta H_{WS})_P$ is the pump head of the warm seawater pipe, which can be given as [110]:

$$(\Delta H_{WS})_P = (\Delta H_{WS})_{SP} + (\Delta H_{WS})_B \quad (5.226)$$

where $(\Delta H_{WS})_{SP}$ is the friction loss of the straight pipe and $(\Delta H_{WS})_B$ is the bending loss on the warm seawater pipe, which are given as [110]:

$$(\Delta H_{WS})_{SP} = 6.82 \frac{L_{WS}}{{d_{WS}}^{1.17}} \times \left(\frac{V_{WS}}{C_{WS}}\right)^{1.85}, C_{WS} = 100 \quad (5.227)$$

$$(\Delta H_{WS})_B = \sum \lambda_m \frac{{V_{WS}}^2}{2g} \quad (5.228)$$

Here, L_{WS} is the length of the warm seawater pipe, d_{WS} is the warm seawater inner pipe diameter and V_{WS} is the velocity of warm seawater inside the pipe. Also, $(\Delta H_{WS})_E$ is the pressure difference of warm seawater in the evaporator, expressible as

$$(\Delta H_{WS})_E = \lambda_E \frac{{V_{WS}}^2}{2g} \frac{L_E}{(D_{eq})_W} \quad (5.229)$$

Here, L_E is the length of the evaporator plate which is 4m in this study and λ_E is taken from reference [110] which is 0.068. Also, D_{eq} is the equivalent diameter, which is calculated as

$$D_{eq} = 2\delta \quad (5.230)$$

where δ is the clearance.

- **Cold seawater pumping power**

The cold seawater pumping power is expressed as

$$\dot{W}_{CS} = \frac{\dot{m}_{CS}\,\Delta H_{CW}\,g}{\eta_{CSP}} \quad (5.231)$$

where η_{CSP} is the cold seawater pump efficiency and ΔH_{CW} is the total pump head of the cold seawater piping, given as

$$\Delta H_{CS} = (\Delta H_{CS})_P + (\Delta H_{CS})_C + (\Delta H_{CS})_d \quad (5.232)$$

Here, $(\Delta H_{CS})_P$ is the pump head of the cold seawater pipe [110]:

$$(\Delta H_{CS})_P = (\Delta H_{CS})_{SP} + (\Delta H_{CS})_B \quad (5.233)$$

These two terms are similar to the terms in equations. (5.227) and (5.228). Also, $(\Delta H_{CS})_C$ is the cold seawater pressure difference in the condenser, defined as

$$(\Delta H_{CS})_C = \lambda_C \frac{{V_{CS}}^2}{2g} \frac{L_C}{(D_{eq})_C} \quad (5.234)$$

where L_C is the length of the evaporator plate and λ_C is taken from reference [110]. Also, D_{eq} is the equivalent diameter given in equation (5.230) and $(\Delta H_{CS})_d$ is the pressure difference caused by the density difference between the warm seawater surface and cold deeper seawater, calculated as [110]:

$$(\Delta H_{CS})_d = L_{CS} - \frac{1}{\rho_{CS}} \left(\frac{1}{2} (\rho_{WS} + \rho_{CS}) L_{CS} \right) \quad (5.235)$$

5.7.1.3 Solar PV/T system

In this integrated multigeneration energy system, a PV/T solar panel is considered as shown on the left side of Fig. 4.3. In order to model the PV/T system, the equation used by Joshi et al. [111]. The equation to calculate power produced by the PV module is given as

$$\dot{W} = \eta_c \dot{I}\, \beta_c \tau_g A \quad (5.236)$$

where η_c is the solar cell efficiency which is equal to 0.38 in this study, β_c is the packing factor of solar cell with the value of 0.83 in this thesis based on research by Joshi et al. [111] and τ_g is the transitivity of the solar panel glass with the value of 0.95 and A is the solar area in m^2. The rate of useful thermal energy obtained from the PV/T air collector is thus obtained as follows:

$$\dot{Q}_{solar} = \frac{\dot{m}_{air} Cp_{air}}{U_L} \left\{ \left(h_{P2Z} Z\dot{I} \right) - U_L (T_{air,in} - T_0) \right\} \times \left[1 - \exp\left(\frac{-bU_L L}{\dot{m}_{air} Cp_{air}} \right) \right] \quad (5.237)$$

where Z is defined as

$$Z = \alpha_b {\tau_g}^2 (1 - \beta_c) + h_{P1G} \tau_g \beta_c (\alpha_c - \eta_c) \quad (5.238)$$

Here α_c is absorptivity of solar cell with the value of 0.85 and α_b is absorptivity of black surface with the value of 0.9 respectively. In equation (5.237) U_L is the overall heat transfer coefficient from solar cell to ambient through top and back surface of insulation with the value of 4.71 $\frac{W}{m^2 K}$. The air outlet temperature of the PV/T panel is calculated based on the energy balance for the PV/T panel and it is expressed as follows:

$$T_{air,out} = \left[T_0 + \frac{h_{P2G} Z\dot{I}}{U_L} \right] \left\{ 1 - \frac{1 - \exp\left(\frac{-bU_L L}{\dot{m}_{air} Cp_{air}} \right)}{\frac{bU_L L}{\dot{m}_{air} Cp_{air}}} \right\} + T_{air,in} \left[\frac{1 - \exp\left(\frac{-bU_L L}{\dot{m}_{air} Cp_{air}} \right)}{\frac{bU_L L}{\dot{m}_{air} Cp_{air}}} \right] \quad (5.239)$$

The thermal efficiency of the PV/T collector is defined as

$$\eta_{th} = \frac{\dot{Q}}{\dot{I} bL} \quad (5.240)$$

Here, $\dot{I}$ is the solar intensity and *b* and *L* are width and length of the PV/T panel.

5.7.1.4 Absorption Chiller

The principle of mass conservation and the first and second laws of thermodynamics are applied to each component of the single-effect absorption chiller. In our analysis, each component is considered as a control volume with inlet and outlet streams, and heat and work interactions are considered. Mass balances are applied for the total mass and each material of the working fluid solution. The governing and conservation equations for total mass and each material of the solution for a steady state and steady flow case follow [96]:

$$\sum \dot{m}_i = \sum \dot{m}_o \tag{5.241}$$

$$\sum (\dot{m}x)_i = \sum (\dot{m}x)_0 \tag{5.242}$$

Here, $\dot{m}$ is the working fluid mass flow rate and *x* is mass concentration of Li-Br in the solution. For each component of the absorption system, a general energy balance is written:

$$\dot{Q} - \dot{W} = \sum \dot{m}_o h_o - \sum \dot{m}_i h_i \tag{5.243}$$

The cooling load of the absorption chiller is defined as

$$\dot{Q}_{cooling} = \dot{m}(h_{28} - h_{27}) \tag{5.244}$$

Further information about the thermodynamic modeling and energy balances for each component is given in [97].

5.7.1.5 PEM Electrolyzer

Thermodynamic modeling of the PEM electrolyzer was already explained in details in section 5.5.1.6. Same thermodynamic modeling is considered for this multigeneration system. The simulation code for the PEM electrolyzer is developed in a way that electricity is the input of the program and the output of the simulation code is the H_2 production rate and exergy efficiency of the PEM Electrolyzer.

5.7.1.6 Reverse osmosis (RO) desalination unit

Since OTEC system is installed near the sea and costal area, production of fresh water is found necessary. Therefore, in this integrated OTEC multigeneration energy system RO desalination

system is considered. The thermodynamic formulas were already explained and given in section 5.6.1.5 as shown in Fig. 4.3.

5.7.2 Exergy analysis of system II

Here, the exergy of each flow is calculated at all states and the changes in exergy are determined for each major component. The exergy destructions for all components in this multigeneration system (Fig. 4.3) are shown in Table 5.7.

- **Energy efficiency**

The energy, or first law, efficiency is defined as the ratio of useful energy produced by the system (cold, heat, electricity) to the input energy of the fuel supplied to the system. In this study, we consider three energy efficiencies for the system: the biomass ORC cycle, the CHP portion of the system and the overall multigeneration system. The energy efficiency of the OTEC power generation system is defined as the net power output of the system divided by input energy at evaporator, which can be expressed as

$$\eta_{power} = \frac{\dot{W}_{net,OTEC}}{\dot{Q}_{EVP}} \tag{5.245}$$

where $\dot{W}_{net}$ is given in equation (5.222), and $\dot{Q}_{EVP}$ is expressible as

$$\dot{Q}_{EVP} = \dot{m}_{WF}(h_5 - h_8) \tag{5.246}$$

$$\eta_{CHP} = \frac{\dot{W}_{net,OTEC} + \dot{W}_{PV/T}}{\dot{Q}_{EVP}} \tag{5.247}$$

$$\eta_{multi} = \frac{\dot{W}_{net,OTEC} + \dot{W}_{PV/T} + \dot{Q}_{cooling,chiller} + \dot{m}_{H_2} LHV_{H_2} + \dot{m}_{15} h_{15}}{\dot{Q}_{EVP}} \tag{5.248}$$

- **5.7.2.3 Exergy efficiency**

The exergy efficiency is defined as the product exergy output divided by the exergy input. According to Yamada et al. [88], the exergy efficiency of the ORC power generation cycle in an OTEC system is given as

$$\Psi_{Power} = \frac{\dot{W}_{net}}{\dot{Ex}_{in}} = \frac{\dot{W}_{net,OTEC}}{\dot{Ex}_{in,WS} + \dot{Ex}_{in,CS}} \tag{5.249}$$

Table 5.7: Expressions for exergy destruction rates for components of the system

Component	Exergy destruction rate expression
Warm sea water pump	$\dot{E}x_{D,P} = \dot{E}x_1 + \dot{W}_P - \dot{E}x_2$
Cold sea water pump	$\dot{E}x_{D,P} = \dot{E}x_9 + \dot{W}_P - \dot{E}x_{10}$
Solar collector	$\dot{E}x_{D,collector} = \dot{E}x_2 + \dot{E}x_{sun} - \dot{E}x_3$
Turbine	$\dot{E}x_{D,T} = \dot{E}x_5 - \dot{W}_T - \dot{E}x_6$
Condenser	$\dot{E}x_{D,Cond} = \dot{E}x_6 + \dot{E}x_{10} - \dot{E}x_7 - \dot{E}x_{11}$
WF pump	$\dot{E}x_{D,P} = \dot{E}x_7 + \dot{W}_P - \dot{E}x_8$
Solar PV/T	$\dot{E}x_{D,collector} = \dot{E}x_{41} + \dot{E}x_{sun} - \dot{E}x_{40}$
Absorption condenser	$\dot{E}x_{D,Cond} = \dot{E}x_{39} - \dot{E}x_{26} - \dot{E}x_Q$
Absorption expansion valves	$\dot{E}x_{D,EXV} = \dot{E}x_{26} + \dot{E}x_{37} - \dot{E}x_{27} - \dot{E}x_{38}$
Absorption evaporator	$\dot{E}x_{D,EVP} = \dot{E}x_{27} - \dot{E}x_{29} + \dot{E}x_Q$
Absorber	$\dot{E}x_{D,Abs} = \dot{E}x_{28} + \dot{E}x_{38} + \dot{E}x_{31} - \dot{E}x_{32} - \dot{E}x_{33}$
Absorption pump	$\dot{E}x_{D,P} = \dot{E}x_{33} + \dot{W}_P - \dot{E}x_{34}$
Absorption heat exchanger	$\dot{E}x_{D,HEX} = \dot{E}x_{34} + \dot{E}x_{36} - \dot{E}x_{35} - \dot{E}x_{37}$
Absorption generator	$\dot{E}x_{D,Gen} = \dot{E}x_{35} + \dot{E}x_{40} - \dot{E}x_{41} - \dot{E}x_{33} - \dot{E}x_{36}$
PEM electrolyzer	$\dot{E}x_{D,PEM} = \dot{E}x_{29} + \dot{W}_{PEM} - \dot{E}x_{22} - \dot{E}x_{21}$
RO pump	$\dot{E}x_{D,RO\ Pump} = \dot{E}x_{13} + \dot{W}_P - \dot{E}x_{14}$
RO desalination unit	$\dot{E}x_{D,RO\ desalination} = \dot{E}x_{14} - \dot{E}x_{10} - \dot{E}x_{15}$
RO hydraulic turbine	$\dot{E}x_{D,h\ turbine} = \dot{E}x_{16} - \dot{W}_T - \dot{E}x_{17}$

$$\Psi_{CHP} = \frac{\dot{W}_{net,OTEC} + \dot{W}_{PV/T}}{\dot{E}x_{in,WS} + \dot{E}x_{in,CS}} \tag{5.250}$$

$$\Psi_{multi} = \frac{\dot{W}_{net,ORC} + \dot{W}_{PV/T} + \dot{E}x_{cooling} + \dot{E}x_{H_2} + \dot{E}x_{22} + \dot{E}x_{22}}{\dot{E}x_{in,WS} + \dot{E}x_{in,CS}} \tag{5.251}$$

where

$$\dot{E}x_{in,WS} = \dot{m}_{in,WS}\left[\left(h_{WS,in} - h_0\right) - T_0(s_{WS,in} - s_0)\right] \tag{5.252}$$

$$\dot{E}x_{in,CS} = \dot{m}_{in,CS}\left[\left(h_{CS,in} - h_0\right) - T_0(s_{CS,in} - s_0)\right] \tag{5.253}$$

Here, the reference-environment state is taken to be P_0 = 1.01 bar and T_0 = 298.15 K.

5.7.3 Economic analysis of system III

Renewable based multigeneration system shown in Fig 4.3 has some similar parts as the first multigeneration system. Here, the cost functions of the ones that differ from the first system are provided.

5.7.3.1 PV/T solar collector

The purchase cost of PV/T solar collector is a function of collector area that can be expressed as follows [112]:

$$Z_{PV/T}(\$) = 310\, n_x n_y Lb \tag{5.254}$$

where n_x and n_y is the number of PV/T in series and parallel, L and b are the PV/T length and width respectively.

5.7.3.2 Flat plate solar collector in OTEC cycle

As shown in Fig. 4.3, a flat plate solar collector is used for the OTEC system to increase the efficiency of the system. The purchase cost of solar flat plate collector can be expressible as

$$Z_{FPC}(\$) = 235\, A_{FPC} \tag{5.255}$$

Here, A_{FPC} is the flat plate collector area in m^2.

5.7.3.3 OTEC cycle

The OTEC cycle has 4 major components. The purchase cost of each component can be found as follows:

- **For OTEC turbine and generator**

The cost function of the ORC turbine can be calculated using the following formula [103]:

$$Z_T(\$) = 4750\left(\dot{W}_T\right)^{0.75} + 60\left(\dot{W}_T\right)^{0.95} \tag{5.256}$$

Here, $\dot{W}_T$ is the work generated by the turbine in kW.

- **For OTEC evaporator**

The purchase cost of OTEC evaporator can be calculated as follows [103]:

$$Z_{EVP}(\$) = 276(A_{EVP})^{0.88} \tag{5.257}$$

where

$$A_{EVP} = \frac{\dot{Q}_{EVP}}{U_{EVP}\Delta T_{\ln}} \tag{5.258}$$

Here, U_{EVP} is the overall heat transfer coefficient for evaporator with the value of 4.39 $\frac{kW}{m^2K}$.

- **For Condenser**

The purchase cost of OTEC condenser can be calculated as follows [85, 103]:

$$Z_{Cond}(\$) = 150(A_{Cond})^{0.8} \quad (5.259)$$

where

$$A_{EVP} = \frac{\dot{Q}_{Cond}}{U_{Cond}\Delta T_{\ln}} \quad (5.260)$$

Here, U_{Cond} is the overall heat transfer coefficient for evaporator with the value of 4.69 $\frac{kW}{m^2K}$ [85].

- **For Pumps**

The following expression is used to calculate the cost of OTEC pumps [113]:

$$Z_{Pump}(\$) = 3500(\dot{W}_P)^{0.41} \quad (5.261)$$

Chapter 6: Results and discussion

6.1 Introduction

In order to enhance the understanding of the system's performance, it is important to use several analyses to see how this performance varies with design parameters. In this chapter, the results of thermodynamic modeling, exergy, economic and environmental impact assessment, and optimization are explained. Exergy analysis can help develop strategies and guidelines for more efficient and effective use of energy, and is utilized to study various thermal processes, especially power generation, CHP, trigeneration and multigeneration. The exergy analysis includes the determination of the exergy destruction rate and exergy efficiency of each component in the system and also determines the overall exergy efficiency of the multigeneration system. Exergy analysis also helps to identify and quantify the source of irreversibilities in the systems that are associated with each component. Economic analysis shows the total cost rate of the system, cost of each component, cost of electricity and cost of environmental impacts.

The environmental impact assessment shows how much reduction in greenhouse gases is possible when shifting from conventional power generation units to CHPs and multigeneration energy systems. Further improvement of a thermal system can be obtained by using optimization. Since both efficiency and total cost rate of the systems are important, single objective optimization will not yield a true optimum. Therefore, a multi-objective optimization should be applied to the system. In this chapter, different output key parameters are investigated for three different systems. These parameters are overall exergy efficiency, total exergy destruction rate, cooling and heating load, hydrogen production rate, fresh water mass flow rate, CO_2 emission of the system and net power output of each system. Also, to enhance the understanding of the system performance, a comprehensive parametric study is conducted to see the result of variation in several major design parameters of system performance. Finally, by defining some objective functions, the optimum design parameters are obtained using a multi-objective genetic algorithm optimization technique.

6.2 Results of system I

For thermodynamic modeling, the multigeneration system considered here (Fig. 4.1) is divided into five main parts: gas turbine (Brayton) cycle, Rankine cycle with double pressure HRSG, a single effect absorption chiller, organic Rankine cycle (ORC), domestic water heater and PEM electrolyzer. The fuel injected to the combustion chamber is natural gas. We determine the temperature profile in the plant, input and output enthalpy and exergy flow rates, exergy destructions rates, and energy and exergy efficiencies. In order to model the system, energy balances are considered for each system component. The dead state is taken to be P_0 = 1.01 bar and T_0 = 293.15 K.

6.2. 1 Modeling results

Several simplifying assumptions are made here to render the analysis more tractable, while retaining adequate accuracy and allowing the principal points of the article to be illustrated:

- All processes occur at steady state.
- Air and combustion products are ideal-gas mixtures as the temperature is high the pressure is low so the ideal gas assumption is reasonable.
- Heat loss from the combustion chamber is 2% of the fuel lower heating value, and all other components are adiabatic.
- Both HP and LP pinch temperatures are constant at 10ºC.
- The flow across the throttle valve is isenthalpic.
- The ORC working fluid at the evaporator outlet is a saturated vapor.
- Pressure drops in ORC cycle are negligible.
- Heat losses from piping and other auxiliary components are negligible.

To model the gas turbine based multigeneration system, some parameters are selected as input data for the simulation. The input data for the simulation are listed in Table 6.1. Also, Table 6.2 lists the parameters used to simulate the PEM electrolyzer. To ensure the accuracy and validity of the developed computer simulation code, the PEM electrolyzer simulation is validated with experimental data from the literature.

Table 6.1: Input parameters used to model the system.

Parameter	**Value**	**Parameter**	**Value**
Compressor pressure ratio, r_{AC}	10	ORC evaporator pinch point, (^{o}C)	10
Compressor isentropic efficiency, η_{AC}	0.83	ORC condenser pressure, P_{Cond} (kPa)	90
Gas turbine inlet temperature, *GTIT* (K)	1400	ORC turbine inlet pressure, P_{ORC} (kPa)	700
Gas turbine isentropic efficiency, η_{GT}	0.88	ORC extraction pressure, $P_{ex,ORC}$ (kPa)	220
HRSG low pressure, PLP (bar)	3	ORC evaporator pressure, (kPa)	25
HRSG high pressure, PHP (bar)	20	PEM temperature, T_{PEM} (^{0}C)	80
Low pressure pinch point PP_{LP} (^{0}C)	10	PEM electrolyzer thickness, D (μm)	100
High pressure pinch point PP_{HP} (^{0}C)	10	Chiller weak solution concentration	57.6
chiller evaporator temperature, (^{o}C)	5	Chiller strong solution concentration	58.2
Pump isentropic efficiency, η_{Pump}	0.78	P_0 (kPa)	101
Steam turbine isentropic efficiency, η_{ST}	0.80	T_0 (^{0}C)	25
Condenser pressure, P_{Cond} (kPa)	10		

Specifically, the electrochemical model is used to simulate experiments published in the literature and the modeling results and experimental data are compared. The electrolyte used in the experiments [114, 115] is Nafion, a polymer widely used as electrolyte in fuel cells and electrolyzers. The thicknesses of the electrolytes tested by Ioroi et al. [114] and Millet et al. [115] were 50 μm and 178 μm, respectively. Platinum was used as the electrode catalyst. The simulation code for the *J–V* characteristics for PEM electrolysis are compared with experimental data of Ioroi et al. [114] as shown in Fig. 6.1. The modeling results agree well with the experimental data, supporting the validity of the present simulation. It is found that the cell potential increases rapidly when current density is less than 300 A/m^2. When *J* exceeds 300 A/m^2, the cell potential increases slightly with *J*. To enhance the understanding of the electrochemical performance of the PEM electrolyzer, ohmic and activation overpotentials are examined and shown individually in Fig. 6.2. This figure shows that the ohmic overpotential is very small and increases slightly with current density. This observation is attributable to the fact

that the membrane ionic conductivity (σ_{PEM}) is high at typical values of $\boldsymbol{\lambda}$ and the operating temperature, leading to a lower R_{PEM} (see equations. (5.69) and (5.70)), which means the lower the overall ohmic resistance the lower the ohmic overpotential.

Table 6.2: Input parameters used to model PEM electrolysis [114].

Parameter	**Value**
P_{O_2} (atm)	1.0
P_{H_2} (atm)	1.0
T_{PEM} (^{0}C)	80
$E_{act,a}$ (kJ/mol)	76
$E_{act,c}$ (kJ/mol)	18
$\boldsymbol{\lambda}_a$	14
$\boldsymbol{\lambda}_c$	10
D (μm)	100
J_a^{ref} **(A/m^2)**	1.7×10^5
J_c^{ref} **(A/m^2)**	4.6×10^3

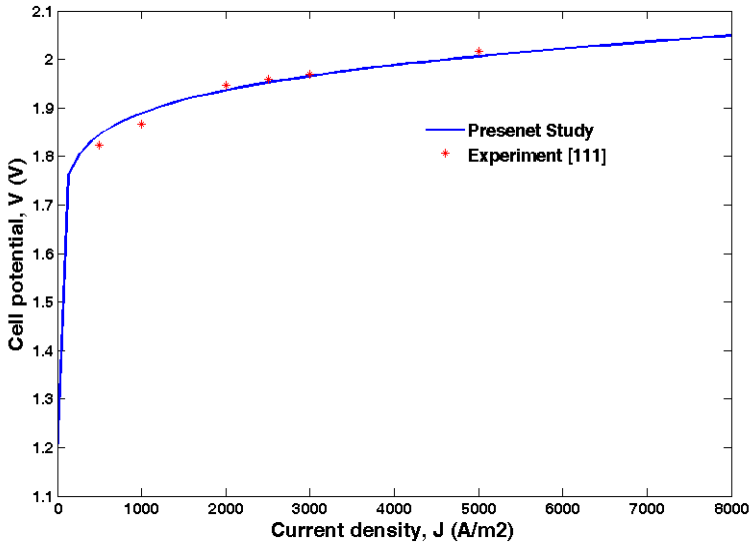

Figure 6.1: Comparison of present model with experimental data for PEM electrolyzer.

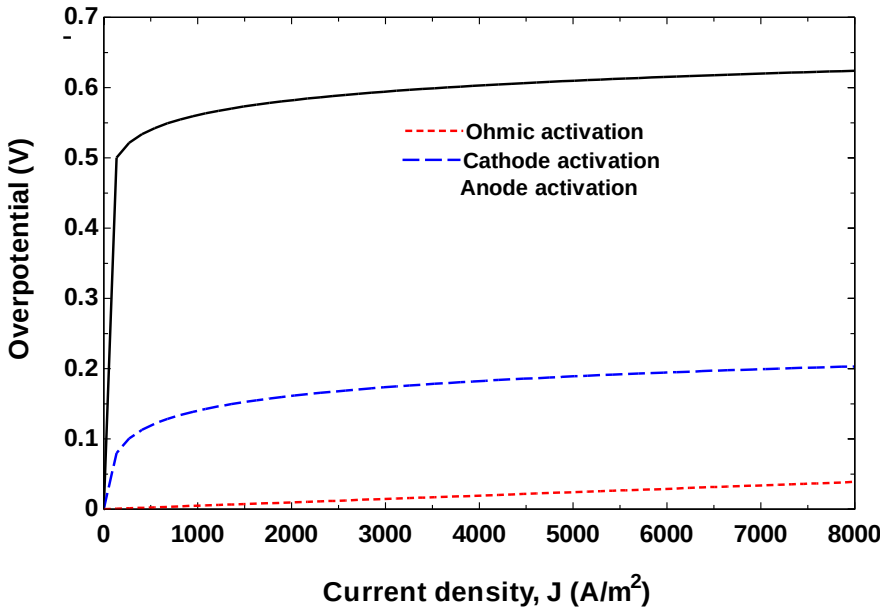

Figure 6.2: Variations of electrolyzer overpotentials at various current densities.

Table 6.3 lists the thermodynamic specifications of the multigeneration system, including heating and cooling loads, electricity generated by the turbines, COP of the absorption chiller, combustion chamber mass flow rate, hydrogen production rate, hot water mass flow rate and cost of environmental impact.

Table 6.3 : Parameter values resulting from energy and exergy analyses of the system.

Parameter	**Value**
$\dot{m}_f$ (kg/s)	0.64
$\dot{Q}_{heating}$ (kW)	5788
$\dot{Q}_{cooling,absorption}$ (kW)	1219
$\dot{Q}_{cooling,ORC}$ (kW)	43
$\dot{W}_{GT}$ (kW)	10000
$\dot{W}_{ST}$ (kW)	786
$\dot{W}_{ORC}$ (kW)	252
η_{multi} (%)	61
Ψ_{multi} (%)	59
$\dot{m}_{H_2}$(kg/h)	1.25
$\dot{m}_{DWH}$(kg/s)	3.58
Absorption chiller COP	0.44
CO_2 emissions (kg/kWh)	132
CO emissions (kg/kWh)	7
$\dot{C}_{env}$ ($/h)	67.65
Total costa rate ($/h)	1090
Total exergy destruction rate (MW)	19.6
Sustainability index	1.73

6.2. 2 Exergy and economic analyses results

The exergy analysis results are summarized in Fig. 6.3, and show that the highest exergy destruction occurs in the combustion chamber (CC), mainly due to the irreversibilities associated with combustion and the large temperature difference between the air entering the CC and the flame temperature. The condenser in the Rankine cycle exhibits the next largest exergy destruction, mainly due to the temperature difference between two fluid streams passing through it, but also due to the pressure drop across the device.

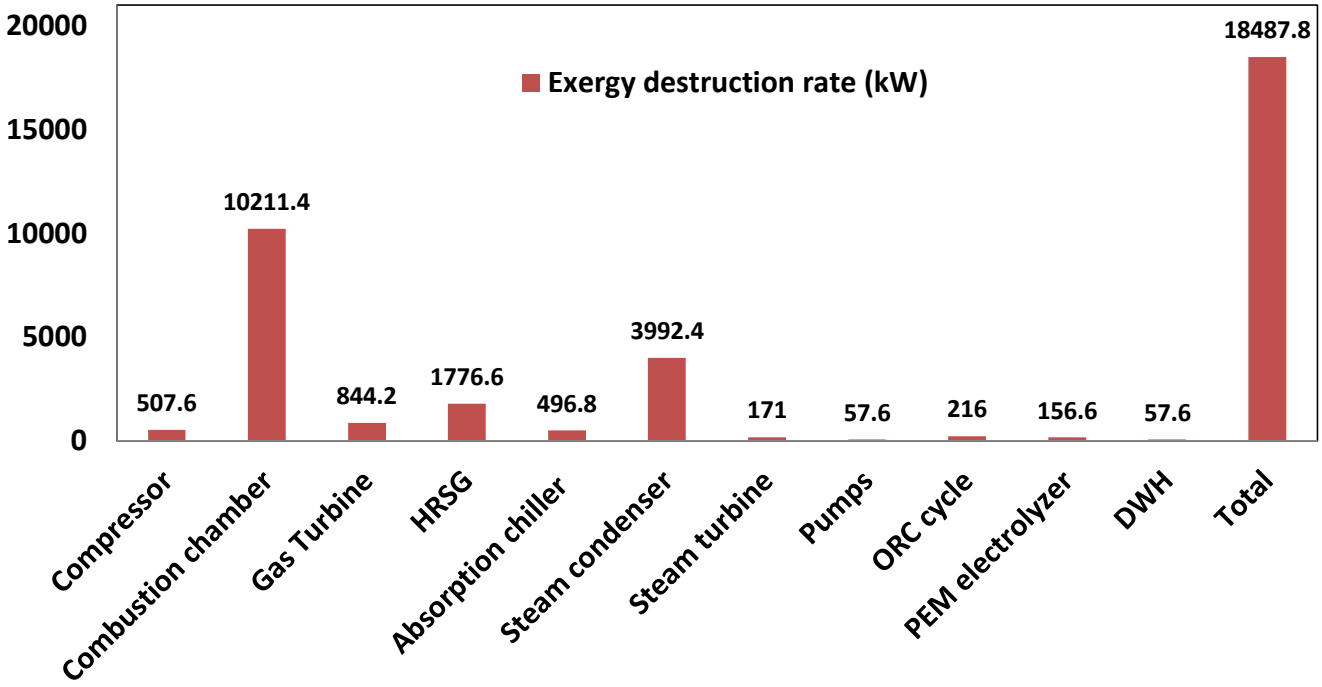

Figure 6.3: Exergy destruction rates for the multigeneration system and its components.

Fig. 6.4 shows for each component the dimensionless exergy destruction ratio. This measure is useful for prioritizing exergy losses in an intuitive manner. Both exergy destruction and the dimensionless exergy destruction ratio are higher in the combustor than in other components, suggesting that it would likely be worthwhile to focus improvement efforts on this component. Moreover, the results show that the absorption cycle does not exhibit significant exergy destructions, in part because it does not directly utilize fuel energy but instead uses steam produced by the HRSG.

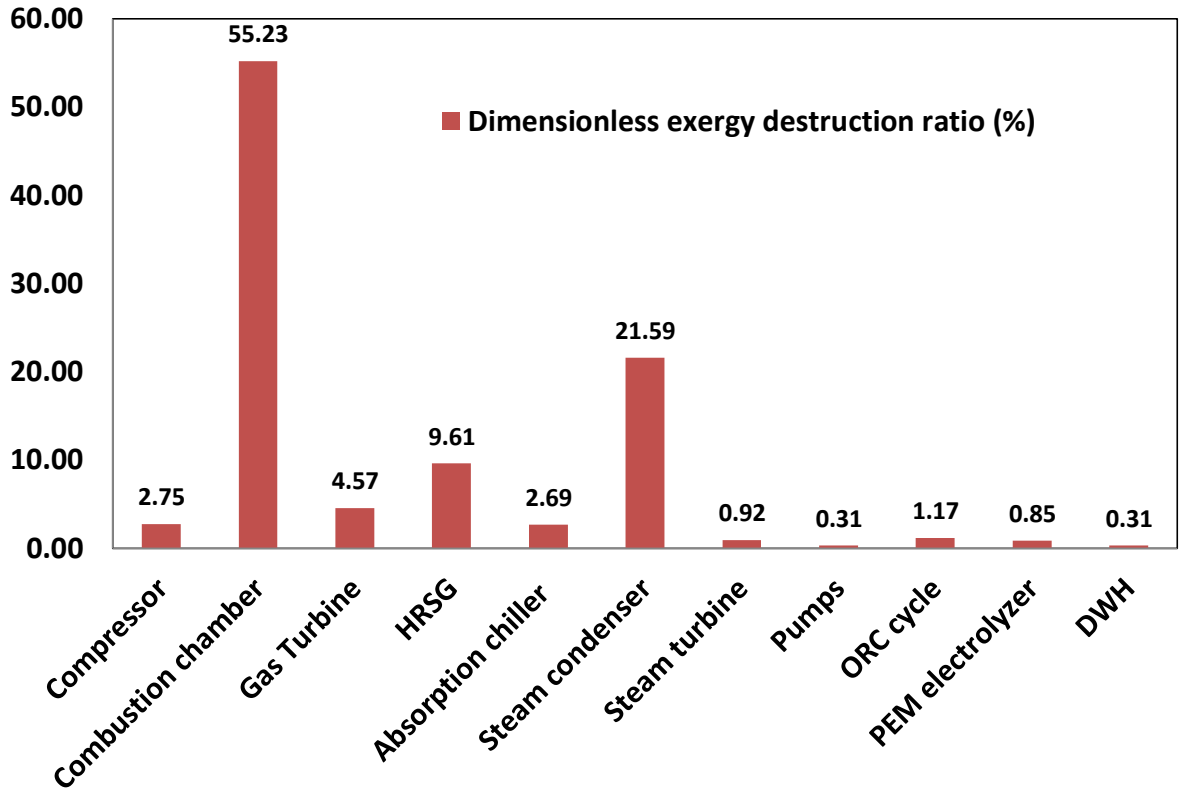

Figure 6.4: Dimensionless exergy destruction ratio for the multigeneration system and its components.

In order to better understand the system performance, energy and exergy efficiency of each subsystem are calculated (see Fig. 6.5). It is seen that energy and exergy efficiencies are higher for the multigeneration system compared to other cycles when it is not configured in an integrated manner. It is also seen that both energy and exergy efficiencies for the multigeneration system are almost double those of a power generation system, mainly due to an increase in the numerator of equation (5.182).

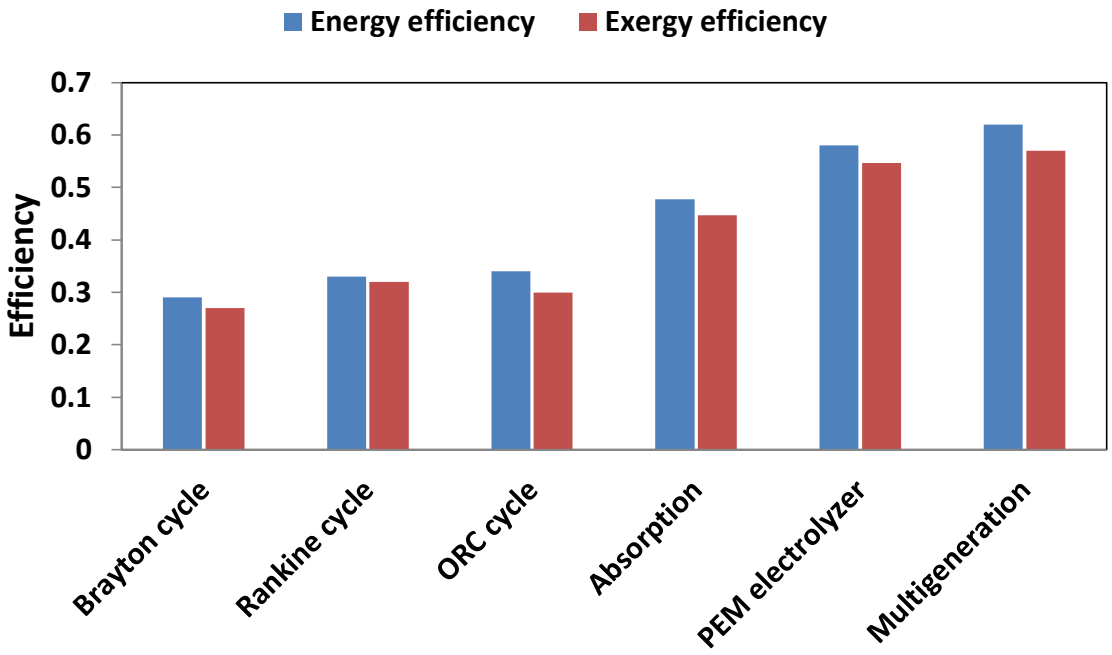

Figure 6.5: Energy and exergy efficiency for the subsystems of the multigeneration system.

6.2.2.1 Effect of varying compressor pressure ratio on system performance

Compressor pressure ratio (r_{AC}) significantly affects system performance like energy and exergy efficiencies. Fig.6.6 shows the variation with compressor pressure ratio of exergy efficiencies, for the system and its sections like power generation. It is observed that fuel consumption decreases as the compressor pressure ratio increases, mainly due to the increase of the air temperature entering the combustion chamber and the corresponding reduction in fuel consumption. The exergy efficiency of the multigeneration cycle is observed to increase with gas turbine isentropic efficiency, due to the corresponding increase in product yield. In addition, it can be seen that there is a sharp increase in exergy efficiency first. The reason is that, at lower pressure ratios, increasing the pressure ratio increases the outlet temperature of the compressor and decreases the fuel mass flow rate injected to the combustion chamber, increasing the efficiency. However, at a certain air compressor pressure ratio, increasing r_{AC} increases the compressor work more than it decreases the fuel mass flow rate. This effect leads to a decrease in the output power. Consequently, the network output first increases significantly and then decreases as compressor pressure ratio increases.

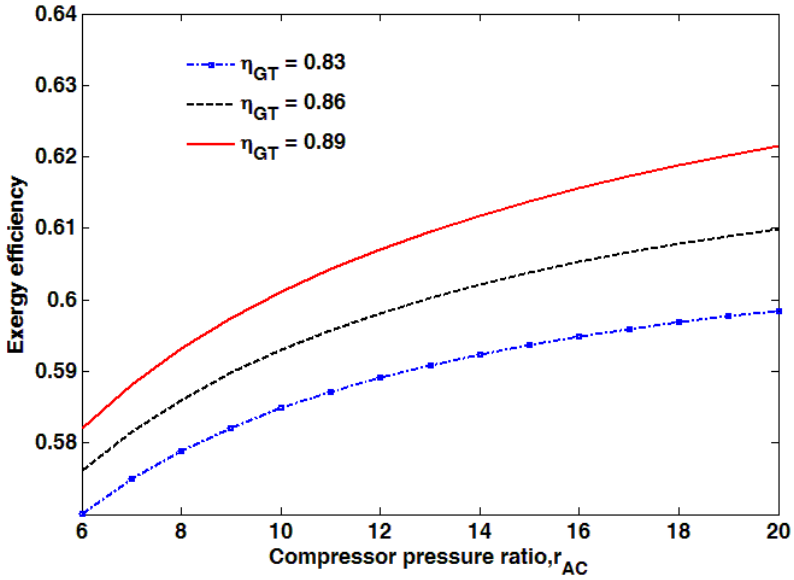

Figure 6.6: Variations with compressor pressure ratio of the trigeneration exergy efficiency for several gas turbine isentropic efficiencies

To understand more comprehensively the effect of varying compressor pressure ratio on the exergy efficiencies, three cycles of the system ranging from power generation to multigeneration are examined (see Fig. 6.7). It is seen in Fig. 6.7 that the multigeneration cycle has higher energy and exergy efficiencies than the GT and CHP cycles. This observation results from the large quantity of energy lost to the environment from the outlet of the gas turbine in the GT cycle. The variations of exergy efficiency in Fig. 6.7 more accurately reflect thermodynamic performance. The exergy efficiency of the cogeneration cycle is higher than the exergy efficiency of the gas turbine cycle, but the difference is less compared to the difference between the energy efficiencies of both cycles, because the exergy associated with heating is less than the energy of the process heat. In addition, the energy efficiency of the multigeneration cycle is higher than the energy efficiency of the cogeneration cycle, which is higher than the energy efficiency of gas turbine cycle.

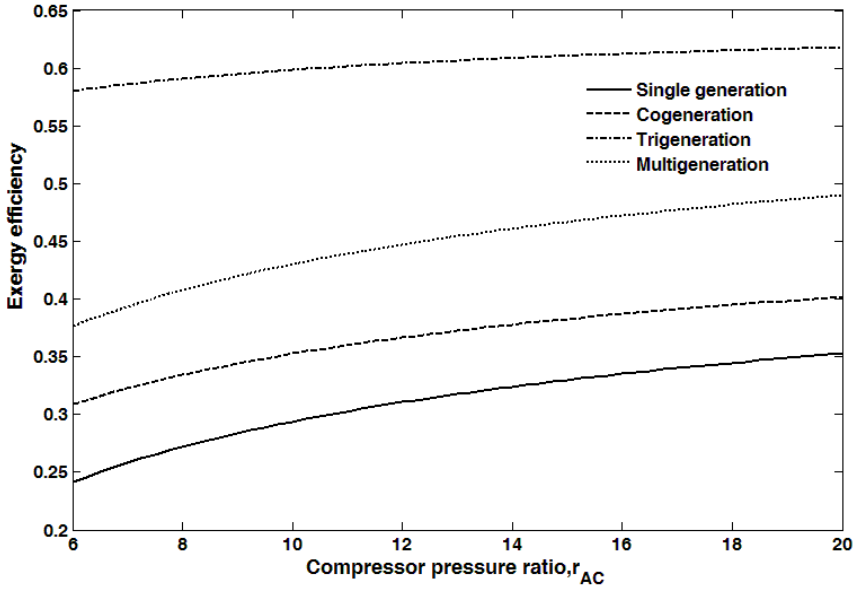

Figure 6.7: Variations with compressor pressure ratio of energy and exergy efficiencies

This observation is due to the fact that the flue gases from the gas turbine are used to produce the cold in the multigeneration plant. The exergy efficiency of the multigeneration cycle is slightly higher than that of the cogeneration cycle because the exergy associated with the cooling load is small.Fig. 6.8 shows the variation with compressor pressure ratio of both exergy efficiency and exergy destruction rate for the system. It is observed that fuel consumption decreases as the compressor pressure ratio increases, mainly due to the increase of the air temperature entering the combustion chamber and the corresponding reduction in fuel consumption. The reason is that, at lower pressure ratios, increasing the pressure ratio increases the outlet temperature of the compressor and decreases the fuel mass flow rate injected to the combustion chamber, increasing the efficiency (see Fig. 6.9). Fig. 6.10 shows the variation with compressor pressure ratio of both heating and cooling load for the system. It is observed that both heating and cooling load of the system decreases as compressor pressure ratio increases. It is due to the fact that an increase in pressure ratio results in a decrease in both gas turbine outlet temperature and gas turbine mass flow rate which is the inlet energy for the bottoming cycles which are Rankine and absorption chiller systems. The more the input energy the higher the heating and cooling load can be achieved.

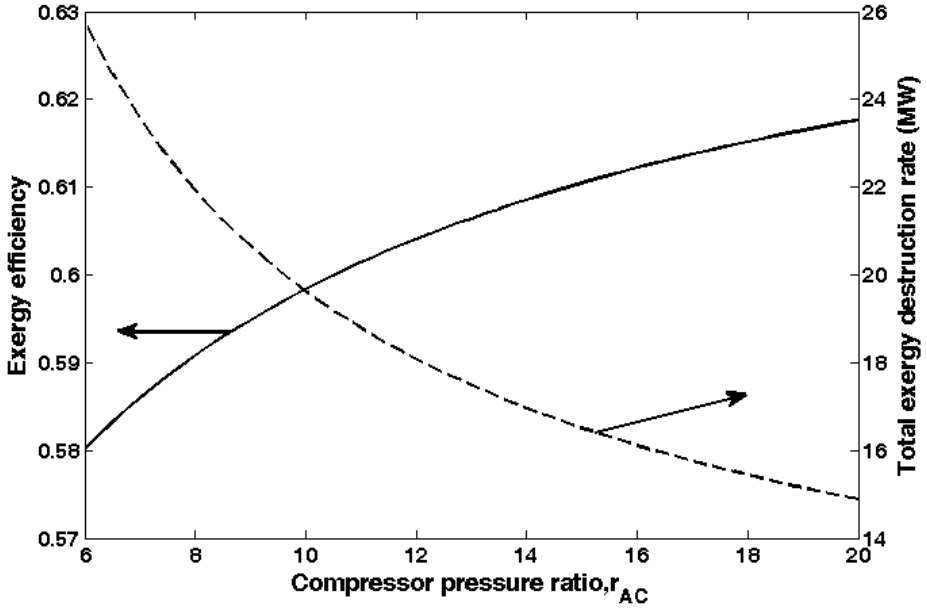

Figure 6.8: Variations with compressor pressure ratio of exergy efficiency and exergy destruction rate for the trigeneration system

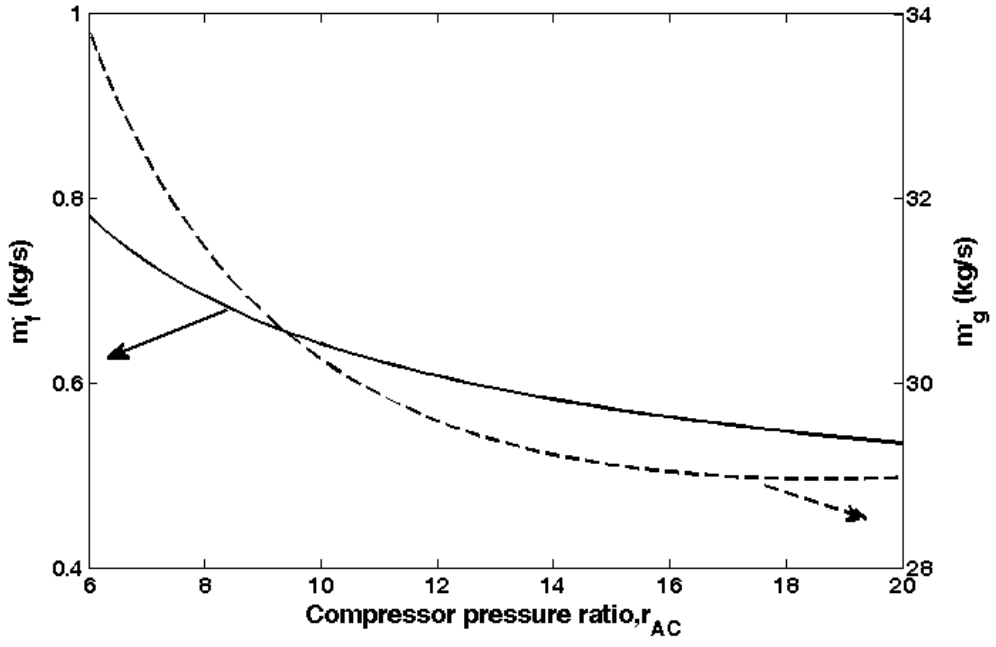

Figure 6. 9: Variations with compressor pressure ratio of combustion chamber and gas turbine mass flow rate

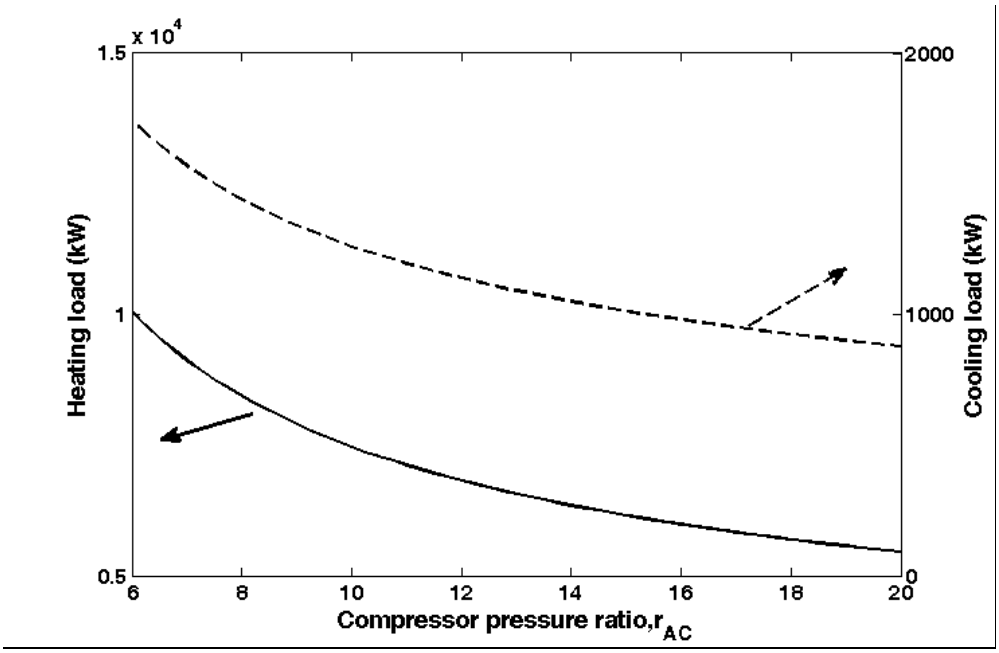

Figure 6.10: Variations with compressor pressure ratio of heating and cooling load of the multigeneration.

Fig. 6.11 shows the variation with compressor pressure ratio of both steam cycle and ORC power output. It is observed that and increase in pressure ration results in a decrease in both power outputs which is due to a reduction of gas turbine outlet temperature which leads to a decrease in energy input for both systems. Therefore, the lower the input energy to steam and ORC cycles, the lower the power output.

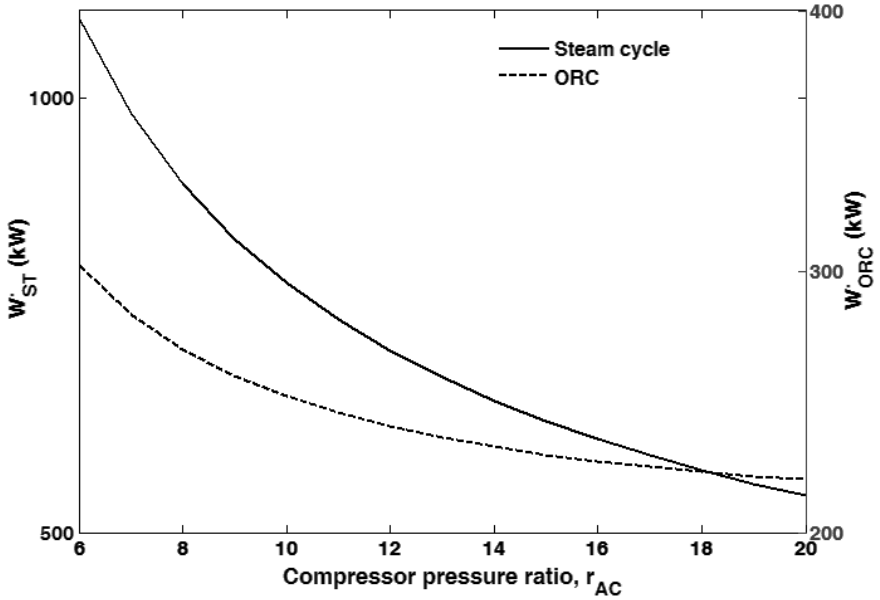

Figure 6.11: Variations with compressor pressure ratio of steam turbine and ORC net power output.

6.2.2.2 Effect of varying gas turbine inlet temperature (GTIT) on system performance

The gas turbine inlet temperature (GTIT) is a significant design parameter in a gas turbine cycle. Raising this parameter can increase gas turbine output power. But an energy balance of the combustion chamber indicates that the fuel mass flow input rate also decreases as the GTIT rises (see Fig. 6.12). The decreased fuel input is also reflective of the increase in turbine exhaust temperature, following equations. (5.29) and (5.30).

Fig. 6.13 shows the variations with turbine inlet temperature of the exergy efficiencies for the power generation, CHP and multigeneration cycles. The exergy efficiencies are observed to increase with increasing in turbine inlet temperature, because of the corresponding increase in net work output and relatively smaller increase in heat addition to the cycle. The same trend is observed for the exergy destruction rate which is shown in Fig. 6.14.

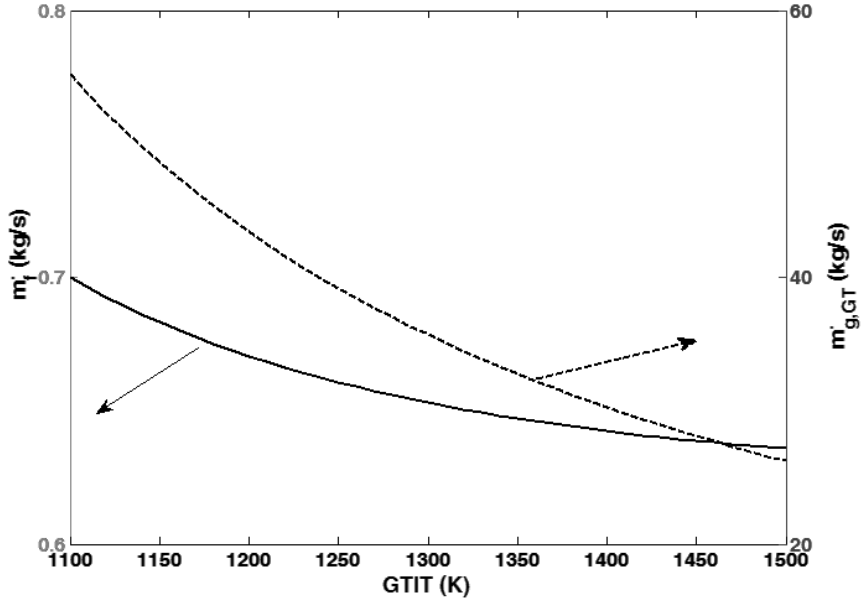

Figure 6.12: Variations with gas turbine inlet temperature of total combustion chamber mass flow rate and flue gas mass flow rate.

Fig. 6.15 shows the variation with GTIT of both heating and cooling load of the system. It is observed that an increase in GTIT results in an increase in both heating and cooling load of the system. This is due to the fact that an increase in GTIT leads to an increase in gas turbine outlet temperature while other parameters are fixed due to equation (5.29).

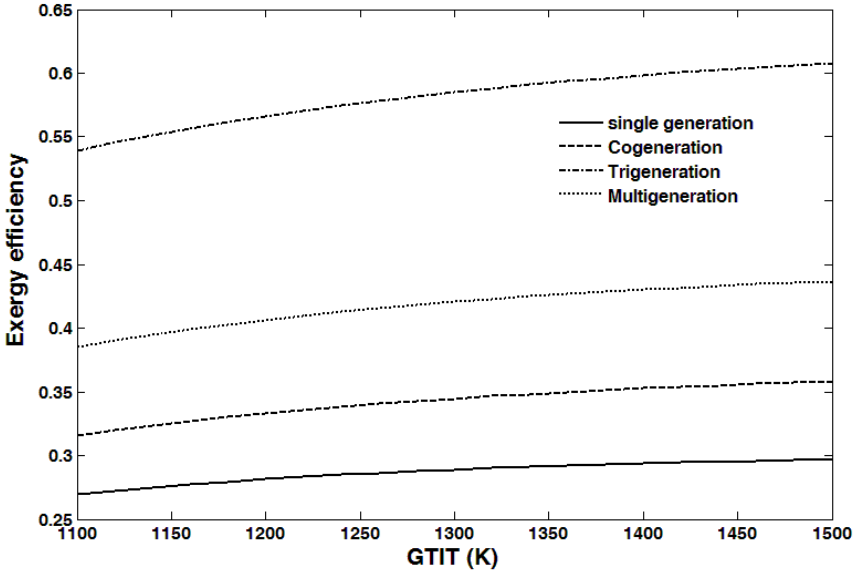

Figure 6.13: Variations of gas turbine inlet temperature of exergy efficiency

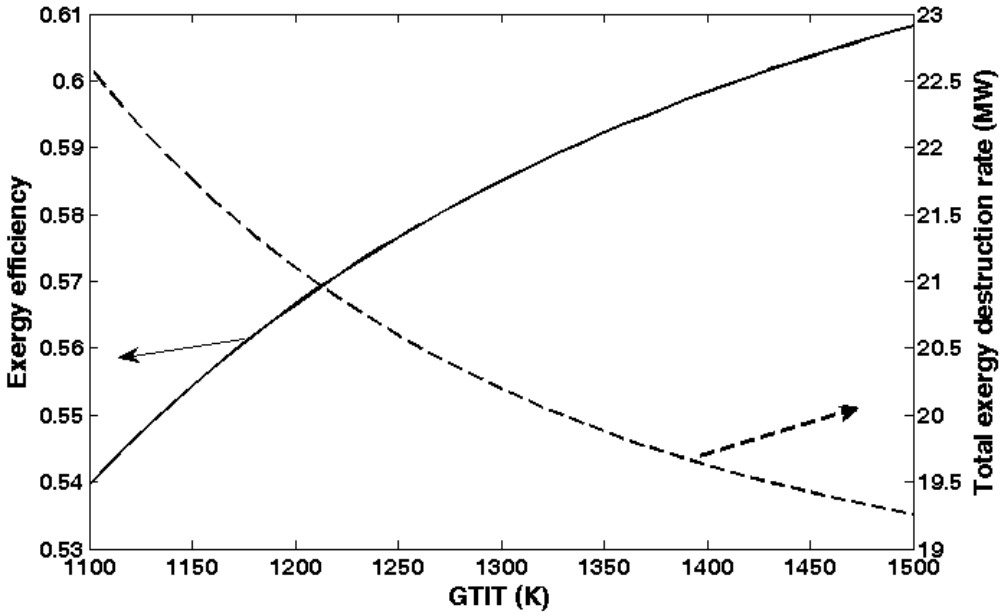

Figure 6.14: Variations with gas turbine inlet temperature of exergy efficiency total exergy destruction rate

Since gas turbine outlet temperature is the input of the bottoming cycles, an increase in this input results in an increase in heating and cooling load of the system. Fig. 6.16 shows the variation with GTIT of both steam cycle and ORC cycle power output.

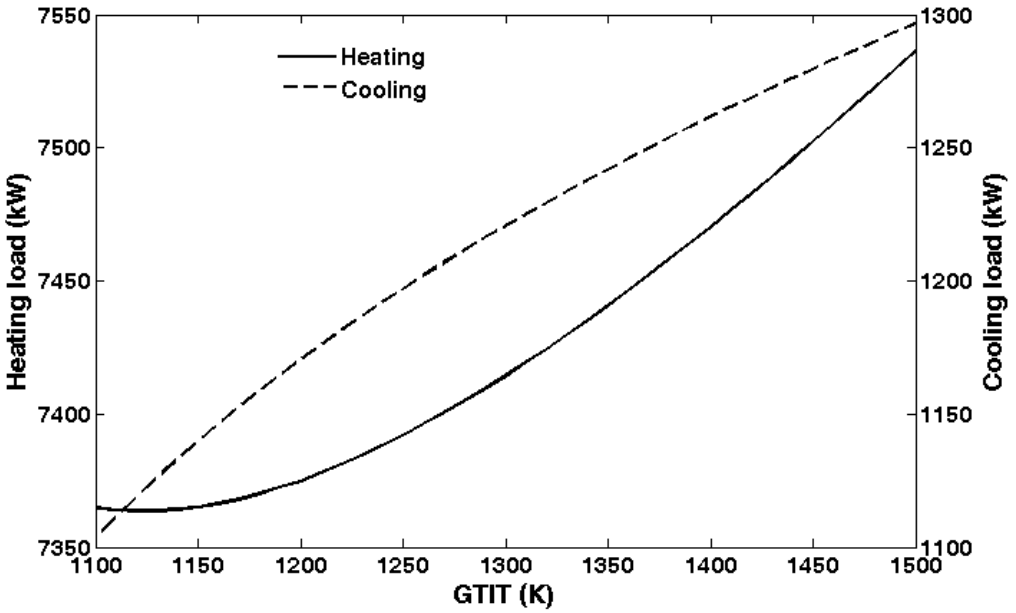

Figure 6.15: Variations with gas turbine inlet temperature of heating and cooling load of the system.

It is seen that and increase in GTIT results in an increase in steam cycle power output while in decreases the ORC power output. An increase in steam cycle power is due to the fact that an increase in GTIT leads to an increase in gas turbine outlet temperature and a decrease in gas turbine mass flow rate as shown in Fig.6.12; however an increase in GTIT dominates the decrease in gas turbine mass flow rate in a sense that the total input energy entering the HRSG increases.

An increase in HRSG inlet energy results in an increase in steam turbine inlet enthalpy which finally results in an increase in steam turbine power output. However, an increase in GTIT leads to a decrease in ORC power output.

Since the outlet energy of HRSG is the main source of ORC cycle, an increase in GTIT results in a decrease in HRSG outlet energy which decrease the ORC power output. Same trend is observed for hydrogen production mass flow rate and hot water mass flow rate as shown in Fig. 6.17. When the HRSG inlet temperature increases while keeping other design parameters constant, the HRSG outlet temperature decreases as the pinch point temperature is constant.

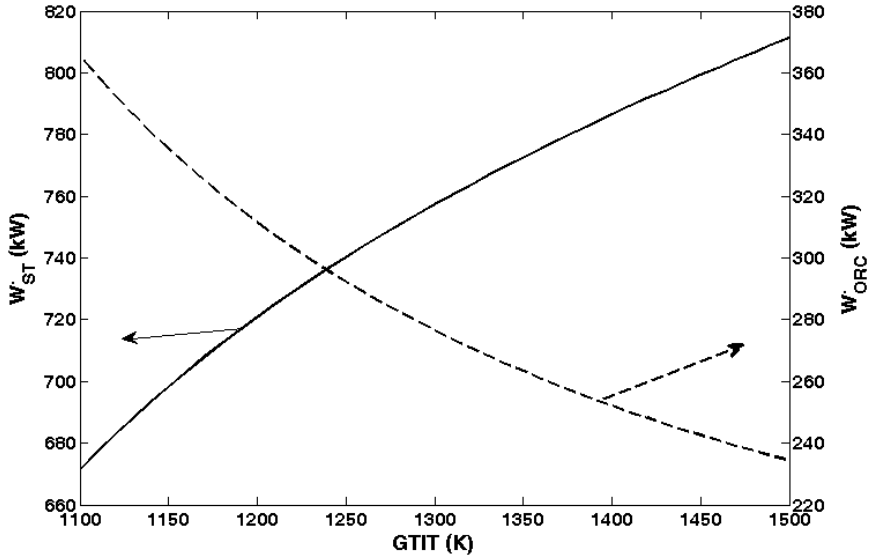

Figure 6.16: Variations with gas turbine inlet temperature of steam and ORC power output.

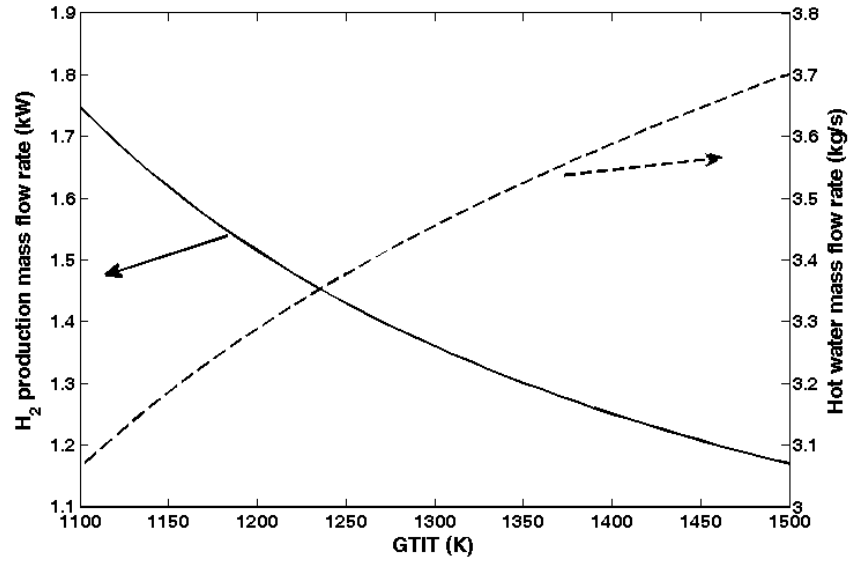

Figure 6.17: Variations with gas turbine inlet temperature of hydrogen production and hot water mass flow rate.

6.2.2.3 Effect of varying other cycle parameters on system performance

The effect of varying several other design parameters on the performance of the cycle is examined. Since the steam pressure produced in the HRSG is an important design parameter, the effect of this pressure on efficiencies is discussed. Fig. 6.18 shows the impact of high-pressure steam on system performance.

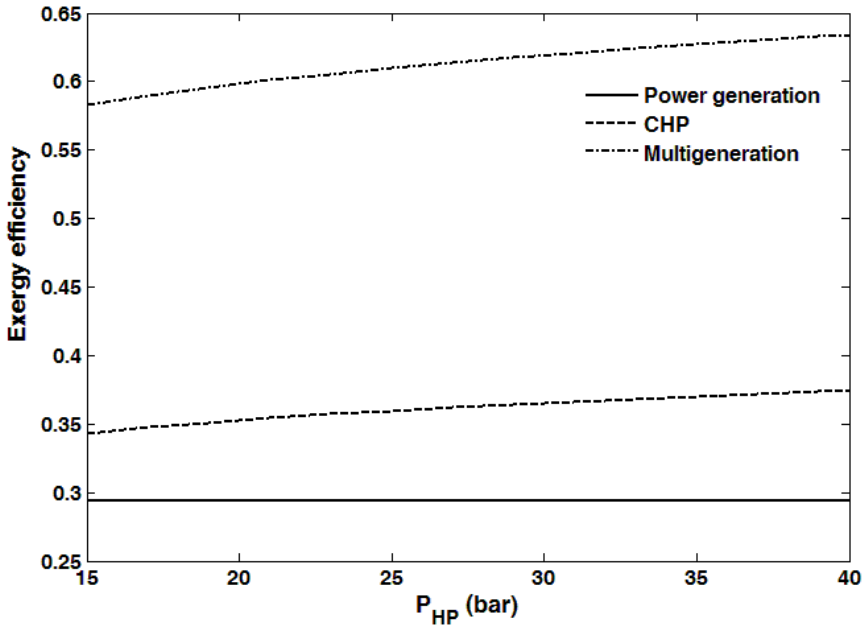

Figure 6.18: Variations with pressure of high-pressure steam, P_{HP}, on system energy and exergy efficiencies.

It is found that the CHP exergy efficiency increases with the HP steam pressure if the turbine exhaust temperature is relatively high. The multigeneration exergy efficiency also increases with increasing process heat pressure, but the increase in multigeneration exergy efficiency is more significant than CHP. It is also shown that exergy efficiency of the power generation cycle does not change with high pressure as it is the upper cycle and it does not include any heating or cooling in its definition. An increase in high pressure leads to an increase in the turbine inlet enthalpy which finally results in an increase in turbine power output. Fig. 6.19 shows this trend. An increase in high pressure also has an effect on ORC power output as shown in Fig. 6.19.

Fig.6.20 shows the effect of varying evaporator temperature in the absorption cycle on the system performance, in terms of exergy efficiencies. The exergy efficiencies of both the gas turbine cycle and the CHP system are not significantly dependent on evaporator temperature. The exergy efficiency of the multigeneration cycle also increases with increasing evaporator temperature, but the increase is small because the exergy associated with the cold is small. Generally, evaporator temperature does not have a significant effect on the system performance.

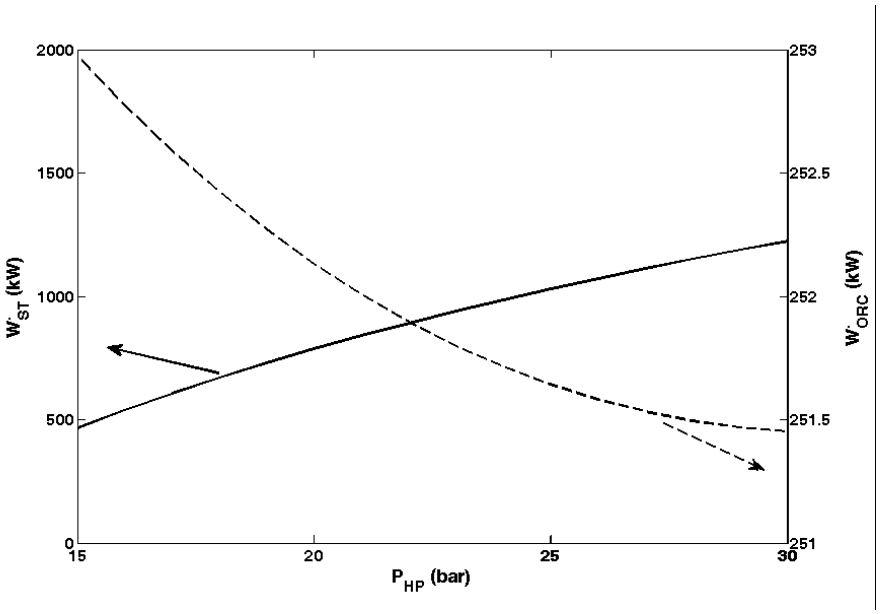

Figure 6.19: Variations with HRSG high pressure of steam cycle and ORC power output.

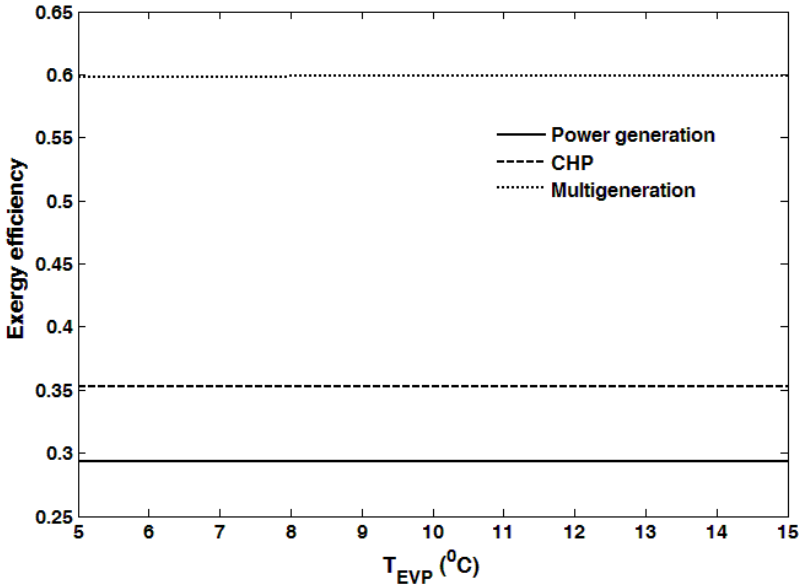

Figure 6.20: Variations with T_{EVP} of various system exergy efficiencies.

Fig. 6.21 shows the variation with high pressure pinch point temperature (PP_{HP}) of both steam exergy efficiency and total exergy destruction rate. It is seen that an increase in PP_{HP} temperature results in a decrease in system exergy efficiency. This is due to the fact that the higher the pinch point temperature, the lower the energy being utilized in HRSG which leads to a reduction of steam turbine power output. Also, an increase in PP_{HP} leads to an increase in total exergy destruction due to an increase in HRSG irreversibilities.

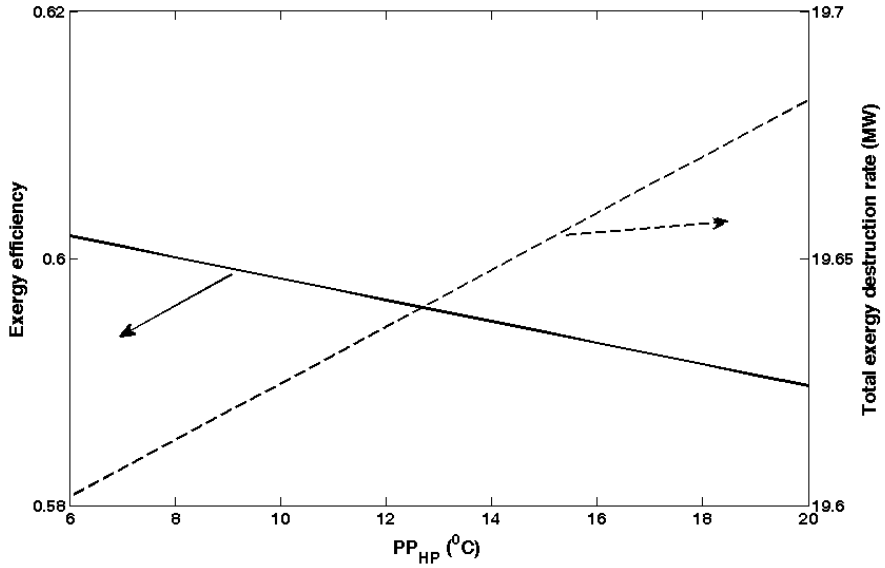

Figure 6.21: Variations with high pressure pinch point temperature of exergy efficiency and total exergy destruction rate.

Fig. 6.22 shows the variation with high pressure pinch point temperature (PP_{HP}) of total cost rate of the system. It is observed that an increase in PP_{HP} decrease the total cost rate of the system. An increase in pinch point temperature while fixing other design parameters, results in a decrease in heat transfer area for the HRSG component. This is why the total cost rate of the system decreases.

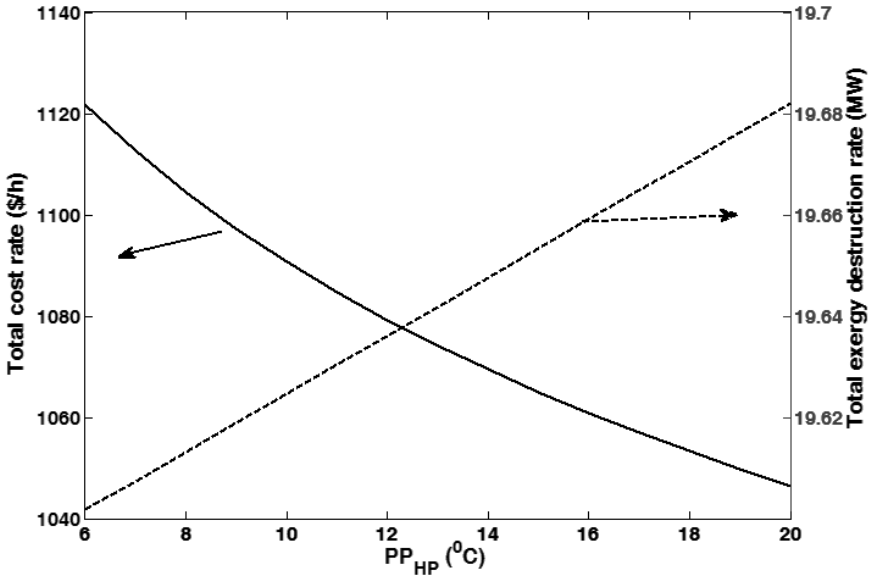

Figure 6.22: Variations with high pressure pinch point temperature of total cost rate and total exergy destruction rate.

6.2. 3 Environmental impact assessment

To provide environmental insights, the environmental impact of the gas turbine cycle is compared to that of the multigeneration system in Fig. 6.23. It is seen that the multigeneration cycle has less CO_2 emissions than the GT and CHP cycles, providing a significant motivation for the use of multigeneration cycles. It is also observed that the multigeneration system has a higher exergy efficiency than the other cycles. Fig. 6.24 also shows that the multigeneration cycle has less CO emissions than the GT and CHP cycles, providing another motivation for the use of multigeneration cycles. However, the amount of CO emission is significantly less that the amount of CO_2 emissions of the system.

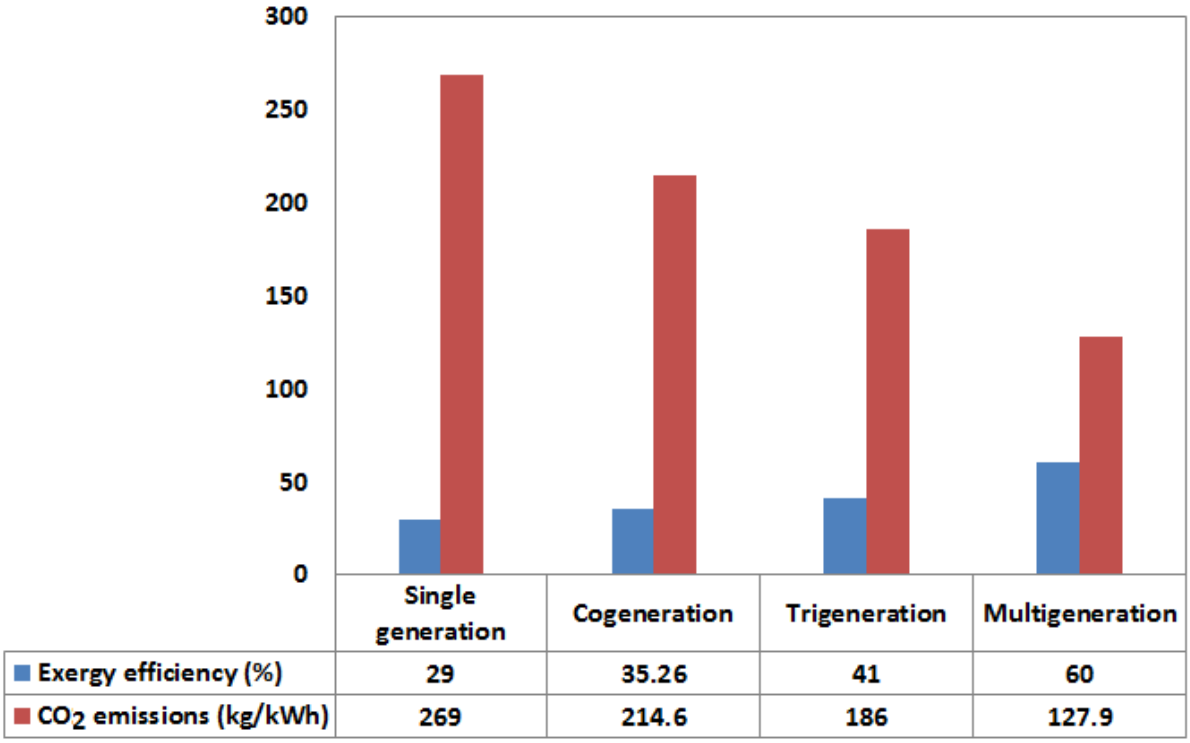

Figure 6.23: Comparison of exergy efficiency and unit CO_2 emissions of selected types of plants.

Fig. 6.25 shows the effect on compressor pressure ratio on the CO_2 emissions for various cases. It is seen that the multigeneration cycle has less CO_2 emissions than the power and CHP cycles, another benefit of multigeneration. In addition, increasing the compressor pressure ratio is seen to decrease CO_2 emissions for the power cycle, CHP and multigeneration cycles.

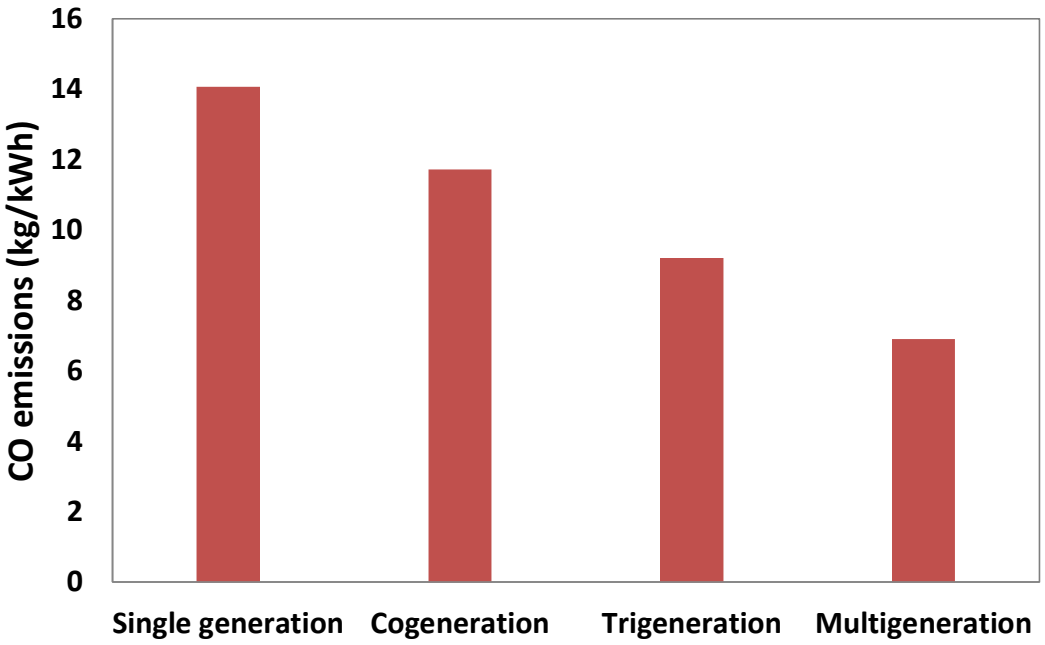

Figure 6.24: Unit CO emissions of selected types of plants.

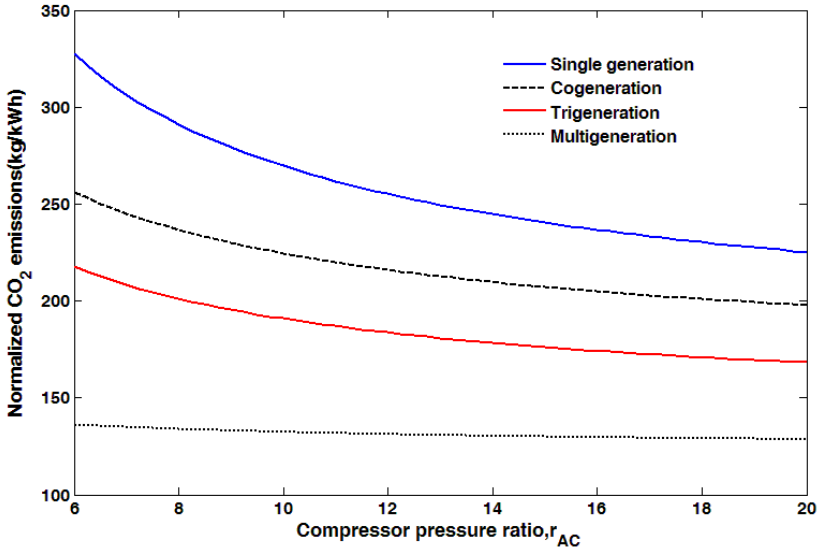

Figure 6.25: Variations of unit CO_2 emissions with compressor pressure ratio for selected cases.

When the compressor pressure ratio increases, the gas turbine outlet temperature decreases. Since this temperature has a significant effect in producing heating and cooling, the unit CO_2 emission of the cycle increases, where the CO_2 emission is in units of kg of CO_2 per MWh of electricity, cooling and heating. Similar results are obtained for CO emissions of the system, as shown in Fig. 6.26. The desire of preserving the environment while converting energy

resources into different forms can be assessed quantitatively using an environmental index of performance. The outputs of the energy conversion process are not only the desired products like electricity, heating and cooling, but also pollutant emissions (e.g., NO_x and CO), CO_2 emissions, thermal pollution (e.g., warming of process air and water), solid wastes, etc.

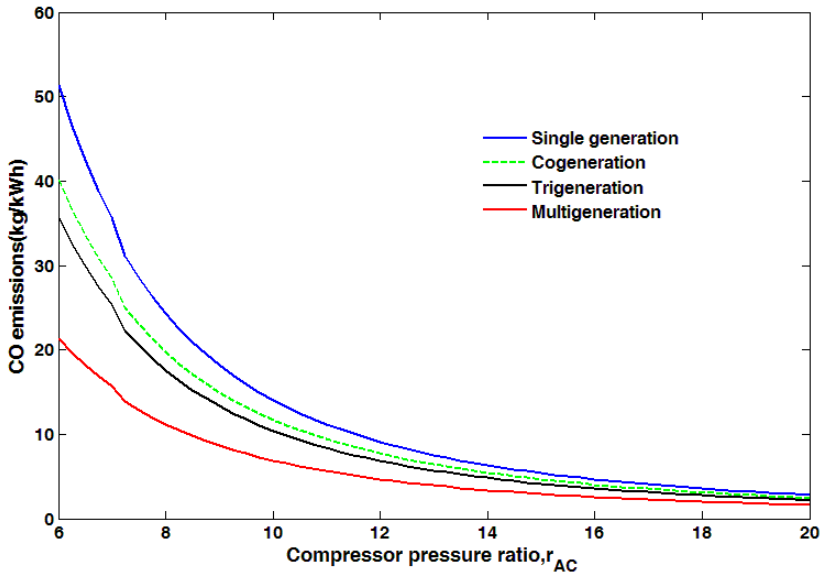

Figure 6.26: Variations of unit CO emissions with compressor pressure ratio for selected cases.

Reduction or minimization of these undesired effects may be an objective from the energetic perspective. A single pollutant can be considered in such an environmental impact assessment objective according to its degree of harmfulness. If more than one pollution source is taken into account, their degrees of harmfulness can be introduced as relative weights of each pollutant measure. The weighting may also be considered from economic point of view when the unit damage cost of each pollutant is available. These criteria can also be combined to form a hybrid criterion which includes information from each.

In this analysis, we express the environmental impact as the total cost rate of pollution damage ($/s) due to CO, NO_x and CO_2 emissions by multiplying their respective flow rates by their corresponding unit damage costs (C_{CO}, C_{NOx} and C_{CO2}, which are taken to be equal to 0.02086 $/kg, 6.853 $/kg and 0.024 $/kg, respectively) [116]. The cost of pollution damage is assumed here to be added directly to other system costs.Expanding the results for CO_2 emissions, we investigate the effect of compressor pressure ratio on cost of environmental impact and sustainability index. Fig. 6.27 shows that increasing the compressor pressure decreases the cost of environmental impact, due to the reduction of mass flow rate injected into the combustion

chamber. The sustainability index increases correspondingly for all three cycles considered (GT, CHP and multigeneration).

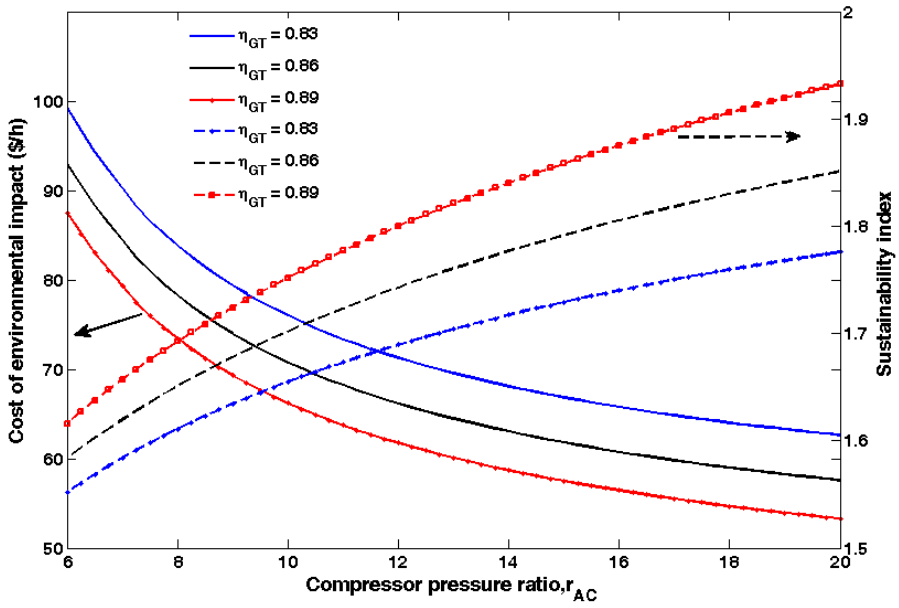

Figure 6.27: Variations with compressor pressure ratio of sustainability index and cost rate of environmental impact.

Fig. 6.28 shows the effect of compressor pressure ratio on total exergy destruction of the cycle and sustainability index, and similar results are obtained as in Fig. 6.27. That is, the overall exergy destruction of the cycle decreases and the sustainability index increases with increasing compressor pressure ratio. Exergy efficiency, exergy destruction, environmental impact and sustainability are thus observed to be linked in such systems, supporting the utility of exergy and environmental impact assessment. Fig. 6.29 shows the effect of compressor pressure ratio on total cost rate and cost of environmental impact. An increase in compressor pressure ratio leads to a decrease in both costs. The reason for the compressor pressure ratio effect is that an increase in this parameter increases the outlet temperature and decreases the mass flow rate injected to the combustion chamber. As the first term in the total cost rate is directly associated with the mass flow rate of the fuel cost, any decrease in this term results in a decrease in the total cost of the system. A significant design parameter is the gas turbine inlet temperature (*GTIT*). Raising this parameter can increase gas turbine output power. But an energy balance of the combustion chamber indicates that the fuel input rate also decreases as the *GTIT* rises.

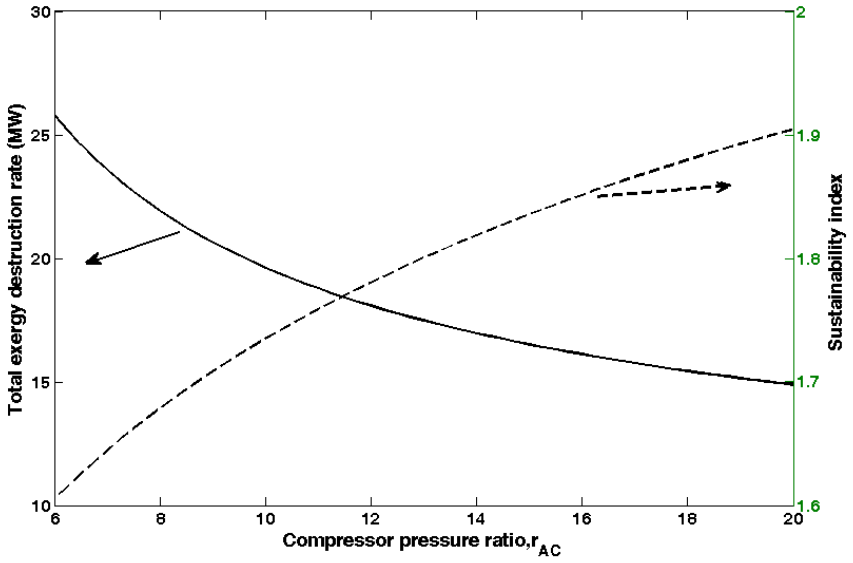

Figure 6.28: Variations with compressor pressure ratio of total exergy destruction rate and sustainability index.

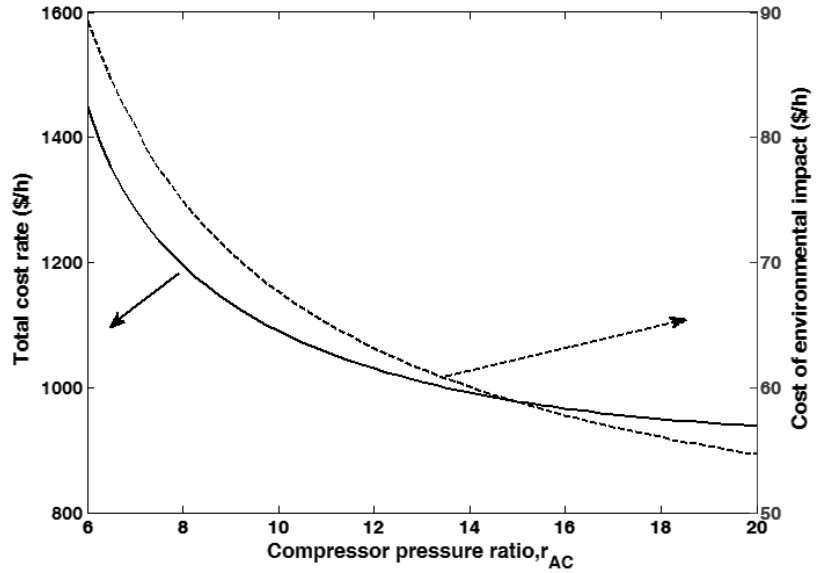

Figure 6.29: Variations with compressor pressure ratio of total cost rate and cost of environmental impact.

The decreased fuel input is also reflective of an increase in turbine exhaust temperature. The variations of CO_2 emissions for the cycles with gas turbine inlet temperature are shown in Fig. 6.30. CO_2 emissions are seen to decrease with increasing *GTIT*. The mass flow rate of gases through the combustion chamber decreases with an increase in *GTIT*, and also the net output power and the heating and cooling loads increase. Multigeneration is observed to be the most advantageous option from an environmental point of view.

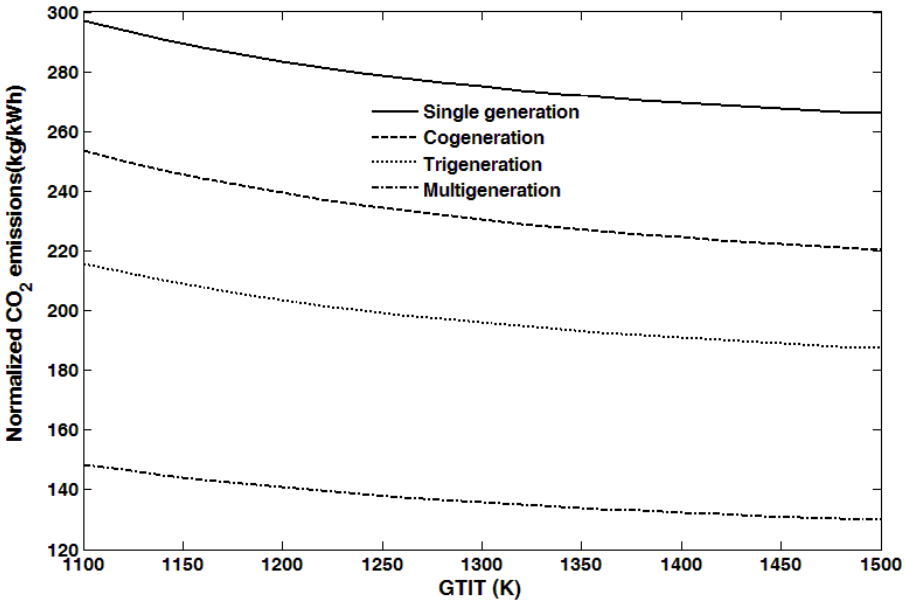

Figure 6.30: Variations of gas turbine inlet temperature (*GTIT*) on normalized CO_2 emissions.

Same results were obtained for the CO emissions of the system as shown in Fig. 6.31. The variations with GTIT of both cost of environmental impact and sustainability index are shown in Fig. 6.32, where the cost of environmental impact is seen to decrease with increasing *GTIT*.

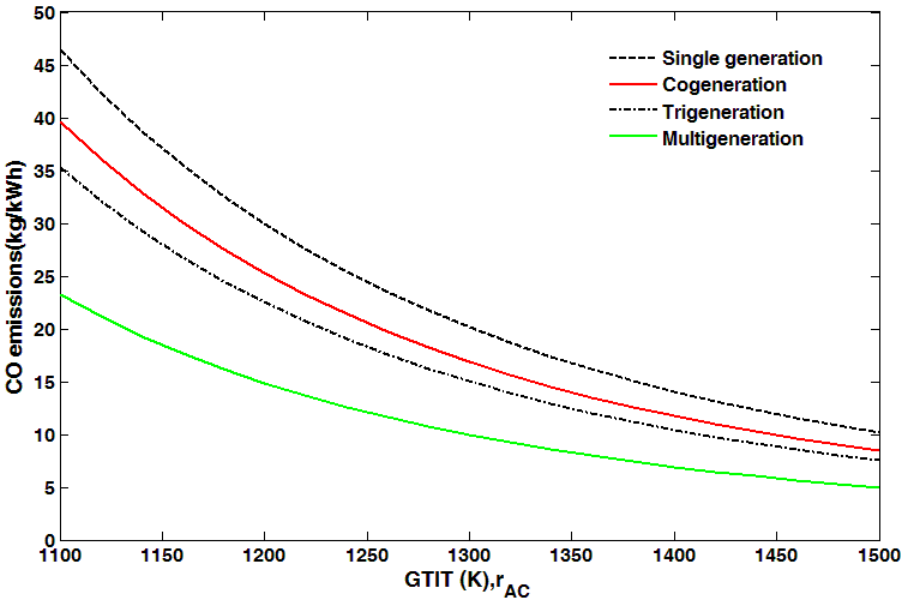

Figure 6.31: Variations of gas turbine inlet temperature (GTIT) on normalized CO emissions.

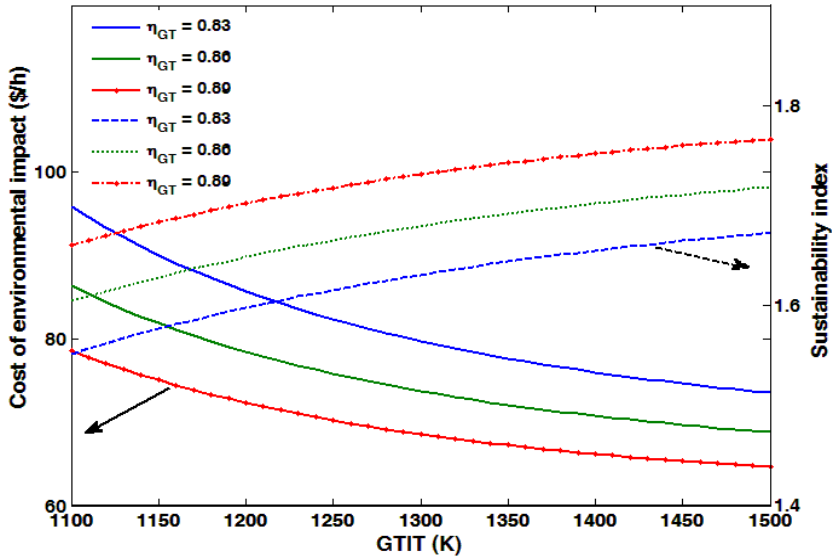

Figure 6.32: Variations with gas turbine inlet temperature of sustainability index and cost rate of environmental impact.

6.2.4 Multi-objective optimization

A multi-objective optimization method based on an evolutionary algorithm is applied optimization to the multigeneration system for heating, cooling, electricity, hot water and hydrogen to determine the best design parameters for the system. Objective functions, design parameters and constraints, and overall optimization are described in this section.

6.2.4.1 Definition of objectives

Two objective functions are considered here for multi-objective optimization: exergy efficiency (to be maximized) and total cost rate of product (to be minimized). The cost of pollution damage is assumed to be added directly to the expenditures that must be paid, making the second objective function the sum of thermodynamic and environmental objectives. Consequently, the objective functions in this analysis can be expressed as follows:

Exergy efficiency

$$\Psi_{multi} = \frac{\dot{W}_{net,GT}+\dot{W}_{net,ST}+\dot{W}_{net,ORC}+\dot{E}x_{heating}+\dot{E}x_{cooling,chiller}+\dot{E}x_{cooling,ORC}+\dot{E}x_{H_2}+\dot{E}x_{18}}{\dot{E}x_f} \quad (6.1)$$

Total cost rate

$$\dot{C}_{tot} = \sum_k \dot{Z}_k + \dot{C}_f + \dot{C}_{env} \quad (6.2)$$

where the cost rates of environmental impact and fuel are expressed as

$$\dot{C}_{env} = C_{Co}\dot{m}_{Co} + C_{NOx}\dot{m}_{NOx} + C_{Co_2}\dot{m}_{Co_2} \;\&\; \dot{C}_f = c_f\dot{m}_f\, LHV \tag{6.3}$$

Here, $\dot{Z}_K$ is the purchase cost of each component. More details about equipment purchase cost can be found elsewhere [64].The purchase cost of each component in this multigeneration system was explained in section 5.12.1. Also c_f is the fuel cost which is taken to be 0.003 $/MJ in this study. In this analysis, we express the environmental impact as the total cost rate of pollution damage ($/s) due to CO, NO_x and CO_2 emissions by multiplying their respective flow rates by their corresponding unit damage costs (C_{CO}, C_{NOx} and C_{CO2}, which are taken to be equal to 0.02086 $/kg, 6.853 $/kg and 0.024 $/kg, respectively) [64]. The cost of pollution damage is assumed here to be added directly to other system costs.

6.2.4.2 Decision variables

The following decision variables (design parameters) are selected for this study: compressor pressure ratio (r_{AC}), compressor isentropic efficiency (η_{AC}), gas turbine isentropic efficiency (η_{GT}), gas turbine inlet temperature (*GTIT*), high pressure pinch point temperature (PP_{HP}) difference, low pressure pinch point temperature (PP_{LP}) difference, high pressure (P_{HP}), low pressure (P_{LP}), steam turbine isentropic efficiency (η_{ST}), pump isentropic efficiency (η_p), condenser pressure (P_{Cond}), absorption chiller evaporator temperature (T_{EVP}), ORC turbine inlet pressure (P_{ORC}), ORC turbine extraction pressure ($P_{ex,ORC}$) and ORC evaporator pressure ($P_{EVP,ORC}$). Although the decision variables may be varied in the optimization procedure, each is normally required to be within a reasonable range. Such constraints, based on earlier reports are listed in Table 6.4.

6.2.4.3 Evolutionary algorithm: Genetic algorithm

Genetic algorithms apply an iterative, stochastic search strategy to find an optimal solution and imitate in a simplified manner principles of biological evolution [93]. A characteristic of an evolutionary algorithm is a population of individuals, where an individual consists of the values of the decision variables (structural and process variables here) and is a potential solution to the optimization problem [14]. More details about genetic algorithm and its procedure are given elsewhere [14, 93].

6.2.4.4 Results and discussion

The genetic algorithm optimization is performed for 250 generations, using a search population size of M = 100 individuals, crossover probability of p_c = 0.9, gene mutation probability of p_m = 0.035 and controlled elitism value c = 0.55. The results of the optimization are given and described.

6.2.4.4.1 Optimization results

Fig. 6.33 shows the Pareto frontier solution for this multigeneration system with objective functions indicated in equation. (6.1) and (6.2) in multi-objective optimization. It can be seen in this figure that the total cost rate of products increases moderately as the total exergy efficiency of the cycle increases to about 65 %. Increasing the total exergy efficiency from 65 % to 68 % increases the cost rate of product significantly.

Table 6.4: Optimization constraints and their rationales

Constraint	**Reason**
$GTIT$ < 1550 K	Material temperature limit
P_2/P_1 < 22	Commercial availability
η_{AC} < 0.9	Commercial availability
η_{GT} < 0.9	Commercial availability
P_{HP} < 40 bar	Commercial availability
P_{LP} < 5.5 bar	Commercial availability
10 ºC < PP_{HP} < 22 ºC	Heat transfer limit
12 ºC < PP_{LP} < 22 ºC	Heat transfer limit
η_{ST} < 0.9	Commercial availability
η_p < 0.9	Commercial availability
2 ºC < T_{EVP} < 6 ºC	Cooling load limitation
8 kPa < P_{Cond} < 10 kPa	Thermal efficiency limit
500 kPa < P_{ORC} < 750 kPa	ORC commercial availability
180 kPa < $P_{ex,ORC}$ < 250 kPa	ORC commercial availability
20 kPa < $P_{EVP,ORC}$ < 35 kPa	Cooling load limitation

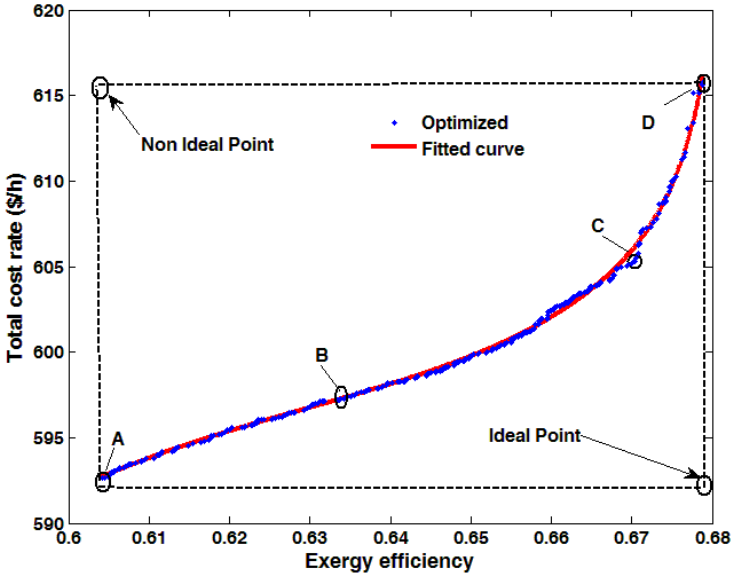

Figure 6.33: Pareto Frontier: Best trade off values for the objective functions

The results of optimum exergy efficiency and total cost rate for all points evaluated over 300 generations are shown in Fig. 6.34.

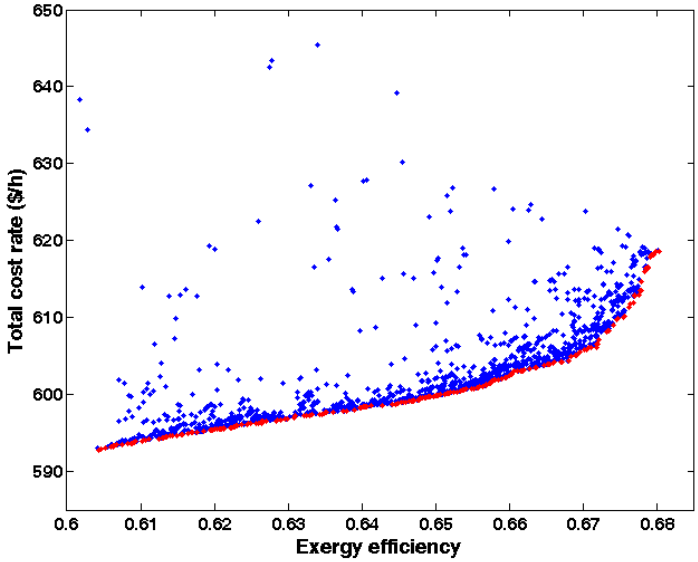

Figure 6.34: Results of all evaluations during 300 generations using genetic algorithm. A clear approximation of the Pareto front is visible on the lower part of the figure.

The Pareto-optimal curve (best rank) is clearly visible in the lower part of the figure (red line) which is separately shown in Fig. 6.33. As shown in Fig. 6.33, the maximum exergy efficiency exists at design point *D* (67.89 %), while the total cost rate of products is the greatest

at this point (615.75 $/hr). On the other hand, the minimum value for the total cost rate of product occurs at design point *A* which is about 592.6 $/hr. Design point *A* is the optimal situation when total cost rate of product is the sole objective function, while design point *D* is the optimum point when exergy efficiency is the sole objective function. In multi-objective optimization, a process of decision-making for selection of the final optimal solution from the available solutions is required. The process of decision-making is usually performed with the aid of a hypothetical point in Fig. 6.33 (the ideal point), at which both objectives have their optimal values independent of the other objectives. It is clear that it is impossible to have both objectives at their optimum point simultaneously and, as shown in Fig. 6.33, the ideal point is not a solution located on the Pareto Frontier.

The closest point of the Pareto frontier to the ideal point might be considered as a desirable final solution. Nevertheless, in this case, the Pareto optimum frontier exhibits weak equilibrium i.e., a small change in exergy efficiency from varying the operating parameters causes a large variation in the total cost rate of product. Therefore, the ideal point cannot be utilized for decision-making in this problem. In selection of the final optimum point, it is desired to achieve a better magnitude for each objective than its initial value for the base case problem. Note that in multi-objective optimization and the Pareto solution, each point can be utilized as the optimized point. Therefore, the selection of the optimum solution depends on the preferences and criteria of the decision maker, suggesting that each may select a different point as for the optimum solution depending on his/her needs. Table 6.5 shows all the design parameters for points *A*-*D*.

As shown in Fig. 6.33, the optimized values for exergy efficiency on the Pareto frontier range between 60 % and 68 %. To provide a good relation between exergy efficiency and total cost rate, a curve is fitted on the optimized points obtained from the evolutionary algorithm. This fitted curve is shown in Fig. 6.33. The expression for this fitted curve is given as follows:

$$\dot{C}_{total} = \frac{692.4\psi^3 - 2284\psi^2 + 1429\psi - 129.7}{\psi^5 + 51.48\psi^4 - 136.1\psi^3 + 130.7\psi^2 - 55.98\psi + 9.27} \quad (6.4)$$

To study the variation of thermodynamic characteristics, four different points (*A* to *D*) on the Pareto frontier are considered. Table 6.6 shows total cost rate of the system, the total exergy destruction, the system efficiency, the heating and cooling loads of the system and the CO_2 emission of the system.

Table 6.5: Optimized values for design parameters of the system based on multi-objective optimization

Design parameter	***A***	***B***	***C***	***D***
η_{AC}	0.88	0.88	0.88	0.87
η_{GT}	0.90	0.89	0.90	0.90
r_{AC}	14.90	14.90	14.90	14.97
GTIT (K)	1498	1495	1499	1496
P_{LP} (bar)	2.01	2.00	4.90	4.90
P_{HP} (bar)	12.29	23.40	29.90	29.90
PP_{HP} (^{o}C)	14.98	14.90	14.90	4.46
PP_{LP} (^{o}C)	14.92	14.90	14.80	14.95
T_{EVP} (^{o}C)	5.00	1.10	2.31	2.10
η_{FWP}	0.84	0.84	0.75	0.87
η_{ST}	0.77	0.78	0.87	0.88
P_{Cond} (kPa)	10.00	9.86	8.04	8.10
P_{ORC} (kPa)	718	689	503	506
$P_{ex,ORC}$ (kPa)	249	248	246	249
$P_{EVP,ORC}$ (kPa)	24.84	34.9	21.20	27.6

From point *A* to point *D* in this table both total cost rate of the system and exergy efficiencies increase. As already stated, point *A* is preferred when total cost rate is a single objective function and design point *D* when exergy efficiency is a single objective function. Design point *C* has better results for both objective functions. Other thermodynamic properties correctly confirm this trend. For instance, from point *B* to *C*, the total exergy destruction rate decreases when the exergy efficiency increases.

Table 6.6: Thermodynamic characteristics of four different points on the Pareto frontier.

Point	$\dot{W}_{net}$ (kW)	Ψ	$\dot{E}x_{D,tot}$ kW	$\dot{Q}_{cooling}$ kW	$\dot{Q}_{heating}$ kW	$\dot{C}_{tot}$ \$/h	CO_2 kg/kWh	$\dot{m}_{H_2}$ kg/h	$\dot{m}_{DWH}$ kg/h
A	10304	0.60	14911	929.95	4858	592.61	136.94	0.71	2983
B	10817	0.63	14437	915.10	5207	597.44	130.13	0.71	2938
C	11393	0.67	13909	904.34	6625	605.31	116.46	1.25	2981
D	11451	0.68	13845	930.35	6833	615.75	114.78	1.29	3064

To better understand the variations of all design parameters, the scattered distribution of the design parameters are shown in Figs. 6.35 to 6.38. The results show that compressor isentropic efficiency (Fig. 6.35a), gas turbine inlet temperature (Fig. 6.35b), compressor pressure ratio (Fig. 6.35d), and ORC extraction pressure (Fig. 6.38b) tend to become as high as possible. This observation means that an increase in these parameters leads to the better optimization results. For example, an increase in these design parameters leads to improvement for both objective functions in multi-objective optimization.

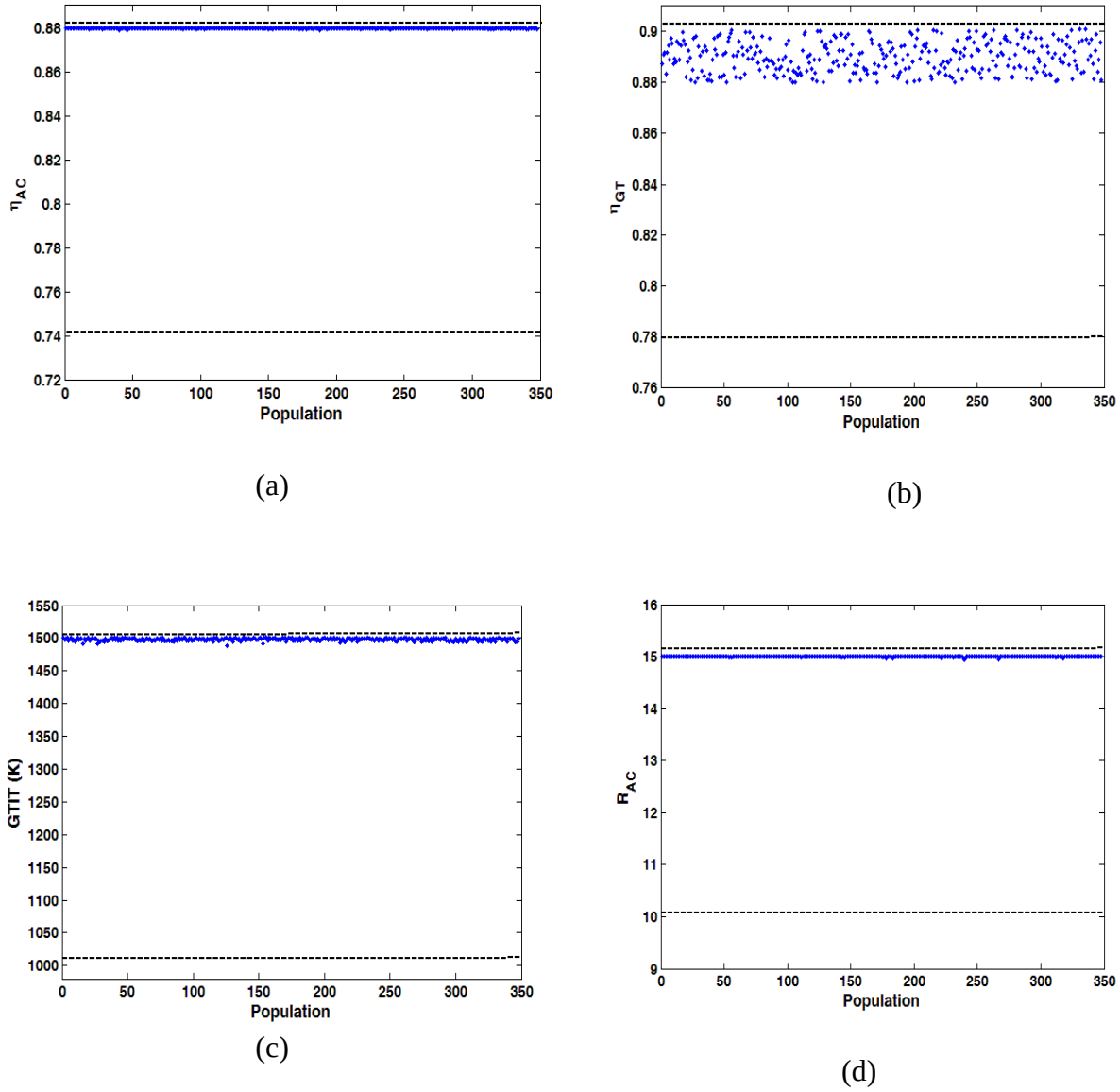

Figure 6.35: Scattered distribution of decision variables with population in Pareto frontier: (a) compressor isentropic efficiency, (b) gas turbine isentropic efficiency, (c) gas turbine inlet temperature, (d) compressor pressure ratio

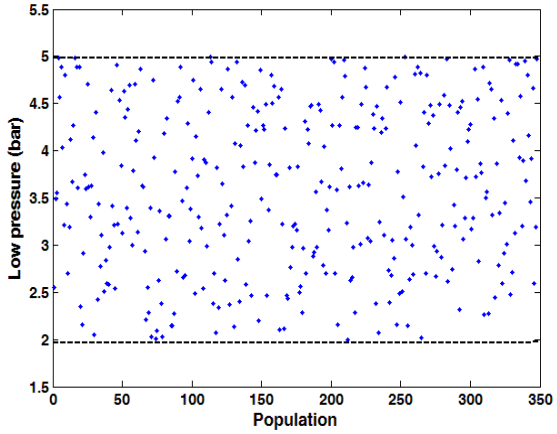

(a)

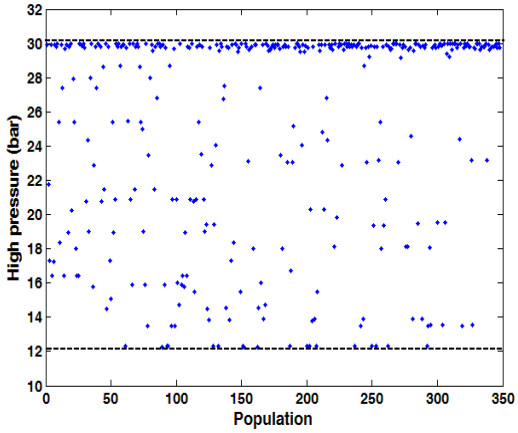

(b)

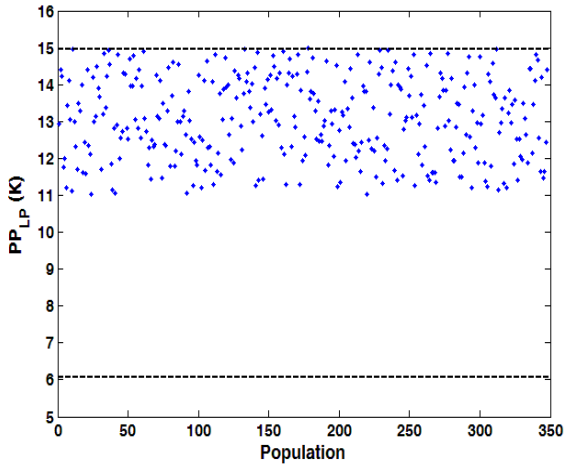

(c)

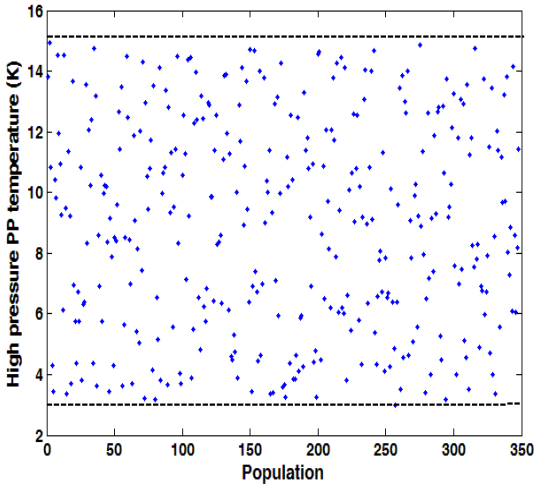

Figure 6.36: Scattered distribution of decision variables with population in Pareto frontier: (a) HRSG low pressure, (b) HRSG high pressure, (c) low pressure pinch point temperature, (d) high pressure pinch point temperature

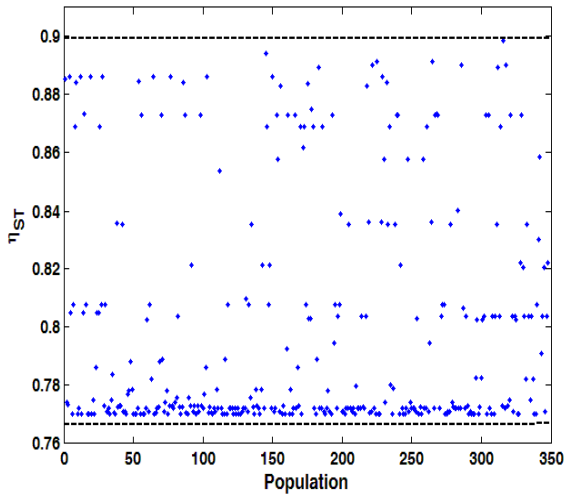

(a)

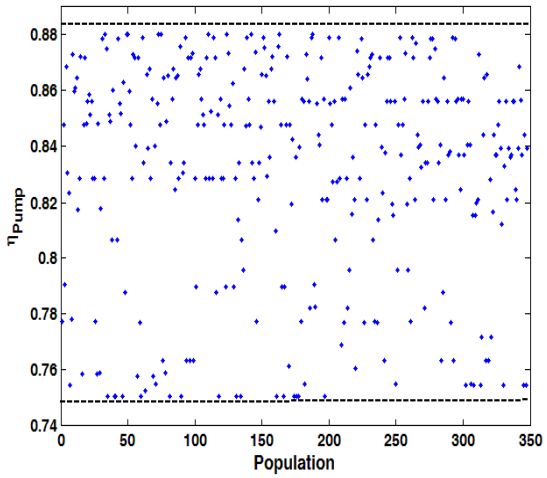

(b)

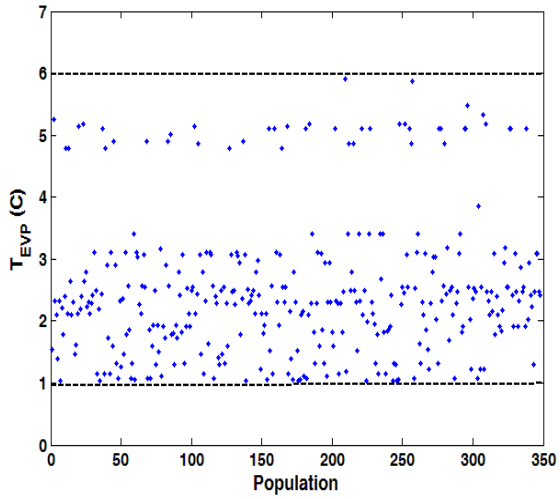

(c)

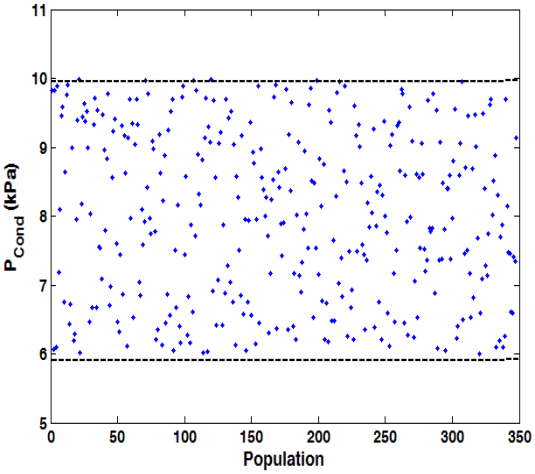

(d)

Figure 6.37: Scattered distribution of decision variables with population in Pareto frontier: HRSG steam turbine isentropic efficiency (a), pump isentropic efficiency (b), absorption chiller evaporator temperature (c) and condenser pressure (d).

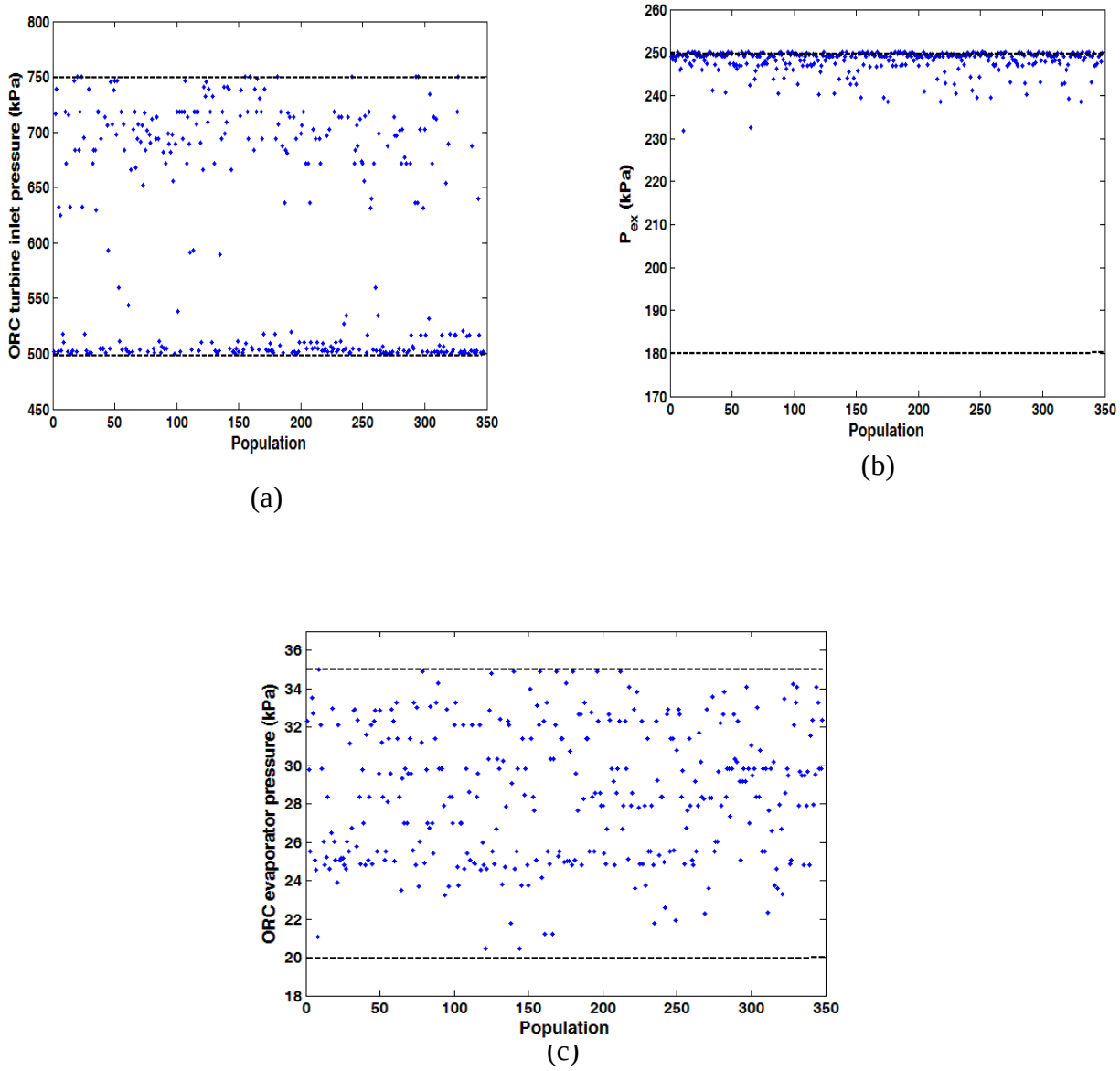

Figure 6.38: Scattered distribution of decision variables with population in Pareto frontier: (a) ORC turbine inlet pressure, (b) ORC turbine extraction pressure, (c) ORC evaporator pressure

In Figs. 6.35-6.38, we observe that the HRSG low and high pressures (Fig. 6.36a and Fig. 6.36b), the HRSG high and low pinch point temperatures (Fig. 6.36c and Fig. 6.36d), the steam turbine and pump isentropic efficiencies (Fig. 6.37a and Fig. 6.37b), the absorption chiller evaporator temperature (Fig. 6.37c), the condenser pressure (Fig. 6.37d), the ORC turbine inlet pressure (Fig. 6.38a) and the ORC evaporator Pressure (Fig. 6.38c) have scattered distributions in their allowable domains, suggesting that these parameters have important effects on the trade-off between exergy efficiency and total cost rate. Design parameters selected with their maximum values indicate that they do not exhibit a conflict between two objective functions, indicating that increasing those design parameters leads to an improvement of both objective functions.

6.2.4.4.2 Sensitivity analysis

In order to have a better understanding of the multi-objective optimization, a comprehensive sensitivity analysis is performed. The effects of each design parameters for point *A-D* on both objective functions are investigated. Fig. 6.39a, shows the effects of compressor isentropic efficiency on system exergy efficiency and total cost rate of the system. As seen in this figure, an increase in compressor isentropic efficiency has positive effect on both objective functions. An increase in compressor isentropic efficiency leads to a decrease in compressor required work which results in less fuel burnt in the combustion chamber. The lower the fuel use the higher the exergy efficiency and the lower the cost.

Fig. 6.39b also shows that an increase in gas turbine isentropic efficiency has a positive effect on both objective functions. The reason is same as for compressor isentropic efficiency. Fig. 6.39c represents the effect of *GTIT* on both objective functions, showing that this parameter has positive effect on both objective functions. The maximum value for the *GTIT* is selected based on the evolutionary algorithm. The higher the *GTIT*, the higher the achieved exergy efficiency will be, since one of the objective functions is supposed to be maximized. As shown in this figure, an increase in *GTIT* has positive effect on both objective functions. This is why, in Fig. 6.35c, points reach at their maximum value for *GTIT*. Fig. 6.39d shows the effect of compressor pressure ratio on both objective functions. An increase in compressor pressure ratio leads to an increase in exergy efficiency and decrease in total cost rate of the system.

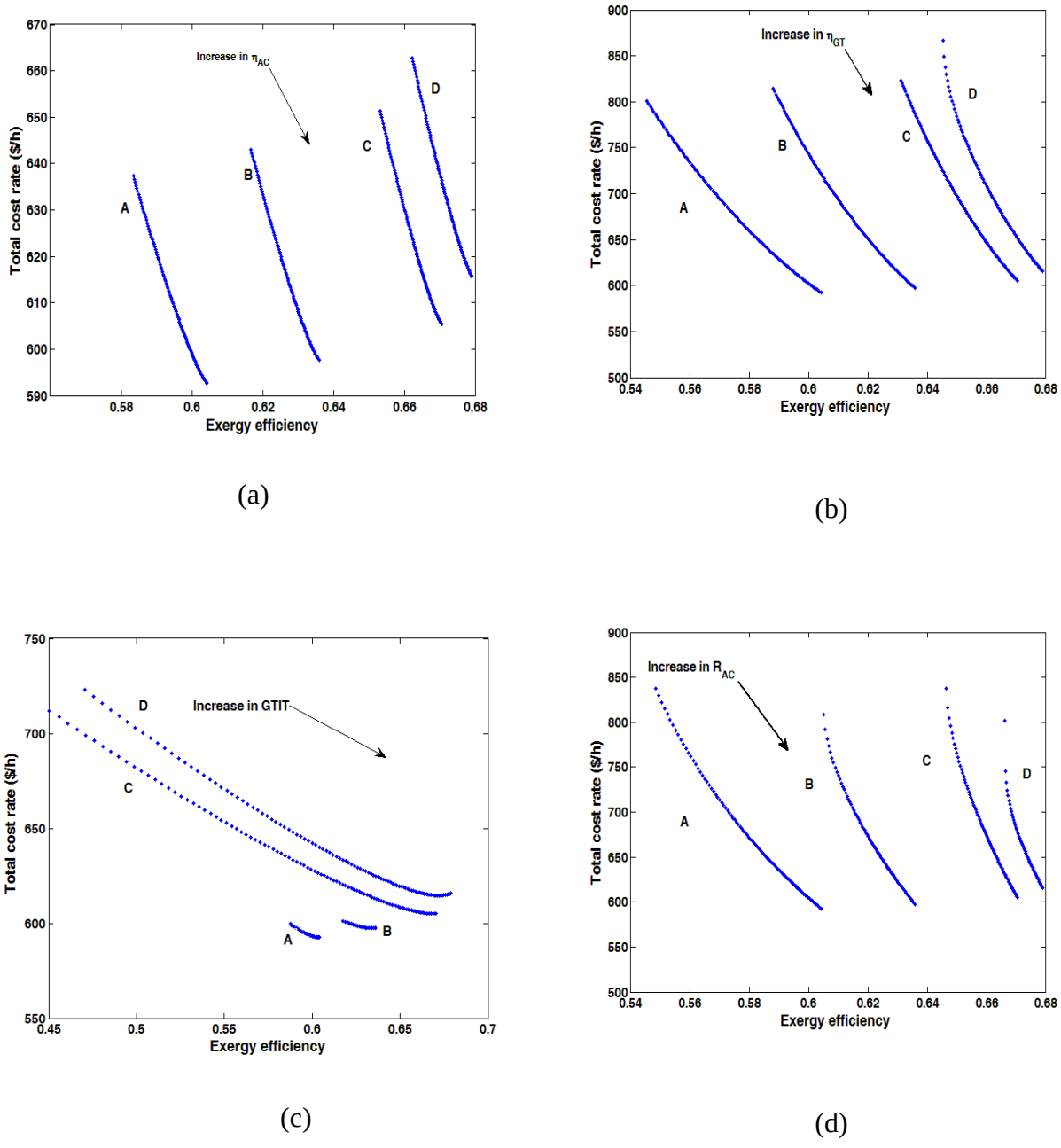

Figure 6.39: Effects of design parameters on both objective functions: (a) compressor isentropic efficiency, (b) gas turbine isentropic efficiency, (c) gas turbine inlet temperature, (d) compressor pressure ratio

The reason for the compressor pressure ratio effect is that an increase in this parameter increases the outlet temperature and decreases the mass flow rate injected to the combustion chamber. As the first term in the total cost rate (equation 6.2) is directly associated with the mass flow rate of the fuel, any decrease in this term results in a decrease in the objective function. This is why the scattered distribution for the compressor pressure ratio achieves a maximum value within its range.

Figs. 6.40a and 6. 40b show the effect of HRSG low and high pressures on both objective functions. An increase in these design parameters is seen to have a positive effect on system exergy efficiency and a negative effect on total cost rate of the system. An increase in HRSG high pressure results in an increase in the steam turbine work and increase in HRSG low pressure, and leads to an increase in absorption chiller cooling load. According to equation (6.1), increases in both $\dot{W}_{net,ST}$ and $\dot{Q}_{cooling,chiller}$ result in an increase in system exergy efficiency. However, an increase in HRSG pressures results in an increase in HRSG purchase and maintenance cost, which leads to an increase in last term of equation (6.2). Since, an increase in HRSG pressures has positive and negative effects on the objective functions, they have scattered distributions within their allowable ranges.

Fig. 6.40c and 6.40d show the effect of HRSG pinch point temperatures on both objective functions. It is seen that an increase in pinch point temperature results in a decrease in system exergy efficiency. This is due to the fact that the higher the pinch point temperature, the lower the energy being utilized in HRSG which leads to a reduction of steam turbine power output. On the other side, an increase in pinch point temperature while fixing other design parameters, results in a decrease in heat transfer area for the HRSG component. This is why the total cost rate of the system decreases.Fig. 6.41a represents the effect of steam turbine isentropic efficiency (η_{ST}) on both objective functions. An increase in η_{ST} results in an increase in system exergy efficiency and increase in total cost of the system. Increasing this parameter results in an increase in the steam turbine power output, which directly leads to an increase in the exergy efficiency. It is also seen that increasing this parameter leads to an increase in steam turbine purchase and maintenance cost. Since an increase in this parameter has positive and negative effects on both objective functions, the variation of this design parameter within its allowable range exhibits a scattered distribution as shown in Fig. 6.37a.

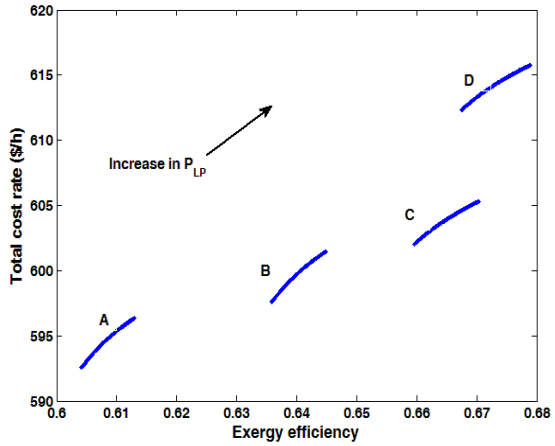

(a)

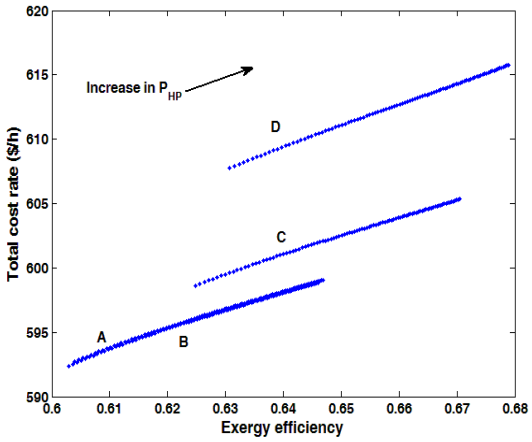

(b)

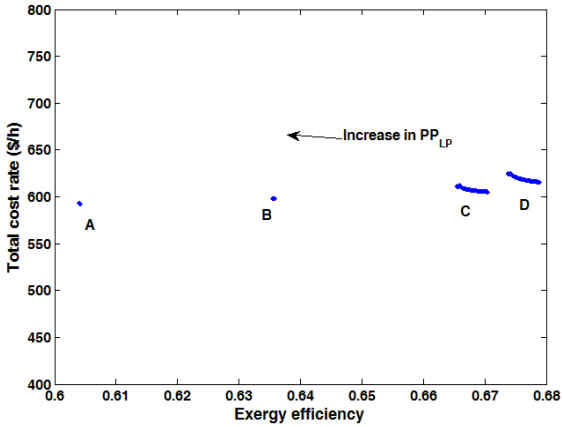

(c)

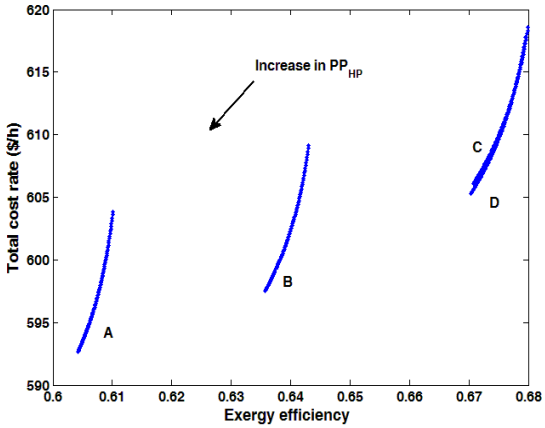

(d)

Figure 6.40: Effects of design parameters on both objective functions: (a) HRSG low pressure, (b) HRSG high pressure, (c) low pressure pinch point temperature, (d) high pressure pinch point temperature (d)

Fig. 6.41b shows that pump isentropic efficiency dese not have a significant effect on both objective functions, as its purchase cost is small. Fig. 6.41c shows the variation of the objective function by changing the absorption chiller evaporator temperature. An increase in evaporator temperature results in an increase in cooling load of the absorption chiller and at a same time increase the cost of the chiller. Fig. 6.41d shows the effect of condenser pressure on both objective functions. As shown in this figure, an increase in condenser pressure results in a decrease in system exergy efficiency, which is due to an increase in the heat rejected to the surroundings.

Fig. 6.42a shows the effect of ORC turbine inlet pressure on the objective functions. An increase in ORC turbine inlet pressure leads to a decrease in system exergy efficiency and a decrease in the total cost rate of the system. Fig. 6.42b shows the variation of objective functions with ORC extraction pressure. It is seen that this parameter has positive effect on both objective functions. An increase in extraction pressure results in an increase in ejector entrainment ratio which results in an increase in ORC cooling load. Fig. 6.42c illustrates the effect of ORC evaporator pressure on objective functions. An increase in this parameter increases the exergy efficiency of the system while it increases the total cost rate of the system. However, this increase is not significant. Therefore, since evaporator pressure has positive and negative effect on the objective functions, the distribution of this parameter within its allowable range has a scattered distribution, as shown in Fig. 6.38c.

6.2.4.4.3 Closing remarks

The comprehensive thermodynamic modeling and multi-objective optimization of a multigeneration energy system provides useful information. A calculus-based optimization approach using evolutionary algorithms (i.e. genetic algorithms) allows multi-objective optimization of the multigeneration plant. Environmental impacts are quantified conveniently as pollution-related costs in the economic objective function, transforming the environmental objective to a cost function. Merging the new environmental cost function with the thermoeconomic objective yields a useful thermoenvironomic function. Fitting a curve on the optimized points provides a closed form equation.

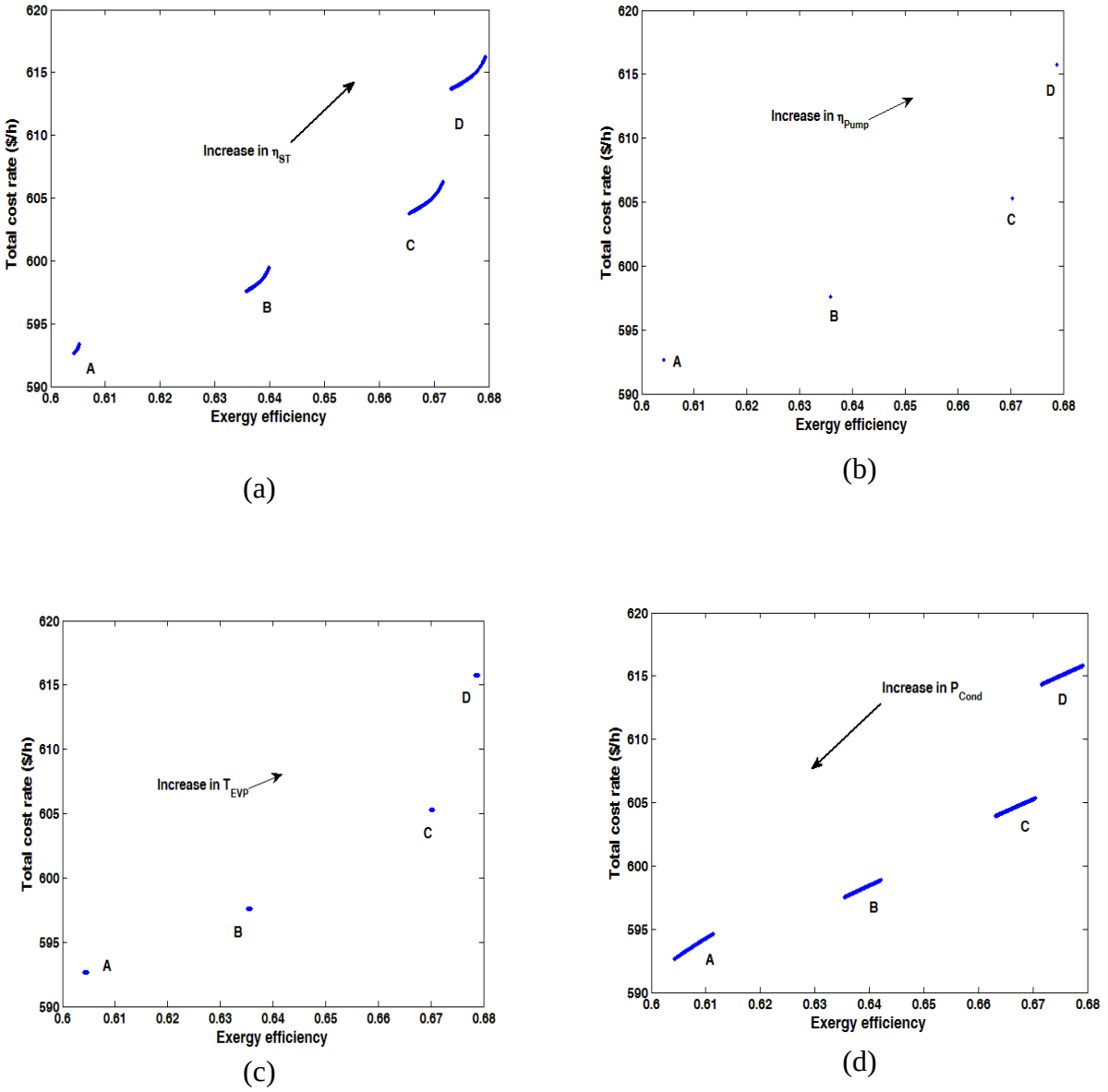

Figure 6.41: Effects of design parameters on objective functions, (a) steam turbine isentropic efficiency, (b) pump isentropic efficiency, (c) absorption chiller evaporator efficiency, (d) condenser pressure

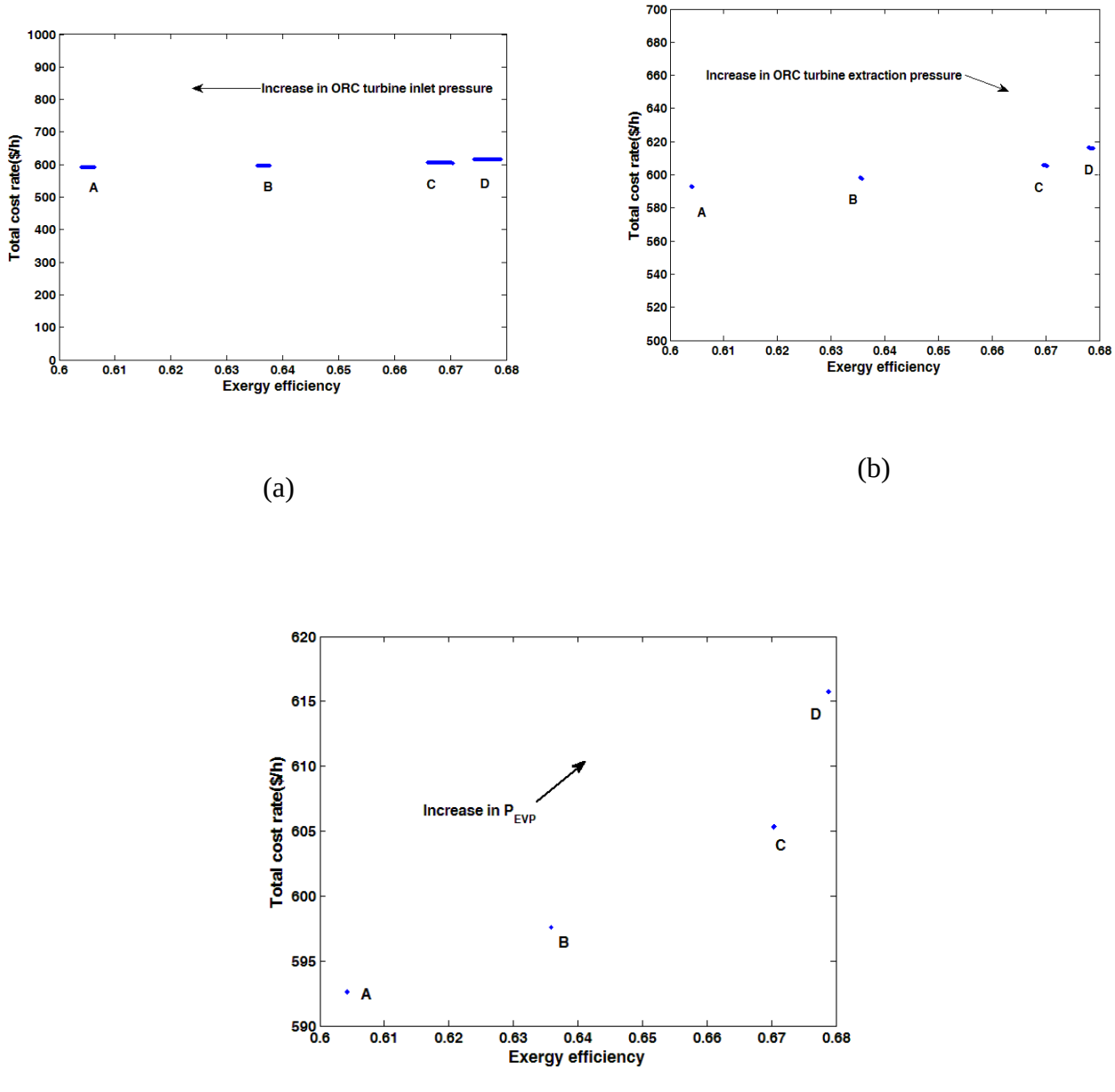

Figure 6.42: Scattered distribution of decision variables with population in Pareto frontier: (a) ORC turbine inlet pressure, (b) ORC turbine extraction pressure, (c) ORC evaporator pressure

The results suggest that compressor isentropic efficiency, gas turbine inlet temperature, compressor pressure ratio and ORC extraction pressure tend to maximum values, and that an increase in these parameters results in better system performance. Other concluding remarks follow:

- An increase in compressor pressure ratio, gas turbine inlet temperature and ORC turbine extraction pressure has a positive effect on both objective functions.
- An increase in HRSG pressures increases system exergy efficiency and decreases the total cost rate of the system.
- An increase in HRSG pinch point temperatures reduces the system exergy efficiency.
- An increase in steam turbine isentropic efficiency results in an increase in system exergy efficiency an increase in total cost of the system.
- An increase in evaporator temperature results in an increase in cooling load of the absorption chiller.

6.3 Results of system II

The thermodynamic modeling of the multigeneration system considered here (Fig. 4.2) is divided into five sub-systems: 1) biomass combustor, 2) organic Rankine cycle and domestic water heater, and 3) double-effect absorption chiller 4) proton exchange membrane (PEM) electrolyzer and reverse osmosis (RO) desalination unit. We determine the temperature profile in the multi-generation plant, input and output enthalpies, exergy flows, environmental impacts, exergy destructions and exergy efficiencies.

6.3. 1 Modeling results

The results of the present thermodynamic modeling and exergy and environmental analyses are presented here, including assessments of the effects of varying several design parameters on cycle performance. Table 6.7 lists the thermodynamic properties of the multigeneration system shown in Fig. 4.2. In this exergy analysis, the dead state is defined to have a pressure of P_0 = 1.01 bar and a temperature of T_0 = 293.15 K. Energy and exergy balances are used to model the system, while invoking reasonable assumptions The following simplifying assumptions are made here to render the analysis more tractable, while retaining adequate accuracy to illustrate the principal points of this study [75, 117]:

- All processes operate at steady state.
- Air and combustion products are ideal-gas mixtures.
- The fuel injected to the combustor is pine sawdust biomass with a composition as given in Table 5.5.
- The ORC turbine and pump isentropic efficiencies are 85%.
- The ORC pump inlet temperature is 85 ^{0}C.
- The organic fluid enters the turbine at 400 ^{0}C.
- About 5% of the net power output is used to operate the PEM electrolyzer.
- In these examinations, it is assumed that the volumetric composition of the inlet air is 0.7567 N_2, 0.2035 O_2, 0.003 CO_2 and 0.036 H_2O [47].

To model the biomass based multigeneration system, some parameters are selected as input data for the simulation. The input data for the simulation are listed in Table 6.7.

Table 6.7: Input parameters used to simulate the system.

Parameter	**Value**	**Parameter**	**Value**
Fuel mass flow rate (kg/s)	0.3	Chiller evaporator temperature (^{0}C)	7
ORC pump inlet temperature (^{0}C)	95	Chiller weak solution concentration (%)	52.25
Pinch point temperature (^{0}C)	10	Chiller strong solution concentration (%)	57.32
ORC turbine inlet pressure (kPa)	2000	PEM electrolyzer temperature (^{0}C)	80
ORC turbine inlet temperature (^{0}C)	360	Sea water salinity (ppm)	3600
Turbine isentropic efficiency	0.83	Fresh water salinity (ppm)	1000
Pump isentropic efficiency	0.78	Ro membrane area (m^2)	37
Fuel cost ($/kWh) [79]	0.01	Fresh water productivity (%)	50

Table 6.8 lists the thermodynamic specifications of the multigeneration system, including heating and cooling loads, the electricity generated by the turbines, the COP of the absorption chiller, and the mass flow rates of biomass, hydrogen and hot water.

Table 6.8: Parameter values from modeling and energy and exergy analyses of the system

Parameter	**Unit**	**Value**
Biomass flow rate, $\dot{m}_f$	kg/s	0.30
Heating load, $\dot{Q}_{Heating}$	kW	2383
Cooling load, $\dot{Q}_{Cooling}$	kW	2560
Net output power, $\dot{W}_{Net}$	kW	500.47
Exergy efficiency, ψ	%	28.82
Absorption chiller COP	-	1.63
ORC mass flow rate, $\dot{m}_{ORC}$	kg/s	4.84
Hydrogen production mass flow rate, $\dot{m}_{\mathrm{H_2}}$	kg/day	2
Hot water mass flow rate, $\dot{m}_{\mathrm{HW}}$	kg/s	0.78
Fresh water mass flow rate, $\dot{m}_{fresh}$	Kg/s	1.93
Specific CO_2 emission, ε	kg/MWh	358
Total cost rate	$/h	476
Cost of environmental impact	$/h	48.47
Total exergy destruction rate	kW	5393
Power to cooling ratio	-	0.19
Power to heating ratio	-	0.20

6.3. 2 Exergy and economic analyses results

The analysis described earlier is used to evaluate output parameters including exergy efficiency and exergy destruction rate of the components in the system considered, as well as the carbon dioxide emissions in kg/MWh. These parameters are examined while varying the ORC evaporator pinch point temperature, the ORC pump inlet temperature, the turbine inlet pressure and the biomass mass flow rate. The exergy efficiency and CO_2 emissions are calculated for three cases: electrical power, cogeneration and multigeneration. The exergy analysis results are summarized in Fig. 6.43, and show that the highest exergy destruction occurs in the combustor, mainly due to the irreversibilities associated with combustion and the large temperature difference between the air entering the combustor and the flame temperature. The double-effect absorption chiller heat exhibits the next largest exergy destruction, mainly due to the temperature difference between two fluid streams passing through all heat exchangers as the pressure drop across the device.

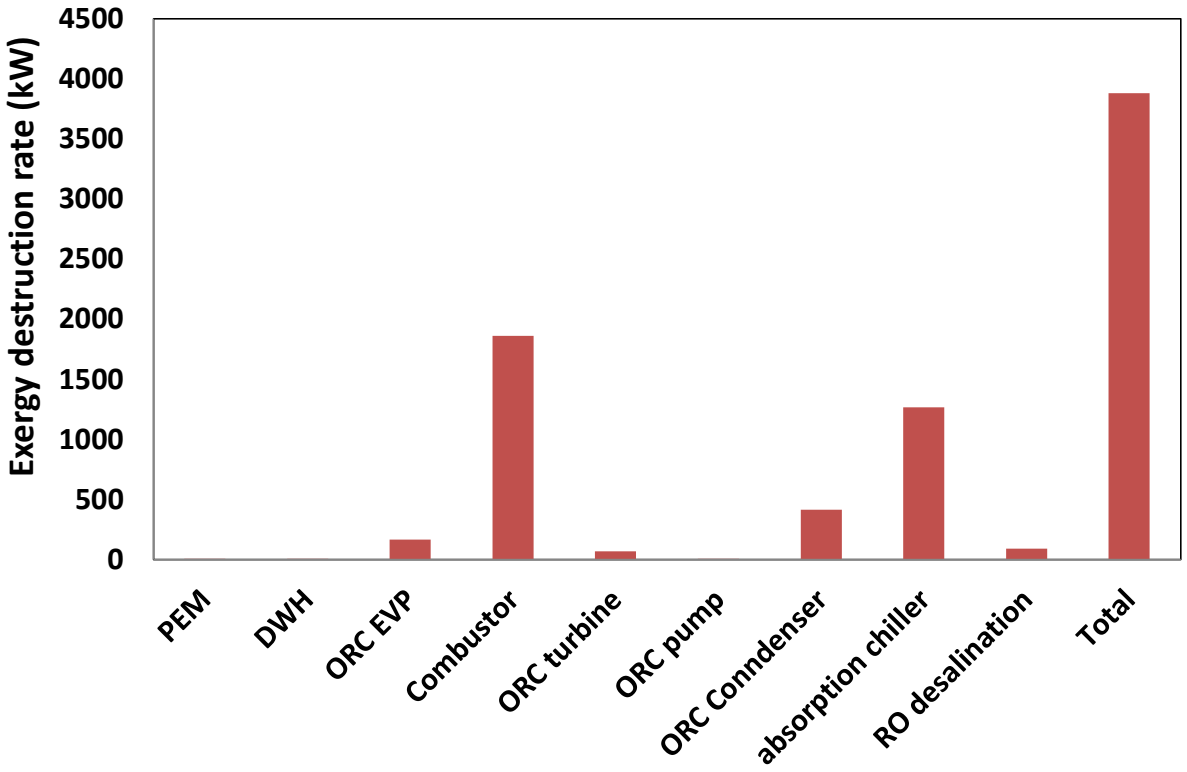

Figure 6.43: Exergy destruction rates for the multi-generation system and its components.

- **Parametric study results**

The effect of variations of several design parameters on the thermodynamic performance of the multigeneration system is assessed. Since pinch point temperature, ORC turbine inlet pressure and ORC pump inlet temperature significantly affect system performance parameters (e.g., energy and exergy efficiencies), we focus on them here. The pinch point (PP) temperature is a significant design parameter in heat exchangers. Raising this temperature can reduce the efficiency of the system by reducing the energy recovered by the heat exchanger. Fig. 6.44 shows the effect of varying pinch point temperature on the cycle's overall exergy efficiencies for three the cases considered. As seen in this figure, the exergy efficiency of the multigeneration system is almost double that of a power generation system, mainly due to an increase in the numerator of equation (5.193).

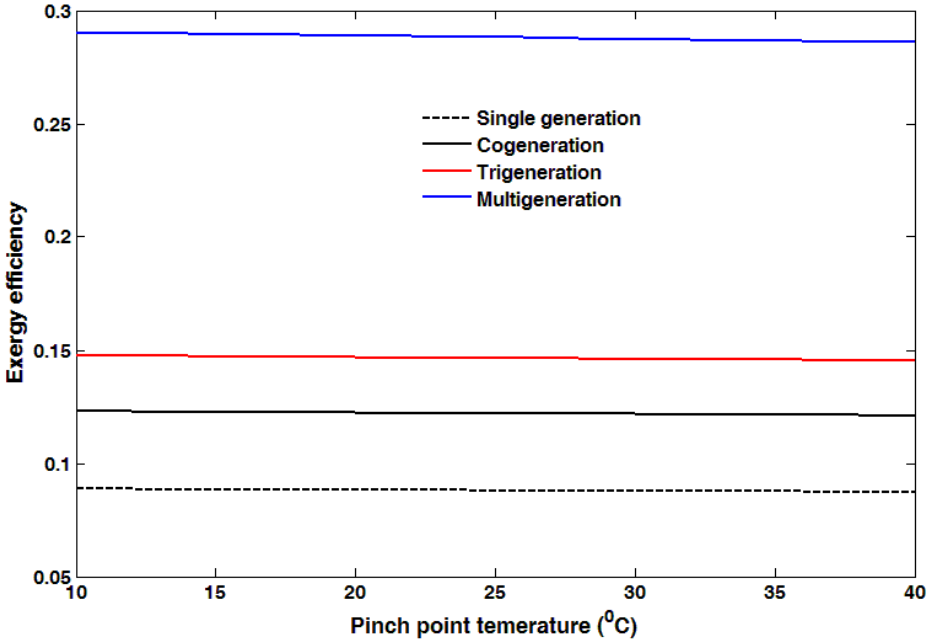

Figure 6.44: Effects of varying pinch point temperature on exergy efficiency for several cycles.

Also, an increase in pinch point temperature leads to a slight decrease in exergy efficiency. Fig. 6.45 illustrates the effect of pinch point temperature on heating and cooling loads of the system. Both heating and cooling loads of the multigeneration system are observed to decrease with an increase in pinch point temperature. When the pinch point temperature increases, the flue gas temperature leaving the ORC evaporator increases, which results in a decrease in the ORC mass flow rate based on an energy balance for a control volume around ORC evaporator. Therefore, the lower the ORC mass flow rate, the lower are the heating and cooling loads.

An increase in pinch point temperature increases the hot water mass flow rate leaving the domestic water heater. Since an increase in pinch point temperature leads to a rise in the temperature at point 33 of the system shown in Fig. 4.2, the flue gases enter the domestic water heater with a higher temperature, which results in an increase in hot water production. However, the pinch temperature has a negative effect on hydrogen production rate since an increase in pinch point temperature reduces the turbine power output. These results are shown in Fig. 6.46

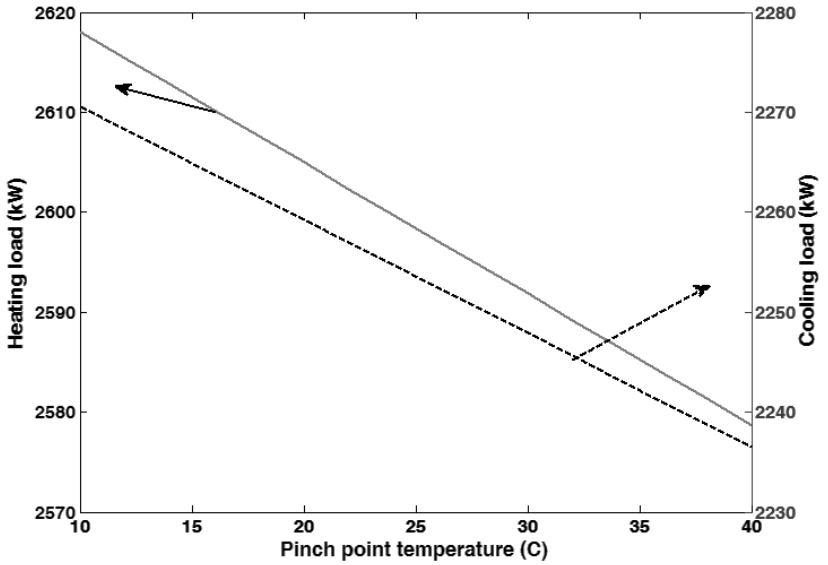

Figure 6.45: Effects of varying pinch point temperature on heating and cooling loads of the system.

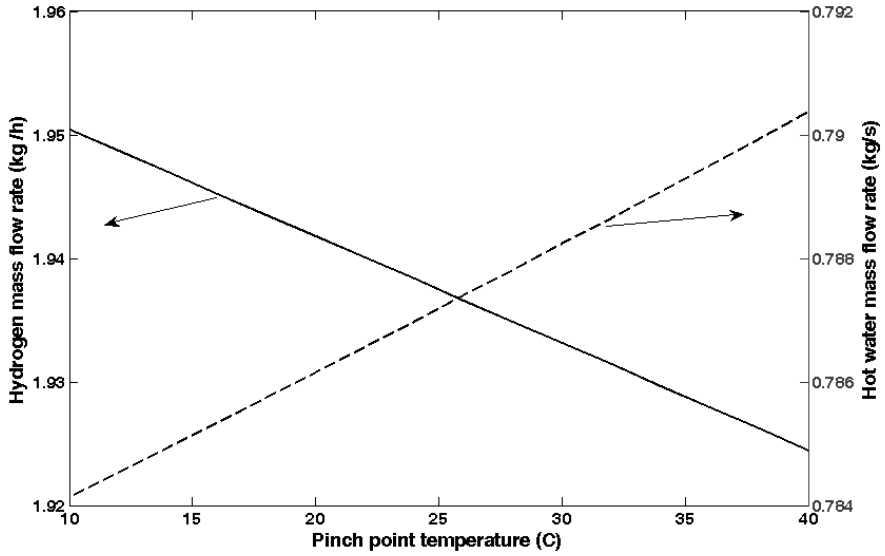

Figure 6. 46: Effects of varying pinch point temperature on hot water and hydrogen production rates.

Fig. 6.47 shows the effect of pinch point temperature on the system exergy efficiency and total exergy destruction rate of the system. It is observed that an increase in pinch point temperature results in a decrease in exergy efficiency and increase in total exergy destruction rate. When the pinch point temperature increases, the flue gas temperature leaving the ORC evaporator increases, which results in a decrease in the ORC mass flow rate based on an energy balance for a control volume around ORC evaporator. Therefore, the lower the ORC mass flow rate, the lower

are the heating and cooling loads. Therefore, a decrease in both heating and cooling load leads to a decrease in exergy efficiency and increase in the irreversibilities of the system.

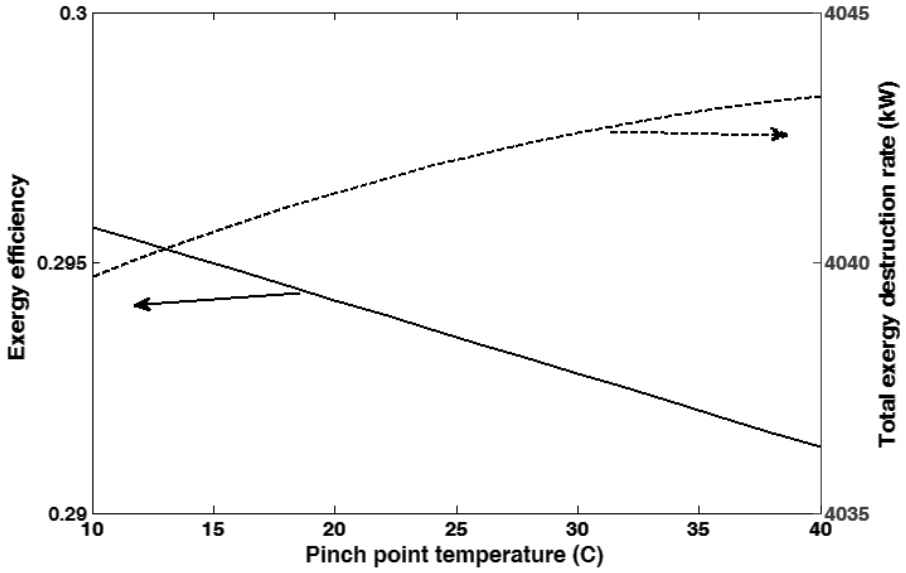

Figure 6.47: Effects of varying pinch point temperature on exergy efficiency and total exergy destruction rate.

The effect of pinch point temperature on net power output and fresh water production is shown in Fig. 6.48. It is seen that an increase in pinch point temperature has a negative effect on both net power output. When the pinch point temperature increases, the ORC mass flow rate decreases according to energy balance for the evaporator which finally leads to a decrease in turbine work. Since the input of the RO system is the electricity form the turbine, a decrease in net power output results in a reduction in fresh water production. Fig. 6.49 shows the effect of pinch point temperature on total cost rate of the system. It is observed that and increase in pinch point temperature results in a decrease in total cost rate of the system. An increase in pinch point temperature while fixing other design parameters, results in a decrease in heat transfer area for the evaporator component.

This is why the total cost rate of the system decreases. Another important design parameter in this system is ORC inlet turbine pressure, which affects the system performance.

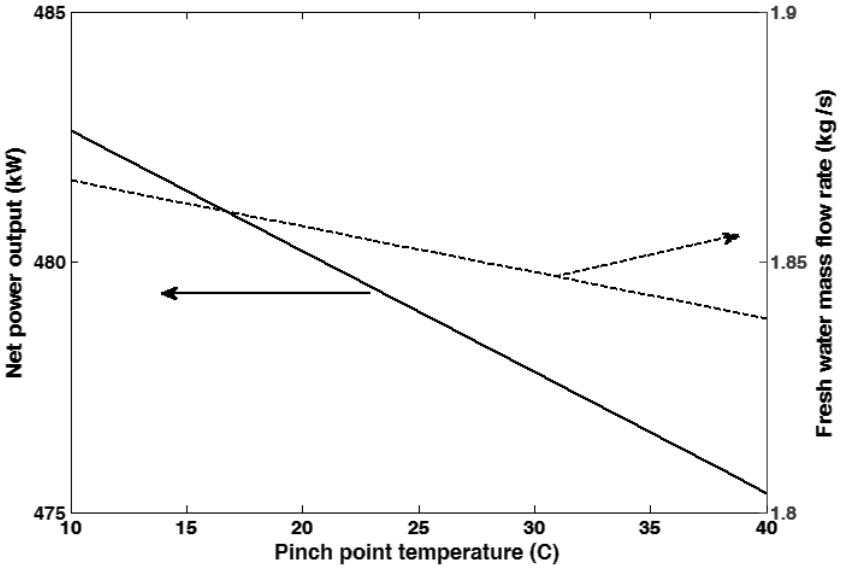

Figure 6.48: Effects of varying pinch point temperature on net power output and fresh water mass flow rate.

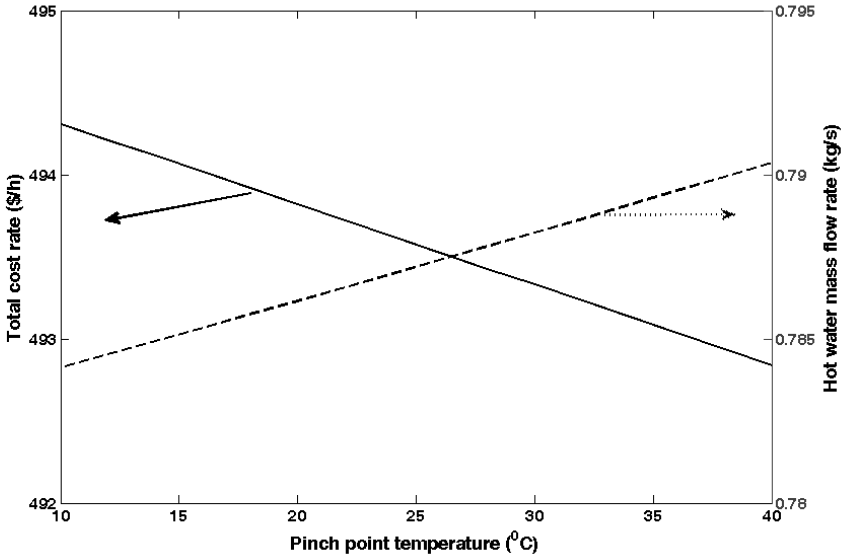

Figure 6.49: Effects of varying pinch point temperature total cost rate and fresh water mass flow rate.

Fig. 6.50 shows the effect of ORC turbine inlet pressure on exergy efficiency of the multigeneration, the CHP and the power generation systems. This figure also shows that an increase in this pressure raises the exergy efficiency for these cases. To better understand the effect of ORC turbine inlet pressure on exergy efficiency, we should focus on the effect of this pressure on heating and cooling load and net power output of the system.

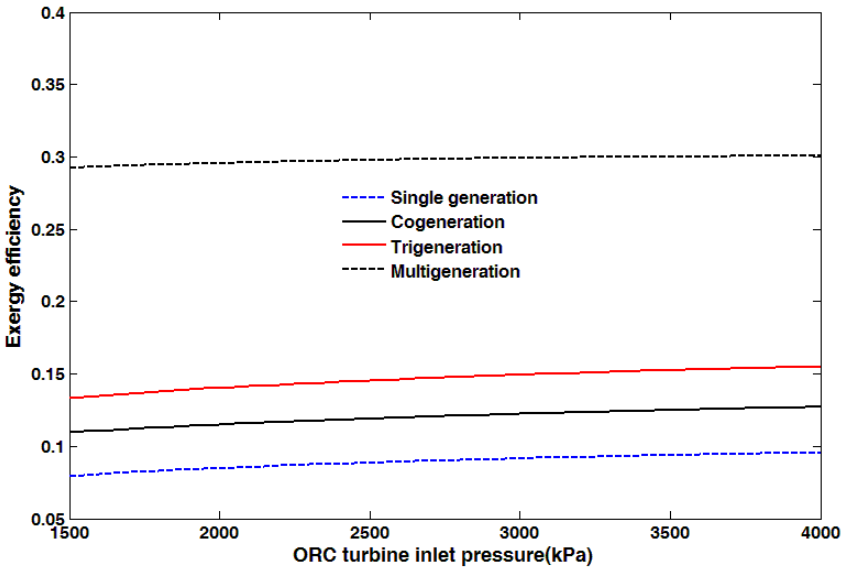

Figure 6.50: Effects of varying ORC turbine inlet pressure on exergy efficiency.

Fig. 6.51 shows the effect of ORC turbine inlet pressure on the heating and cooling load of the system. As shown in this figure, an increase in this pressure reduces the heating load of the system while an increase in this pressure has a positive effect on cooling load of the system. An energy balance for a control volume around the ORC evaporator shows that when the energy input from biomass is constant, a reduction in turbine inlet enthalpy increases the ORC mass flow rate. Since inlet and outlet enthalpies of the generator in the absorption cycle are constant, an increase in the ORC mass flow rate leads to an increase in energy input to the absorption system, which increases the cooling load of the system.

For the heating load, an increase in ORC turbine inlet pressure, while fixing other design parameters, decreases the turbine inlet enthalpy and, since the turbine outlet enthalpy is a function of the turbine inlet enthalpy and turbine isentropic efficiency, this a corresponding decrease in turbine outlet enthalpy (h_{28}), which is the inlet energy for the heating process unit. Although the ORC mass flow rate increases as already discussed, the reduction in enthalpy of the heating process dominates.

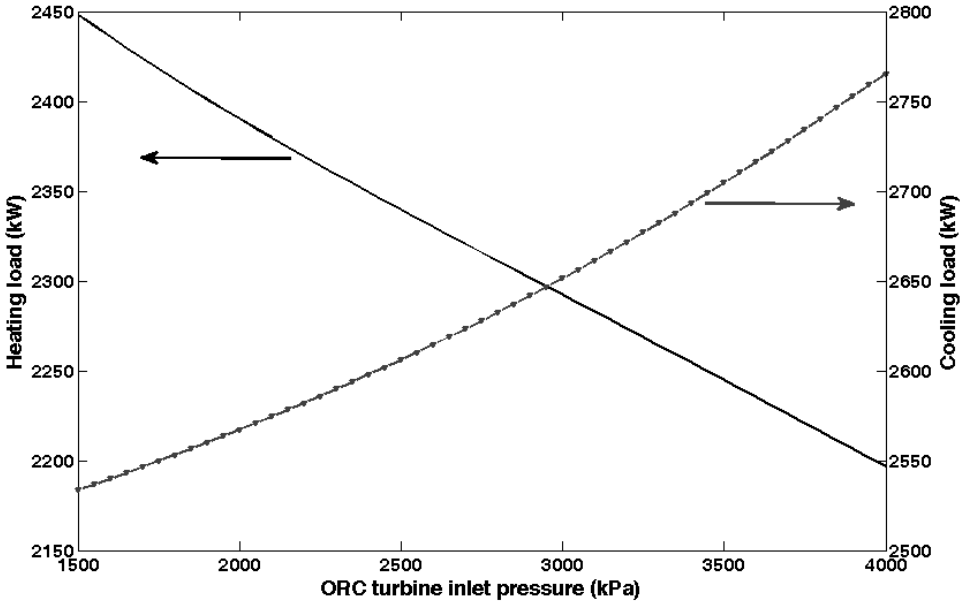

Figure 6.51: Effects of varying ORC turbine inlet pressure on heating and cooling loads of the system.

Fig. 6.52 shows the effect of ORC turbine inlet pressure on the power to cooling and heating ratios. An increase in this pressure results in an increase in both ratios confirming the trend of increasing exergy efficiency shown in Fig. 6.50 since the numerator of equation (5.193) increases. Fig. 6.53 shows the variation of hydrogen production rate and the total exery destruction rate of the system. As seen in Fig. 6.53, an increase in ORC turbine inlet pressure always raises the hydrogen production rate, due to the increase in turbine work as aforementioned. Thus, the higher the turbine work, the higher is the hydrogen production rate achieved. However, the ORC turbine inlet pressure has two different effects on the total exergy destruction rate of the system.

The total exergy destruction rate decreases with turbine inlet pressure to a minimum value, followed by an increase. This is due to the fact that the exergy destruction rate of the ORC cycle decreases and the exergy destruction rate of absorption chiller increases, while the exergy destruction rate (shown in Fig. 6.54) remains constant for the other components.

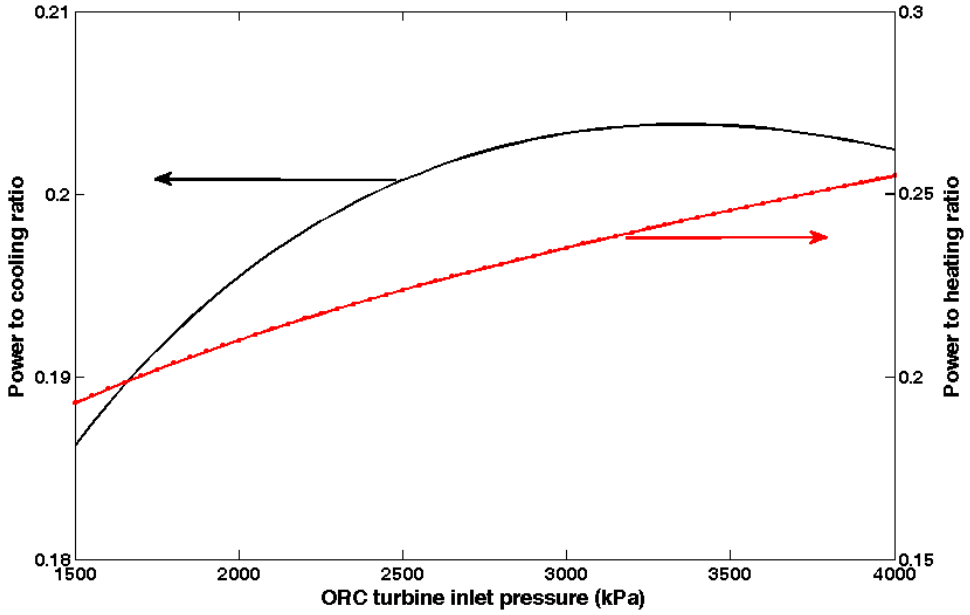

Figure 6.52: Effects of varying ORC turbine inlet pressure on the power to heating and cooling ratios.

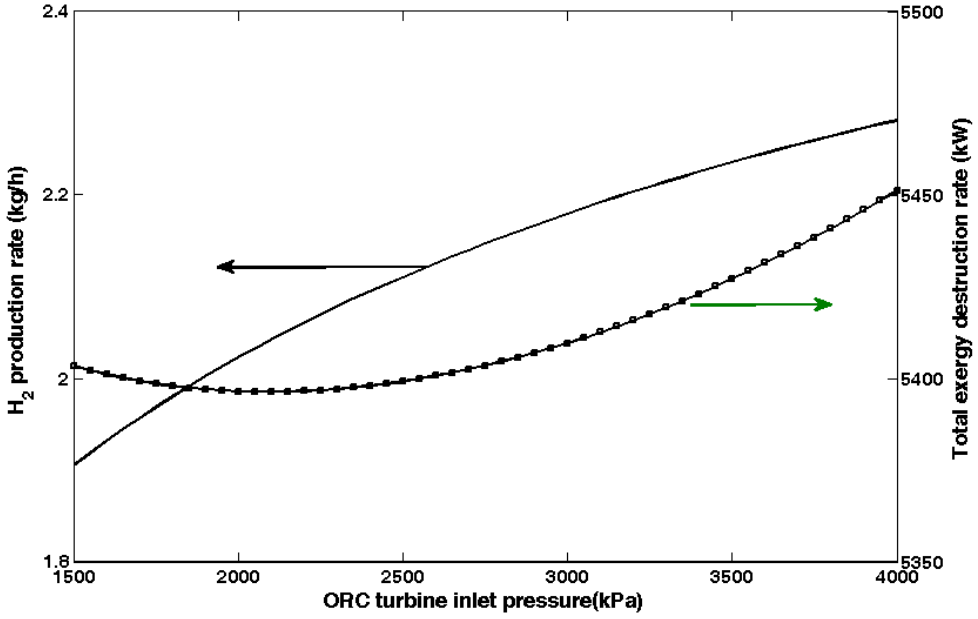

Figure 6.53: Effects of varying ORC turbine inlet pressure on hydrogen production and total exergy destruction rate.

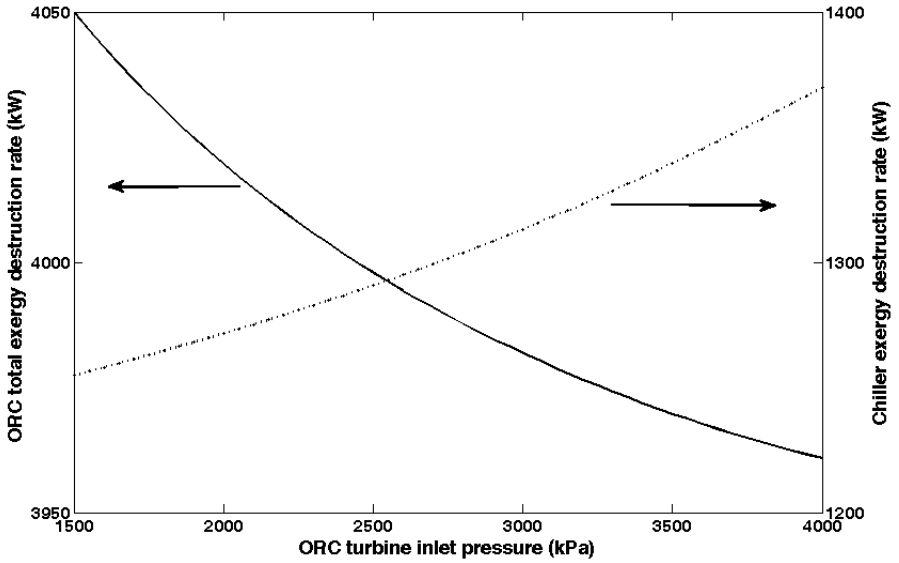

Figure 6.54: Effects of varying ORC turbine inlet pressure on exergy destruction rate for ORC cycle and absorption chiller.

Fig. 6.55 shows the variation of total cost rate and the total exergy destruction rate of the system. As seen in Fig. 6.55, an increase in ORC turbine inlet pressure results in an increase in total cost rate of the system. This is due to the fact that an increase in this pressure leads to an increase in turbine work and this increase in turbine work leads to an increase in the purchase cost of the turbine which results in an increase in total cost arte of the system.

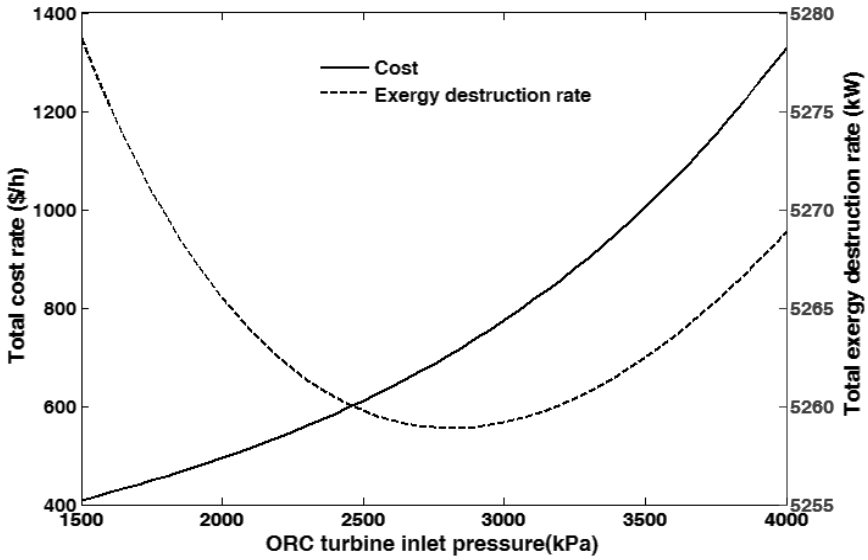

Figure 6.55: Effects of varying ORC turbine inlet pressure on total cost rate and total exergy destruction rate.

Fig. 6.56 confirms this trend. Also, an increase in ORC turbine inlet pressure has a positive effect on total cost rate of the system and net power output.

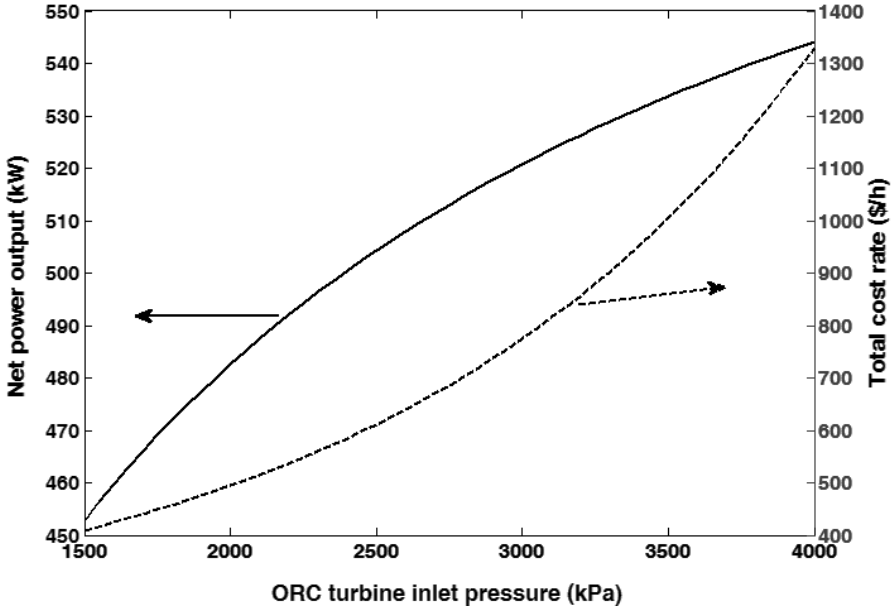

Figure 6.56: Effects of varying ORC turbine inlet pressure on total cost rate net power output.

Another important factor that affects system performance is the ORC pump inlet temperature. Fig. 6.57 shows the effect of pump inlet temperature on exergy efficiency and total exergy destruction rate. An increase in pump inlet temperature increases the heating process pressure which increases the enthalpy at point 28 in Fig. 4.2. Thus, an increase in this enthalpy results in an increase in heating load of the system. Since an increase in pump inlet temperature increases the pump inlet enthalpy, it increase the energy input for the absorption chiller which is the enthalpy difference between points 24 and 25 (see Fig. 4.2). The trends regarding changes of heating and cooling loads are shown in Fig. 6.58. An increase in pump inlet temperature affects the pump work and increases the ORC evaporator inlet enthalpy which results in an increase in the ORC mass flow rate, based on an energy balance around the ORC evaporator. Fig. 6.57 also shows that an increase in ORC pump inlet temperature reduces the total exergy destruction, due to an increase in the exergy at the ORC turbine outlet, which reduces the exergy destruction rate for the turbine, based on the exergy balance for the turbine.

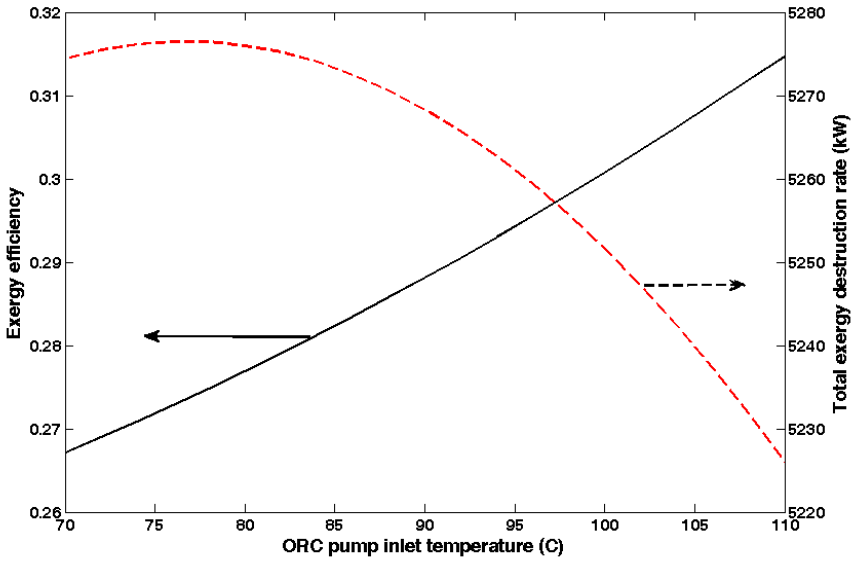

Figure 6.57: Effects of varying ORC pump inlet temperature on exergy efficiency and total exergy destruction rate.

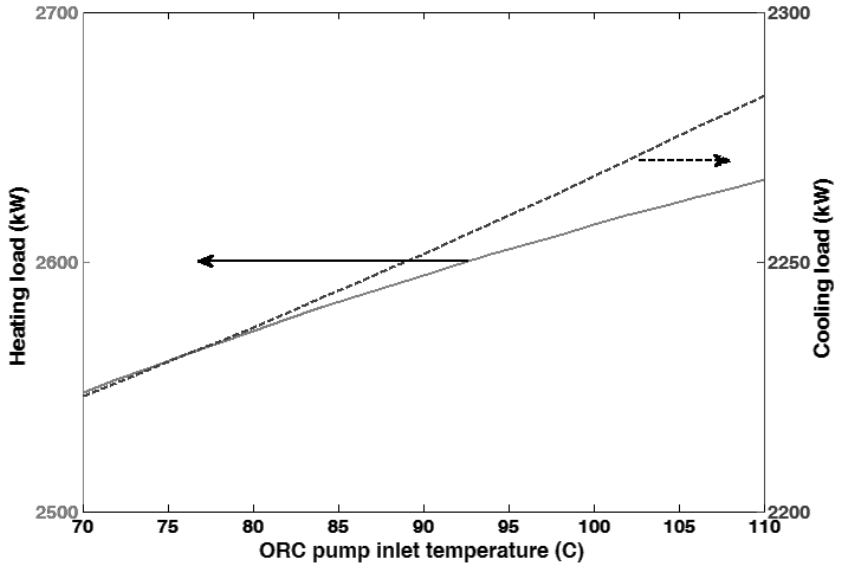

Figure 6.58: Effects of varying ORC pump inlet temperature on heating and cooling loads of the system.

Fig. 6.59 shows the variation of exergy efficiency for three different cycles. It is shown, an increase in pump inlet temperature results in an increase in exergy efficiency for both CHP and multigeneration system which is due to an increase in heating and cooling. However, an increase in ORC pump inlet temperature leads to a reduction of net power output which is due to the fact that an increase in this temperature while keeping other parameters fixed leads to an increase in turbine outlet enthalpy and writing the energy balance equation around the turbine an increase in the outlet

energy results in a decrease in turbine work as shown in Fig. 6.60. This is why in Fig. 6.59 an increase in ORC pump inlet temperature decrease the exergy efficiency for the power generation cycle as it does not include the cooling and heating load.

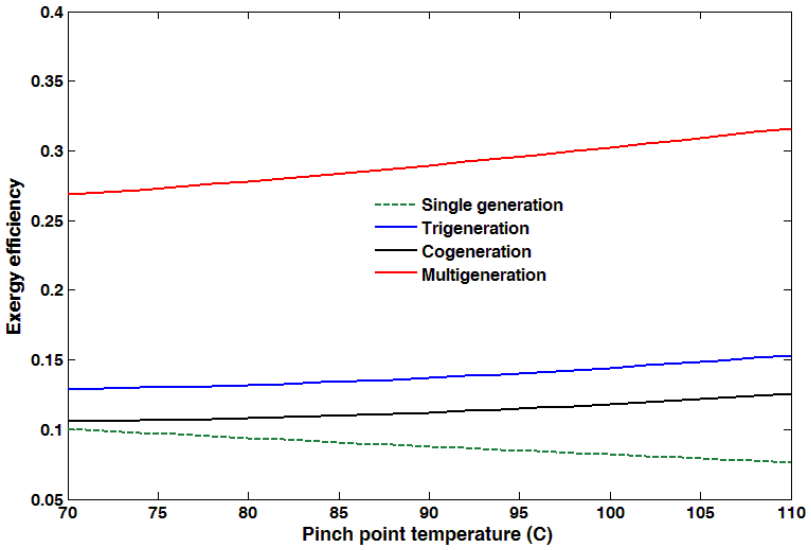

Figure 6.59: Effects of varying ORC pump inlet temperature on exergy efficiency.

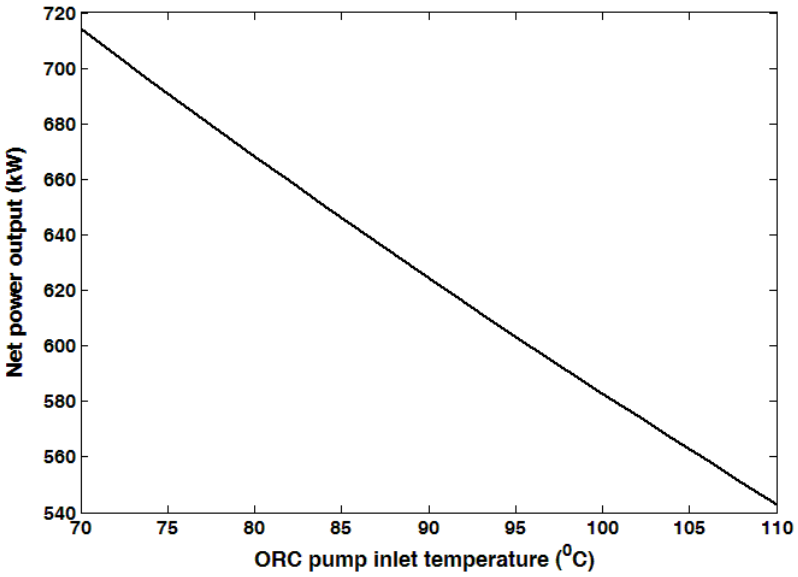

Figure 6.60: Effects of varying ORC pump inlet temperature on net power output.

Fig. 6.61 shows the power to heating and cooling ratio with ORC pump inlet temperature. Both power to heating and cooling ratios decrease with an increase in pump inlet temperature, due to an increase in the turbine outlet enthalpy, which reduces the turbine work, and an increase in heating load.

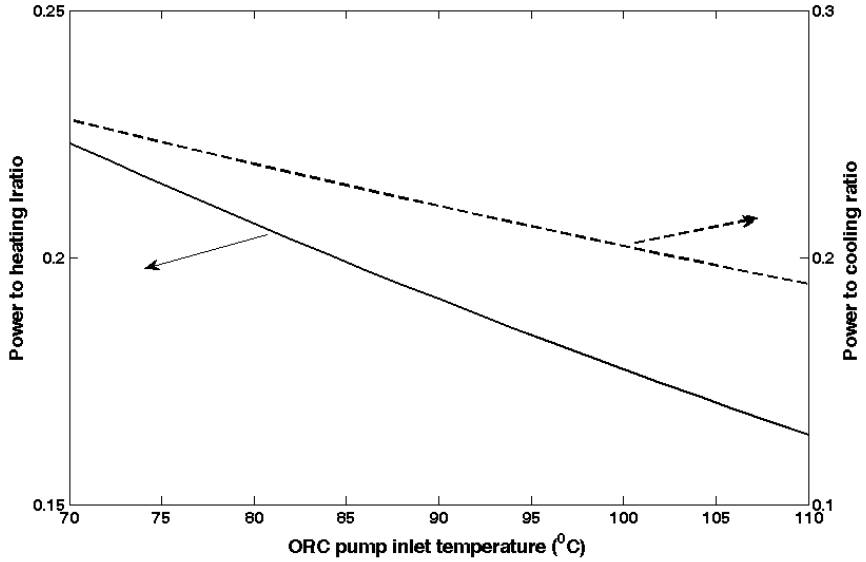

Figure 6.61: Effects of varying ORC pump inlet temperature on power to heating and cooling ratios.

Fig. 6.62 shows the effect of pump inlet temperature on total cost rate of the system. As it is shown, an increase in pump inlet temperature results in a decrease in total cost rate.

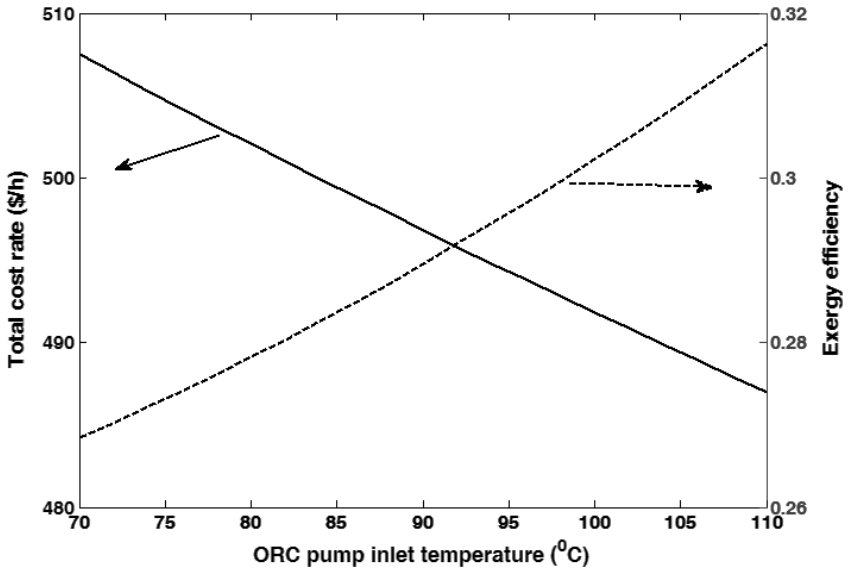

Figure 6.62: Effects of varying ORC pump inlet temperature on total cost rate and exergy efficiency.

As it was already discussed, an increase in pump inlet temperature decrease the turbine work and since the purchase cost of turbine is proportional to the work the cost of turbine decreases which finally leads to a decrease in total cost rate of the system.

6.3. 3 Environmental impact assessment

To provide environmental insights, the environmental impact of the power system is compared to that of the multigeneration in Fig. 6.63. It is seen that the multigeneration cycle has less CO_2 emissions than the power and CHP cycles, providing a significant motivation for the use of multi-generation cycles. It is also observed that multi-generation considered here has a higher exergy efficiency than other cycles.

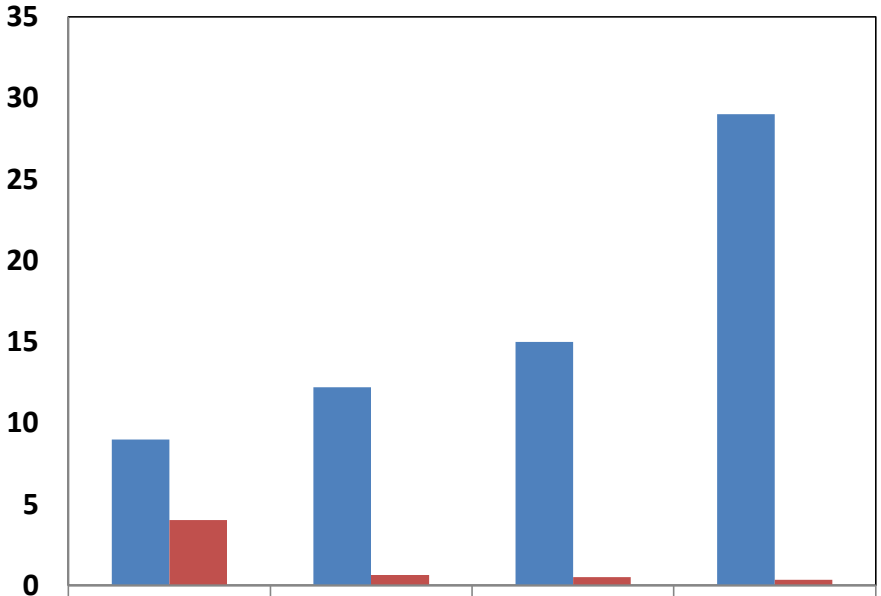

	Single generation	Cogeneration	Trigeneration	Multigeneration
Exergy efficiency (%)	9	12.2	15	29
CO2 emission (t/MWh)	4.035	0.659	0.51	0.358

Figure 6.63: Comparison of exergy efficiencies and environmental impacts for three types of plants.

The variation of CO_2 emissions with ORC turbine inlet pressure is shown in Fig. 6.64. Increasing this pressure decreases the CO_2 emissions for all cycles, however the decrease in CO_2 emissions for the power cycle is greater compared to that for the multigeneration system. This observation is attributable to the fact that an increase in turbine inlet pressure always results in an

increase in turbine work, which is due to an increase in ORC mass flow rate, while an increase in turbine inlet pressure increases the heating load of the system (as discussed in Fig. 6.58),

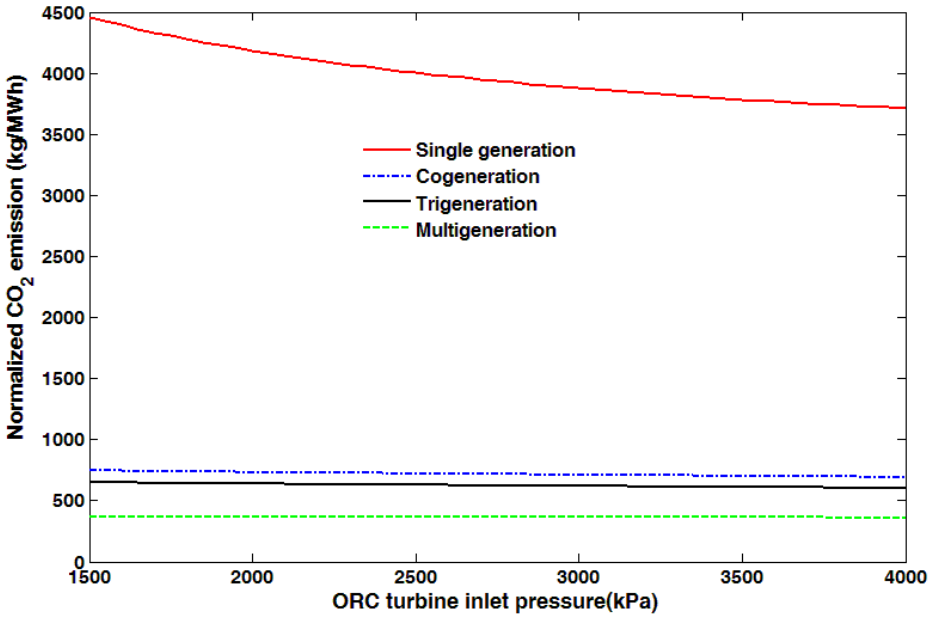

Figure 6. 64: Effect of varying ORC turbine inlet pressure on CO_2 emissions.

Thus, CO_2 emissions for the power system do not include the heating load and, as a result, the CO_2 emissions drastically decrease for the power generation system. Expanding the results for CO_2 emissions, we determine that increasing the pump inlet temperature has a negative effect on CO_2 emissions of the system.

As shown in Fig. 6.65, an increase in this temperature increases the CO_2 emissions for the power generation, CHP and multigeneration systems. This is based on the fact that an increase in this temperature decreases the net power output, which affects the CO_2 emissions. However the rate of increase for the power generation system is higher relative to the CHP and multigeneration systems. Fig. 6.66 shows the effect of pinch point temperature difference on the CO_2 emissions for three cycles. It is observed that an increase in pinch point temperature leads to an increase in normalized CO_2 emissions as an increase in pinch point temperature decreases the net power output as discussed in Fig. 6.48.

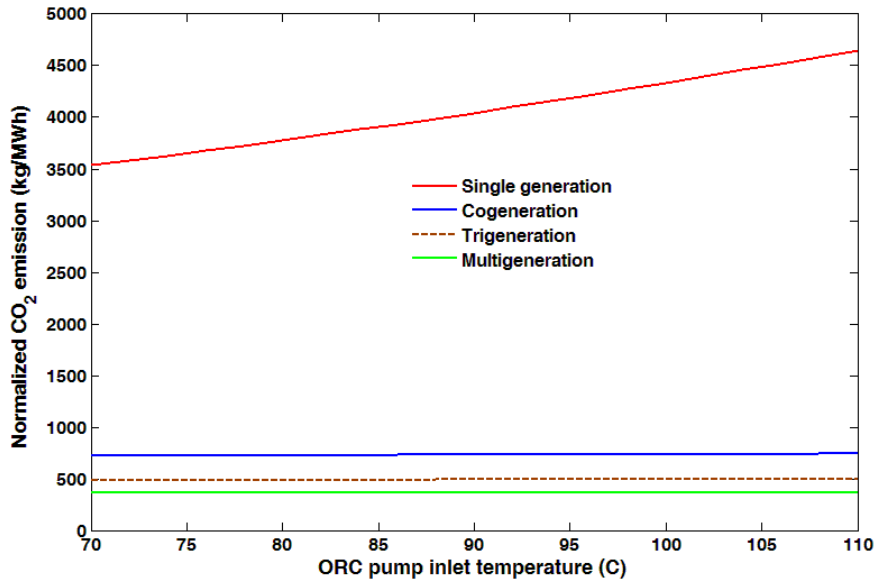

Figure 6.65: Effect of varying ORC pump inlet temperature on CO_2 emissions.

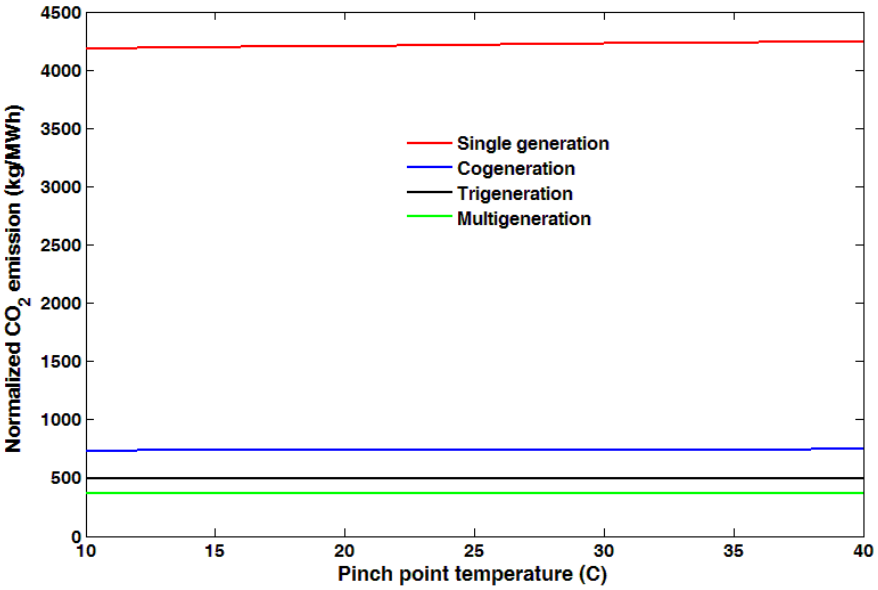

Figure 6.66: Effect of varying pinch point temperature on CO_2 emissions.

6.3.4 Multi-objective optimization

A multi-objective optimization method based on an evolutionary algorithm is applied optimization to the multigeneration system for heating, cooling, electricity, hot water, fresh water and hydrogen to determine the best design parameters for the system. Objective functions, design parameters and constraints, and overall optimization are described in this section.

6.3.4.1 Definition of objectives

Two objective functions are considered here for multi-objective optimization: exergy efficiency (to be maximized) and total cost rate of product (to be minimized). The cost of pollution damage is assumed to be added directly to the expenditures that must be paid, making the second objective function the sum of thermodynamic and environmental objectives. Consequently, the objective functions in this analysis can be expressed as follows:

Exergy efficiency

$$\Psi_{multi} = \frac{\dot{W}_{net,ORC}+\dot{E}x_{heating}+\dot{E}x_{cooling}+\dot{E}x_{H_2}+\dot{E}x_{36}+\dot{E}x_{41}}{\dot{E}x_{biomass}} \quad (6.4)$$

Total cost rate

$$\dot{C}_{tot} = \sum_k \dot{Z}_k + \dot{C}_f + \dot{C}_{env} \quad (6.5)$$

where the cost rates of environmental impact and fuel are expressed as

$$\dot{C}_{env} = C_{Co_2}\dot{m}_{Co_2} \;\&\; \dot{C}_f = c_f \dot{m}_f \, LHV \quad (6.6)$$

Here, $\dot{Z}_K$ is the purchase cost of each component. More details about equipment purchase cost can be found elsewhere [64].The purchase cost of each component in this multigeneration system was explained in section 5.12.2. Also c_f is the fuel cost which is taken to be 0.01 \$/kWh in this study. In this analysis, we express the environmental impact as the total cost rate of pollution damage (\$/s) due to CO_2 emissions by multiplying their respective flow rates by their corresponding unit damage costs (C_{CO2}, which is taken to be equal to and 0.024 \$/kg, respectively) [64]. The cost of pollution damage is assumed here to be added directly to other system costs.

6.3.4.2 Decision variables

The following decision variables (design parameters) are selected for this study: biomass flow rate ($\dot{m}_{biomass}$), ORC pump inlet temperature ($T_{in,Pump}$), ORC evaporator pinch point temperature (PP) difference, ORC turbine inlet pressure (P_{main}), ORC turbine inlet temperature (T_{main}), ORC turbine isentropic efficiency (η_T), pump isentropic efficiency (η_p) and absorption chiller evaporator temperature (T_{EVP}).Although the decision variables may be varied in the optimization procedure, each is normally required to be within a reasonable range. Such constraints, based on earlier reports are listed in Table 6.9.

Table 6.9: Optimization constraints and their rationales

Constraint	**Reason**
0.2 kg/s <$\dot{m}_{biomass}$ <0.4 kg/s	Biomass fuel limitation
$T_{in,Pump}$ < 115 K	Material temperature limit
1500 kPa <P_{main} <3000 kPa	Commercial availability
320 ºC < T_{main} <400 ºC	Commercial availability
10 ºC < PP < 35 ºC	Heat transfer limit
η_T < 0.9	Commercial availability
η_p < 0.9	Commercial availability
2 ºC < T_{EVP} < 6 ºC	Cooling load limitation

6.3.4.3 Evolutionary algorithm: Genetic algorithm

Genetic algorithms apply an iterative, stochastic search strategy to find an optimal solution and imitate in a simplified manner principles of biological evolution [93]. A characteristic of an evolutionary algorithm is a population of individuals, where an individual consists of the values of the decision variables (structural and process variables here) and is a potential solution to the optimization problem [14]. More details about genetic algorithm and its procedure are given elsewhere [14, 93].

6.3.4.4 Results and discussion

The genetic algorithm optimization is performed for 250 generations, using a search population size of M = 100 individuals, crossover probability of p_c = 0.9, gene mutation probability of p_m = 0.035 and controlled elitism value c = 0.55. The results of the optimization are given and described.

6.3.4.4.1 Optimization results

Fig. 6.67 shows the Pareto frontier solution for this multigeneration system with objective functions indicated in equations (6.4) and (6.5) in multi-objective optimization. It can be seen in this figure that the total cost rate of products increases moderately as the total exergy efficiency of the cycle increases to about 32 %. Increasing the total exergy efficiency from 32 % to 34 % increases the cost rate of product significantly.

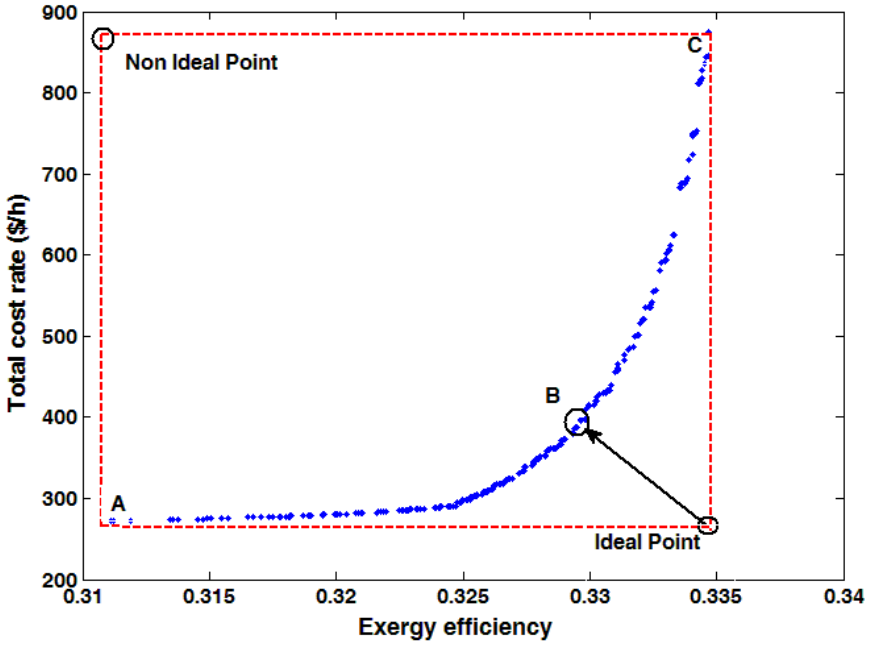

Figure 6.67: Pareto Frontier: Best trade off values for the objective functions

The results of optimum exergy efficiency and total cost rate for all points evaluated over 300 generations are shown in Fig. 6.68. The Pareto-optimal curve (best rank) is clearly visible in the lower part of the figure (red line) which is separately shown in Fig. 6.67. As shown in Fig. 6.67, the maximum exergy efficiency exists at design point *C* (33.5 %), while the total cost rate of products is the greatest at this point (874.62 $/hr).

On the other hand, the minimum value for the total cost rate of product occurs at design point *A* which is about 271.84 $/hr. Design point *A* is the optimal situation when total cost rate of product is the sole objective function, while design point *C* is the optimum point when exergy efficiency is the sole objective function. In multi-objective optimization, a process of decision-making for selection of the final optimal solution from the available solutions is required. The process of decision-making is usually performed with the aid of a hypothetical point in Fig. 6.67 (the ideal point), at which both objectives have their optimal values independent of the other objectives. It is clear that it is impossible to have both objectives at their optimum point simultaneously and, as shown in Fig. 6.67, the ideal point is not a solution located on the Pareto Frontier. The closest point of the Pareto frontier to the ideal point might be considered as a desirable final solution.

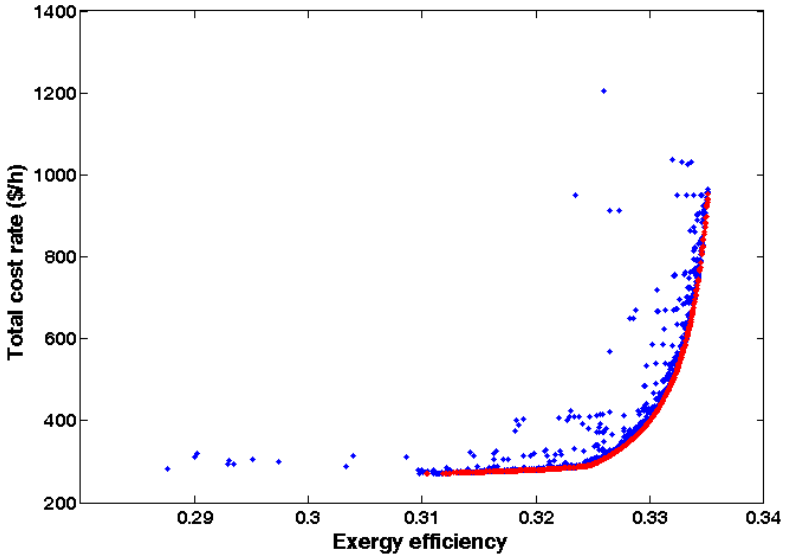

Figure 6.68: Results of all evaluations during 300 generations using genetic algorithm. A clear approximation of the Pareto front is visible on the lower part of the figure.

Nevertheless, in this case, the Pareto optimum frontier exhibits weak equilibrium i.e., a small change in exergy efficiency from varying the operating parameters causes a large variation in the total cost rate of product. Therefore, the ideal point cannot be utilized for decision-making in this problem. In selection of the final optimum point, it is desired to achieve a better magnitude for each objective than its initial value for the base case problem. Note that in multi-objective optimization and the Pareto solution, each point can be utilized as the optimized point. Therefore, the selection of the optimum solution depends on the preferences and criteria of the decision maker, suggesting that each may select a different point as for the optimum solution depending on his/her needs. Table 6.10 shows all the design parameters for points *A*-*C*.

Table 6.10: Optimized values for design parameters of the system based on multi-objective optimization

Design parameter	***A***	***B***	***C***
$\dot{m}_{biomass}$ (kg/s)	0.20	0.2	0.21
$T_{in,Pump}$ (ºC)	115	114	114
P_{main} (kPa)	1500	2049	3818
T_{main} (ºC)	320	400	398.5
PP (ºC)	12	10.3	10.6
η_T	0.80	0.90	0.9
η_p	0.82	0.84	0.85
T_{EVP} (ºC)	5.2	7	6.9

As shown in Fig. 6.67, the optimized values for exergy efficiency on the Pareto frontier range between 31 % and 34 %. To provide a good relation between exergy efficiency and total cost rate, a curve is fitted on the optimized points obtained from the evolutionary algorithm. This fitted curve is shown in Fig. 6.33. The expression for this fitted curve is given as follows:

$$\dot{C}_{total} = \frac{360\psi^3+194.8\psi^2-253.4\psi+49.76}{\psi^3-57.46\psi^2-28.92\psi-3.25} \times 100 \qquad (6.7)$$

This is allowable when the efficiency varies between 0.29 and 0.34. To study the variation of thermodynamic characteristics, three different points (*A* to *C*) on the Pareto frontier are considered. Table 6.11 shows total cost rate of the system, the total exergy destruction, the system efficiency, the heating and cooling loads of the system and the CO_2 emission of the system.

Table 6. 11: Thermodynamic characteristics of three different points on the Pareto frontier.

Point	$\dot{W}_{net}$ (kW)	Ψ	$\dot{E}x_{D,tot}$ kW	$\dot{Q}_{cooling}$ kW	$\dot{Q}_{heating}$ kW	$\dot{C}_{tot}$ \$/h	CO_2 kg/kWh	$\dot{m}_{H_2}$ kg/h	$\dot{m}_{DWH}$ kg/s	$\dot{m}_{fresh}$ kg/s
A	278.35	0.31	3749	2000	1487	271.8	346.8	1.19	0.52	1.08
B	307.10	0.32	3473	1543	1741	362	364	1.30	0.53	1.19
C	351.10	0.33	3477	1614	1644	874	361.7	1.50	0.52	1.4

From point *A* to point *C* in this table both total cost rate of the system and exergy efficiencies increases. As already stated, point *A* is preferred when total cost rate is a single objective function and design point *C* when exergy efficiency is a single objective function. Design point *B* has better results for both objective functions. Other thermodynamic properties correctly confirm this trend. For instance, from point *B* to *C*, the total exergy destruction rate decreases when the exergy efficiency increases.

To better understand the variations of all design parameters, the scattered distribution of the design parameters are shown in Figs. 6.69 to 6.70. The results show that ORC pump inlet temperature (Fig. 6.69b) and absorption chiller evaporator temperature (Fig. 6.70d) tend to become as high as possible. This observation means that an increase in these parameters leads to the better optimization results. For example, an increase in these design parameters leads to improvement for both objective functions in multi-objective optimization. In Figs. 6.69-6.70, we see that the ORC turbine inlet pressure (Fig. 6.69c), the ORC turbine inlet temperature (Fig. 6.69d), the evaporator pinch point temperature difference (Fig. 6.70a), ORC turbine isentropic efficiency (Fig. 6.70b), and the ORC pump isentropic efficiency (Fig. 6.70c) have scattered

distributions in their allowable domains, suggesting that these parameters have important effects on the trade-off between exergy efficiency and total cost rate. Design parameters selected with their maximum values indicate that they do not exhibit a conflict between two objective functions, indicating that increasing those design parameters leads to an improvement of both objective functions.

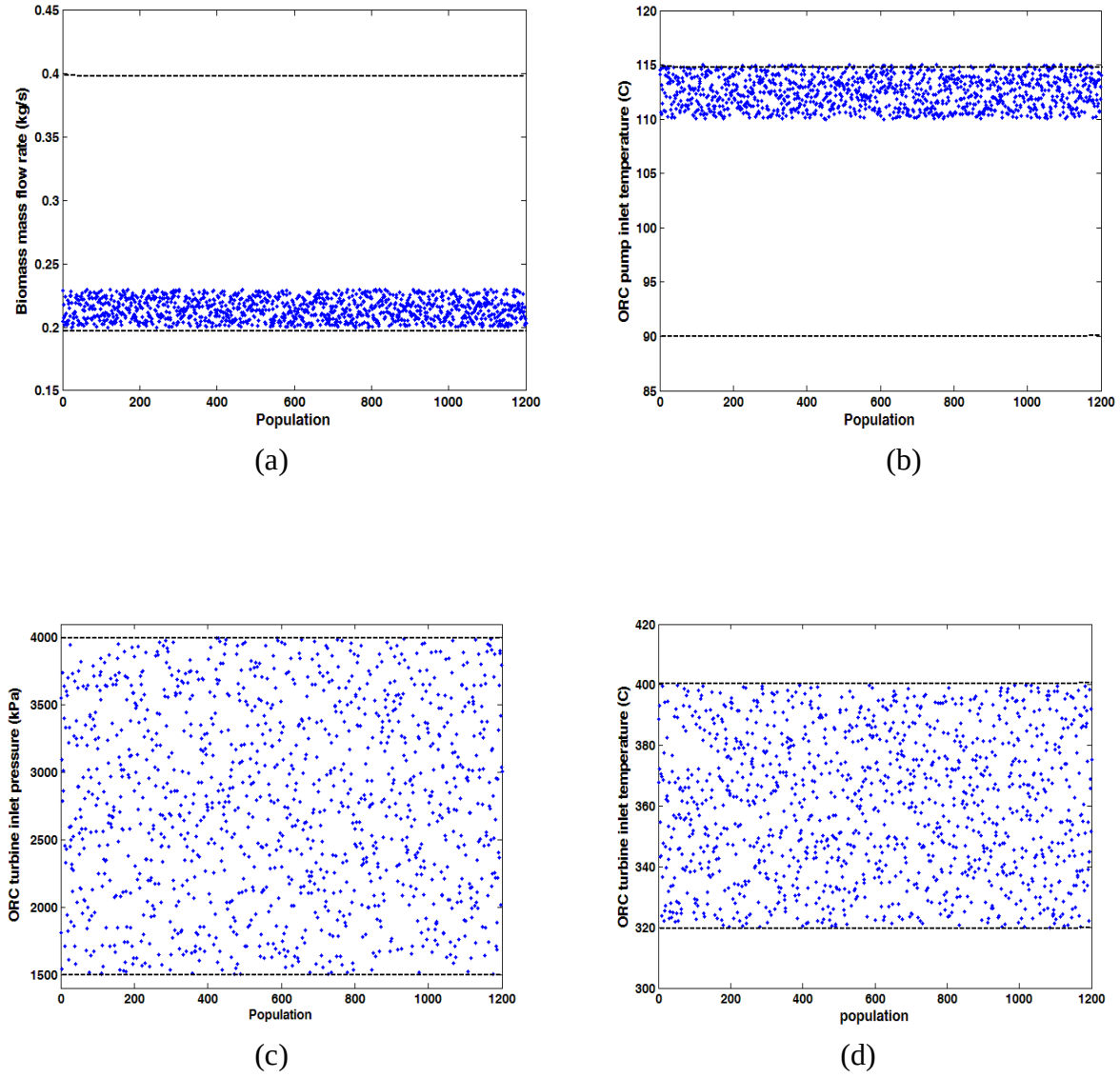

Figure 6.69: Scattered distribution of decision variables with population in Pareto frontier: (a) biomass flow rate, (b) ORC pump inlet temperature, (c) ORC turbine inlet pressure, (d) ORC turbine inlet temperature

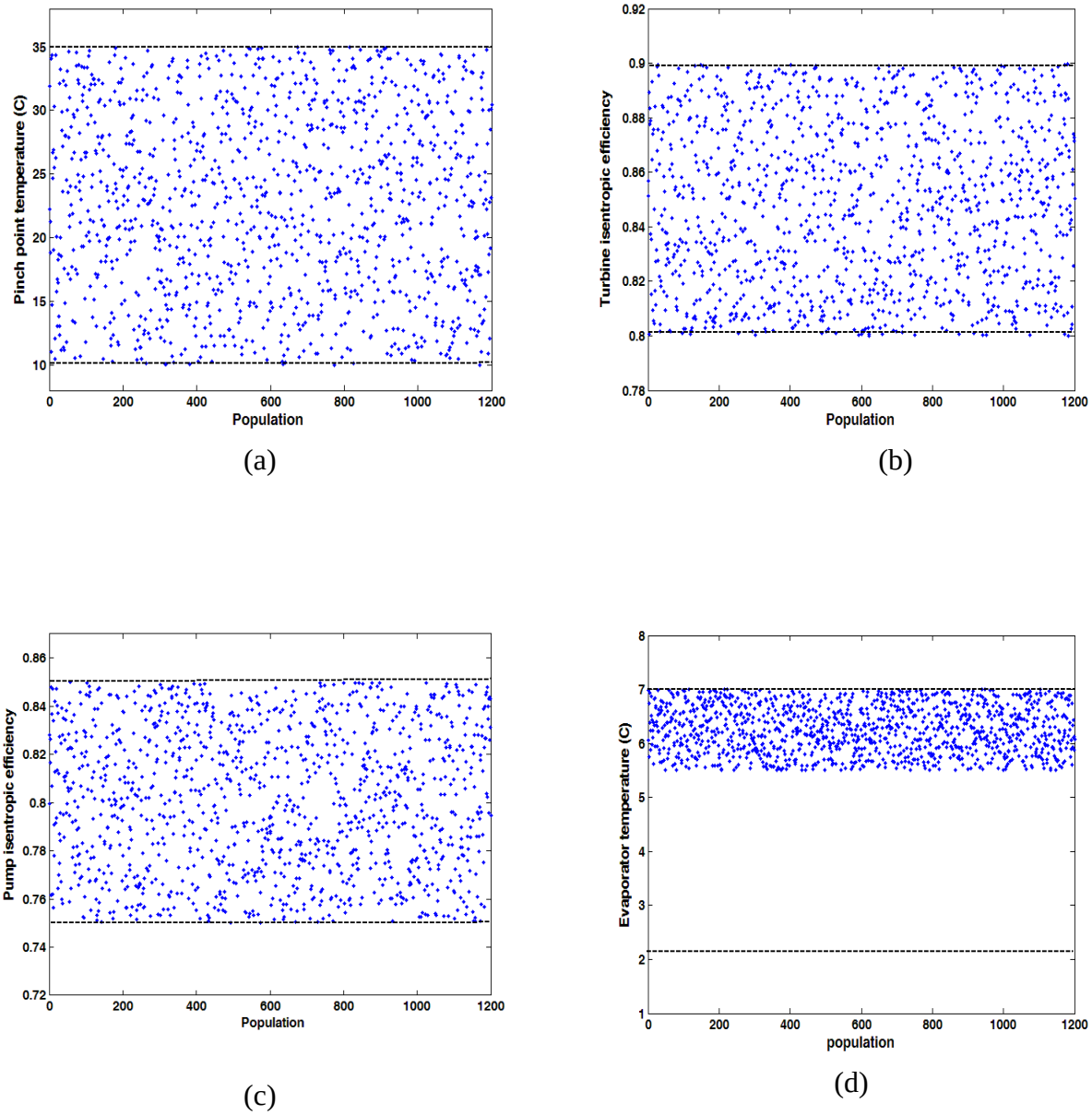

Figure 6.70: Scattered distribution of decision variables with population in Pareto frontier: (a) Pinch point temperature, (b) ORC turbine isentropic efficiency, (c) ORC pump isentropic efficiency, (d) absorption chiller evaporator temperature

6.3.4.4.2 Sensitivity analysis

In order to have a better understanding of the multi-objective optimization, a comprehensive sensitivity analysis is performed. The effects of each design parameters for point *A*-*C* on both objective functions are investigated. Fig. 6.71 shows the effects of biomass flow rate on system exergy efficiency and total cost rate of the system. As seen in this figure, an increase in biomass flow rate has negative effect on both objective functions. An increase in biomass flow rate leads to a decrease in system exergy efficiency as the denominator of equation (6.4) increases. Also, an increase in this parameter increase the total cost rate of the system as the mass flow rate increase the cost associated with the fuel increases which results in an increase in total cost rate of the system.

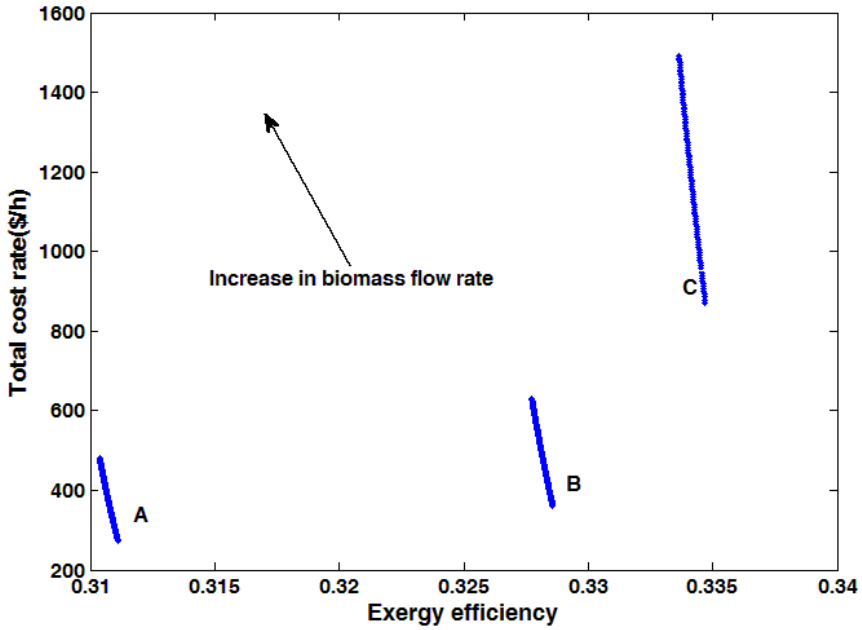

Figure 6.71: Effects of biomass flow rate on both objective functions.

Fig. 6.72 shows the variation of ORC turbine inlet pressure on both objective functions. As shown in this figure, an increase in turbine inlet pressure results in an increase in both objective functions. When the turbine inlet pressure increase the exergy efficiency of the system increases which is due to an increase in cooling load and net power output of the system.

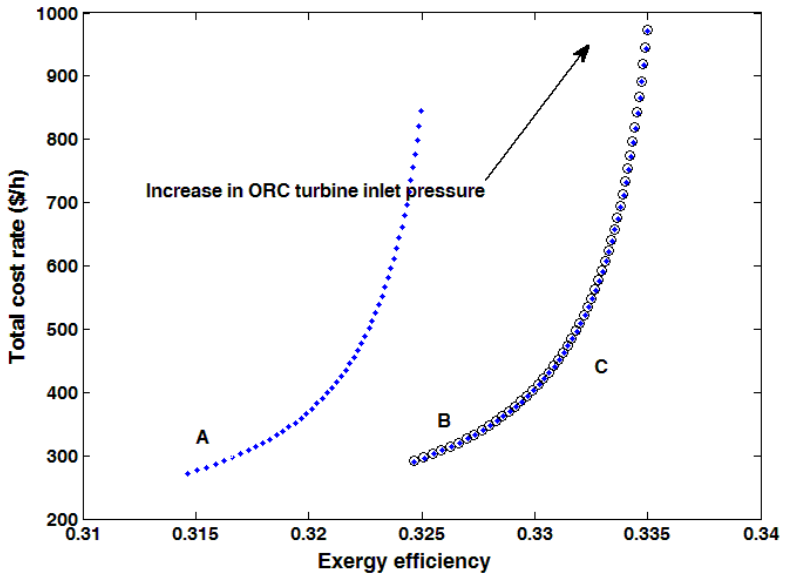

Figure 6.72: Effects of turbine inlet pressure on both objective functions.

An increase in ORC turbine inlet pressure reduces the heating load of the system while an increase in this pressure has a positive effect on cooling load of the system. An energy balance for a control volume around the ORC evaporator shows that when the energy input from biomass is constant, a reduction in turbine inlet enthalpy increases the ORC mass flow rate. Since inlet and outlet enthalpies of the generator in the absorption cycle are constant, an increase in the ORC mass flow rate leads to an increase in energy input to the absorption system, which increases the cooling load of the system.

For the heating load, an increase in ORC turbine inlet pressure, while fixing other design parameters, decreases the turbine inlet enthalpy and, since the turbine outlet enthalpy is a function of the turbine inlet enthalpy and turbine isentropic efficiency, this a corresponding decrease in turbine outlet enthalpy (h_{28}), which is the inlet energy for the heating process unit. Although the ORC mass flow rate increases as already discussed, the reduction in enthalpy of the heating process dominates. In addition, an increase in ORC turbine inlet pressure results in increase in the ORC mass flow rate entering the turbine which results in an increase in turbine output work. Therefore, the combination of these effects leads to an increase in the system exergy efficiency. Fig. 6.72 also shows that an increase in turbine inlet pressure results in an increase in total cost rate of the system which is due to an increase in turbine purchase cost as the inlet pressure increases. As a result, an increase in ORC turbine inlet pressure has a negative and

positive effect on the objective functions. This is why the scattered distribution for the ORC turbine inlet pressure has a scattered distribution.

Fig. 6.73 shows the variation of turbine inlet temperature on both objective functions. It is observed that an increase in turbine inlet temperature increase the exergy efficiency of the system for point *A*-*C* on the Pareto curve. Increasing the turbine inlet temperature leads to an increase in turbine inlet enthalpy while keep other parameters fixed, this increase leads to an increase in turbine work which finally results in an increase in exergy efficiency according to equation (6.4). On the other side, an increase in turbine inlet temperature increase the total cost of the system which is due to an increase in turbine purchase cost. An increase in turbine purchase cost leads to an increase in the total cost of the system. Since an increase in this parameter has positive and negative effects on both objective functions, the variation of this design parameter within its allowable range exhibits a scattered distribution as shown in Fig. 6.69d.

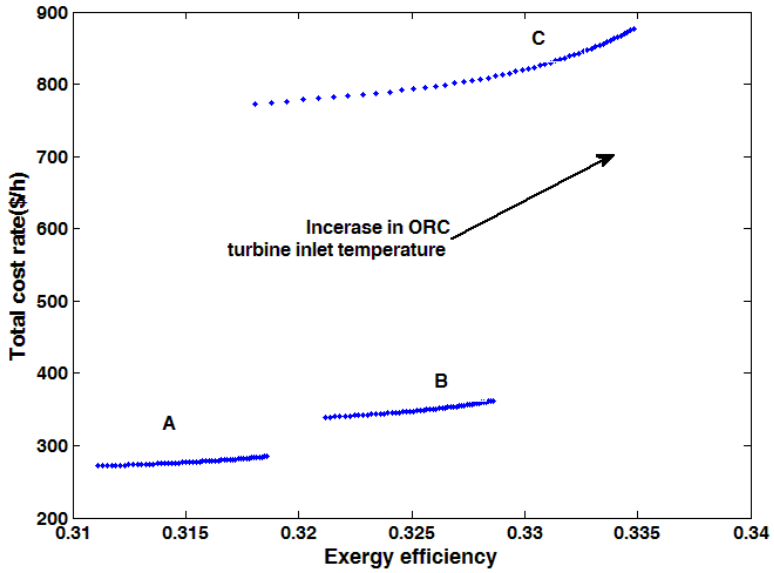

Figure 6.73: Effects of turbine inlet pressure on both objective functions.

Fig. 6.74 shows the effect of evaporator pinch point temperatures on both objective functions. It is seen that an increase in pinch point temperature results in a decrease in system exergy efficiency. This is due to the fact that the higher the pinch point temperature, the lower the energy being utilized in evaporator which leads to a reduction of ORC turbine power output. On the other side, an increase in pinch point temperature while fixing other design parameters,

results in a decrease in heat transfer area for the evaporator. This is why the total cost rate of the system decreases.

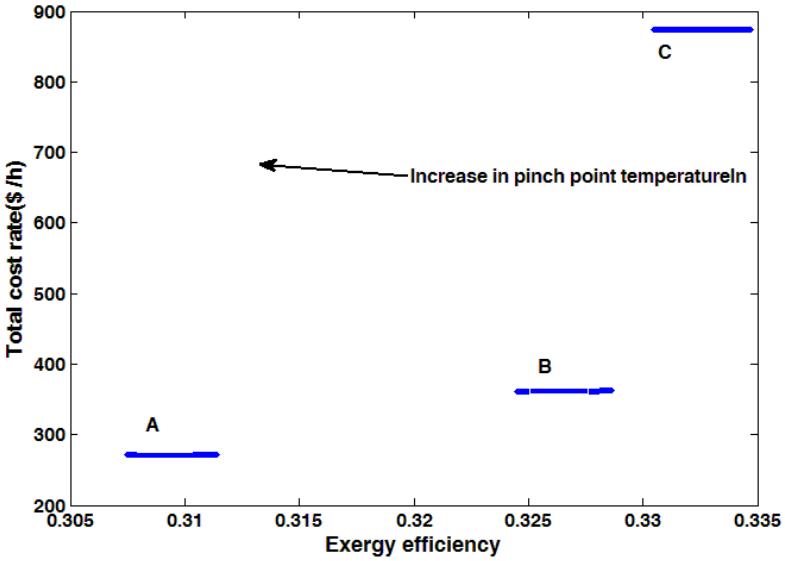

Figure 6.74: Effects of evaporator pinch point temperature on both objective functions.

Since an increase in this parameter has positive and negative effects on both objective functions, the variation of this design parameter within its allowable range exhibits a scattered distribution as shown in Fig. 6.70a. Fig. 6.75 represents the effect of turbine isentropic efficiency (η_T) on both objective functions. An increase in η_T results in an increase in system exergy efficiency and increase in total cost of the system. Increasing this parameter results in an increase in the steam turbine power output, which directly leads to an increase in the exergy efficiency.

It is also seen that increasing this parameter leads to an increase in steam turbine purchase and maintenance cost. Since an increase in this parameter has positive and negative effects on both objective functions, the variation of this design parameter within its allowable range exhibits a scattered distribution as shown in Fig. 6.70b. Fig. 6.76 shows that pump isentropic efficiency does not have a significant effect on both objective functions, as its purchase cost is small. Fig. 6.77c shows the variation of the objective function by changing the absorption chiller evaporator temperature. An increase in evaporator temperature results in an increase in cooling load of the absorption chiller and at a same time increase the cost of the chiller.

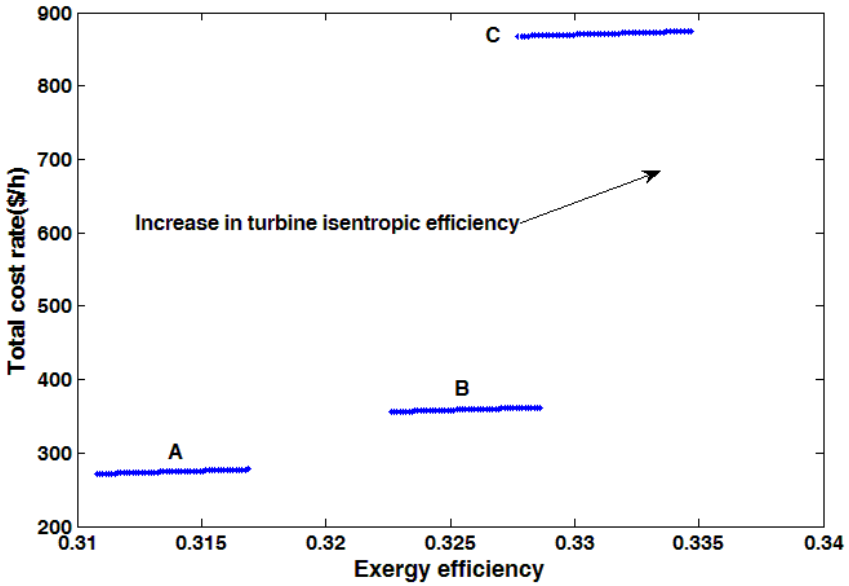

Figure 6.75: Effects of turbine isentropic efficiency on both objective functions.

6.4 Results of system III

The thermodynamic modeling of the multigeneration system considered (Fig. 4.3) is divided into five sub-systems: 1) PV/T solar collector, 2) Ocean thermal energy conversion (OTEC), 3) single-effect absorption chiller 4) proton exchange membrane (PEM) electrolyzer and reverse osmosis (RO) desalination unit. We determine the temperature profile in the multigeneration plant, input and output enthalpies, exergy flows, environmental impacts, exergy destructions and exergy efficiencies.

6.4. 1 Modeling results

Results of the thermodynamic model and exergy analyses are presented here, including assessments based on the effects of varying several design parameters with respect to cycle performance. Table 6.12 lists the thermodynamic properties of the multigeneration system shown in Fig. 4.3.

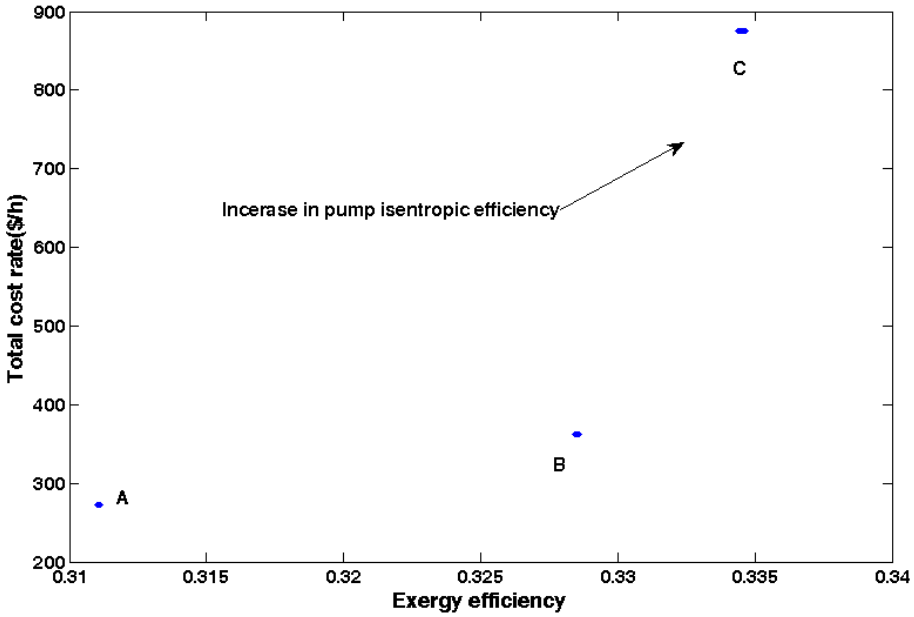

Figure 6.76: Effects of pump isentropic efficiency on both objective functions.

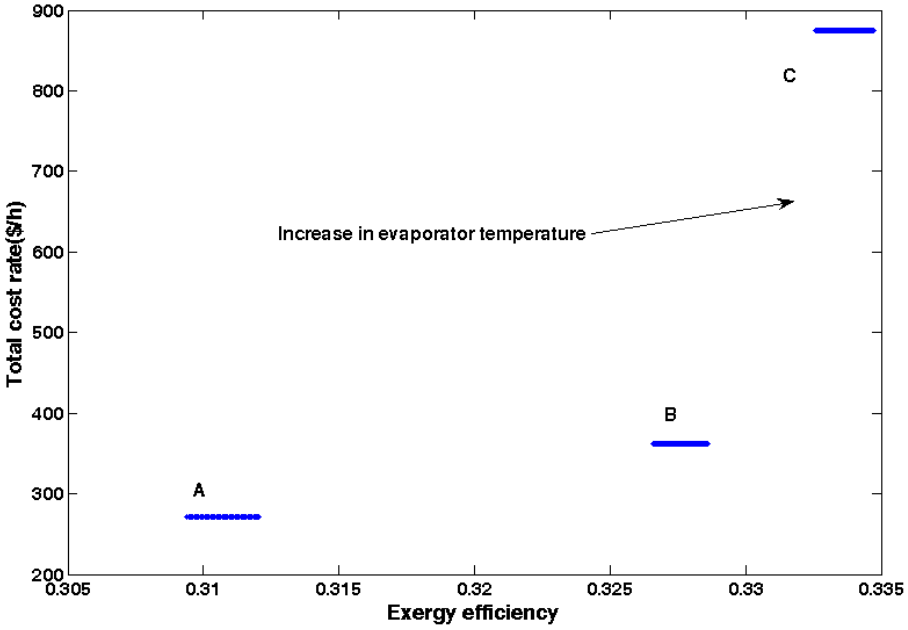

Figure 6.77: Effects of absorption chiller on both objective functions.

In this exergy analysis, the dead state is defined to have a pressure of P_0 = 1.01 bar and a temperature of T_0 = 293.15 K. Energy and exergy balances are used to model the system, while invoking reasonable assumptions. In order to model the integrated OTEC system, a simulation code using Matlab software is developed. Five main parts are first individually modelled, including individual exergy flow rates. Engineering equation solver (EES) is linked to Matlab to calculate the properties of the different working fluids (i.e., water and ammonia) such as pressure, temperature, enthalpy and entropy. Several simplifying assumptions are made here to render the analysis more tractable, while retaining adequate accuracy to illustrate the principal points of the study:

- All processes operate at steady state.
- The thermodynamic cycle of the integrated system in Fig. 4.3 is an ideal saturated Rankine cycle using pure ammonia as the working fluid.
- All the components are adiabatic.
- Pressure drops in ORC cycle are negligible.
- State 5 is saturated vapour.
- Heat losses from piping and other auxiliary components are negligible.

In order to conduct the simulation, input data are required. For each subsystem certain reliable data are inputted to the simulation code in order to determine the outputs. Table 6.12 lists the input parameters for the OTEC system simulation. In addition, Table 6.13 lists the parameter used to simulate the PEM electrolyzer.

Table 6.14 lists the thermodynamic specifications of the multigeneration system, including cooling load, the electricity generated by the turbines, the COP of the absorption chiller, and the mass flow rates of biomass, hydrogen, hot water and fresh water production.

6.4. 2 Exergy and economic analyses results

The exergy analysis results are summarized in Fig. 6.78, and show that the highest exergy destruction occurs in the solar collectors, mainly due to the irreversibilities associated with the high temperature of sun which creates high exergy input. Moreover, the temperature difference between the solar cell and inlet air temperature results in a significant entropy generation. The OTEC Rankine cycle exhibits the next largest exergy destruction, mainly due to the temperature

difference between two fluid streams passing through the components, along with the pressure drop across the device.

Table 6. 12: Input data for the system simulation of OTEC system.

Parameter	Value	Parameter	Value
Turbine isentropic efficiency, η_T	0.80	Warm seawater mass flow rate (kg/s)	150
Generator mechanical efficiency, η_G	0.90	Cold sea water mass flow rate (kg/s)	150
Working fluid pump isentropic efficiency, η_{WFP}	0.78	Cold sea water pipe length (m)	1000
Seawater pumps isentropic efficiency, η_P	0.80	Cold seawater pipe inner diameter (m)	0.70
Ambient temperature (^{0}C)	25	Warm sea water pipe length (m)	50
Solar radiation incident on collector surface, I (W/m^2)	700	Warm sea water pipe length (m)	0.70
Warm sea water temperature, T_{WSI} (^{0}C)	22	Solar collector effective area (m^2)	5000
Cold sea water temperature at depth of 1000 m, T_{CSI} (^{0}C)	4	Electrolyzer working temperature (^{0}C)	80
PV/T solar collector length (m)	1.2	PV/T solar collector width (m)	0.54
Absorption chiller evaporator temperature (^{0}C)	5	OTEC evaporator pinch point temperature (^{0}C)	3
Sea water salinity (ppm)	36000	PV/T air mass flow rate (kg/s)	2

Table 6.13: Input parameters used to model PEM electrolysis.

Parameter	Value
P_{O_2} (atm)	1.0
P_{H_2} (atm)	1.0
T_{PEM} (^{0}C)	80
$E_{act,a}$ (kJ/mol)	76
$E_{act,c}$ (kJ/mol)	18
$\boldsymbol{\lambda}_a$	14
$\boldsymbol{\lambda}_c$	10
D (μm)	100
J_a^{ref} **(A/m^2)**	1.7×10^5
J_c^{ref} **(A/m^2)**	4.6×10^3
F **(C/mol)**	96,486

Table 6.14: Parameter values resulting from energy and exergy analyses of the system.

Parameters	**Value**
Net power output, $\dot{W}_{net}$(kW)	72.49
Exergy efficiency, Ψ (%)	0.37
Sustainability Index, *SI*	1.29
Total exergy destruction rate, $\dot{E}x_{D,tot}$ (kW)	1351
Hydrogen production rate, $\dot{m}_{H_2}$(kg/hr)	0.26
Cooling load (kW)	105
Fresh water mass flow rate (kg/s)	0.23
Total cost rate ($/h)	176.35
PEM electrolyzer exergy efficiency, Ψ_{PEM} (%)	56.32
Warm surface pump power, $\dot{W}_{WS}$ (kW)	1.39
Cold surface pump power, $\dot{W}_{CS}$ (kW)	3.34
Working fluid pump power, $\dot{W}_{WF}(kW)$	1.12

Fig. 6.79 shows the dimensionless exergy destruction ratio for each component. This measure is useful for prioritizing exergy losses in an intuitive manner. Both exergy destruction and the dimensionless exergy destruction ratio are higher in solar collectors than in any other component, suggesting that it would likely be worthwhile to focus improvement efforts on this component. Moreover, the results show that, the absorption cycle and RO desalination unit do not exhibit significant exergy destructions, since it does not directly utilize fuel energy but uses heat produced by the PV/T and work instead.

6.4.2.1 Effect of PV/T parameters on collector performance

In order to enhance the understanding of the system, the effect of certain major PV/T design parameters on the PV/T system performance are investigated in this section. Fig. 6.80 shows the effect of inlet air mass flow rate on the exergy efficiency of the PV/T collector. It is observed that, at constant collector length, an increase in the inlet air mass flow rate results in an increase in exergy efficiency of the collector to a certain value and reaches to its maximum value and decreases thereafter.

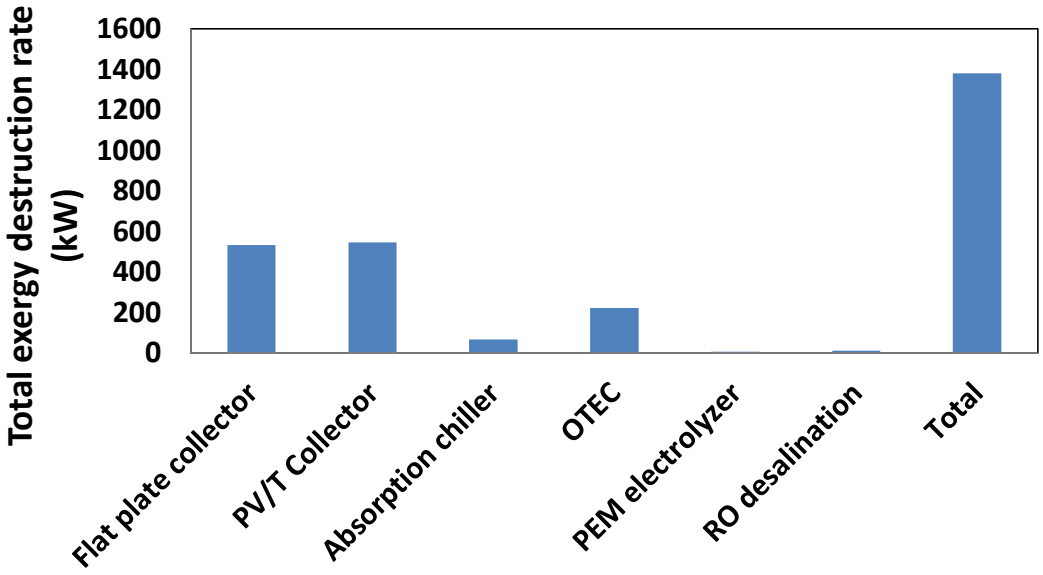

Figure 6.78: Exergy destruction rates for the Integrated OTEC based multigeneration system and its components.

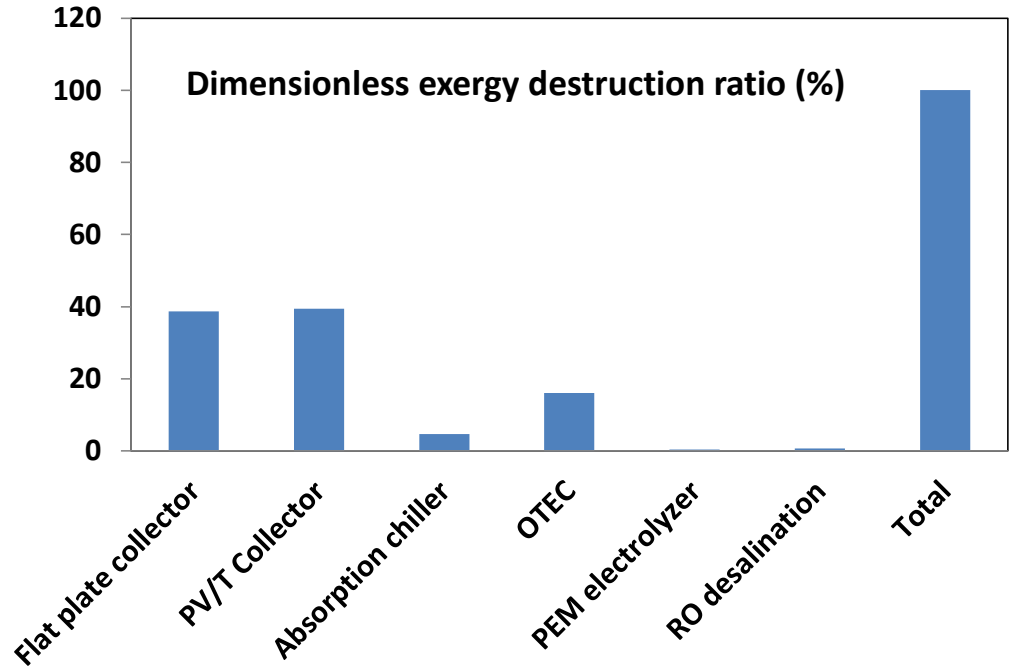

Figure 6.79: Dimensionless exergy destruction ratio for the multigeneration system and its components.

This is due to the fact that an increase in mass flow rate initially leads to an increase in the energy received by the collector, and to a maximum value after that the increase in mass flow rate results in an increase in inlet air velocity increases which cause a pressure drop in air duct, therefore this increase causes a significant drop in the exergy efficiency of PV/T air collector. Therefore, it is imperative to find the optimal value for the air mass flow rate. It is observed from this figure that and increase in collector length increases the exergy efficiency of the collector, which is mainly due to an increase in both heating and electricity production by the collector that is proportional to the collector length.

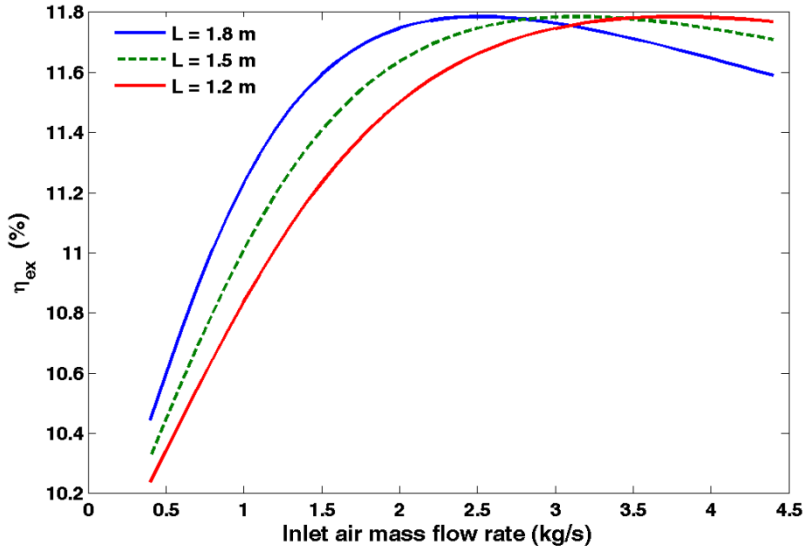

Figure 6.80: Effects of varying inlet air mass flow rate and PV/T length on exergy efficiency of the PV/T collector.

Fig.6.81 shows the variation of PV/T electricity production with PV/T length and width. It is observed that an increase in both PV/T length and width increases the PV/T electricity generation. The reason is due to the effect of collector area on the electricity produced by the collector, where the higher the collector area the more the electricity is generated by the collector. Fig. 6.82 shows the effect of these two parameters on the PV/T heat produced to increase the inlet air temperature. It is observed that an increase in collector length results in an increase in the heat produced by the collector to reach a maximum value, and after that an increase in collector length does not significantly increase the heat gained by the collector as the inlet sun energy reaches to a maximum value.

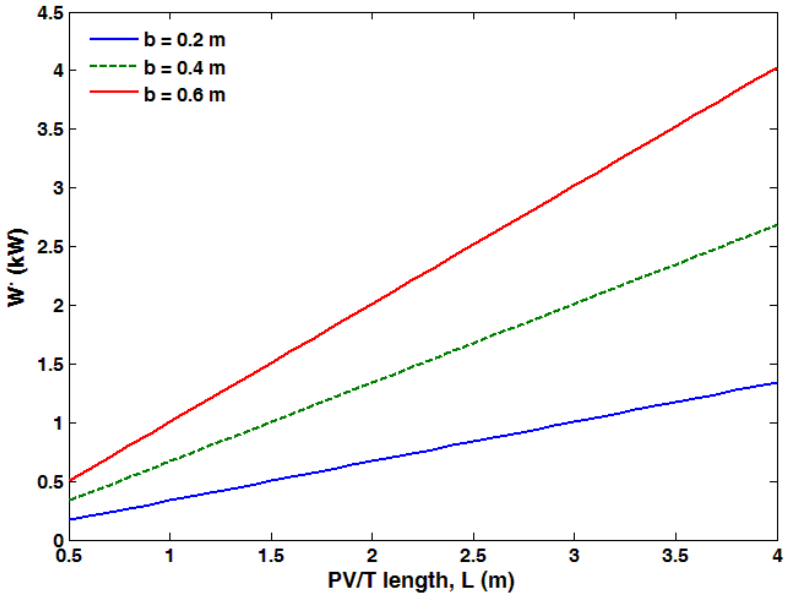

Figure 6.81: Effects of varying PV/T length and width on electricity generated by the PV/T collector.

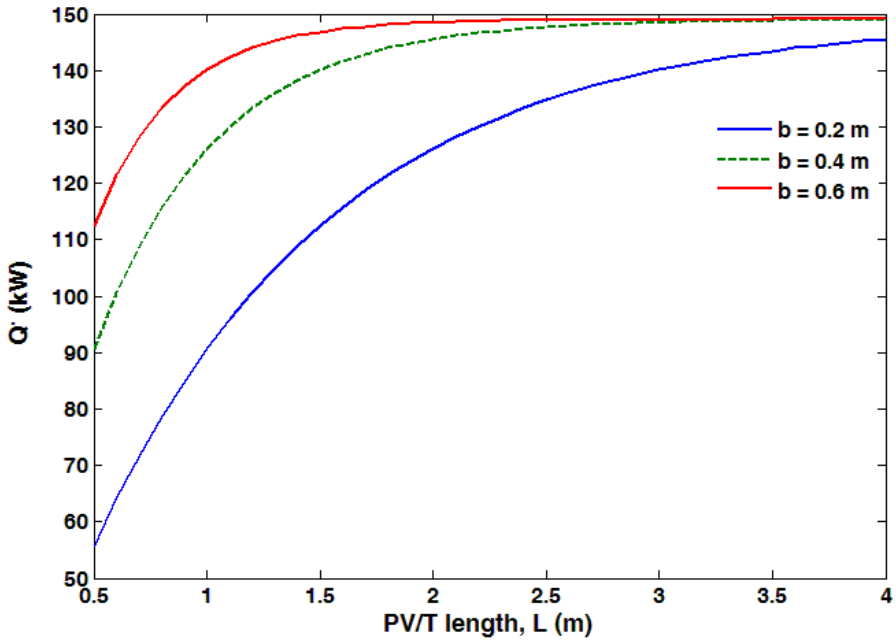

Figure 6. 82: Effects of varying PV/T length and width on electricity generated by the PV/T collector.

6.4.2.1 Parametric study of the integrated OTEC based multigeneration system

The effect of several design parameter variations on the thermodynamic performance of the multigeneration system is assessed in this section. Since warm surface mass flow rate ($\dot{m}_{WS}$), solar radiation intensity ($\dot{I}$), condenser temperature (T_{Cond}), PV/T collector length (L), PV/T collector width (b), PV/T inlet air mass flow rate ($\dot{m}_{air}$), evaporator pinch point temperature difference (PP) significantly affect the system performance parameters (e.g., exergy efficiencies, total cost rate and total exergy destruction), they became the main subject of attention in this section.

Warm surface temperature is an important parameter in the OTEC system as an increase in this parameter results in an increase in the energy input of the OTEC evaporator. Fig. 6.83 shows the effect of warm surface mass flow rate on exergy efficiency and the total exergy destruction of the system. It is observed that an increase in this parameter results in a decrease in exergy efficiency of the system which is due to an increase in energy inputted to the system according to equation (5-206). An increase in this mass flow rate results in an increase in OTEC net power output and increase in the denominator of equation (5-206), however the increase in exergy input of the system becomes the dominant effect. This is why an increase in warm surface mass flow rate decreases the system exergy efficiency.

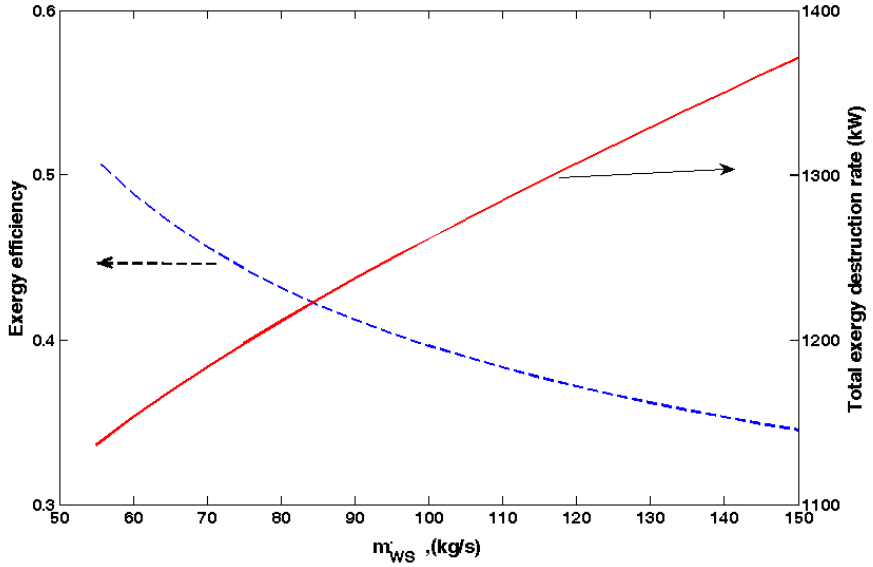

Figure 6.83: Effects of varying seawater warm surface mass flow rate on the system exergy efficiency and exergy destruction rate of the system

Fig. 6.84 shows the effect of warm surface mass flow rate on the net power output and total cost rate of the system. As previously explained, an increase in warm mass flow rate increases the

energy inputted to the OTEC evaporator. Therefore, using the energy balance equation for a control volume around the evaporator, the mass flow rate of the OTEC working fluid increases which finally results in an increase in the turbine work.

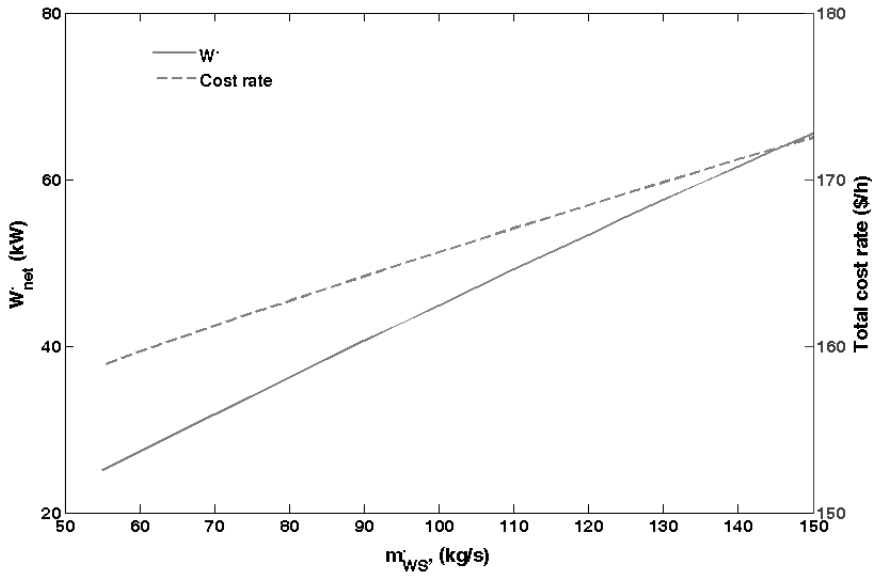

Figure 6.84: Effects of varying seawater warm surface mass flow rate on the net power output and total cost rate of the system

It is also observed form this figure that an increase in warm surface mass flow rate results in an increase in the total cost of the system. This is due to an increase in the purchase cost of the turbine and warm surface working pump as the turbine and pump work increases and as a results the total cost of the system which is the summation of all purchase cost increases. Since the main cycle of this integrated multigeneration system is OTEC system and it is dependent on the warm surface temperature, the effect of solar radiation intensity is significant. Fig. 6.85 shows the effect of solar radiation intensity on the exergy efficiency of the system. It is observed that an increase in solar radiation intensity increases the exergy efficiency of the integrated multigeneration system. This is due to the fact that an increase in solar intensity leads to an increase in the temperature of the warm surface. The higher the warm surface temperature, the higher the energy input to the OTEC evaporator which leads to an increase in the turbine work, which finally results in an increase in the system exergy efficiency. Fig. 6.85 also investigates the effect of condenser temperature on the exergy efficiency. It shows that an increase in condenser temperature reduces the exergy efficiency of the system.

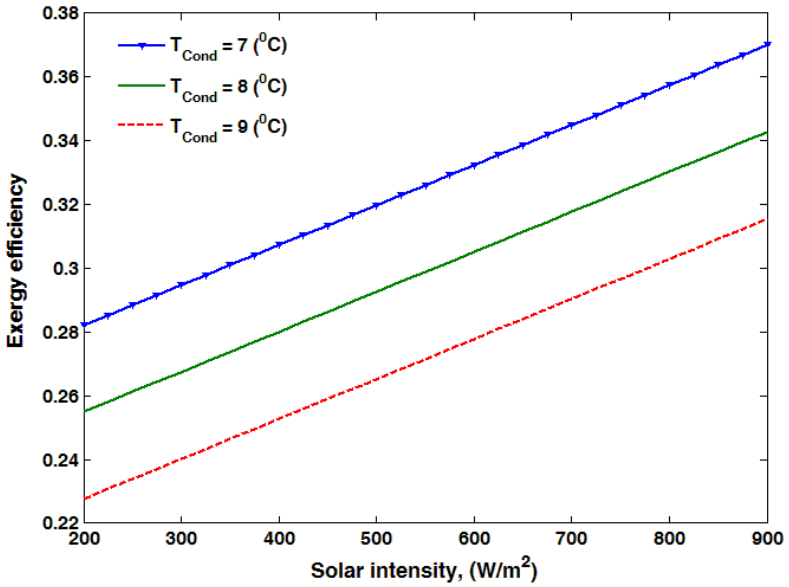

Figure 6.85: Effects of varying solar radiation intensity on the exergy efficiency of the system.

When the condenser temperature increases, while keeping other parameters fixed, leads to an increase in turbine outlet enthalpy and by applying the energy balance equation around the turbine, an increase in the outlet energy results in a decrease in turbine work as shown in Fig. 6.86.

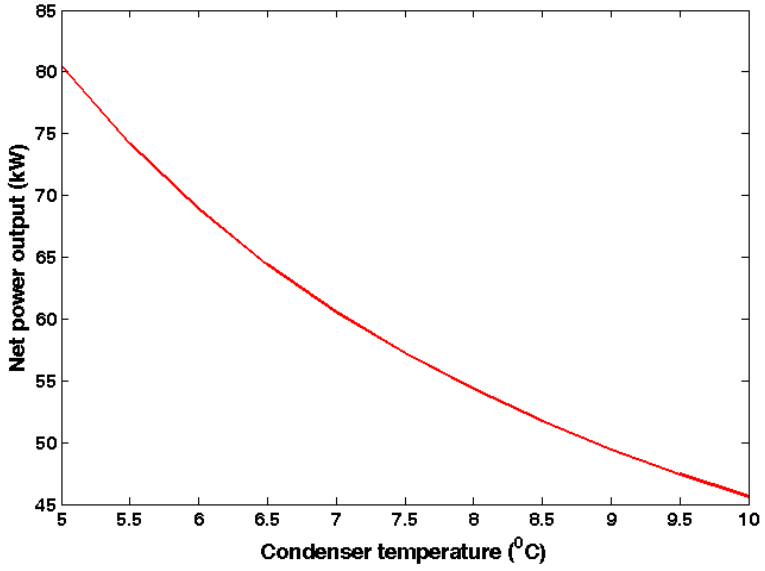

Figure 6.86: Effects of varying condenser temperature on the net power output the system.

Fig. 6.87 shows the variation of solar radiation intensity on the total exergy destruction of the system. As shown in this figure, an increase in solar radiation intensity results in an increase in total exergy destruction rate of the system. This is due to an increase in solar exergy inputted to the PV/T and flat plate collector which increase the exergy destruction of the system. It is also observed that an increase in condenser temperature leads to an increase in the total exergy destruction which is due to an increase in exergy input to the condenser which is a result of an increase in condenser enthalpy. This results in an increase in exergy destruction rate for the condenser.

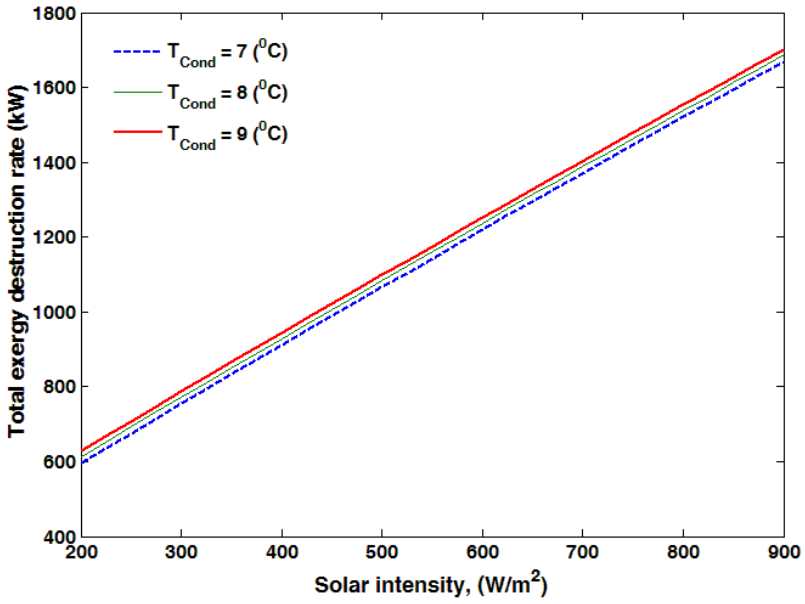

Figure 6.87: Effects of varying solar intensity on the total exergy destruction of the system.

Fig. 6.88 shows the variation of solar radiation intensity and condenser temperature on the total cost rate of the system. It is observed that an increase in solar radiation intensity increases the total cost rate, but not considerably. The main reason is due to an increase in absorption chiller which will affect the cost of the single effect absorption chiller which results an increase in the total cost rate of the system. It is shown that an increase in solar radiation intensity about 700 W/m^2 results in an increase in total cost of the system less than 3 $/h. However, this figure shows that an increase in condenser temperature for 2 ^{0}C at a specific solar tradition intensity results in an increase in solar radiation for about 5 $/h.

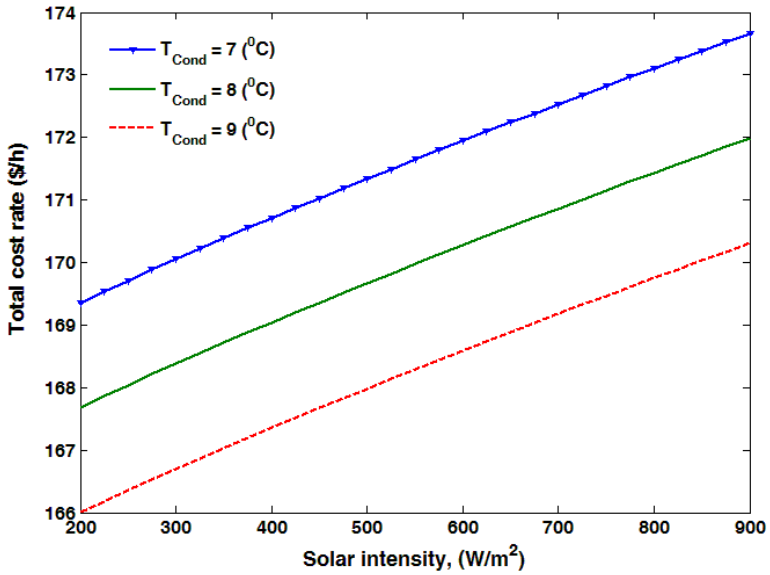

Figure 6.88: Effects of varying solar intensity on the total exergy destruction of the system.

The pinch point (PP) temperature is a significant design parameter in heat exchangers. Raising this temperature can reduce the efficiency of the system by reducing the energy recovered by the heat exchanger. Fig. 6.89 shows the effect of varying pinch point temperature on the cycle's overall exergy efficiency.

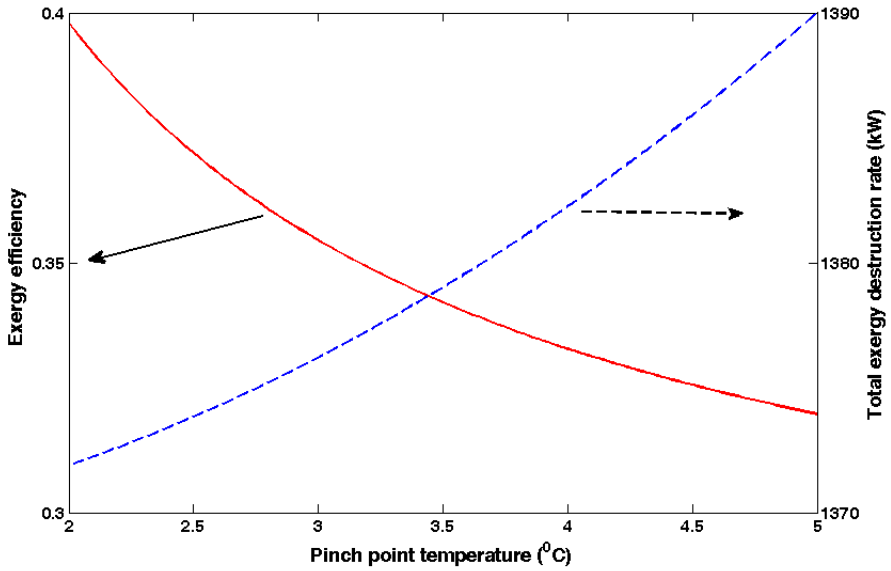

Figure 6.89: Effects of varying pinch point temperature on the exergy efficiency and total exergy destruction rate of the system.

As seen in this figure, the exergy efficiency of the multigeneration system decreases when pinch point temperature increases. Fig. 6.89 shows the effect of pinch point temperature on the system exergy efficiency and total exergy destruction rate of the system. It is observed that an increase in pinch point temperature results in a decrease in exergy efficiency and increase in total exergy destruction rate. When the pinch point temperature increases, the fluid temperature leaving the OTEC evaporator increases, which results in a decrease in the ORC mass flow rate based on an energy balance for a control volume around ORC evaporator. Therefore, the lower the ORC mass flow rate, the less the turbine work becomes.

Fig. 6.90 shows the effect of pinch point temperature on the hydrogen production and total cost rate of the system. It is observed that an increase in pinch point temperature results in a decrease in hydrogen production rate and total cost of the system. Since an increase in the pinch point temperature decreases the net power output and PEM electrolyzer uses the electricity produced by turbine the lower the net power output the lower the hydrogen production rate.

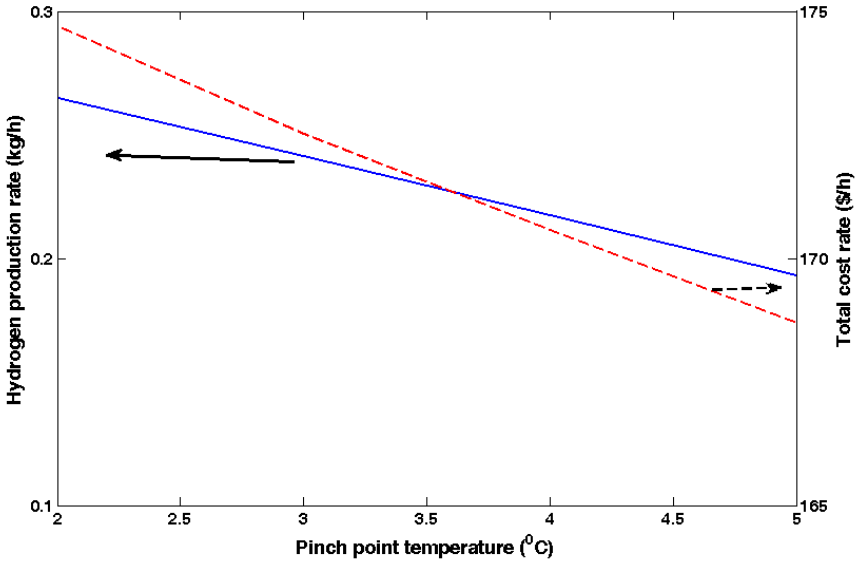

Figure 6.90: Effects of varying pinch point temperature on the hydrogen production and total cost rate of the system.

On the other hand, an increase in pinch point temperature while fixing other design parameters, results in a decrease in heat transfer area for the OTEC evaporator. This is why the total cost rate of the system decreases.

Fig. 6.91 shows the variation of exergy efficiency with PV/T solar collector length and inlet air mass flow rate. It is observed that an increase in collector length increase the exergy efficiency of the system which is due to an increase in electricity produced by the PV/T and heat input to the single effect absorption chiller, since the higher the energy input to the chiller the higher the cooling load of the system (see Fig. 6.92).

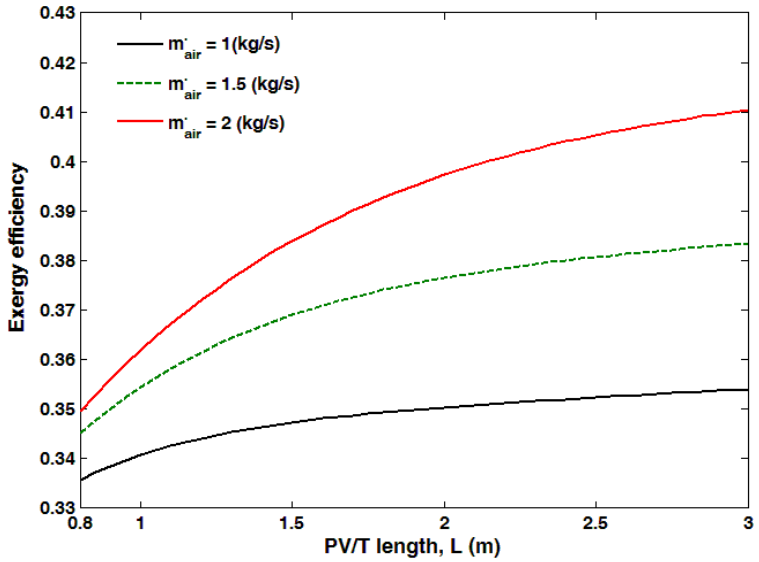

Figure 6.91: Effects of varying PV/T length and inlet air mass flow rate on the exergy efficiency of the system.

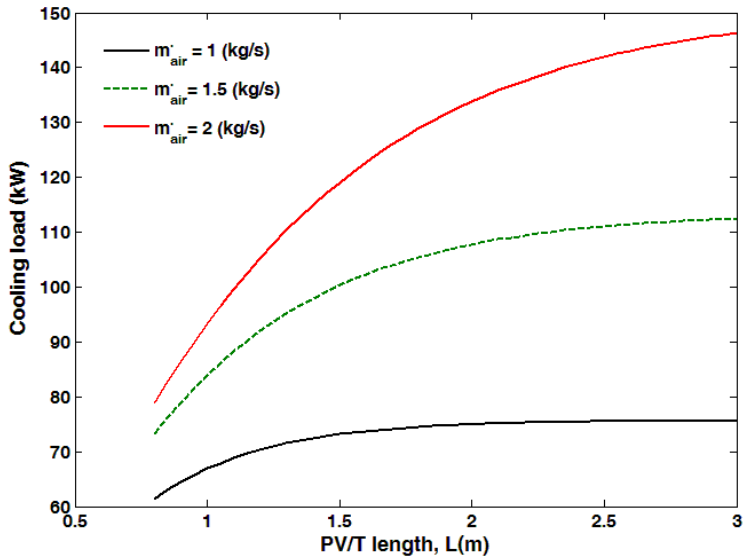

Figure 6.92: Effects of varying PV/T length and inlet air mass flow rate on cooling load of the system.

Fig. 6.93 shows the effect of PV/T length and inlet air mass flow rate on the total cost rate of the system. It is observed that an increase in PV/T solar collector length results in an increase in total cost rate of the system which is due to an increase in collector area which will affect the purchase cost of the collector. At constant collector length, an increase in inlet mass flow rate increases the total cost rate of the system. This is due to the fact that an increase in inlet air mass flow rate increases the chiller cooling load which will affect the purchase cost of the chiller. An increase in chiller cost results in an increase in total cost arte of the system.

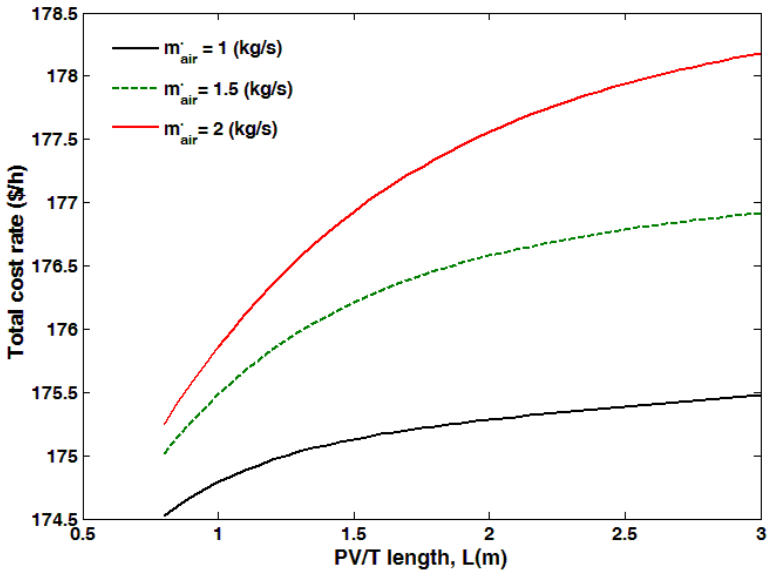

Figure 6.93: Effects of varying PV/T length and inlet air mass flow rate on total cost rate of the system.

6.4.3 Multi-objective optimization of integrated OTEC based multigeneration system

A multi-objective optimization method based on an evolutionary algorithm is applied optimization to the multigeneration system for cooling, electricity, fresh water and hydrogen to determine the most optimum design parameters for the system. Objective functions, design parameters and constraints, and overall optimization are described in this section.

6.4.3.1 Definition of objectives

Two objective functions are considered here for multi-objective optimization: exergy efficiency (to be maximized) and total cost rate of product (to be minimized). Consequently, the objective functions in this analysis can be expressed as follows:

Exergy efficiency

$$\Psi_{multi} = \frac{\dot{W}_{net,ORC}+\dot{W}_{PV/T}+\dot{E}x_{cooling}+\dot{E}x_{H_2}+\dot{E}x_{22}+}{\dot{E}x_{in,WS}+\dot{E}x_{in,CS}} \quad (6.7)$$

Total cost rate

$$\dot{C}_{tot} = \sum_k \dot{Z}_k \quad (6.8)$$

Here, $\dot{Z}_K$ is the purchase cost of each component. More details about equipment purchase cost are given elsewhere [103].

6.4.3.2 Decision variables

The following decision variables (design parameters) are selected for this study: Warm surface mass flow rate ($\dot{m}_{WS}$), OTEC evaporator pinch point temperature (*PP*) difference, OTEC turbine isentropic efficiency (η_T), pump isentropic efficiency (η_p), absorption chiller evaporator temperature (T_{EVP}), PV/T inlet air mass flow rate ($\dot{m}_{air}$), PV/T collector length (*L*), PV/T collector width (*b*) and OTEC condenser temperature (T_{Cond}). Although the decision variables may be varied in the optimization procedure, each is normally required to be within a reasonable range. Such constraints, based on earlier reports are listed in Table 6.15.

Table 6.15: Optimization constraints and their rationales.

Constraint	**Rationales**
100 <$\dot{m}_{WS}$ <150	Due to pump required work limitation
3 < *PP* <6 ºC	Due to heat transfer limit
0.5 kg/s < $\dot{m}_{air}$ <2 kg/s	Due to commercial availability
0.8 m < *L*< 2 m	Due to heat transfer limit
η_T < 0.9	Due to commercial availability
η_p < 0.9	Due to commercial availability
3ºC < T_{EVP} < 7 ºC	Due to cooling load limitation
0.4 m < *b*< 0.7 m	Due to commercial availability
5ºC < T_{Cond} < 9 ºC	Due to heat transfer limit

6.4.3.3 Evolutionary algorithm: Genetic algorithm

Genetic algorithms apply an iterative, stochastic search strategy to find an optimal solution and imitate in a simplified manner principles of biological evolution [93]. A characteristic of an

evolutionary algorithm is a population of individuals, where an individual consists of the values of the decision variables (structural and process variables here) and is a potential solution to the optimization problem [14]. More details about genetic algorithm and its procedure are given elsewhere [14, 93].

6.4.3.4 Results and discussion

The genetic algorithm optimization is performed for 250 generations, using a search population size of M = 100 individuals, crossover probability of p_c = 0.9, gene mutation probability of p_m = 0.035 and controlled elitism value c = 0.55. The results of the optimization are given and described.

6.4.3.4.1 Optimization results

Fig. 6.94 shows the Pareto frontier solution for this multigeneration system with objective functions indicated in equation. (6.7) and (6.8) in multi-objective optimization.

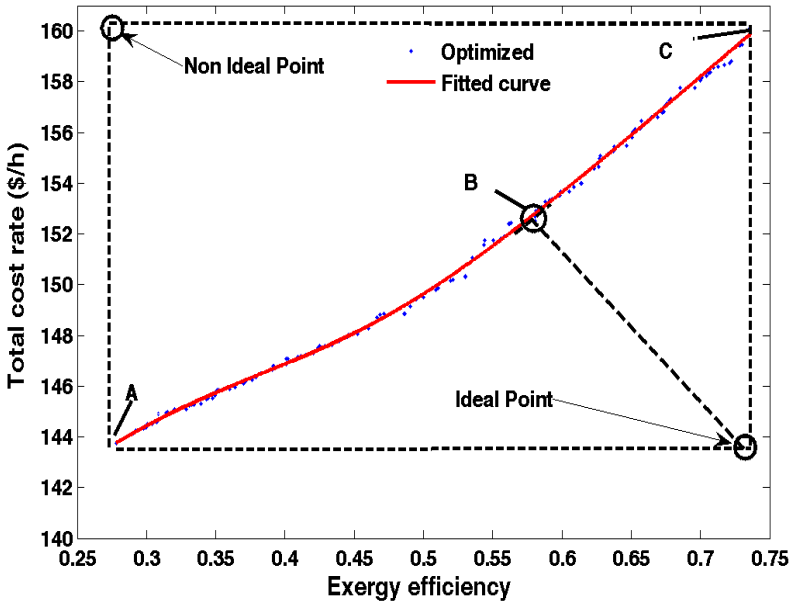

Figure 6.94: Pareto Frontier: Best trade off values for the objective functions

The results of optimum exergy efficiency and total cost rate for all points evaluated over 300 generations are shown in Fig. 6.95. The Pareto-optimal curve (best rank) is clearly visible in the lower part of the figure (red line) which is separately shown in Fig. 6.94.

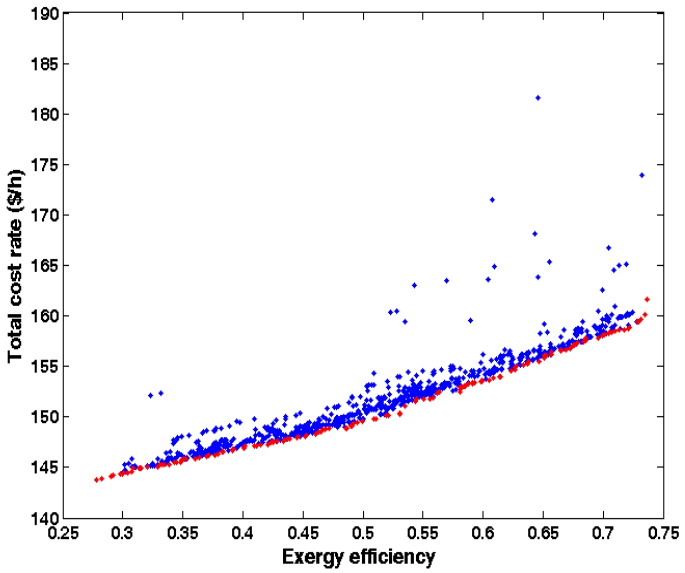

Figure 6.95: Results of all evaluations during 300 generations using genetic algorithm. A clear approximation of the Pareto front is visible on the lower part of the figure

As shown in Fig. 6.94, the maximum exergy efficiency exists at design point *C* (73.63 %), while the total cost rate of products is the greatest at this point (161.58 $/hr).On the other hand, the minimum value for the total cost rate of product occurs at design point *A* which is about 143.7 $/hr. Design point *A* is the optimal situation when total cost rate of product is the sole objective function, while design point *C* is the optimum point when exergy efficiency is the sole objective function. In multi-objective optimization, a process of decision-making for selection of the final optimal solution from the available solutions is required. The process of decision-making is usually performed with the aid of a hypothetical point in Fig. 6.94 (the ideal point), at which both objectives have their optimal values independent of the other objectives. It can be clearly seen that it is not feasible to have both objectives at their optimum point simultaneously and, as shown in Fig. 6.94, the ideal point is not a solution located on the Pareto Frontier.The closest point of the Pareto frontier to the ideal point might be considered as a desirable final solution. Nevertheless, in this case, the Pareto optimum frontier exhibits a weak equilibrium i.e., a small change in exergy efficiency from varying the operating parameters causes a large variation in the total cost rate of product. Therefore, the ideal point cannot be utilized for decision-making in this problem. In selection of the final optimum point, it is desired to achieve a better magnitude for each objective than its initial value for the base case problem.

Note that in multi-objective optimization and the Pareto solution, each point can be utilized as the optimized point. Therefore, the selection of the optimum solution depends on the preferences and criteria of the decision maker, suggesting that each may select a different point as for the optimum solution depending on his/her needs. Table 6.16 shows all the design parameters for points *A*-*C*.

Table 6.16: Optimized values for design parameters of the system based on multi-objective optimization.

Design parameter	***A***	***B***	***C***
L (m)	2	2.2	2.4
$\dot{m}_{WS}$ (kg/s)	100.5	100.6	100.3
PP (ºC)	5	2.5	1.5
η_T (%)	75	83	84
η_p (%)	81	77	76
T_{EVP} (ºC)	3.5	4	3.5
T_{Cond} (ºC)	9	8	6
$\dot{m}_{air}$ (kg/s)	0.5	1.8	2
b (m)	0.6	0.7	0.7

As shown in Fig. 6.94, the optimized values for exergy efficiency on the Pareto frontier range between 27 % and 73 %. In order to provide a good relationship between exergy efficiency and total cost rate, a curve is fitted on the optimized points obtained from the evolutionary algorithm. This fitted curve is shown in Fig. 6.94. The expression for this fitted curve is given as follows:

$$\dot{C}_{total} = \frac{43.55\psi^3+96.17\psi^2-93.68\psi+26.57}{\psi^2-0.78\psi+0.2} \quad (6.9)$$

This is allowable when the efficiency varies between 0.32 and 0.75.In order to study the variation of thermodynamic characteristics, three different points (*A* to *C*) on the Pareto frontier are considered. Table 6.17 shows total cost rate of the system, the total exergy destruction, the system exergy efficiency, the cooling loads of the system fresh water and hydrogen production arte of the system.

Table 6.17: Thermodynamic characteristics of three different points on the Pareto frontier.

Point	$\dot{W}_{net}$ (kW)	Ψ	$\dot{E}x_{D,tot}$ kW	$\dot{Q}_{cooling}$ kW	$\dot{C}_{tot}$ \$/h	$\dot{m}_{H_2}$ kg/h	$\dot{m}_{fresh}$ kg/h
A	29	0.28	1242	40	143.8	0.10	312
B	52.5	0.60	1277	140.5	153.7	0.18	584.7
C	66.6	0.73	1248	146.54	161.6	0.23	720

From point *A* to point *C* in this table, both total cost rate of the system and exergy efficiencies increases. As previously stated, point *A* is preferred when total cost rate is a single objective function, and design point *C* when exergy efficiency is a single objective function. Design point *B* has better results for both objective functions. Other thermodynamic properties correctly confirm this trend. For instance, from point *B* to *C*, the total exergy destruction rate decreases when the exergy efficiency increases. In order to better understand the variations of all design parameters, the scattered distribution of the design parameters are shown in Figs. 6.96 to 6.98.

In Figs. 6.96 to 6.98, it can be seen that the ORC turbine inlet pressure (Fig. 6.69c), the PV/T length (Fig. 6.96a), the pinch point temperature (Fig. 6.96c), the turbine isentropic efficiency (Fig. 6.96d), the pump isentropic efficiency (Fig. 6.97a), the condenser temperature (Fig.6.97c), the PV/T inlet air mass flow rate (6.97d) and the PV/T width (Fig. 6.98) have scattered distributions in their allowable domains, suggesting that these parameters have important effects on the trade-off between exergy efficiency and total cost rate. Design parameters selected with their maximum values indicate that they do not exhibit a conflict between two objective functions, indicating that increasing those design parameters leads to an improvement of both objective functions.

6.4.3.4.2 Sensitivity analysis

In order to have a better understanding of the multi-objective optimization, a comprehensive sensitivity analysis was performed. The effects of each design parameter for points *A*–*C* on both objective functions are investigated. Fig. 6.99 shows the effects of PV/T length on system exergy efficiency and total cost rate of the system. As seen in this figure, an increase in PV/T length has a negative effect on total cost rate, while an increase in this parameter results in an increase in the exergy efficiency of the system. An increase in PV/T length leads to an increase in collector electricity production and heat input to the single effect absorption chiller, resulting in an increase in the useful outputs of the system to increase the efficiency. On the other hand, an increase in this parameter correspondingly increases the purchase cost of the PV/T collector, which affects the total cost rate of the system. Since an increase in this parameter has both positive and negative effects on objective functions, its variation has a scattered distribution as shown in Fig. 6.96 a.

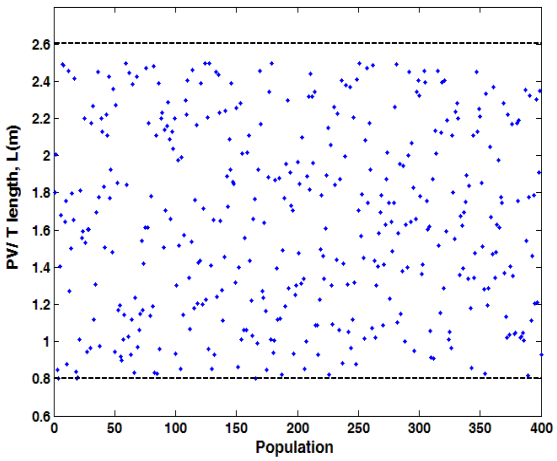

(a)

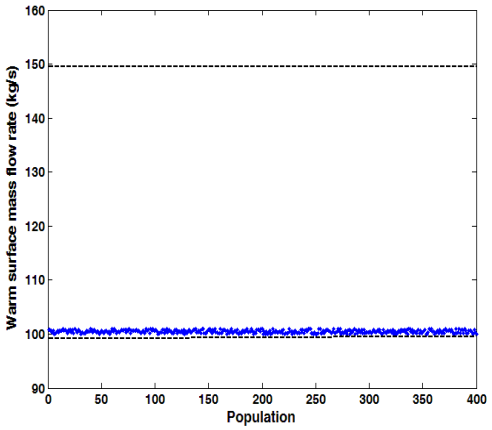

(b)

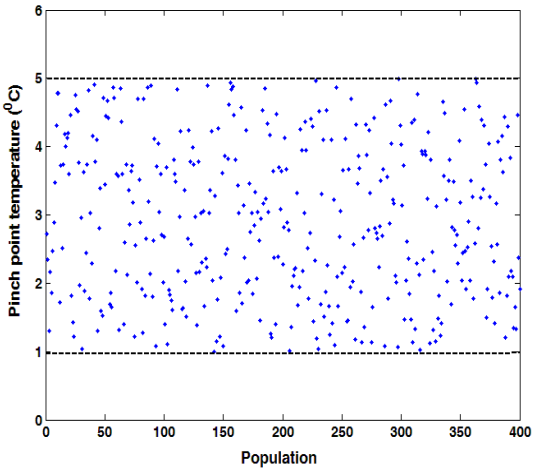

(c)

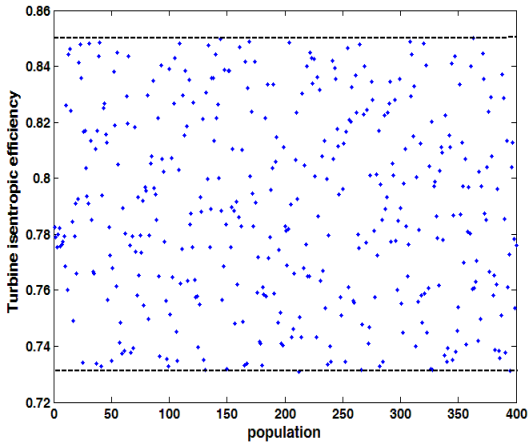

(d)

Figure 6.96: Scattered distribution of decision variables with population in Pareto frontier: (a) PV/T length, (b) warm surface mass flow rate, (c) pinch point temperature, (d) turbine isentropic efficiency

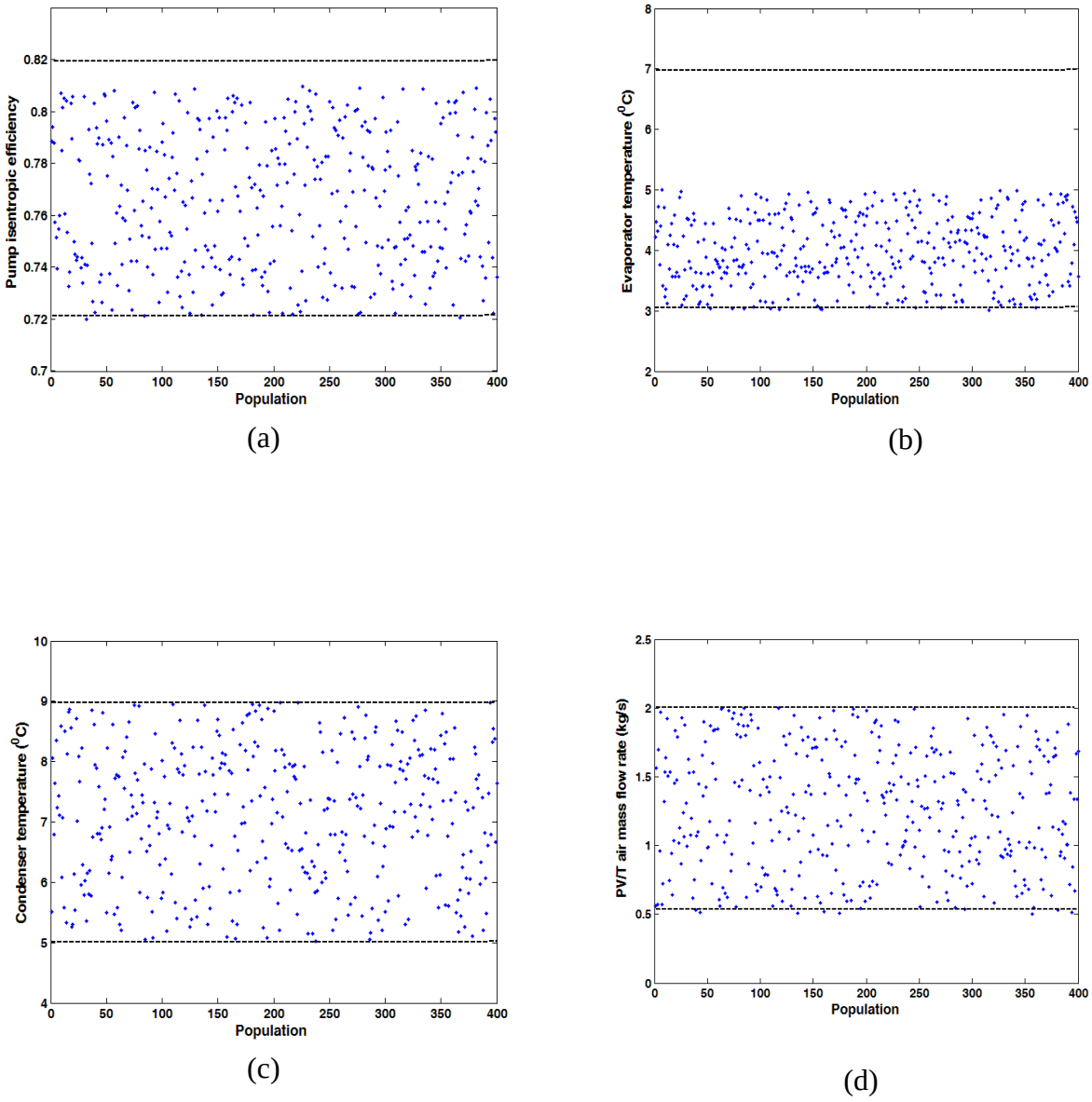

Figure 6.97: Scattered distribution of decision variables with population in Pareto frontier: (a) Pump isentropic efficiency, (b) chiller evaporator temperature, (c) condenser temperature, (d) PV/T mass flow rate

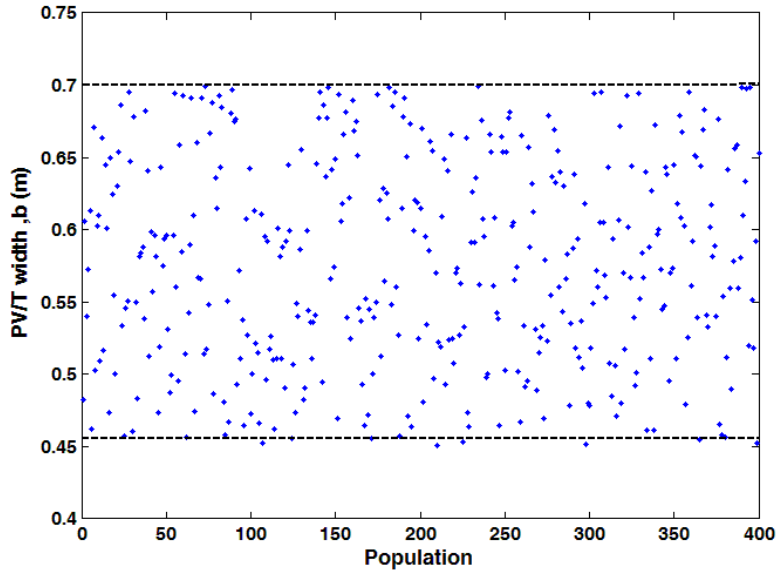

Figure 6.98: Scattered distribution of decision variables with population in Pareto frontier: PV/T width.

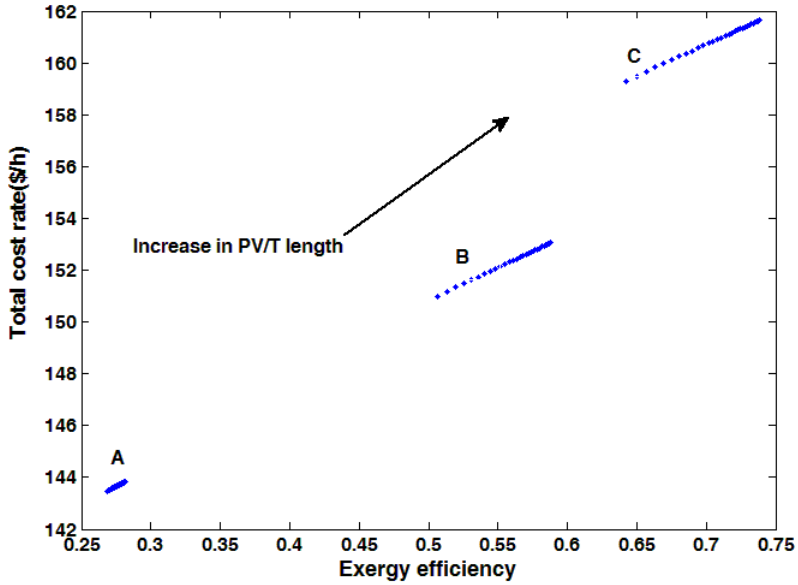

Figure 6.99: Effects of PV/T length on both objective functions.

Fig. 6.100 shows the effect of variation in warm surface mass flow rate on both objective functions. As shown, an increase in this parameter results in an increase in total cost rate while exergy efficiency decreases. As previously explained, an increase in this parameter leads to an increase in net power output; however, at the same time, it increases the exergy input to the

system, which results in a drop in exergy efficiency. An increase in warm surface mass flow rate increases the purchase cost of the OTEC turbine and OTEC pumps increasing the total cost of the system.

Fig. 6.101 shows the effect of evaporator pinch point temperature variation on both objective functions. An increase in this variable results in a decrease in system exergy efficiency. This is due to the fact that the higher the pinch point temperature, the lower the energy being utilized in the evaporator, which leads to a reduction of OTEC turbine power output. On the other hand, an increase in pinch point temperature when other design parameters are fixed results in a decrease in heat transfer area for the evaporator and a corresponding decrease in total cost rate for the system.

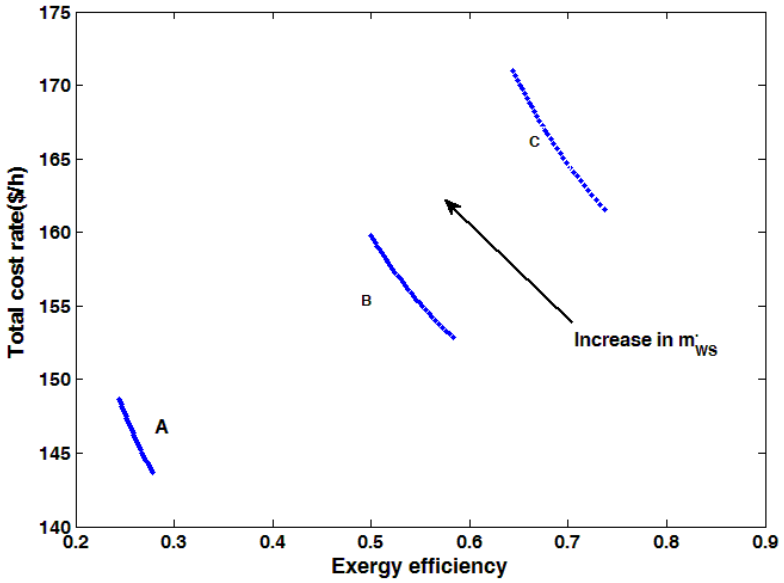

Figure 6.100: Effects of warm surface mass flow rate on both objective functions.

Fig. 6.102 represents the effect of turbine isentropic efficiency (η_T) variation on both objective functions. An increase in η_T results in an increase in system exergy efficiency and in the total cost of the system. An increase also results in an increase in the turbine power output, which directly leads to increased systemic exergy efficiency.

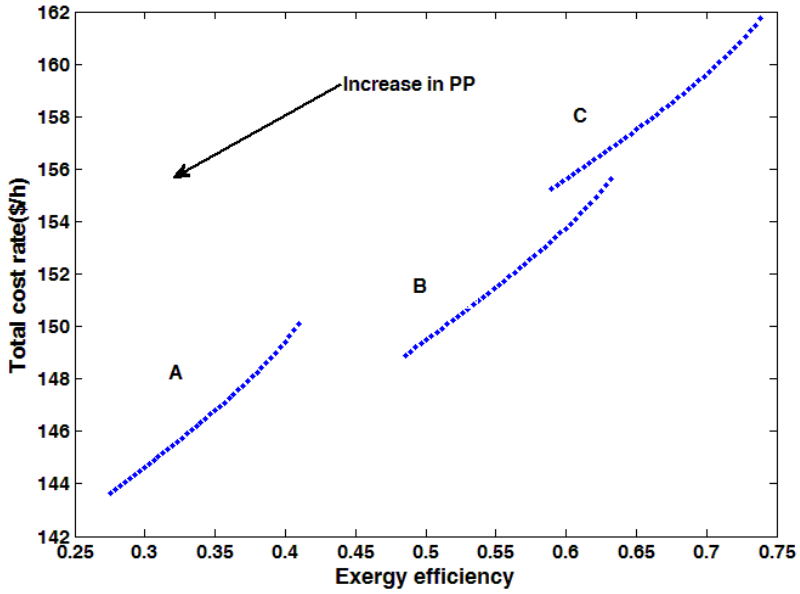

Figure 6.101: Effects of OTEC evaporator pinch point temperature on both objective functions.

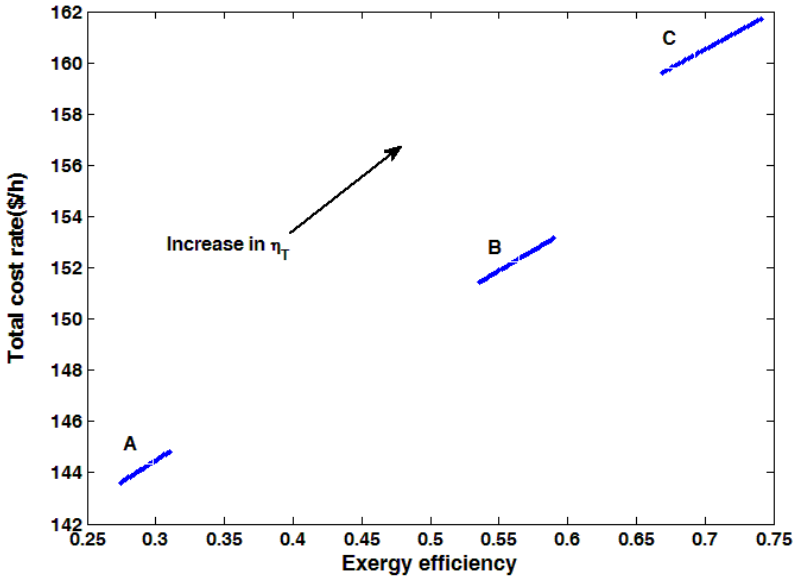

Figure 6.102: Effects of turbine isentropic efficiency on both objective functions.

Fig. 6.102 also shows that increasing this parameter leads to an increase in turbine purchase and maintenance cost. Since an increase in this parameter has positive and negative effects on both objective functions, the variation of this design parameter within its allowable range exhibits a scattered distribution as shown in Fig. 6.96d. Fig. 6.76 shows that pump isentropic efficiency does not have a significant effect on either objective function, as its purchase cost is relatively insignificant.

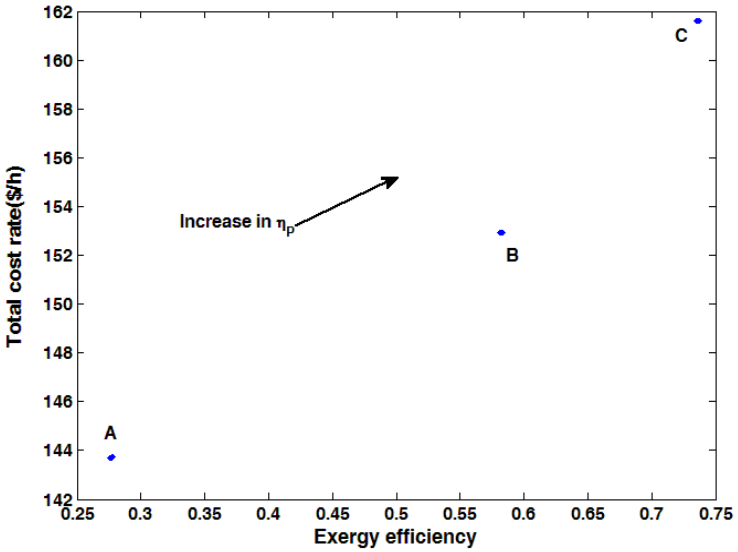

Figure 6.103: Effects of pump isentropic efficiency on both objective functions.

Fig. 6.104 shows the variation of the objective function by changing the absorption chiller evaporator temperature. An increase in evaporator temperature results in an increase in cooling load of the absorption chiller and, at the same time, increases the cost of the chiller. Another important factor in this integrated OTEC-based multigeneration system is the condenser temperature. Fig. 6.105 shows the effect of condenser temperature on both objective functions. It is observed that an increase in condenser temperature results in a decrease in the exergy efficiency of the system. This is due to the fact that an increase in condenser temperature increases the condenser pressure, which in turn results in an increase in heat rejected to the environment and therefore causes an increase in the outlet turbine enthalpy, which finally reduces the turbine work.

However, an increase in condenser temperature has a positive effect on the total cost rate of the system. When the condenser temperature increases, turbine work decreases, thereby decreasing the purchase cost of the turbine—a function of the work generated by the turbine. At the same time, there is an increase in condenser temperature when other design parameters are fixed. Fig. 6.106 shows the effect of PV/T inlet air mass flow rate on both objective functions. An increase in inlet air mass flow rate increases the exergy efficiency of the system.

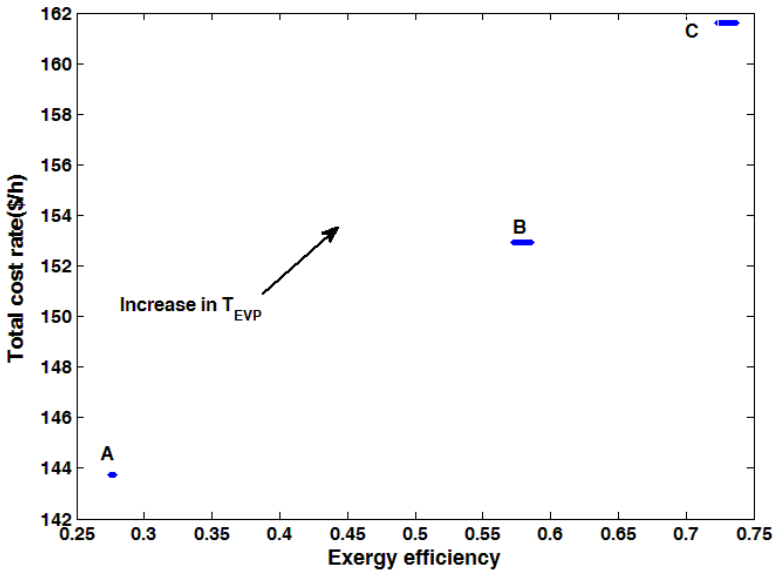

Figure 6.104: Effects of chiller evaporator temperature on both objective functions.

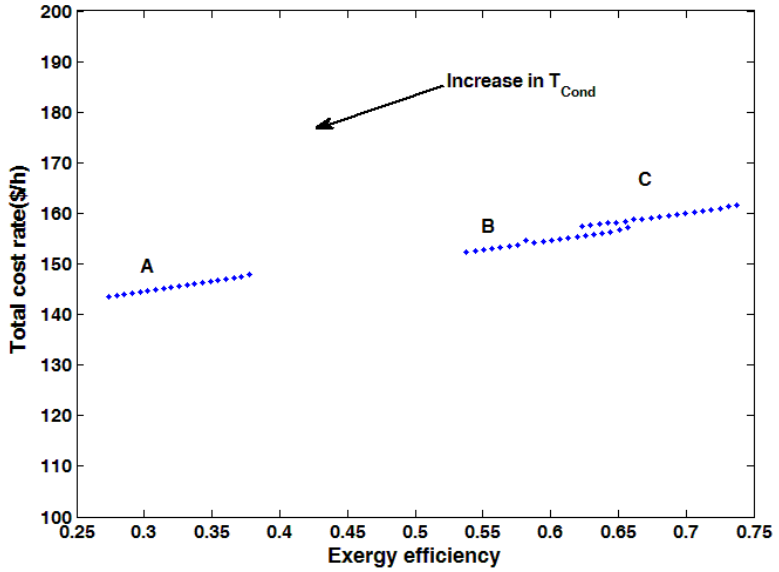

Figure 6.105: Effects of condenser temperature on both objective functions.

When inlet air mass flow rate increases, input heat into the absorption chiller generator increases and the higher the input energy to the generator, the higher the cooling load of the system. An increase in cooling load of the system increases the exergy efficiency of the system. Increasing PV/T inlet air mass flow rate also results in an increase in the total cost rate of the

system, mainly due to an increase in the cooling load of the system, which in turn increases the purchase cost of the system. Since an increase in this parameter has positive and negative effects on both objective functions, the variation of this design parameter within its allowable range exhibits a scattered distribution as shown in Fig. 6.97d.

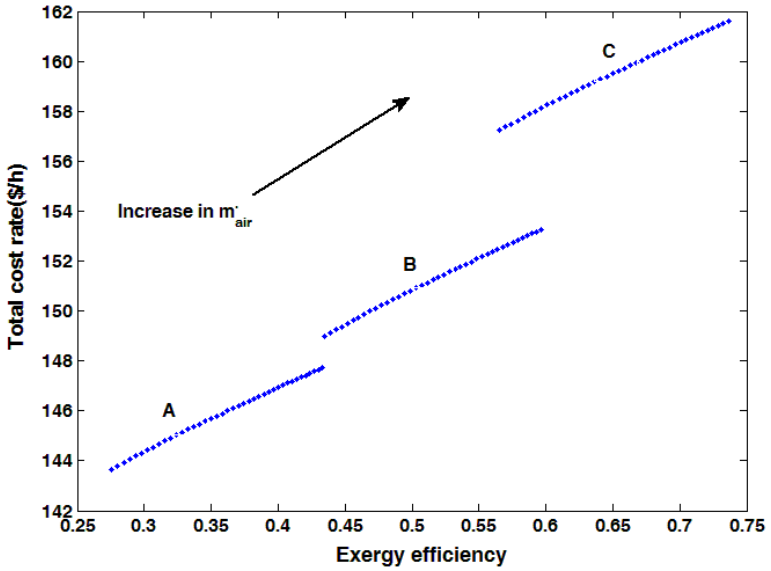

Figure 6.106: Effects of PV/T inlet air mass flow rate on both objective functions.

Fig. 6.107 shows the effect of PV/T width on both objective functions. As depicted, an increase in PV/T collector width increases the exergy efficiency of the system. This is due to an increase in collector area, which increases the electricity generated by the PV/T and increases in the absorption chiller energy input; this, in turn, increases the exergy efficiency of the system. An increase in this parameter also resulted in an increase in the purchase cost of the PV/T, which is a function of collector area. Therefore, the higher the PV/T purchase cost, the higher the total cost rate of the system. Since an increase in this parameter has positive and negative effects on both objective functions, the variation of this design parameter within its allowable range exhibits a scattered distribution as shown in Fig. 6.98.

6.5 Comparison and generalization

In this chapter, the comprehensive thermodynamic modelling, exergy analyses, environmental impact assessments, and multi-objective optimization of three newly proposed multigeneration systems for heating, cooling, electricity generation, hydrogen, hot water and fresh water productions are reported for insights they provide.

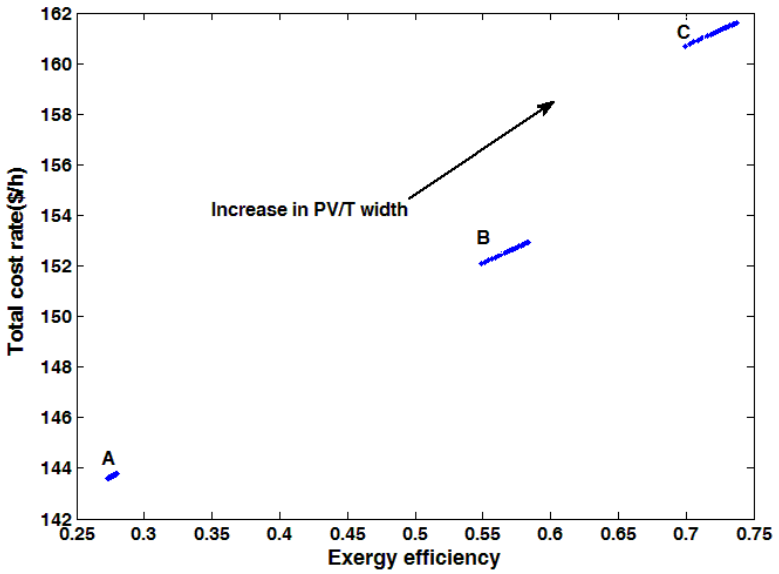

Figure 6.107: Effects of PV/T width on both objective functions.

Since these three systems have different prime movers, the comparison needs different criteria. Table 6.18 lists the useful outputs of each multigeneration energy system. This data shows that although the net power output of system I is much higher than that of alternative systems, the CO_2 emissions and total cost rate are higher compared to other systems.

Table 6.18: Comparison of three different multigeneration systems.

Parameter	$\dot{W}_{net}$ (kW)	$\dot{Q}_{heat}$ (kW)	$\dot{Q}_{cooling}$ (kW)	H_2 (Kg/h)	$\dot{m}_{DWH}$ (Kg/s)	$\dot{m}_{FW}$ (Kg/s)	$\dot{Z}_{tot}$ $/h	Ψ	CO_2 (Kg/kWh)
System I	11038	5788	1262	1.25	3.58	NA	1090	0.60	132
System II	500	2383	2560	0.08	0.8	1.9	476	0.3	0.36
System III	73	NA	105	0.2	NA	0.2	152	0.37	0

Since the capacity of each system is different, it is difficult to meaningfully compare them. One approach is to normalize each system and then compare them. In order to normalize the cost, the total cost rate of each system is divided by the energy of useful outputs and the final cost per kWh of products is compared. The following equations are used to normalize the cost:

$$C_{System} = \frac{\dot{Z}_{tot,I}}{\sum \dot{W}_{net} + \sum \dot{Q}_{heat} + \sum \dot{Q}_{cooling} + \dot{E}n_{H_2} + \dot{E}n_{DWH} + \dot{E}n_{FW}} \quad (6.10)$$

Here, En_{H_2} is the energy of hydrogen production, En_{DWH} is the energy of hot water at 60 ^{0}C and En_{FW} is the energy of fresh water production. Table 6.19 lists the normalized cost for each multigeneration system. The results show that the normalized cost of the gas turbine multigeneration energy system is less those other systems; however, the CO_2 emissions are relatively high. By contrast, the normalized cost of the integrated OTEC multigeneration system is higher than the other two, but does not have any CO_2 emissions at all. In conclusion, the comparison between multigeneration systems strongly depends on the stated priorities of the designers and engineers. For example, if the priority is to have a system without any emissions and the location is close to the sea, the OTEC system is the best choice. If the plant is going to be installed in a rural area with sufficient biomass, the second multigeneration system is preferred. In addition, the amount of each useful output can help designers to decide which system they should select. For instance, the gas turbine multigeneration system can provide 10 MW of electricity, while OTEC system can only provide 100 kW of electricity.

Table 6.19: Comparison of normalized cost for each multigeneration system.

Name of system	**Normalized cost ($/kWh)**
System I (Gas turbine based)	0.06
System II (Biomass based)	0.08
System III (OTEC based)	0.77

In summary, the comparison of systems indicates that there are several criteria to be considered before undertaking the design of a multigeneration energy system:

- Location of the plant.
- Electricity, heating and cooling requirements of the system.
- Budget for the system.
- Environmental concerns and global warming mitigation.
- Availability and cost of fuel for each system component.

Chapter 7: Conclusions and Recommendations

This PhD thesis provides several useful conclusions and recommendation for future research as follows:

7.1 Conclusions

The following concluding remarks are drawn from this study regarding the studied multigeneration systems:

System I: Gas turbine-based multigeneration

The exergy results show that the combustion chamber, steam condenser and HRSG are the main sources of irreversibility, with the high exergy destruction attributable to the high temperature difference for heat transfer in both devices and the reaction in the combustion chamber. In addition, the multigeneration cycle exhibits less CO_2 and CO emissions than micro gas turbine and CHP cycles. Additional conclusions are as follows:

- The exergy efficiency of the multigeneration cycle increases with gas turbine isentropic efficiency.
- The overall exergy destruction of the cycle decreases and the sustainability index increases with increasing compressor pressure ratio.
- The exergy efficiency and sustainability index for the multigeneration, gas turbine and CHP cycles increases with turbine inlet temperature, and the exergy efficiency of the system is slightly lower than the energy efficiency.
- The cost of environmental impact for the multigeneration system is significantly less than the cost associated with the power and CHP cycles.
- Multigeneration energy systems are good options to mitigate global warming as they can reduce CO_2 and CO emissions and also help reduce the cost of environmental impacts by producing several useful outputs from one energy input.
- The optimization results suggest that the compressor isentropic efficiency, gas turbine inlet temperature, compressor pressure ratio and ORC extraction pressure tend to have maximum values within their specified ranges, and that an increase in these parameters results in better system performance. Other concluding remarks follow:

I. Increase in compressor pressure ratio, gas turbine inlet temperature and ORC turbine extraction pressure have positive effects on both objective functions.
II. An increase in HRSG pressures increases system exergy efficiency and decreases the total cost rate of the system.
III. An increase in HRSG pinch point temperatures reduces the system exergy efficiency.
IV. An increase in steam turbine isentropic efficiency results in an increase in system exergy efficiency and in the total cost of the system.
V. An increase in evaporator temperature results in an increase in the cooling load of the absorption chiller.

System II: Biomass-based multigeneration

The comprehensive thermodynamic modelling, exergy analysis, and environmental impact assessments of this newly proposed multigeneration system for heating, cooling, electricity generation, hydrogen and hot water production have provided useful insights. The exergy results show that the combustor and ORC evaporator are the two main sources of irreversibility, with the highest exergy destruction rate due to the high temperature difference of heat transfer in both devices and the reaction in the combustor. System performance is notably affected by pinch point temperature, ORC turbine inlet pressure, and ORC pump inlet temperature. Additional conclusions follow:

- An increase in pinch point temperature does not significantly change the exergy efficiency of the system, but decreases both the heating and cooling loads of the system.
- An increase in pinch point temperature increases the hot water mass flow rate leaving the domestic water heater; however, it also reduces the hydrogen production rate.
- An increase in ORC turbine inlet pressure increases the net power output, the exergy efficiency of the system, the heating load and the hydrogen production of the system; however, this increase results in a decrease in the cooling load of the system.

- An increase in pump inlet temperature increases the exergy efficiency and the heating load of the system, while also resulting in a slight decrease in the cooling load of the system.
- This multigeneration system exhibits lower CO_2 emissions than the more conventional power generation and CHP systems.
- The optimization results show that ORC turbine inlet pressure, ORC turbine inlet temperature, evaporator pinch point temperature difference, ORC turbine isentropic efficiency, and ORC pump isentropic efficiency have scattered distributions in their allowable domains, suggesting that these parameters have important effects on the trade-off between exergy efficiency and total cost rate. Other concluding remarks follow:
    i. An increase in biomass flow rate leads to a decrease in system exergy efficiency.
    ii. Increase in turbine inlet temperature and turbine inlet pressure result in increases in exergy efficiency and total cost rate of the system. Since an increase in this parameter has positive and negative effects on both objective functions, the variation of this design parameter within its allowable range exhibits a scattered distribution.
    iii. An increase in pinch point temperature results in a decrease in system exergy efficiency and, when other design parameters are fixed, results in a decrease in heat transfer area for the evaporator. This is why the total cost rate of the system decreases.

System III: Integrated OTEC-based multigeneration

The comprehensive thermodynamic modelling and exergy and exergoeconomic analyses of this proposed multigeneration system for cooling, electricity generation, hydrogen and fresh water production has, as with the preceding systems, provided useful insights. System performance is notably affected by warm surface mass flow rate, solar radiation intensity, condenser temperature, PV/T collector length, PV/T collector width, PV/T inlet air mass flow rate and evaporator pinch point temperature difference (*PP*). Both exergy destruction and the dimensionless exergy destruction ratio are higher in solar collectors than in other components, suggesting that it would be worthwhile to focus efforts on improving this component.

Additional specific conclusions follow:

- An increase in warm surface mass flow rate results in a decrease in the exergy efficiency of the system due to an increase in energy input, while at the same time increasing the net power output of the system.
- An increase in solar radiation intensity increases the exergy efficiency of the integrated multigeneration system. This is due to the fact that an increase in solar intensity leads to an increase in the temperature of the warm surface. The higher the warm surface temperature, the higher the energy input to the OTEC evaporator, which leads to an increase in the turbine work and finally results in an increase in the system's exergy efficiency.
- An increase in condenser temperature results in a decrease in both exergy efficiency and net power output of the integrated system.
- An increase in pinch point temperature results in a decrease in exergy efficiency and an increase in total exergy destruction rate.
- Multi-objective optimization showed that OTEC evaporator pinch point temperature difference, OTEC turbine isentropic efficiency, pump isentropic efficiency, absorption chiller evaporator temperature, PV/T inlet air mass flow rate, PV/T collector length, PV/T collector width and OTEC condenser temperature have scattered distributions in their allowable domains, suggesting that these parameters have important effects on the trade-off between exergy efficiency and total cost rate. Other concluding remarks follow:
    i. Increase in PV/T collector length, turbine isentropic efficiency, pump isentropic efficiency, absorption chiller evaporator temperature and PV/T collector inlet air mass flow rate result in increased exergy efficiency and total cost rate of the system.
    ii. An increase in pinch point temperature results in a decrease in system exergy efficiency and, when other design parameters are fixed, also results in a decrease in heat transfer area for the evaporator, finally resulting in a decrease in the total cost rate of the system.

7.2 Recommendations

The results of this PhD thesis can be used for designing new multigeneration systems. These outcomes can assist designers in developing more energy efficient systems in an integration fashion. In this study, three multigeneration systems were analyzed and optimized. The results obtained from this thesis research also suggest several areas for future studies, as summarized below:

- To design and build multigeneration energy systems using different sources.
- To conduct experimental studies in order to enhance the body of knowledge.
- To use advanced exergy end exergoeconomic analysis to understand the effect of the avoidable and unavoidable parts of exergy destruction in each component and optimize based on minimization of the avoidable exergy destruction in each component.
- To perform the analyses for different climate and inflation rates and to investigate the effect of related parameters on optimized values.
- To apply other optimization techniques, like the particle swarm and ant colony methods, in order to compare results.
- To integrate a solid oxide fuel cell with gas turbine cycles for better fuel utilization and enhanced power production efficiency.
- To use coal gasification coupled to gas turbine generators, again for better power generation efficiency.

References

1. Dincer I: Renewable energy and sustainable development: a crucial review. *Renewable and Sustainable Energy Reviews* 2000, 4:157-175.
2. Ozgur Colpan C, Dincer I, Hamdullahpur F: The reduction of greenhouse gas emissions using various thermal systems in a landfill site. *International Journal of Global Warming* 2009, 1:89-105.
3. Spahni R, Chappellaz J, Stocker TF, Loulergue L, Hausammann G, Kawamura K, Flückiger J, Schwander J, Raynaud D, Masson-Delmotte V: Atmospheric methane and nitrous oxide of the late Pleistocene from Antarctic ice cores. *Science* 2005, 310:1317-1321.
4. Ahmadi P, Dincer I: Exergoenvironmental analysis and optimization of a cogeneration plant system using Multimodal Genetic Algorithm (MGA). *Energy* 2010, 35:5161-5172.
5. Al-Sulaiman FA, Dincer I, Hamdullahpur F: Exergy analysis of an integrated solid oxide fuel cell and organic Rankine cycle for cooling, heating and power production. *Journal of power sources* 2010, 195:2346-2354.
6. Ahmadi P, Rosen MA, Dincer I: Greenhouse gas emission and exergo-environmental analyses of a trigeneration energy system. *International Journal of Greenhouse Gas Control* 2011, 5:1540-1549.
7. Dincer I, Zamfirescu C: Renewable-energy-based multigeneration systems. *International Journal of Energy Research* 2012.
8. Ahmadi P, Rosen MA, Dincer I: Multi-objective exergy-based optimization of a polygeneration energy system using an evolutionary algorithm. *Energy* 2012, 46:21-31.
9. Khaliq A, Kumar R, Dincer I: Performance analysis of an industrial waste heat-based trigeneration system. *International journal of energy research* 2009, 33:737-744.
10. Havelský V: Energetic efficiency of cogeneration systems for combined heat, cold and power production. *International Journal of Refrigeration* 1999, 22:479-485.
11. Horlock JH: *Advanced gas turbine cycles.* Pergamon Press; 2003.
12. Haseli Y, Dincer I, Naterer G: Thermodynamic modeling of a gas turbine cycle combined with a solid oxide fuel cell. *International Journal of hydrogen energy* 2008, 33:5811-5822.
13. Ratlamwala T, Dincer I, Gadalla M: Energy and exergy analyses of an integrated solar-based desalination quadruple effect absorption system for freshwater and cooling production. *International Journal of Energy Research* 2012.
14. Srinivas N, Deb K: Muiltiobjective optimization using nondominated sorting in genetic algorithms. *Evolutionary computation* 1994, 2:221-248.
15. Huangfu Y, Wu J, Wang R, Xia Z: Experimental investigation of adsorption chiller for Micro-scale BCHP system application. *Energy and buildings* 2007, 39:120-127.
16. Mago PJ, Hueffed A, Chamra LM: Analysis and optimization of the use of CHP–ORC systems for small commercial buildings. *Energy and Buildings* 2010, 42:1491-1498.
17. Mago PJ, Smith AD: Evaluation of the potential emissions reductions from the use of CHP systems in different commercial buildings. *Building and Environment* 2012, 53:74-82.
18. Mago PJ, Hueffed AK: Evaluation of a turbine driven CCHP system for large office buildings under different operating strategies. *Energy and Buildings* 2010, 42:1628-1636.

19. Bianchi M, De Pascale A, Melino F: Performance analysis of an integrated CHP system with thermal and Electric Energy Storage for residential application. *Applied Energy* 2013.
20. Mıguez J, Murillo S, Porteiro J, Lopez L: Feasibility of a new domestic CHP trigeneration with heat pump: I. Design and development. *Applied thermal engineering* 2004, 24:1409-1419.
21. Porteiro J, Mıguez J, Murillo S, Lopez L: Feasibility of a new domestic CHP trigeneration with heat pump: II. Availability analysis. *Applied thermal engineering* 2004, 24:1421-1429.
22. Cihan A, Hacıhafızoglu O, Kahveci K: Energy–exergy analysis and modernization suggestions for a combined-cycle power plant. *International journal of energy research* 2006, 30:115-126.
23. Barelli L, Bidini G, Gallorini F, Ottaviano A: An energetic–exergetic analysis of a residential CHP system based on PEM fuel cell. *Applied Energy* 2011, 88:4334-4342.
24. Bingöl E, Kılkış B, Eralp C: Exergy based performance analysis of high efficiency poly-generation systems for sustainable building applications. *Energy and Buildings* 2011, 43:3074-3081.
25. El-Emam RS, Dincer I: Energy and exergy analyses of a combined molten carbonate fuel cell–Gas turbine system. *International Journal of Hydrogen Energy* 2011, 36:8927-8935.
26. Akkaya AV, Sahin B, Huseyin Erdem H: An analysis of SOFC/GT CHP system based on exergetic performance criteria. *International Journal of Hydrogen Energy* 2008, 33:2566-2577.
27. Al-Sulaiman FA, Dincer I, Hamdullahpur F: Energy analysis of a trigeneration plant based on solid oxide fuel cell and organic Rankine cycle. *International Journal of Hydrogen Energy* 2010, 35:5104-5113.
28. Rosen MA, Dincer I: Exergoeconomic analysis of power plants operating on various fuels. *Applied Thermal Engineering* 2003, 23:643-658.
29. Ameri M, Ahmadi P, Hamidi A: Energy, exergy and exergoeconomic analysis of a steam power plant: A case study. *International Journal of Energy Research* 2009, 33:499-512.
30. Balli O, Aras H, Hepbasli A: Exergetic performance evaluation of a combined heat and power (CHP) system in Turkey. *International journal of energy research* 2007, 31:849-866.
31. Balli O, Aras H, Hepbasli A: Exergoeconomic analysis of a combined heat and power (CHP) system. *International Journal of Energy Research* 2008, 32:273-289.
32. Kwak HY, Byun GT, Kwon YH, Yang H: Cost structure of CGAM cogeneration system. *International journal of energy research* 2004, 28:1145-1158.
33. Pospisil J, Fiedler J, Skala Z, Baksa M: Comparison of cogeneration and trigeneration technology for energy supply of tertiary buildings. *WSEAS Transactions on Heat and Mass Transfer* 2006, 1:262-267.
34. Al-Sulaiman FA, Hamdullahpur F, Dincer I: Performance comparison of three trigeneration systems using organic rankine cycles. *Energy* 2011, 36:5741-5754.
35. Martins L, Fábrega F, d'Angelo J: Thermodynamic Performance Investigation of a Trigeneration Cycle Considering the Influence of Operational Variables. *Procedia Engineering* 2012, 42:2061-2070.
36. Calva ET, Núnez MP, Toral M: Thermal integration of trigeneration systems. *Applied Thermal Engineering* 2005, 25:973-984.

37. Huang Y, Wang Y, Rezvani S, McIlveen-Wright D, Anderson M, Hewitt N: Biomass fuelled trigeneration system in selected buildings. *Energy Conversion and Management* 2011, 52:2448-2454.
38. Rocha M, Andreos R, Simões-Moreira J: Performance tests of two small trigeneration pilot plants. *Applied Thermal Engineering* 2012, 41:84-91.
39. Huicochea A, Rivera W, Gutiérrez-Urueta G, Bruno JC, Coronas A: Thermodynamic analysis of a trigeneration system consisting of a micro gas turbine and a double effect absorption chiller. *Applied Thermal Engineering* 2011, 31:3347-3353.
40. Chicco G, Mancarella P: Planning aspects and performance indicators for small-scale trigeneration plants. In *Future Power Systems, 2005 International Conference on*. IEEE; 2005: 6 pp.-6.
41. Chicco G, Mancarella P: Planning evaluation and economic assessment of the electricity production from small-scale trigeneration plants. *WSEAS Transactions on Power Systems* 2006, 1:393-400.
42. Aghahosseini S, Dincer I, Naterer G: Integrated gasification and Cu–Cl cycle for trigeneration of hydrogen, steam and electricity. *International Journal of Hydrogen Energy* 2011, 36:2845-2854.
43. Minciuc E, Le Corre O, Athanasovici V, Tazerout M, Bitir I: Thermodynamic analysis of tri-generation with absorption chilling machine. *Applied thermal engineering* 2003, 23:1391-1405.
44. Moya M, Bruno J, Eguia P, Torres E, Zamora I, Coronas A: Performance analysis of a trigeneration system based on a micro gas turbine and an air-cooled, indirect fired, ammonia–water absorption chiller. *Applied Energy* 2011, 88:4424-4440.
45. Velumani S, Enrique Guzmán C, Peniche R, Vega R: Proposal of a hybrid CHP system: SOFC/microturbine/absorption chiller. *International Journal of Energy Research* 2010, 34:1088-1095.
46. Buck R, Friedmann S: Solar-assisted small solar tower trigeneration systems. *TRANSACTIONS-AMERICAN SOCIETY OF MECHANICAL ENGINEERS JOURNAL OF SOLAR ENERGY ENGINEERING* 2007, 129:349.
47. Dincer I, Rosen MA: *Exergy: energy, environment and sustainable development.* Elsevier Science; 2012.
48. Santo D: Energy and exergy efficiency of a building internal combustion engine trigeneration system under two different operational strategies. *Energy and Buildings* 2012.
49. Ebrahimi M, Keshavarz A, Jamali A: Energy and exergy analyses of a micro-steam CCHP cycle for a residential building. *Energy and Buildings* 2012, 45:202-210.
50. Khaliq A: Exergy analysis of gas turbine trigeneration system for combined production of power heat and refrigeration. *International Journal of Refrigeration* 2009, 32:534-545.
51. Kong X, Wang R, Huang X: Energy efficiency and economic feasibility of CCHP driven by stirling engine. *Energy Conversion and Management* 2004, 45:1433-1442.
52. Ziher D, Poredos A: Economics of a trigeneration system in a hospital. *Applied Thermal Engineering* 2006, 26:680-687.
53. Temir G, Bilge D: Thermoeconomic analysis of a trigeneration system. *applied thermal engineering* 2004, 24:2689-2699.

54. Ehyaei M, Mozafari A: Energy, economic and environmental (3E) analysis of a micro gas turbine employed for on-site combined heat and power production. *Energy and Buildings* 2010, 42:259-264.
55. Ozgener O, Hepbasli A: Exergoeconomic analysis of a solar assisted ground-source heat pump greenhouse heating system. *Applied Thermal Engineering* 2005, 25:1459-1471.
56. Ozgener O, Hepbasli A, Ozgener L: A parametric study on the exergoeconomic assessment of a vertical ground-coupled (geothermal) heat pump system. *Building and environment* 2007, 42:1503-1509.
57. Dincer I: Environmental and sustainability aspects of hydrogen and fuel cell systems. *International Journal of Energy Research* 2007, 31:29-55.
58. Amrollahi Z, Ertesvåg IS, Bolland O: Thermodynamic analysis on post-combustion CO< sub> 2</sub> capture of natural-gas-fired power plant. *International Journal of Greenhouse Gas Control* 2011, 5:422-426.
59. Petrakopoulou F, Boyano A, Cabrera M, Tsatsaronis G: Exergoeconomic and exergoenvironmental analyses of a combined cycle power plant with chemical looping technology. *International Journal of Greenhouse Gas Control* 2011, 5:475-482.
60. Sahoo P: Exergoeconomic analysis and optimization of a cogeneration system using evolutionary programming. *Applied thermal engineering* 2008, 28:1580-1588.
61. Sayyaadi H, Sabzaligol T: Exergoeconomic optimization of a 1000 MW light water reactor power generation system. *International Journal of Energy Research* 2009, 33:378-395.
62. Haseli Y, Dincer I, Naterer G: Optimum temperatures in a shell and tube condenser with respect to exergy. *International Journal of Heat and Mass Transfer* 2008, 51:2462-2470.
63. Sayyaadi H, Nejatolahi M: Multi-objective optimization of a cooling tower assisted vapor compression refrigeration system. *International Journal of Refrigeration* 2011, 34:243-256.
64. Ahmadi P, Dincer I, Rosen MA: Exergy, exergoeconomic and environmental analyses and evolutionary algorithm based multi-objective optimization of combined cycle power plants. *Energy* 2011, 36:5886-5898.
65. Sayyaadi H, Babaelahi M: Multi-objective optimization of a joule cycle for re-liquefaction of the Liquefied Natural Gas. *Applied Energy* 2011, 88:3012-3021.
66. Ghaebi H, Saidi M, Ahmadi P: Exergoeconomic optimization of a trigeneration system for heating, cooling and power production purpose based on TRR method and using evolutionary algorithm. *Applied Thermal Engineering* 2012, 36:113-125.
67. Kavvadias K, Maroulis Z: Multi-objective optimization of a trigeneration plant. *Energy Policy* 2010, 38:945-954.
68. Al-Sulaiman FA, Dincer I, Hamdullahpur F: Thermoeconomic optimization of three trigeneration systems using organic Rankine cycles: Part I–Formulations. *Energy Conversion and Management* 2013.
69. Wang J, Yan Z, Wang M, Li M, Dai Y: Multi-objective optimization of an organic Rankine cycle (ORC) for low grade waste heat recovery using evolutionary algorithm. *Energy Conversion and Management* 2013, 71:146-158.
70. Shirazi A, Aminyavari M, Najafi B, Rinaldi F, Razaghi M: Thermal–economic–environmental analysis and multi-objective optimization of an internal-reforming solid oxide fuel cell–gas turbine hybrid system. *International Journal of Hydrogen Energy* 2012.

71. Hosseini M, Dincer I, Ahmadi P, Avval HB, Ziaasharhagh M: Thermodynamic modelling of an integrated solid oxide fuel cell and micro gas turbine system for desalination purposes. *International Journal of Energy Research* 2011.
72. Ratlamwala T, Gadalla M, Dincer I: Performance assessment of an integrated PV/T and triple effect cooling system for hydrogen and cooling production. *International Journal of Hydrogen Energy* 2011, 36:11282-11291.
73. Ratlamwala T, Dincer I, Gadalla M: Performance analysis of a novel integrated geothermal-based system for multi-generation applications. *Applied Thermal Engineering* 2012, 40:71-79.
74. Ozturk M, Dincer I: Thermodynamic analysis of a solar-based multi-generation system with hydrogen production. *Applied Thermal Engineering* 2012.
75. Ahmadi P, Dincer I, Rosen MA: Exergo-environmental analysis of an integrated organic Rankine cycle for trigeneration. *Energy Conversion and Management* 2012, 64:447-453.
76. Ahmadi P, Dincer I, Rosen MA: Development and assessment of an integrated biomass-based multi-generation energy system. *Energy* 2013.
77. Cohce M, Dincer I, Rosen M: Energy and exergy analyses of a biomass-based hydrogen production system. *Bioresource technology* 2011, 102:8466-8474.
78. Hughes EE, Tillman DA: Biomass cofiring: status and prospects 1996. *Fuel processing technology* 1998, 54:127-142.
79. Lian Z, Chua K, Chou S: A thermoeconomic analysis of biomass energy for trigeneration. *Applied Energy* 2010, 87:84-95.
80. Mujeebu M, Jayaraj S, Ashok S, Abdullah M, Khalil M: Feasibility study of cogeneration in a plywood industry with power export to grid. *Applied Energy* 2009, 86:657-662.
81. Tchanche BF, Lambrinos G, Frangoudakis A, Papadakis G: Low-grade heat conversion into power using organic Rankine cycles–A review of various applications. *Renewable and Sustainable Energy Reviews* 2011, 15:3963-3979.
82. Faizal M, Rafiuddin Ahmed M: On the ocean heat budget and ocean thermal energy conversion. *International Journal of Energy Research* 2011, 35:1119-1144.
83. Meegahapola L, Udawatta L, Witharana S: The Ocean Thermal Energy Conversion strategies and analysis of current challenges. In *Industrial and Information Systems, 2007 ICIIS 2007 International Conference on*. IEEE; 2007: 123-128.
84. Esteban M, Leary D: Current developments and future prospects of offshore wind and ocean energy. *Applied Energy* 2012, 90:128-136.
85. Uehara H, Nakaoka T: OTEC using plate-type heat exchanger (using ammonia as working fluid). *Transactions of JSME* 1984, 50:1325-1333.
86. Uehara H, Ikegami Y: Optimization of a closed-cycle OTEC system. *Journal of Solar Energy Engineering;(USA)* 1990, 112.
87. Uehara H, Miyara A, Ikegami Y, Nakaoka T: Performance analysis of an OTEC plant and a desalination plant using an integrated hybrid cycle. *Journal of solar energy engineering* 1996, 118.
88. Yamada N, Hoshi A, Ikegami Y: Performance simulation of solar-boosted ocean thermal energy conversion plant. *Renewable Energy* 2009, 34:1752-1758.
89. Cengel YA, Boles MA, Kanoğlu M: *Thermodynamics: an engineering approach.* McGraw-Hill New York; 2011.
90. Bejan A, Tsatsaronis G, Moran M: *Thermal design and optimization.* Wiley-Interscience; 1995.

91. Barzegar Avval H, Ahmadi P, Ghaffarizadeh A, Saidi M: Thermo-economic-environmental multiobjective optimization of a gas turbine power plant with preheater using evolutionary algorithm. *International Journal of Energy Research* 2011, 35:389-403.
92. Gulder OL: Flame temperature estimation of conventional and future jet fuels. *Journal of engineering for gas turbines and power* 1986, 108:376-380.
93. Ghaffarizadeh A, Ahmadi K, Flann NS: Sorting unsigned permutations by reversals using multi-objective evolutionary algorithms with variable size individuals. In *Evolutionary Computation (CEC), 2011 IEEE Congress on*. IEEE; 2011: 292-295.
94. Goldberg DE: Genetic algorithms in search, optimization, and machine learning. 1989.
95. Schaffer JD: Multiple objective optimization with vector evaluated genetic algorithms. In *Proceedings of the 1st international Conference on Genetic Algorithms*. L. Erlbaum Associates Inc.; 1985: 93-100.
96. Farshi LG, Mahmoudi SS, Rosen MA, Yari M: Use of low grade heat sources in combined ejector–double effect absorption refrigeration systems. *Proceedings of the Institution of Mechanical Engineers, Part A: Journal of Power and Energy* 2012, 226:607-622.
97. Palacios-Bereche R, Gonzales R, Nebra SA: Exergy calculation of lithium bromide–water solution and its application in the exergetic evaluation of absorption refrigeration systems LiBr-H2O. *International Journal of Energy Research* 2012, 36:166-181.
98. Wang J, Dai Y, Sun Z: A theoretical study on a novel combined power and ejector refrigeration cycle. *International Journal of Refrigeration* 2009, 32:1186-1194.
99. Ahmadi P, Dincer I, Rosen MA: Energy and exergy analyses of hydrogen production via solar-boosted ocean thermal energy conversion and PEM electrolysis. *International Journal of Hydrogen Energy* 2012.
100. Ni M, Leung MK, Leung DY: Energy and exergy analysis of hydrogen production by a proton exchange membrane (PEM) electrolyzer plant. *Energy conversion and management* 2008, 49:2748-2756.
101. Kotas TJ: The exergy method of thermal plant analysis. 1985.
102. Roosen P, Uhlenbruck S, Lucas K: Pareto optimization of a combined cycle power system as a decision support tool for trading off investment vs. operating costs. *International Journal of Thermal Sciences* 2003, 42:553-560.
103. Peters MS, Timmerhaus KD, West RE, Timmerhaus K, West R: *Plant design and economics for chemical engineers.* McGraw-Hill New York; 1968.
104. Mabrouk AA, Nafey A, Fath H: Thermoeconomic analysis of some existing desalination processes. *Desalination* 2007, 205:354-373.
105. Genç G, Çelik M, Serdar Genç M: Cost analysis of wind-electrolyzer-fuel cell system for energy demand in Pınarbaşı-Kayseri. *International Journal of Hydrogen Energy* 2012.
106. Basu P: *Combustion and gasification in fluidized beds.* CRC press; 2006.
107. Salcedo R, Antipova E, Boer D, Jiménez L, Guillén-Gosálbez G: Multi-objective optimization of solar Rankine cycles coupled with reverse osmosis desalination considering economic and life cycle environmental concerns. *Desalination* 2012, 286:358-371.
108. Bruno JC, Lopez-Villada J, Letelier E, Romera S, Coronas A: Modelling and optimisation of solar organic rankine cycle engines for reverse osmosis desalination. *Applied Thermal Engineering* 2008, 28:2212-2226.

109. Farahat S, Sarhaddi F, Ajam H: Exergetic optimization of flat plate solar collectors. *Renewable Energy* 2009, 34:1169-1174.
110. Nihous G, Vega L: Design of a 100 MW OTEC-hydrogen plantship. *Marine structures* 1993, 6:207-221.
111. Joshi A, Tiwari A, Tiwari G, Dincer I, Reddy B: Performance evaluation of a hybrid photovoltaic thermal (PV/T)(glass-to-glass) system. *International Journal of Thermal Sciences* 2009, 48:154-164.
112. Al-Alili A, Hwang Y, Radermacher R, Kubo I: A high efficiency solar air conditioner using concentrating photovoltaic/thermal collectors. *Applied Energy* 2012, 93:138-147.
113. Uehara H, Dilao CO, Nakaoka T: Conceptual design of ocean thermal energy conversion (OTEC) power plants in the Philippines. *Solar energy* 1988, 41:431-441.
114. Ioroi T, Yasuda K, Siroma Z, Fujiwara N, Miyazaki Y: Thin film electrocatalyst layer for unitized regenerative polymer electrolyte fuel cells. *Journal of Power sources* 2002, 112:583-587.
115. Millet P, Andolfatto F, Durand R: Design and performance of a solid polymer electrolyte water electrolyzer. *International Journal of Hydrogen Energy* 1996, 21:87-93.
116. Ehyaei M, Mozafari A, Alibiglou M: Exergy, economic & environmental (3E) analysis of inlet fogging for gas turbine power plant. *Energy* 2011, 36:6851-6861.
117. Al-Sulaiman FA, Dincer I, Hamdullahpur F: Energy and exergy analyses of a biomass trigeneration system using an organic Rankine cycle. *Energy* 2012.